

Haptic Interface Based on Tactile Sensors for Assistive Devices

Andrés Trujillo León

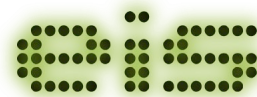
Department of Electronics
Instituto de Investigación Biomédica de Málaga
Escuela de Ingenierías Industriales
Universidad de Málaga

A doctoral thesis submitted for the degree of
Philosophiæ Doctor (PhD) in Mechatronics Engineering

January 2018



UNIVERSIDAD DE MÁLAGA



*Electronics for
Instrumentation
and Systems*


UNIVERSIDAD
DE MÁLAGA





UNIVERSIDAD
DE MÁLAGA

AUTOR: Andrés Trujillo León

 <http://orcid.org/0000-0003-4798-1777>

EDITA: Publicaciones y Divulgación Científica. Universidad de Málaga



Esta obra está bajo una licencia de Creative Commons Reconocimiento-NoComercial-SinObraDerivada 4.0 Internacional:

<http://creativecommons.org/licenses/by-nc-nd/4.0/legalcode>

Cualquier parte de esta obra se puede reproducir sin autorización pero con el reconocimiento y atribución de los autores.

No se puede hacer uso comercial de la obra y no se puede alterar, transformar o hacer obras derivadas.

Esta Tesis Doctoral está depositada en el Repositorio Institucional de la Universidad de Málaga (RIUMA): riuma.uma.es



Haptic Interface Based on Tactile Sensors for Assistive Devices

Andrés Trujillo León

Department of Electronics
Instituto de Investigación Biomédica de Málaga
Escuela de Ingenierías Industriales
Universidad de Málaga

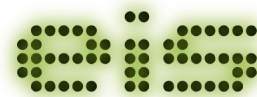
Supervisors: Fernando Vidal Verdú
Wael Bachta

A doctoral thesis submitted for the degree of
Philosophiæ Doctor (PhD) in Mechatronics Engineering

February 2018



UNIVERSIDAD DE MÁLAGA



*Electronics for
Instrumentation
and Systems*





UNIVERSIDAD
DE MÁLAGA

El Dr. Fernando Vidal Verdú, catedrático del Departamento de Electrónica de la Universidad de Málaga, y el Dr. Wael Wachta, profesor titular de la Universidad Pierre et Marie Curie, Paris VI, e investigador del Institut des Systèmes Intelligents et de Robotique, París,

CERTIFICAN:

Que D. Andrés Trujillo León, Ingeniero T. Telecomunicaciones e Ingeniero en Electrónica por la Universidad de Málaga, ha realizado bajo su dirección la Tesis Doctoral que tiene por título "Haptic Interface Based on Tactile Sensors for Assistive Devices" para optar al grado de Doctor en Ingeniería Mecatrónica, alcanzando los objetivos de investigación propuestos y estando debidamente cualificada para su defensa.

Málaga,
Enero 2018

Directores de Tesis: Dr. Fernando Vidal Verdú y Dr. Wael Wachta.

Tutor de Tesis: Dr. Fernando Vidal Verdú.



UNIVERSIDAD
DE MÁLAGA

A vosotros...

... que os habéis acostumbrado a vivir con la maleta siempre a mano. Que a menudo pasáis tiempo lejos de vuestras familias. Que a veces os sentís solos e incomprendidos. Que sois vilipendiados por vuestro gobierno. Que sufrís unas condiciones laborales indignas. Que cuando los medios se toman la "molestia" de incluiros en el debate, sois víctimas de la falsa equidistancia. Que en ocasiones sois acusados de ser mercenarios por quienes toman la -pequeñísima- parte por el todo.

... por dedicar vuestras vidas a hacer que las de los demás sean más sencillas, agradables y largas. Por arrojar luz donde hasta ahora había oscuridad. Por, además, luchar por que no volvamos a las cavernas empleando tiempo que no tenéis, ya que publicáis o perecéis. Por vuestra inmensurable vocación y talento. A vosotros, héroes anónimos.



UNIVERSIDAD
DE MÁLAGA

Acknowledgements / Agradecimientos

La realización de una tesis doctoral es un proceso largo, muchas veces arduo y fatigoso. Esta se ha sustentado en muchas personas que han estado ahí de una forma u otra y que, a veces sin ser conscientes, han tenido que ver con que llegue a buen término.

Me gustaría dar las gracias a / I would like to thank:

Todas aquellas personas que han participado en los experimentos. Más de un centenar de voluntarios de distintas nacionalidades han usado los prototipos presentados en esta tesis en los distintos experimentos planteados dando lugar a los resultados que la respaldan. Su participación desinteresada ha sido crucial. En especial, resaltaría la siempre presta disponibilidad mostrada por mis colegas del grupo EIS Óscar, José, Julián y Rafa, y por mi amiga y coetánea doctorando Estrella. Sois unos conejillos de indias estupendos.

Fernando Vidal. Cuando la relación que te une a tu director de tesis está más cercana a la amistad que a la supervisión formal académica todo es más sencillo.

Mi madre, que imagino con sentimientos encontrados, consciente de que este es un trabajo bonito, pero a menudo complicado y poco reconocido; *a mi padre,* por empeñarse en demostrarme que la divulgación científica es más necesaria que nunca.

Mi abuela Valle, fuente de inspiración para todos los que la conocemos.

Wael Bachtá, for his valuable comments and recommendations on my work. For inviting me to stay at the ISIR and make me feel at home.

The ISIR's staff and my colleagues and PhD candidates of AGATHE group, for their warm welcome and hospitality. At this time all of them are already doctors. In my defense, doctoral theses are shorter in France (seriously).

Isa. You know that I love you and that sort of thing. However, this document is about science. In this sense, the results reported by the authors of [1–3] suggest that the following may be a pertinent question: will you marry me?

* * *

El autor de la presente tesis doctoral ha sido beneficiario de un contrato para la Formación de Profesorado Universitario (FPU), perteneciente a los subprogramas de Formación y de Movilidad dentro del Programa Estatal de Promoción del Talento y su Empleabilidad, en el marco del Plan Estatal de Investigación Científica y Técnica y de Innovación 2013-2016 en I+D+i. Asimismo, esta tesis doctoral también se ha financiado a través del "*Proyecto Sensores táctiles en sistemas mecatrónicos para salud*", con referencia TEC2015-67642-R, a cargo del Plan Nacional de Investigación y fondos FEDER. Durante las estancias en el *Institut des Systèmes Intelligents et de Robotique* (Université Pierre et Marie Curie), París, Francia, la investigación se llevó a cabo parcialmente en el marco del proyecto *Labex SMART*, con referencia ANR-11-LABX-65 - ANR-11-IDEX-0004-02.

Abstract

Developed countries must cope with the increasing aging of their population. Aging well requires functional capacity in the daily life activity. This way, assistive technologies have to face one of the main age related issues: mobility decline. Canes and walkers are prescribed for people with reduced mobility but still able to walk. However, there is a numerous group among the elderly with limited walking ability that requires other kind of aid. In this sense, powered wheelchairs are reported as a means of extending the activity and participation of their users. These chairs are normally driven through a joystick located at the armrest. However, this device is not a suitable for all users. Some of them find it difficult and others need the assistance of another person (those suffering from nervous system diseases, spinal cord injuries, mental disability, etc). This way, there are cases in which the help of an assistant is required. Since propelling a wheelchair in day to day life is a hard task that may cause health problems, it is useful that assistants can benefit from powered wheelchairs advantages. The common commercial driving solution aimed at assistants consists in another joystick placed at the rear part of the chair. As it has been previously reported, this device is not very comfortable and intuitive. Regarding research, many of the related robotic assistive devices base their interface on force sensors. These devices are costly and hence are a barrier to market entry.

Considering the above, the present work is dedicated to develop a haptic interface aimed to fully assist the driving of powered wheelchairs. It is a handlebar intended to be used by caregivers in the same way as a regular one. Moreover, it is based on tactile sensors, which are a cost-effective alternative in human-machine haptic interaction. Two prototypes of handlebar are proposed and the acquisition electronics are described. Besides, a series of experiments are performed. They are devoted to the study of the issues and specific characteristics of this tactile interface. A haptic-based driving control is proposed based on the results of the these tests. This is evaluated in a controlled experiment in which it is compared with the common attendant joystick. Both objective performance data and the perception of the users about the driving experience with the handlebar are positive. Results suggest that the haptic handlebar is a viable proposal to assist caregivers in an intuitive and effortless way. Finally, the interface is extended to another assistive device such as a cane.

A tactile handle is developed and attached to an instrumented cane. Experiments show that parameters closely related to the trajectory pitch angle and the load force on the cane can be provided by the haptic handle. They may be useful for monitoring and improving the physical therapy of, for example, post-stroke patients that undergo rehabilitation.

Structure of the manuscript

This document is organized in 6 chapters and 4 appendixes as follows:

- Chapter 1 introduces the topic of the thesis, analyzing the background and the state of the art. A number of shortcomings that justify the proposal of this work are identified. It also presents the framework within which the thesis has been developed.
- Chapter 2 describes the design and implementation of the haptic handlebar. Prototypes and their conditioning electronics are detailed. A preliminary driving experiment is performed.
- Chapter 3 is centered on the work lines that arose from the preliminary experiment explained in Chapter 2. Four experiments are described and, as a result, a driving control algorithm is proposed.
- Chapter 4 presents the evaluation of the haptic handlebar. An experiment aimed to obtain objective and subjective data from the users driving experience is detailed. Then, the results are discussed.
- Chapter 5 is devoted to the adaptation of the haptic interface to a cane handle. The implementation of the device and an experiment to evaluate its use in rehabilitation are presented. The results of the latter are commented.
- Lastly, Chapter 6 summarizes the conclusions of the thesis and provides the ongoing work and future prospects.

Four appendixes have been included in the manuscript to provide complementary information. Appendix A gathers the data extracted from the experiments that were not included in the main body of the document. Appendix B lists the scientific contributions which have resulted from this work. Appendix C presents the analysis, through simulations, of the haptic handlebar effect on the system performance. Finally, Appendix D includes a discussion about a related proposal in which the authors suggest a control quite similar to that developed in this thesis.

Table of contents

List of figures	xv
List of tables	xxiii
Acronyms and clarifications	xxv
1 Introduction	1
1.1 Background	1
1.1.1 Wheelchair as mobility device	3
1.1.2 The caregiver	6
1.1.3 Wheelchair driving options aimed at caregivers	7
1.2 Haptic interface for wheelchair attendants	9
1.2.1 Tactile sensors	10
1.2.1.1 Capacitive tactile sensors	11
1.2.1.2 Piezoelectric tactile sensors	11
1.2.1.3 Inductive tactile sensors	12
1.2.1.4 Optical tactile sensors	12
1.2.1.5 Strain gauges	12
1.2.1.6 Piezoresistive tactile sensors	12
1.3 Haptic interface for other assistive systems	13
1.4 Framework of the thesis	15
1.4.1 Research group	15
1.4.2 Research projects	16
2 Haptic handlebar implementation	17
2.1 System architecture	18
2.2 Tactile handlebar	19
2.3 Control electronics	25
2.3.1 Joystick emulation	27



2.4	Preliminary analysis	30
2.4.1	Testing algorithm	32
2.4.1.1	Acceleration/deceleration processing	33
2.4.1.2	Turn processing	36
2.4.1.3	Linear speed correction	37
2.4.2	Preliminary results	37
3	Haptic-based driving control	41
3.1	Haptic-based movement control based on force/torque analysis	42
3.1.1	Experimental setup	43
3.1.2	Experiment and results (E1)	44
3.1.2.1	Force and torque analysis	45
3.1.2.2	Proposed control variables	48
3.2	Study of grip force effect	58
3.2.1	Tactels response characterization	58
3.2.2	Grip force impact on the coupling between the parameters extracted from the force sensor and those captured by the tactile handlebar . .	61
3.2.3	Grip force impact on <i>CoMs</i> excursion (E2)	62
3.2.3.1	Correction of <i>GF</i> effect on <i>CoMs</i> excursion	73
3.3	Study of the effect of the arrangement of the tactile array (E3)	77
3.4	Study of the handlebar grasp (E4)	82
3.4.1	Grip stabilization	85
3.4.2	Influence of attendant's height	87
3.4.3	<i>CoM</i> evolution during the grasp onset	91
3.5	Vibro-haptic feedback to prevent overexertion	97
3.6	Processing of control parameters based on <i>CoM</i>	102
4	Haptic handlebar evaluation	109
4.1	Haptic handlebar and attendant joystick comparison (E5)	110
4.1.1	Assessment of driving performance (E5.1)	110
4.1.1.1	Experimental setup	110
4.1.1.2	Protocol and methods	111
4.1.1.3	Results	115
4.1.2	Gathering of participants perception (E5.2)	120
4.1.2.1	Form questions	121
4.1.2.2	Form responses	124
4.2	Discussion	128

5	Haptic interface in another assistive systems	131
5.1	Instrumented cane (E6)	132
5.1.1	Tactile cane handle	132
5.1.2	Experimental setup	134
5.1.3	Protocol and methods	136
5.1.4	Results	137
5.2	Discussion	138
6	Conclusions and future work	143
6.1	Conclusions	143
6.2	Ongoing and future work	146
	References	151
	Appendix A Extension of experiments results	165
	Appendix B Scientific contributions	181
B.1	Journals	181
B.2	Conferences	181
B.3	Patent	182
	Appendix C Dynamic system modeling and simulations	183
C.1	Modeling of a powered wheelchair as a differential wheeled robot	183
C.1.1	Powered wheelchair kinematics	183
C.1.2	Powered wheelchair dynamics	186
C.2	Simulations	187
	Appendix D Discussion about a related proposal	191
	Appendix Summary of the thesis in Spanish	195



UNIVERSIDAD
DE MÁLAGA

List of figures

1.1	Predicted population pyramid for Western Europe in 2030 [4].	2
1.2	Manual (left) and powered wheelchair (right).	4
1.3	Senior couple in which the wife has the role of wheelchair attendant.	7
1.4	Attendant joystick mounted on a wheelchair (left). Add-on to assist electrically a MW (right).	8
2.1	System operation scheme.	18
2.2	4x4 mesh with tactels arranged individually (left) and in form of columns and rows (right).	19
2.3	Resistance/Force dependance for the FSR® 400 series (extracted from [5]).	20
2.4	FSR® 402 sensor structure.	21
2.5	GF/diameter dependance when grasping a circular handle (left). Force components on the handle (right). (Both extracted from [6]).	22
2.6	Matrix schematic of the first handlebar prototype.	22
2.7	Tactile sensors matrix prior to embrace the PVC bar (left). Resulting implementation (right).	23
2.8	Matrix schematic of the second prototype (left). Handlebar implementation (right).	24
2.9	Second prototype mounted on a commercial PW.	24
2.10	Conditioning and control electronics schematic.	26
2.11	Conditioning and control electronics implementation.	27
2.12	PW speeds according to the control voltajes V_{linear} and $V_{angular}$ (previously named V_{WHITE} and V_{YELLOW} , respectively).	29
2.13	PW movement is a composition of linear and angular speeds.	30
2.14	Tactile image (right) and its center of mass (left) in one of the handles of the first prototype.	30



2.15	Displacement of the $CoMs$ under different maneuvers registered with the first prototype: (a) forward movement, (b) backward movement, (c) turn to the right and (d) turn to the left.	31
2.16	CoM shift over the tactels group in the second prototype.	32
2.17	Spatial parameters used by the testing algorithm.	33
2.18	Acceleration (left) and deceleration (right) patterns.	33
2.19	Left turns patterns.	34
2.20	Right turns patterns.	34
2.21	Graphical representation of the parameters Δ_L (left) and Δ_R (right).	36
2.22	V_{linear} limit modulation according to $V_{angular}$	37
2.23	Preliminary test path.	38
2.24	Participant following the path in the preliminary test.	38
2.25	Participant driving on a ramp with the handlebar mounted on a PW.	39
3.1	Experimental setup scheme including a F/T sensor.	44
3.2	Path of experiment E1.	45
3.3	Experimental setup of E1.	46
3.4	Location of F_y , F_z , T_z and T_x	46
3.5	Angle formed by the arms of shorter (left) and taller (right) attendants when grasping the handlebar.	47
3.6	F_y and F_z at the moment in which the handlebar is grasped.	47
3.7	Typical parameters of the ellipse that describes the object pressing on the tactels in manipulation tasks, in this case, a bottle opener (based on the Figure presented in [7]).	49
3.8	Experiment results for participants P1-P5: coupling between the couples $\langle SUB_{CoM}, T_z \rangle$ (left column) and $\langle SUM_{CoM}, F_y \rangle$ (right column) with the corresponding first order linear functions superimposed.	54
3.9	Experiment results for participants P6-P10: coupling between the couples $\langle SUB_{CoM}, T_z \rangle$ (left column) and $\langle SUM_{CoM}, F_y \rangle$ (right column) with the corresponding first order linear functions superimposed.	55
3.10	SUM_{CoM} versus F_y for P7. The red line is computed from the data of P7 by linear regression. The green dashed line, which has a lower slope, fits better with the data captured during pulling maneuvers.	56
3.11	T_z and F_y from the F/T sensor (first and third plot). SUB_{CoM} and SUM_{CoM} (second plot and fourth plot) obtained from processing of the pressure values.	56

3.12	From top to bottom: T_z , CoM_L , CoM_R , SUM_{CoM} and F_y . During the data acquisition the chair was moving ahead and, afterwards, a right and a left turns were introduced.	57
3.13	Tactile handlebar in the characterization platform.	59
3.14	Vertical axis: force captured by the ATI F/T Nano17. Horizontal axis: digitized pressure from the left top handlebar tactel. In red and blue sensors output for upward and downward force, respectively. In yellow the mean between the previous curves. The dashed line represents the linear approximation of this mean. According to the sensor reference, F_z decreases when pressing so the slope of the curve would be negative; this way, in order to facilitate the visualization, what is showed is the absolute value.	60
3.15	GF 's effect on the couplings between $\langle SUM_{CoM}, F_y \rangle$ and $\langle SUB_{CoM}, T_z \rangle$ (1 st order functions superimposed).	62
3.16	Experimental setup scheme of E2. The handlebar is fixed to a laboratory table.	63
3.17	During the 1 st sequence P/P maneuvers are exerted (top). In the 2 nd sequence, turns are performed (bottom).	64
3.18	Participants P1-P3: CoM_L and CoM_R versus F_y (upper graphs) during P/P maneuvers (1 st sequence). Linear approximations (lower graphs). The	65
3.19	Participants P4-P6: CoM_L and CoM_R versus F_y (upper graphs) during push/pull maneuvers (1 st sequence). Linear approximations (lower graphs).	66
3.20	Participant P7: CoM_L and CoM_R versus F_y (upper graphs) during push/pull maneuvers (1 st sequence). Linear approximations (lower graphs).	67
3.21	Participants P1-P3: CoM_L and CoM_R versus T_z (upper graphs) during turn maneuvers (2 nd sequence). Linear approximations (lower graphs). The	68
3.22	Participants P4-P6: CoM_L and CoM_R versus T_z (upper graphs) during turn maneuvers (2 nd sequence). Linear approximations (lower graphs).	69
3.23	Participant P7: CoM_L and CoM_R versus versus T_z (upper graphs) during turn maneuvers (2 nd sequence). Linear approximations (lower graphs).	70
3.24	From top to bottom: T_z and GF_{HB} during the performance of the sequence of turns of E2 by one average participant for "strong", "normal" and "weak" grip.	71
3.25	Output of the tactels of the left (in blue) and right (in red) handles during the "normal" grip exercise plotted in Figure 3.24.	72
3.26	1 st order approximations for the tests included in the category G_{T3} and mean of these functions (thicker line in black) for the left and the right handle.	74
3.27	Gripping force-dependent gain functions for SUM_{CoM} (left) and SUB_{CoM} (right).	76

3.28	Tactels arrangements for the calculation of the <i>CoM</i> of the tests from the experiment E3.	78
3.29	Percentage of times that each tactel arrangement led to the maximum excursion (left chart - deeper blue for left handle, right chart - deeper orange for right handle). Percentage of times that each tactel arrangement led to the second largest excursion (left chart - lighter blue for left handle, right chart - lighter orange for right handle). All the test carried out with a handlebar height of h_1 were included.	79
3.30	Percentage of times that each tactel arrangement led to the maximum excursion (left chart - deeper blue for left handle, right chart - deeper orange for right handle). Percentage of times that each tactel arrangement led to the second largest excursion (left chart - lighter blue for left handle, right chart - lighter orange for right handle). Only the test carried out during the sequence of P/P maneuvers were included (height= h_1).	79
3.31	Percentage of times that each tactel arrangement led to the maximum excursion (left chart - deeper blue for left handle, right chart - deeper orange for right handle). Percentage of times that each tactel arrangement led to the second largest excursion (left chart - lighter blue for left handle, right chart - lighter orange for right handle). Only the test carried out during the sequence of turns maneuvers were included (height= h_1).	80
3.32	Percentage of times that each tactel arrangement led to the maximum excursion (left chart - deeper blue for left handle, right chart - deeper yellow for right handle). Percentage of times that each tactel arrangement led to the second largest excursion (left chart - lighter blue for left handle, right chart - lighter yellow for right handle). All the test carried out with a handlebar height of h_2 were included.	80
3.33	Percentage of times that each tactel arrangement led to the maximum excursion (left chart - deeper blue for left handle, right chart - deeper yellow for right handle). Percentage of times that each tactel arrangement led to the second largest excursion (left chart - lighter blue for left handle, right chart - lighter yellow for right handle). Only the test carried out during the sequence of P/P maneuvers were included (height= h_2).	80

3.34	Percentage of times that each tactel arrangement led to the maximum excursion (left chart - deeper blue for left handle, right chart - deeper yellow for right handle). Percentage of times that each tactel arrangement led to the second largest excursion (left chart - lighter blue for left handle, right chart - lighter yellow for right handle). Only the test carried out during the sequence of turns maneuvers were included (height= h_2).	81
3.35	Area that produces biggest CoM excursions when selected as origin of the tactile array (dashed line, left). Arrangement chosen as new tactel configuration by default (right).	83
3.36	Scheme of experimental setup of the E4.	85
3.37	Visual example of the parameter Δ_{CoM}	86
3.38	Link between the centers of mass with stabilized grip and the attendants' height. Corresponding 1 st order functions superimposed.	87
3.39	Tendency of CoM_r evolution as the height of the attendant changes (left). Grips from a taller (top right) and a shorter user (bottom right).	88
3.40	Handle grip with an angle between the forearm and the closed hand that is almost zero (left). Handle grips for which the angle is significant in both directions (center and right).	89
3.41	Gripping force versus height from participants of E4.	91
3.42	Twelve examples, extracted from the data of E4, of the evolution of CoM_L (left) and CoM_R (right) when the handlebar is just grasped. The parameters are normalized to be expressed in tactels coordinates.	93
3.43	Hand surface in contact with the handles when they are grasped (lighter area in left). Six people grasping the left handle in rest condition (right). The photos have been taken from the rear, in a point between the handlebar and the person.	94
3.44	Process of the handlebar grasp (ordered from top to bottom). The lighter area in the open hand represents the contact with the handle in each step ([1]-[6]).	95
3.45	CoM (top) and GF (bottom) from a test in which there is a rebound.	96
3.46	Evolution of the pairs CoM_L and GF_L (left side, top and bottom respectively) and CoM_R and GF_R (right side, top and bottom respectively) during a performance of E4.	97
3.47	Twelve examples, extracted from the data of E4, of the evolution of CoM_L (left) and CoM_R (right) when the handlebar is released. The parameters are normalized to be expressed in number of tactels.	98

3.48	Evolution of the pairs CoM_L and GF_L (left side, top and bottom) and CoM_R and GF_R (right side, top and bottom) during the driving of the PW by the participant of E4 whose GF was the highest. The dashed line represents the mean GF	100
3.49	Vibration motor and piece where it is placed (left). The whole set inserted in the left handle end (right).	101
3.50	Schematic of the motor activation circuit.	101
3.51	Processing of SUB_{CoM} to estimate turns.	102
3.52	Processing of SUM_{CoM} to estimate forward and backward motion.	103
3.53	Static and dynamic dead bands (left and right).	104
3.54	Ideal scenarios in which the PW is stopped, turning around itself and moving straight (from left to right).	105
3.55	Real scenarios with the PW stopped, performing a turn around the PW vertical axis and performing a pushing maneuver (from left to right).	105
3.56	Linear speed limitation based on angular speed.	106
4.1	Path of experiment E5.	111
4.2	Experimental setup of E5.	112
4.3	Laser pointer and cam attached to the PW seat, from below (left). The same structure from above (right). The laser circular reflection is visible on the tape.	112
4.4	Corridor and laboratory used in the first part of the experiment E5. Continuous and dashed lines refer to the PW going forward and backward, respectively.	114
4.5	Example of the color-based segmentation in the video processing of experiment E5.1.	114
4.6	Graphical representation of the tape borders detection for the first 80 frames of one test (top). The dashed line refers to the laser light position. Distance from the reference laser light to the tape (bottom).	115
4.7	Trajectory error for participants P1-P5 in experiment E5.1 using the attendant joystick (left, in blue) and the haptic handlebar (right, in red).	116
4.8	Trajectory error for participants P6-P10 in experiment E5.1 using the attendant joystick (left, in blue) and the haptic handlebar (right, in red).	117
4.9	From top to bottom: mean trajectory error, maximum trajectory error, test duration, product of mean trajectory error by test duration. The results for the attendant joystick are showed in blue and those for the haptic handlebar in red.	118

4.10	Number of collisions during driving in the second location with the attendant joystick (in blue) and with the haptic handlebar (in red) (* represents zero collisions).	120
4.11	Participants' opinion about different aspects of the driving with both devices: ease of use (top-left), comfort (top-right), training (center-left), usefulness (center-right), safety (bottom-left) and fatigue (bottom-right).	125
4.12	Participants' previous experience with a joystick, an assistive handlebar and wheelchair attendant role (left). Participant's ages (right).	127
4.13	Evolution of SUB_{CoM} , the dashed line represents the absence of turns (top). Evolution of SUM_{CoM} , the dashed line represents a constant forward speed (bottom).	130
5.1	Tactile cane handle schematic (left). Handle implementation (right).	133
5.2	Cane handle conditioning electronics scheme.	134
5.3	Cane handle conditioning electronics board.	135
5.4	Experimental setup of E6.	135
5.5	Pressure map obtained from the tactile handle.	136
5.6	Experiment results for participants P1-P5: coupling between the couples $\langle \bar{P}_U, F_z \rangle$ (left column) and $\langle CoM_U, Pitch \rangle$ (right column) with the corresponding first order linear functions superimposed.	139
5.7	Experiment results for participants P6-P10: coupling between the couples $\langle \bar{P}_U, F_z \rangle$ (left column) and $\langle CoM_U, Pitch \rangle$ (right column) with the corresponding first order linear functions superimposed.	140
5.8	Test of P8: on the left, mean F_z measured by the ATI Mini45 sensor (red) and estimation using the parameter \bar{P}_U (blue dashed line). On the right, mean pitch angle trajectory (red) captured by the IMU and its estimation based on the CoM_U (blue dashed line).	140
6.1	With the current prototype, a rotation of 45° in the coordinates of the elements takes place between one tactels arrangement and the next.	147
6.2	Tactile handle equipping 16 tactels. At the bottom, the electrodes are covered with a piezoresistive sheet.	147
6.3	Tactile cane handle. On the right, the tactels electrodes are exposed. On the left, they have been covered with piezoresistive sheets for testing purposes.	149
C.1	Kinematics of a differential wheeled vehicle.	184
C.2	Experimental setup for the dynamic characterization of the haptic handlebar.	188

C.3	Simulation of a slalom path (dashed line) tracking considering the three following situations: 1) Only the PW model (in orange), 2) the PW and the driver model (in yellow) and 3) the PW, the driver and the haptic handlebar model (in purple).	189
C.4	Trajectory errors when the driver model is included (in blue) and when the handlebar model is also added (in orange).	189
D.1	Experimental setup of the proposal in [8] (Figure extracted from the article).	191
D.2	Results of the replication of the test performed in [8]: signal captured by the F/T sensor (top), parameter proposed in this thesis (center) and parameter proposed in [8] (bottom).	192
D.3	Extract from a test of E1 for an average participant: T_z (top), SUB_{CoM} (center) and SUB_{AO} (bottom).	193

List of tables

2.1	REM24SD - Joystick interface signals.	28
3.1	Rule of thumb for correlation interpretation.	52
3.2	Gradients of the mean of the linear functions for the tests in the categories associated with push/pull maneuvers (second column for CoM_L and third for CoM_R). Gradient of SUM_{CoM} computed from the latter (fourth column). Accumulated $m_{SUM_{CoM}}$ decline (fifth row).	75
3.3	Gradients of the mean of the linear functions for the tests in the categories associated with turns maneuvers (second column for CoM_L and third for CoM_R). Gradient of SUB_{CoM} computed from the latter (fourth column). Accumulated $m_{SUB_{CoM}}$ decline (fifth row).	75
3.4	Example of different arrangements of the tactile array. From one to the next, the beginning of the array is rotated one position. y refers to the variable of Equation 2.5.	78
3.5	Variability of CoM in rest condition: statistical measures.	86
3.6	CoM_s of reference from the participants of E4: statistical measures.	88
3.7	Difference in the parameter CoM_r in two consecutive grips of the same participant: statistical measures.	89
3.8	Gripping force exerted for the participants of E4, once the grip is steady: statistical measures.	90
4.1	Pe coefficient, $Median(\bar{x})$ and U – value of Mann-Whitney Test (one-tailed, with $U_{critical_{p<0.05}} = 27$) for the Likert scale results of the questionnaire.	126
A.1	Pearson (r) and Spearman’s rank-order (ρ) correlation coefficients for the pair of variables formed by the center of mass of each hand (CoM_L/CoM_R) and F_y during the 1 st sequence of maneuvers (push/pull) of the experiment E2. They are classified by the type grip that the participant intended to perform (‘weak’, ‘normal’ and ‘strong’).	166



A.2	Pearson (r) and Spearman's rank-order (ρ) correlation coefficients for the pair of variables formed by the center of mass of each hand (CoM_L/CoM_R) and T_z during the 2 nd sequence of maneuvers (turns) of the experiment E2. They are classified by the type grip that the participant intended to perform ('weak', 'normal' and 'strong').	167
A.3	Participants P1-P6: arrangements of tactels for which the CoM excursion was maximum (Arr_{1^aExc}) and those for which it was the second largest (Arr_{2^aExc}). In parentheses, the normalized value of the calculated excursion. PP1 and PP2 refer to the two tests of P/P maneuvers whereas T1 and T2 are related to the two tests in which turns were performed. The height of the handlebar for these data was h_1	168
A.4	Participants P7-P12: arrangements of tactels for which the CoM excursion was maximum (Arr_{1^aExc}) and those for which it was the second largest (Arr_{2^aExc}). In parentheses, the normalized value of the calculated excursion. PP1 and PP2 refer to the two tests of P/P maneuvers whereas T1 and T2 are related to the two tests in which turns were performed. The height of the handlebar for these data was h_1	169
A.5	Participants P1-P6: arrangements of tactels for which the CoM excursion was maximum (Arr_{1^aExc}) and those for which it was the second largest (Arr_{2^aExc}). In parentheses, the normalized value of the calculated excursion. PP1 and PP2 refer to the two tests of P/P maneuvers whereas T1 and T2 are related to the two tests in which turns were performed. The height of the handlebar for these data was h_2	170
A.6	Participants P7-P12: arrangements of tactels for which the CoM excursion was maximum (Arr_{1^aExc}) and those for which it was the second largest (Arr_{2^aExc}). In parentheses, the normalized value of the calculated excursion. PP1 and PP2 refer to the two tests of P/P maneuvers whereas T1 and T2 are related to the two tests in which turns were performed. The height of the handlebar for these data was h_2	171
A.7	Parameters from the tests of the experiment E5.1 for the attendant joystick driving. From left to right: mean and maximum trajectory errors, test duration, mean trajectory error and test duration product. The last row gathers the mean of all the latter parameters considering all the tests.	172
A.8	Same parameters of those explained for Table A.7, this time for the haptic handlebar.	172

Acronyms and clarifications

In order of appearance:

SCI: Spinal Cord Injury

AT: Assistive Technology

MW: Manual Wheelchair

PW: Powered Wheelchair

FSR: Force Sensing Resistor

ADC: Analog-to-Digital Converter

GF: Gripping Force

PCB: Printed Circuit Board

PVC: Polyvinyl Chloride

DAC: Digital-to-Analog Converter

CoM: Center of Mass

P/P: Pushing and Pulling (maneuvers)

F/T: Force and Torque

E_i: Experiment (sorted by appearance in the document, with *i* from 1 to 6)

P_j: Experiment Participant ('*j*' is used to distinguish between different volunteers that participated)

AO: Aggregate Output

SUM_{CoM}: Sum of left and right handle CoMs

SUB_{CoM}: Subtraction of left and right handle CoMs

DOU: Digital Output Unit

AD: Analog-to-Digital

IMU: Inertial Measurement Unit

AHRS: Attitude and Heading Reference System

Subscript *L*: The parameter with which it appears is calculated for the left handle tactile cover

Subscript *R*: The parameter with which it appears is calculated for the right handle tactile

cover

Subscript *HB*: The parameter with which it appears is calculated considering the whole handlebar tactile cover. It may refer also to the haptic handlebar driving, when it is compared with the attendant joystick.

Subscript *r*: The parameter with which it appears is computed in *rest condition*

Subscript *measured*: The parameter with which it appears is computed from the raw captured sample

Subscript *AJ*: The parameter with which it appears is computed for the attendant joystick driving

Subscript *U*: The parameter with which it appears is computed for the upper side of the cane handle

Plurals: parameters in plural are indicated by adding the letter 's' at the end of the acronym. For example, *CoMs* refers to the pair formed by *CoM_L* and *CoM_R*.

1

Introduction

"Somewhere, something incredible is waiting to be known."

— Carl Sagan

1.1 Background

Developed societies are getting old, so that facing the increasing aging of their inhabitants must be a crucial goal. In the coming decades, the predicted population pyramid for these countries will lose their triangular shape [4, 9]. From 2000 until 2050, the world's population aged 60 and over will more than triple from 600 million to 2 billion [10]. The direct causes behind the lack of young people and the increment of the elderly are a fall in the birth rates and the rising of life expectancy [11].

Aging well requires health and functional capacity in the daily life activity [12]. Statistics show that one in six people suffers some kind of disability in the European Union (EU).

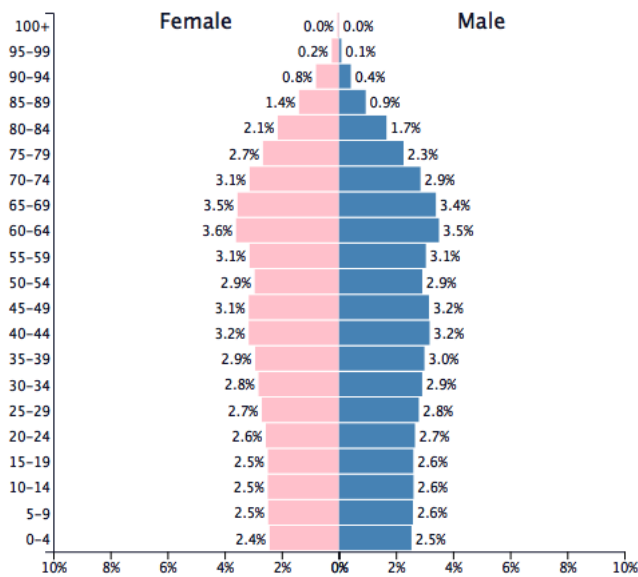


Fig. 1.1 Predicted population pyramid for Western Europe in 2030 [4].

Approximately, a third of population over 75 have disabilities that restrict them to some extent and more than 20% are considerably restricted [13]. Inside EU-27¹, the 52.9% of disabled people reported that their incapacity causes them mobility difficulties [14]. This is one of the main barriers to participation and there may be a number of reasons behind it. A stroke is currently the leading cause of disability in developed countries [15]. Spinal cord injury (SCI) has an annual incidence of 22 people per million inhabitants in these societies, which means that more than 130.000 people a year start a life bound to a wheelchair for 40 years or more [16]. Cerebral palsy is also origin of mobility incapacity in people from their childhood, with an estimation of 650.000 European families with a member suffering this disease [17]. Apart from these pathologies, mobility decline is one of the major issues among the elderly; it is strongly linked to aging itself [18, 19]. The oldest old, who are those over 85, represent a particular challenge as they are the fastest growing sector in developed populations and have high rates of physical and cognitive impairment [20].

In this context, assistive technology (AT) becomes a key piece in terms of quality life improvement. This concept comprises any item, piece of equipment, software program, or product system that is used to increase, maintain, or improve the functional capabilities of persons with disabilities [21]. It incorporates a wide range of devices from simple, low-cost devices to complex home monitoring systems that use electronic information and

¹Belgium, Denmark, France, Germany, Greece, Ireland, Italy, Luxembourg, Netherlands, Portugal, Spain, United Kingdom, Austria, Finland, Sweden, Cyprus, Czech Republic, Estonia, Hungary, Latvia, Lithuania, Malta, Poland, Slovakia, Slovenia, Bulgaria and Romania.

communication technology [20]. AT has been found to be especially helpful among elderly, as it allows them to develop the functional activities of daily living safely, increase their independence and autonomy, prevent comorbidities² and therefore improve the quality of life and social inclusion [22]. When users are able to walk, the more commonly used assistive tool to increase gait stability is the cane. A simple single point cane may reduce falls in people with imbalance. Other gait assisting devices are the walkers. Their main characteristics are structural simplicity, low cost and great rehabilitation potential [23]. In recent years, research has provided various examples of these two common assistive tools. The authors of [24–26] worked on robotic versions of a cane. In [27–30], advanced robotic walkers were presented. However, as we have seen, there is a numerous group of people with limited walking ability that require other kind of mobility aid since the latter is not sufficient.

1.1.1 Wheelchair as mobility device

Wheelchairs are often used as an alternative for mobility when a person can not walk at all. In United States (USA), 3.7 million people were wheelchair users in 2010 [31]. This number reached approximately 5 million in Europe [32]. There are, basically, two types of wheelchairs (figure 1.2). The manual wheelchairs (MW) are normally propelled by the seated individual through the effort of his or her upper limbs. This means that the user has to be able to exert the necessary strength to propel the weight of the chair structure plus his or her own body. Although proper for people with arms and hands not affected by any impairment, MW are not a feasible option for many stroke and SCI survivors. They could be not suitable for the oldest old either. In such cases, powered wheelchairs (PW) become a valuable option. For the elderly, PW are reported as a means of extending the activity and participation [33]. In the USA, a study found that the 44% of people with SCI used an external-powered wheelchair [34]. Among the 35% of affected by SCI who have two chairs, a powered version is normally one of them [35]. They normally use it outdoors, where distances to cover are longer.

These wheelchairs have two motors that power the two main wheels independently to allow turning maneuvers, including sharp turns. They are usually driven with a hand-operated joystick located at the end of the armrest. Although a powered mobility is undoubtedly beneficial, there are people who may not be able to operate these devices by themselves. For example, persons with severe disabilities. Clinicians reported that 9-10% of patients find them extremely difficult or impossible to use in their daily life. Regarding maneuvering

²Presence of one or more additional diseases or disorders co-occurring with (that is, concomitant or concurrent with) a primary disease or disorder.



Fig. 1.2 Manual (left) and powered wheelchair (right).

tasks, a 40% find it impracticable. 85% of clinicians see every year patients not able to use a PW since they lack the necessary motor skills, strength or visual sharpness. Up to 9% of individuals require the assistance of another person [36]. Driving a PW is not only a problematic issue for people with acute disabilities but also experienced users report having difficulties performing basic tasks that involve controlling the joystick and maneuvering [37].

Researchers have contributed with many instruments aimed at helping people to drive wheelchairs. In [38], a steering device for quadriplegic patients is presented. Go and stop motion is controlled through electromyography signal and left and right cornering is based on the yaw angle of the user head. Experiments showed that the device was too slow executing certain maneuvers. An interface based on body motion is shown in [39]. A pressure sensor located at the chair back captures the changes of the center of weight produced by the natural body motion when the user wants the chair to move. Besides, a mechanism to assist step climbing when the approach is oblique is proposed. For this purpose, plates were added to the front wheels to increment virtually the radius and the wheel in contact with the step is locked. In [40], the authors make an attempt to improve the straight and circular road driving of a PW by determining the suitable assisted torque for the right and left torque using a fuzzy algorithm. For those patients with limited wrist motion due to upper limbs impairments, an isometric joystick has been developed in [41]. Unlike the conventional version, this is rigid and does not move. The experiments revealed that the participants exerted excessive force using it, probably because its rigid stick does not provide positional feedback.

This kind of joystick showed worse performance than the position one as a mean of control among cerebral palsy patients in this evaluation [42]. The authors of [43] have implemented a wheelchair control based on gestures that the person makes with his or her hand. Each typical chair motion is codified by a gesture that will be identified by an IR sensor. This way, the engines are activated according to the detected command. Other examples like [44] and [45] incorporate a joystick equipped with force feedback in their proposal. The former uses sixteen sensors to detect the nearest obstacles and a Microsoft Sidewinder Force Feedback joystick 2 that provides a feedback modulated for the obstacles recognition to operate the chair. The authors of the latter use a laser rangefinder for the same purpose. They translate the distance to obstacles into force feedback using a commercial device called 3D Haptic PHANTOM Omni that also makes the function of joystick. The same idea has been exploited in [46], where the novelty is that the obstructions are detected by processing the images captured by a camera module. Alternatively, the joystick force feedback of [47] does not try to help the user correcting the trajectory according to the obstacles but it does based on the floor surface orientation. This way, it helps to rectify the wheelchair tendency to flow to the lower direction when going up a slope. In the work showed in [48], authors developed an interface with a touch panel display. The display shows an overhead image from a vision sensor of the chair and its surroundings so that the user can move anywhere by touching directly the image. The prototype presented in [49] allows control a wheelchair by cervical movements. The required signals are extracted from two accelerometers, one in a helmet that the user wears and the other in the chair base. Authors of [50] propose to control the chair by voice commands. Besides, the speed depends on subtle variations of the fundamental frequency of the user's humming.

These are only some examples of the bibliography. Research has been particularly prolific in this field of AT for the last 30 years. However, almost none of the prototypes reach the final user and one of the main reasons is the implementation cost [51]. Moreover, many of them are not suitable for severe disabilities that involved cognitive issues as dementia, common condition among the oldest old, or acute cerebral palsy. Alzheimer and Parkinson patients or those visually impaired are excluded as well. In short, as seen there is a group of wheelchair users for which it turns out impossible to operate it with the current means. In such cases, the assistance of other person that helps them in everyday life with the chair handling is unavoidable. This figure is normally known as caregiver.

1.1.2 The caregiver

According to the Cambridge Dictionary a caregiver is "someone who takes care of a person who is young, old, or sick". Other words referring to the same person can be "carer", "assistant" or "attendant". A common image of this figure is the physician, the nurse or the social worker. However, the term does not describes only healthcare providers. Increasingly, the role of the caregiver role is assumed by family members or friends of the person suffering from chronic illness or disability [52]. Caring is a hard task that, often, has a negative impact on the assisting person. The study in [53] is centered on informal caregivers and found that the 81% have sustained injuries during caring. They suffer also psychological health problems such as fatigue, anxiety and depression. The median age of them was 70.

If we focus on the caregivers whose main responsibility is pushing a wheelchair the situation persists. The majority of these carers reported a broad range of health problems [54]. Most of them are over 50 years and present age-related issues that suppose obstacles to care giving [55]. Musculoskeletal problems, including back and shoulder injuries, were common among the participants of this study [54]. Overall they were spouses and the 75% provided full-time care. The cited work has identified an aging population of carers in which the 83% have at least one problem related to heart, balance, breathing or bodily pain. Other complicated point is going up or down a ramp. Apart from the greater physical effort, coping with this activity may cause psychological anxiety to carers [56]. In view of the above, AT can be a determining support. Its use by disabled people has shown to improve the carers well being as it alleviates the caregiving tasks [57]. The attendants who support users of PW are less likely to suffer physical pain and health problems in comparison with those who propel a MW [54]. Moreover, some National Health System wheelchair and seating services specifies that there are exceptional circumstances that makes a MW impossible to push by a carer [58]. This happens when:

- The seated person weight is over 115 kg and the weight difference between the attendant and the patient plus the chair is greater than 38 Kg.
- A MW for a particular user would require a configuration difficult to propel (extended wheelbase, forwards position of the gravity center, etc.).
- The patient's MW would be inherently heavy to propel because he or she would need medical equipment essential to life, heavy seating systems, etc.

As we have seen, there are situations where the use of a PW is almost mandatory even when an assistant gives support. Nevertheless, despite being an important improvement



Fig. 1.3 Senior couple in which the wife has the role of wheelchair attendant.

compared to MW, it is well worth remembering that this kind of chairs also present a number of problems related, generally, to its handling (see Section 1.1.1)

1.1.3 Wheelchair driving options aimed at caregivers

There are various proposals that aim to provide help when the caregiving labor involves pushing a wheelchair. On the one hand, the most usual commercial solution for PW is the attendant joystick [59] (figure 1.4 left). It is placed at the rear part of the chair to be operated by the caregiver. The idea is exactly the same of the user joystick located on the armrest and, in fact, the control can be dual, that is to say, carried out by the two joysticks. The main weakness of this option is that it has the negative implications already seen. Basic maneuvering can be difficult to perform, all the more considering that the carer is frequently elderly. Besides, works as [60], which involved the figure of the user in the design of smart mobility aid, determined that a joystick may cause oscillatory motion when the person walks using it.

On the other hand, a relatively new offer is the attendant controlled PW. It is a PW specifically designed to be driven by an attendant [61]. There is no joystick for the occupant and the one for the assistant is replaced by a handle that makes the driving more intuitive. The device works as follows: when the carer pushes the wheelchair through the handle, this presses an internal switch that activates an engine that propels onwards the chair. In this way, it can be quite useful when going up hills or ramps. Nonetheless, it does not suffice to steer



Fig. 1.4 Attendant joystick mounted on a wheelchair (left). Add-on to assist electrically a MW (right).

the wheelchair as turn maneuvers are not assisted and they fall entirely on the carer. Another inconvenient point is that if the user wants to go backwards, the chair must be stopped and he or she has to switch the operation mode through buttons, which makes the driving more contrived. A similar proposal available on the market is the electrically assisted MW [62]. This solution consists in adding an accessory to a MW that assists its driving propelling it in the same way as the previous system. The major components are the handle and a engine attached to a wheel (figure 1.4 right). As can be inferred, it has the same advantages and drawbacks of the former option.

Although not so extensive as that focused on the occupant, research targeted at the assistants has given rise to some approaches. The one reported in [63] presents an assisting controller based on the force-velocity relationship. It generates an assisting force when the attendant's propelling force exceeds a threshold. However, it does not contemplate steering and only simulations results are presented, so no hardware is proposed or evaluated to measure the input force. Kakimoto et al. also propose a prototype of a power-assisted attendant propelled wheelchair that detects the caregiver propulsion force through a force sensor placed on the shaft of the handling bar [64]. Although the impulsion force is reduced by 50 to 60%, the behavior is unstable under certain conditions. Again, it was not intended to help in steering but in climbing ramps. In the same vein, authors of [65] introduce a haptic handlebar to assist a shopping trolley driving. Although the weight to propel does not come from a wheelchair, the idea is the same: assisting the push of a heavy load on wheels. The device uses strain gauges to measure forces. The tests performed for its evaluation did not

provide good results since most participants did not find the trolley easy to move [66]. A power assist system for omni-directional transport of wheelchairs is exposed in [67]. The input force of the attendant is measured by a force sensor attached to the handle of the chair. The effectiveness of the proposal was tested, although only in the laboratory and not in real situations. Another interesting device is presented in [68]. It is a combination of wheelchair and walker, so it can be useful to both the occupant and an elderly caregiver that needs walking support. The admittance based controller the authors used has proven to have a good performance controlling the pushing force, which is first acquired from the carer through a force sensor placed between the handle and the robot structure. Murakami et al. [69] propose a sensorless power-assist control that detect the caregiver's input, classified into straight or cornering mode, according to a reactive acceleration estimation observer. This feature is based on the translational velocity and the chair direction angle. The same author also participated in other version of the system which incorporated the function of step passage [70]. Both proposals would be less robust than the equivalent that uses force sensors since it seemed to be based on positive feedback control loop. In the work presented in [71], the authors combine the user input, acquired by two force sensors, with an estimation of the environment disturbance detected using a reaction force estimation observer. The result is an adaptive force control that allows an improved operability and ride quality.

1.2 Haptic interface for wheelchair attendants

In the preceding section, many driving options centered on caregivers were presented. However, they all present some kind of inconvenience. On one side, the commercial proposals have principally two drawbacks. They consist in either awkward and difficult to operate instruments or systems that do not provide complete assistance to the caregiver. On the other side, although the exposed research examples have had more or less success coping with these problems, they are not a valid and realistic alternative. As seen in Section 1.1.1, unfortunately, the implementation cost prevents them from reaching the market and most of them will never make it out of the laboratory. One of the main reasons behind this has to do with the way in which the user interacts with the system. Typically, the user intention is identified by measuring the force that the person exerts and this is usually made using force sensors. This type of sensors can be very expensive. Considering the above, our approach must pursue the following goals:

1. It has to be easy to use and does not need much training. Usability is directly related to intuitiveness.

2. It must provide complete steering assistance. The system has to help the caregiver with the typical maneuvers carried out when driving a wheelchair.
3. It must be cost-effective. It supposes to avoid working on a project whose implementation cost is a known obstacle from the very beginning.

In order to achieve the first objective, the form chosen for the interface presented in this document is the **handlebar**. A handlebar is a familiar tool for most people. They are linked to everyone's life from the childhood since they are the key steering component of bicycles, motorbikes, supermarket or airport trolleys, etc. This way, normally, all of us know how to operate a vehicle through its handlebar. The idea is to take advantage of this common ability to design a device that can be used from the very first moment without the need for a complicated training. The second point will be pursued throughout the design of the system, as it will be seen in the next chapter. Finally, the cost-effectiveness of the proposal will be based on the choice of the proper technology. As it can be supposed, the interaction between the user and the device will be haptic. *Haptics* is a term not too well known to the public that comes from a Greek word that means "to come in contact with" [72]. Hence, this concept has to do with all that associated with the sense of touch and, as the Oxford Dictionary points out, "in particular relating to the perception and manipulation of objects using the sense of touch". Most of the bibliography examples reported in the Section 1.1.1 and 1.1.3 included a haptic interface since they increase the intuitiveness and ease the handling. Thus, the user of our system will use his or her hands to grasp the handlebar in the same manner as conventional one and he or she will exert forces according to his or her intentions. Inferring what the user wants to do requires measuring the stimuli on the handlebar. This is a key point since this task must be performed avoiding force sensors. A cheaper alternative to the latter are the **tactile sensors**.

1.2.1 Tactile sensors

Tactile sensors are often used not only in human-machine interaction, but also in autonomous or remotely controlled robots. In this case, they are arranged forming a tactile skin whose function is to equip the robot, normally its arms or hands, with tactile sensing [73]. The main robotic tasks involving these sensors are object manipulation, object exploration -features as texture, temperature or softness/hardness can be measured- and reaction tasks where the robot reacts to the stimuli applied at a contact point or area [74].

Tactile sensors are widely used in biomedical applications. They are a basic component in minimally invasive surgery, in which their function can range from tissue and tumors palpation to micro-tactile perception in intravascular neurosurgery [75–80]. They are also used in prostate cancer detection and biopsy samples analysis [81, 82]. Moreover, they are helpful to measure blood pressure [83] and to perform intelligent colonoscopes [84], laparoscopes [85] and endoscopes [86]. They contribute in the detection of cognitive failures while driving [87], in the treatment of children with autism [88] or to improve the body balance and thus to prevent pressure sores formation in patients with spinal cord injuries and falls in older and/or disabled adults [89].

A common way of classifying tactile sensors is according to their principle of transduction [73, 90]. Following this criterion, some of the the best-known are:

1.2.1.1 Capacitive tactile sensors

Capacitive tactile sensors are made up of two conductive plates with a dielectric material between them. They share the same operation principle as parallel plate capacitors, for which the capacitance is:

$$C = \frac{A\epsilon_0\epsilon_r}{d} \quad (1.1)$$

Where A is the overlapping area of the two plates, ϵ_0 is the vacuum permittivity, ϵ_r is the dielectric permittivity and d the distance between the plates. The most usual approach is based on the variation of d when they are pressed. Changes in this parameter makes the capacitance, C , vary and become a pressure-dependent variable. They are very sensitive and have a good frequency response, a high spatial resolution and a wide dynamic range. However, its conditioning electronics is complex since they are susceptible to noise, field interactions and parasitic capacitance.

1.2.1.2 Piezoelectric tactile sensors

Piezoelectric materials generate a voltage potential that depends on the applied pressure due to deformations in their crystal lattice. These sensors are built with certain ceramics, crystals and polymers with the latter characteristic. They are suitable for dynamic tactile sensing such as vibrations since they show a good high-frequency response but they are not capable of measuring static stimuli.

1.2.1.3 Inductive tactile sensors

They consist of two coils so that one of them (the primary) induces a magnetic field which is measured by the other (the secondary). The modulation of the mutual inductance between the coils, for instance modifying the length of an iron core, is translated into a modulation of the amplitude and phase of the voltage sensed in the secondary coil. This kind of sensors have a high dynamic range and are often robust. Nevertheless, they are bulky in size and therefore not suitable for mesh configurations. Besides, their repeatability is very poor due to their mechanical realization and the fact that coils do not return to the same position in consecutive readings.

1.2.1.4 Optical tactile sensors

These sensors measure the pressure through the change in light intensity. The transduction occurs when the pressure causes changes in the tactile medium modulating the transmission or reflectance intensity or the spectrum of the light. Their main benefit is immunity to electromagnetic interference commonly produced by electrical systems. Among their drawbacks we find low spatial resolution as they are bulky and rigid. In addition, the loss of light because of microbending and chirping leads to signal distortion.

1.2.1.5 Strain gauges

Strain gauges are used to measure force rather than to sense pressure or contact. Nevertheless, due to their popularity they have been included in this section. They are sensitive to mechanical strain and are normally attached to a substrate. The changes of the exerted force are measured through variations of the electrical resistance. Their main advantage is their low cost. Some of their weaknesses are that they are significantly affected by temperature changes, they have hysteresis and a non-linear response. Besides, they can not be retrieved after being overloaded. These were the sensors used in the haptic handlebar presented in [65] and, as mentioned in Section 1.1.3, the results were not good.

1.2.1.6 Piezoresistive tactile sensors

They usually consist of a piezoresistive material, that is to say, that one whose electrical resistance depends on the applied pressure and the contact location. They are an economic option since its construction is as simple as placing a piezoresistive film onto or between two

electrodes. They are easy to arrange in mesh configuration as well. The sensing material is often a conductive rubber, an elastomer or a conductive ink. Apart from the cost-effectiveness, they have a good sensitivity, low noise and require simple conditioning electronics. On the negative side, they have large hysteresis and a power consumption higher than other options.

This has been the option chosen for the proposal of this manuscript. On the one hand, it fulfills our requirement of using cost-effective sensors. Not only because of the sensors cost but also because the electronics is simple and, therefore, cheaper than for other alternatives. On the other hand, they have good features such as high sensitivity and readings relatively unaffected by noise. Regarding the first of the mentioned drawbacks, the processing will have to be realized in a way that hysteresis does not alter the proper functioning of the system. With respect to the other, the consumption will not be an obstacle; the sensors circuit power supply will come from the PW high-capacity batteries. Thus, it will be negligible compared to the power that the wheel engines need. The specific models of sensor used to cover the handles and, thus, implement the tactile skin in our device are the Force Sensing Resistor (FSR) 402 and 408®, by Interlink Electronics [91, 92], a mature and reliable product with proven good performance.

1.3 Haptic interface for other assistive systems

Although the device this thesis is centered on is a haptic handlebar to help caregivers involving wheelchairs operating, the presented ideas could be exploited by other assistive devices that suffer from the already commented implementation cost difficulty. Many of the research works cited in previous sections have an user interface based on force sensors so that if they were replaced by tactile sensors the chances in getting the market could improve. Two concrete examples of instruments whose interaction with the user have been often carried out with force sensors are robotic walkers and canes. Regarding the former, in [29], the authors have developed a walker that provides guidance for old people with cognitive impairment. The walker presented in [30], in addition to the gait assistance, has the ability of navigating autonomously to its owner without collision, what is useful among elderly people which sometimes forget the location of their assistive device or are not able to walk by themselves to the place where the walker is. The function of the walker shown in [93] is to help people work their remaining locomotion potentials when they have to undergo rehabilitation. In this vein, the walker in [94] intends to be useful for ataxia³ rehabilitation. The device introduced in [95] helps elderly people during the sit to stand transfer. Besides, assisting

³Lack of muscle coordination when a voluntary movement is attempted.

force is provided in case of instability. All these prototypes have one point in common: their handles or forearm support are equipped with force sensors.

The situation is not different if we look at canes. The authors of [26] work on an active haptic cane that can provide efficient gait training modes to chronic stroke patients. The intention is detected thanks to a tilt sensor placed in the handle and a force sensor located in the middle of the shaft. The cane robot developed by the authors of [96, 97] detects falls analyzing the center of pressure and improves the stability through real-time posture control. A force sensor has been included in the handle. The user interface is also based on force sensors in the canes presented in [98], [99] and [100]. The aim of the first two is to avoid falls whilst the third one, additionally, improves the assistance taking into consideration the proper usage of an ordinary cane using on-shoe sensors that the user wears. The omnidirectional-type cane robot shown in [101] is designed for aiding walking of elderly and handicapped people, so its functions include guiding, fall preventing and rehabilitation training. The user intention is inferred from the readings of a force sensor embedded in the handle, again. The reported experiment results are good. This publication is specially paradigmatic since the authors themselves recognize the problem and suggest a possible solution in the Conclusion section: “[...] the interface between the human and the robot is the multiaxis force sensor, which is expensive and fragile. To lower the cost and improve the system reliability, in the future, we would like to construct a low-cost sensing system comprising cheaper force sensors (e.g., force sensing resistors) [...]”

In this doctoral thesis, a first approximation to cope with this issue has been developed. The proposal consists in the design and implementation of a haptic cane handle based on tactile sensors, specifically FSR sensors. The idea is to have a tactile handle that can be attached to different types of canes (robotic active canes, monitoring canes, etc.) and provide information about the patient interaction during its use. The details of its implementation, the experiments and the results achieved will be addressed in Chapter 5.

In addition to benefiting walkers and canes interfaces, it goes without saying that the extension of the haptic handlebar could be direct in the case of common mobility devices such as supermarket trolleys, floor cleaning machines, gurneys, etc.

1.4 Framework of the thesis

1.4.1 Research group

This thesis has been developed within the research group "*Electronics for Instrumentation and Systems*" (EIS), of which the author is member. This group is formed by eight researchers and is mainly devoted to the field of the smart tactile sensors, with an special interest in their applications in assistance to disabled or elderly people. Generally speaking, four research lines can be described:

1. *Characterization and modeling*. It involves the research on tactile sensors based on polymers on flexible printed circuit boards or made with screen-printing. The key point of this technology is the cost-effectiveness. Sensors are characterized to know they performance in terms of linearity, hysteresis, drift, etc., information that is used in the design loop of new sensors. In addition, these results are useful to build models to simulate different approaches without the need of implementing the real sensor and, therefore, saving resources.
2. *Hardware*. The group has implemented conditioning electronics specialized in the acquisition of tactile sensors. Circuits based on a PSoC and a microcontroller has been designed. Moreover, a innovative hardware based on a FPGA that does not need external analog-to-digital converters has been proposed.
3. *Algorithms*. They are aimed at compensating the errors of linearity, hysteresis, drift and mismatching between the different tactile elements in a post-processing stage. Besides, this line is also focus on studying which information extracted from the sensor is relevant at the application level.
4. *Applications*. The main idea behind this line is to put the knowledge acquired through the other research lines into practice with specific applications. As said before, assistance and rehabilitation are fields the group is interested in. This way, it is here where the work that will be presented in this document becomes relevant. Both the tactile handlebar and the tactile cane handle are two implementations whose differentiating factor is the use of cost-effective tactile sensors in a haptic interface. The experience in sensors (acquisition hardware, behavior, etc.) has been exploited in the development of the latter devices. This has given arise to new challenges that will be discussed throughout the manuscript.

1.4.2 Research projects

This PhD has been carried out in the context of two projects funded by the Spanish Government and the European Commission through EFDR funds:

- The project "Tactile Instrumentation and Assistive Living", with reference number TEC2012- 38653, ended in December of 2015. The team of the project was formed by eight researches from the University of Málaga and four researchers from CIDETEC, which is a Technology Center specialized in the areas of materials, surfaces and energy, and is located in San Sebastián (Basque Country, Spain).
- The project "Tactile Sensors in Mechatronic Systems for Health", with reference number TEC2015-67642-R, started in January of 2016. The team of the project is composed of eight researches from the University of Málaga and two researchers from the group Assistance aux Gestes et Applications Therapeutiques (AGATHE) of the institute *Institut des Systèmes Intelligents et de Robotique* (ISIR) at the Pierre et Marie Curie University (Paris, France). This group is devoted to assistive robotics. The researchers from the University of Málaga are also affiliated to the *Institute of Biomedical Research in Málaga* (IBIMA), which facilitates the access to resources in the biomedical area and also collaborations with other professionals in the field to achieve the transfer of the research results.

2

Haptic handlebar implementation

"Every honest researcher I know admits he's just a professional amateur. He's doing whatever he's doing for the first time. That makes him an amateur. He has sense enough to know that he's going to have a lot of trouble, so that makes him a professional."

— Charles Franklin Kettering

In this chapter, the implementation of the haptic handlebar will be introduced. Firstly, the system scheme and its main operating principle is presented. Later, the physical implementation of two prototypes of the device is detailed. Moreover, the conditioning and control electronics that captures the sensor information and activates the powered wheelchair engines is also described. Lastly, a preliminary control algorithm and an little experiment aimed to test the first version of the system are explained. The conclusions of the latter are given.

2.1 System architecture

In order to understand the system operation, Figure 2.1 can be helpful. As explained in the previous chapter, PWs can be steered with a joystick and, normally, all of them incorporate one. The strategy that has been employed consists in making use of this fact to develop a direct and convenient PW-haptic handlebar interface. The handlebar control electronics has been designed so that it can be directly connected to the PW joystick socket. This way, the control signals are the same of those provided by the joystick. Details about the emulation of the joystick will be exposed in Section 2.3.1. Considering the above, the PW can be driven using either the handlebar or the joystick, alternatively.

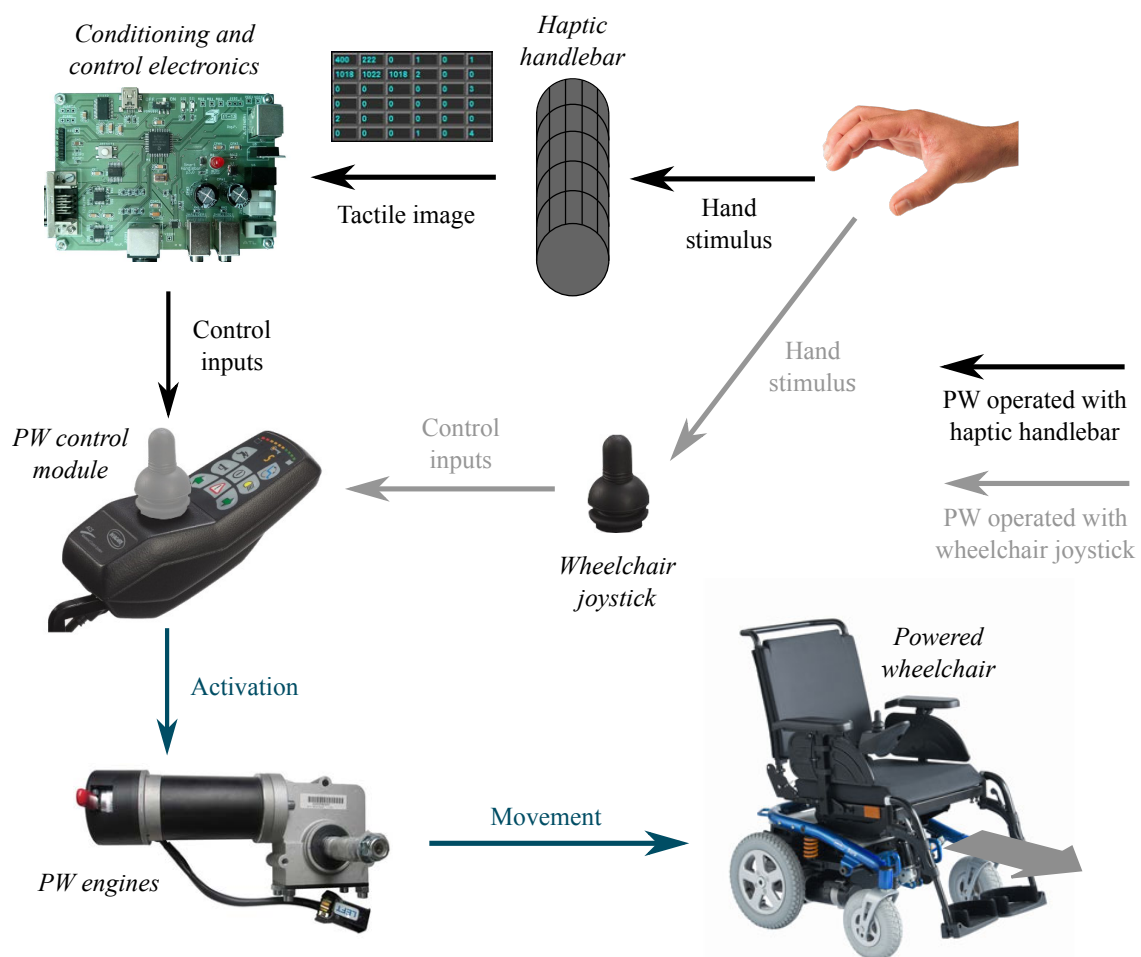


Fig. 2.1 System operation scheme.

Black arrows in Figure 2.1 represents the workflow of the handlebar operation. Firstly, the user grasps the handlebar. This will result in certain pressure on the tactile sensors. Gathering the sensors reading a pressure map can be built. The control and conditioning

electronics is in charge of this task. Besides, it performs an analysis of the data in order to infer the attendant steering intention. In accordance with the latter, the appropriate signals are generated. These are the inputs of the PW control module. This element comprises, on the one hand, the PW user interface so that it includes several buttons and a joystick, and, on the other hand, the PW central processing unit. Hence, it controls all the PW functions. According to its inputs, it communicates to the PW power module how the wheel engines have to be activated. Once the power is supplied to the engines, the PW moves based on the inferred user intention. In the next sections, the relevant components of the operation scheme will be covered.

2.2 Tactile handlebar

Tactile sensors are often arranged in mesh configurations. This option provides information about the pressure distribution in an specific area, that is to say, it is possible to know both the contact points and the pressure on each of them. This way, the reading of the group of sensors corresponds to a pressure map, also known as tactile image. Every individual sensor, which represents a point of the tactile image, is called *tactel*, a term formed by the union of the words "tactile element". The origin is in an analogy with traditional images and the word *pixel*, that comes from "picture element". A tactel contains information about the pressure in one spatial point in the same way that a pixel does likewise with brightness/color.

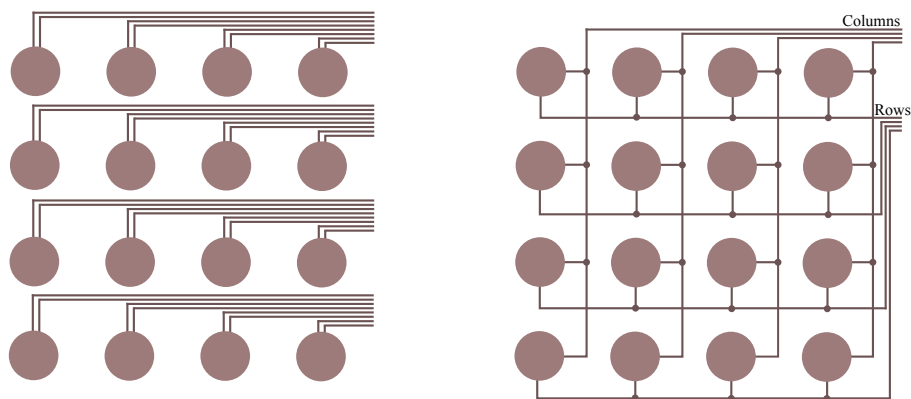


Fig. 2.2 4x4 mesh with tactels arranged individually (left) and in form of columns and rows (right).

In order to obtain a pressure map, all the tactels have to be read. Scanning them simultaneously would be the most accurate way of getting the pressure information. However, this method would require many resources since every sensor should be wired individually to the conditioning electronics, which should have a large addressing capacity (see Figure 2.2 left).

Besides, it would also imply that the electronics had one analog-to-digital converter (ADC) per tactel. This approach is too costly and not normally used. Pressure maps are commonly obtained by reading the tactels value sequentially. Moreover, they are usually arranged in rows and columns, configuration that minimizes the addressing and analog-to-digital conversion necessities (see Figure 2.2 right). This is as it has been done in this work.

Regarding the physical implementation, and reminding that the selected tactile technology was the piezoresistive, there are mainly two ways of building a tactel mesh. One of them implies the use of an array of interconnected discrete force sensing resistors. This way, every tactel in Figure 2.2 would be an individual FSR element that can be a commercial model and that is connected with the others according to the chosen organization. The other consists in the implementation of the whole structure as a single matrix, normally through an array of electrodes with a continuous conductive rubber or polymer sheet placed atop [102]. Each tactel is formed by a pair of electrodes covered by a little area of this material, which acts as piezoresistive link between the contacts. This method is cheaper since no commercial sensors are used. However, it usually presents a worse response as it is more sensitive to interferences between tactels. The first alternative was that used in the design of the handlebar.

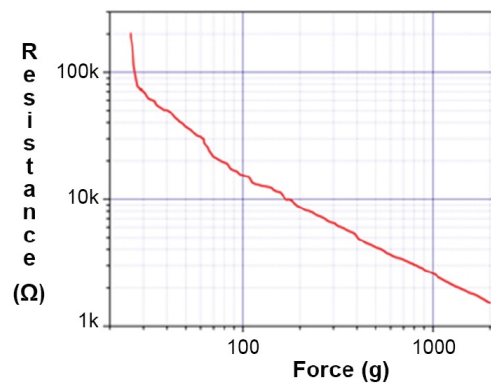


Fig. 2.3 Resistance/Force dependence for the FSR® 400 series (extracted from [5]).

A first prototype was developed using the commercial sensor FSR® 402 [91] as tactel. FSRs are piezoresistive tactile sensors made of polymer thick film that can be seen, from the electrical point of view, as variable resistors. Therefore, the higher the force applied, the lower their electrical resistance. Figure 2.3 can be found in the product data sheet and quantifies this phenomenon. These sensors consist of four distinct parts stacked one above the other (see Figure 2.4).

The bottom layer is the substrate where the electrodes are printed. The contacts have the shape of combs whose teeth are intermingled, what enhances the response to pressure

stimuli. A spacer is placed between this layer and the piezoresistive substrate. Its function is to prevent the electrodes and the piezoresistive material from being in contact in the absence of pressure. This way, only when the sensor is pressed, the piezo-layer is deformed, it passes through the spacer and touches the electrodes allowing the current to flow. Note that if a rigid object with flat bottom is deposited on the sensor, the conductive material does not make contact with the electrodes and the sensor registers no data [103]. Nevertheless, the hands surface is soft and penetrates the spacer gap when grasping the handlebar, so it is not affected by this issue. The last part is just an adhesive to fix the sensor where necessary.

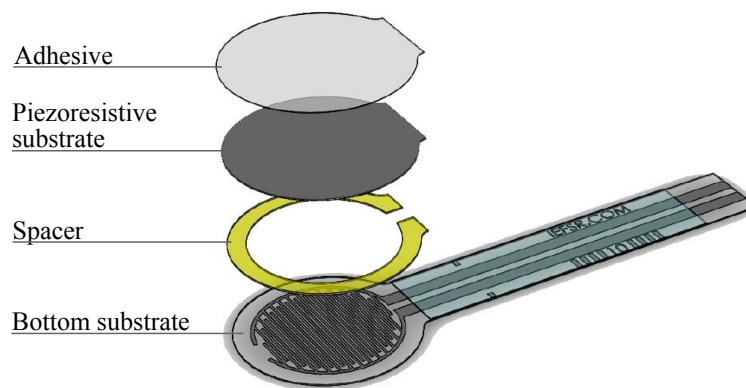


Fig. 2.4 FSR® 402 sensor structure.

Once tactels are grouped, the structure dimensions have to be taken into account. On the one hand, the handles should be long enough to ensure that the hand surface is in contact with the tactile area, having in mind those users with wide hands. On the other hand, the handlebar diameter is specially important since it affects the performance. If it is too small, there is space for very few rows and the matrix vertical resolution decreases. If it is too big, the handlebar can be awkward to use. Moreover, the work of Edgren et al. [6] shows that the diameter influences clearly the gripping force (GF). An appropriate handlebar diameter can reduce the effort, what prevents fatigue and overexertion. According to this study, when the diameter is 38.1mm the registered GF is maximum. Since the tactel size is a geometric constraint, we tried to keep it as close as possible to the latter value. The closest to 38.1mm diameters tested by the authors were 25.4mm and 50.8mm. As plotted in Figure 2.5, the force was higher for 50.8mm than for 25.4mm. That is to say, if a diameter of exactly 38.1mm is not possible, GF is higher by exceeding this number than remaining below. Besides, if we are rigorous, capturing GF for these concrete diameters what the authors have proven is that the force peak is withing the range of [38.1mm,50.8mm), probably nearer the first value.

Additionally, the study also found that a diameter close to that value increases the force component parallel to the ground plane (F_y in Figure 2.5 right). This is particularly

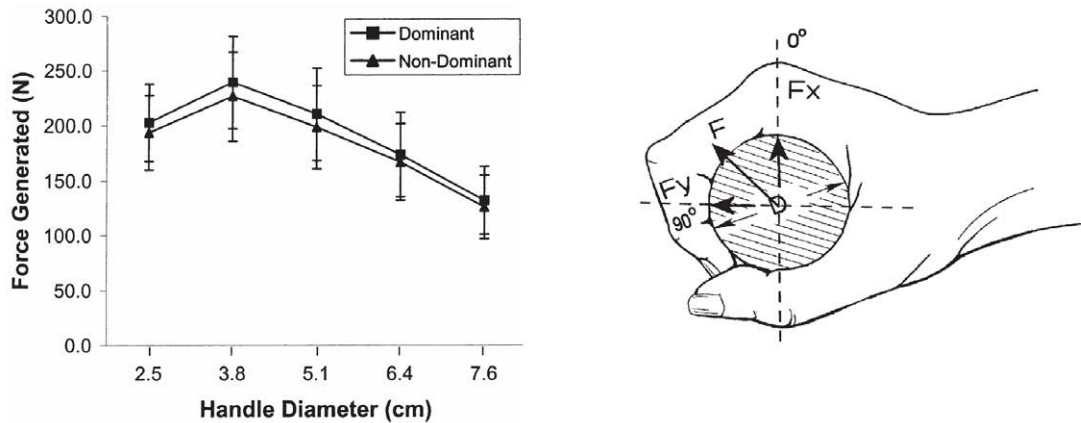


Fig. 2.5 GF/diameter dependence when grasping a circular handle (left). Force components on the handle (right). (Both extracted from [6]).

interesting in our application, since it is the wheelchair movement plane and that in which forces to perform the different maneuvers are exerted. This way, it contributes equally to prevent fatigue in the driving process.

Given the above, an array of 6×12 elements was built as the handlebar tactile cover. As it is shared by the left and right hands, the structure was divided into two sub-arrays of 6×6 tactels, one for the the left handle and the other for the right one. The tactile matrix schematic is shown in Figure 2.6.

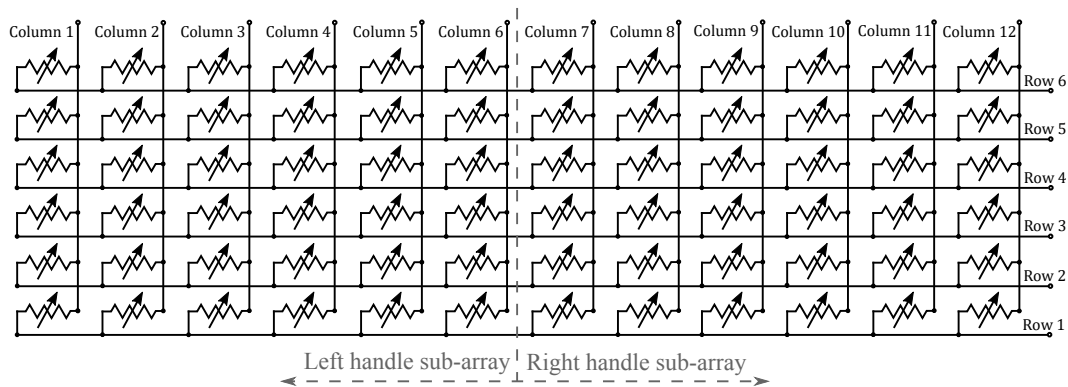


Fig. 2.6 Matrix schematic of the first handlebar prototype.

It was composed of one rigid printed circuit board (PCB) per row in each sub-array. The PCBs were joined together with soldered flexible tinned bridges that make the columns of the matrix. The tactels were soldered on the upper side of the PCBs. They must lie on a flat surface as they are sensitive to folds that cause undesired interferences [103]. The assembled structure was mounted embracing a bar of vinyl polychloride (PVC). It can be

seen in Figure 2.7. The resulting handlebar has a diameter of approximately 42mm and an active area length of 117mm in each handle.

This first prototype was used to carry out preliminary experiments that focused on studying how the force maps evolved while an attendant interacted with the handlebar. Despite the tactile response was good, the tinned bridges that join the PCBs were fragile so that, when someone grasped the structure tightly, they frequently broke and the cover had to be taken apart for repair. This fact was a source of persistent delays and led to the development of a second prototype.



Fig. 2.7 Tactile sensors matrix prior to embrace the PVC bar (left). Resulting implementation (right).

The new version was more robust. It was also cheaper than the old one since the number of tactels was reduced from 72 to 16 by removing the horizontal dimension of each sub-array (this measure will be explained in Section 2.4). This reduction also made the scanning faster. Besides, the vertical resolution was increased in two tactels. Hence, the new tactile matrix had 8×2 elements. The pressure sensor used was the FSR® 408 [92]. It is also manufactured by Interlink Electronics and has the same parts that were previously described for the model FSR® 402. It is marketed in form of strips with a length up to 609.6mm. In order to adapt it to our requirements, the sensor length was modified to obtain a tactel of 120×16.5 mm. One tactel were fixed on each side of two PVC octagonal pieces, one per handle, with the purpose of having a flat support surface. The electrical contacts were oriented toward the handlebar center. Thus, the connections were out of the grip area and could be protected with a plastic cylindrical covering. This made it resistant to excessively high gripping forces. Both handles were covered with plastic transparent film to protect the tactels from the environment. A LCD display was added in the middle in order to show messages to the user. The diameter of the resulting handlebar is 42.5mm. The length of the active area of the handles is 120mm.

Figure 2.9 shows the second prototype of tactile handlebar mounted on a commercial PW. Note that it is fixed on the ends and there are no elastic joints in the resultant structure.

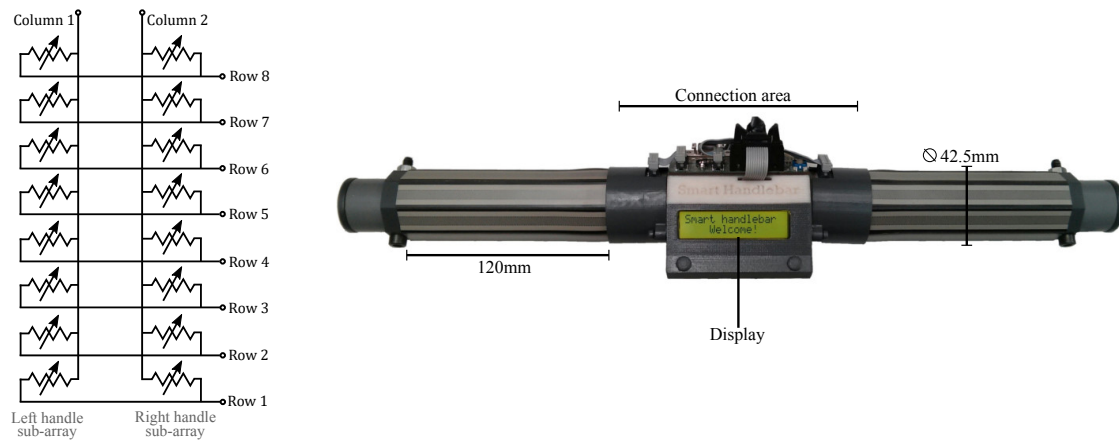


Fig. 2.8 Matrix schematic of the second prototype (left). Handlebar implementation (right).



Fig. 2.9 Second prototype mounted on a commercial PW.

Once the implementation of the tactile handlebar has been explained, the next section will be focused on the electronics in charge of carrying out the pressure maps readings and activating PW engines accordingly.

2.3 Control electronics

The conditioning electronics has been designed to be able to scan piezoresistive matrices, considering the undesirable effects that appear in this configuration. As tactels are interconnected, parasite resistive paths may arise between them. This could produce crosstalk that affects to the read value. The electronics schematic can be seen in Figure 2.10. It is based on a PIC18F4680 microcontroller by Microchip Technology, which is a versatile and cheap device. The matrix rows are connected to analog switches which are activated through the microcontroller digital outputs. Each column is wired to the inverting input of a transimpedance amplifier. The reading procedure is as follow: digital ports activate the switches so that the selected row is grounded. At the same time, the others are connected to a reference voltage, V_{REF} . Note that V_{REF} is also the voltage at the amplifiers non-inverting input. Due to the virtual short across the amplifiers input terminals, the tactels of the non-selected rows have the same voltage in both terminals¹. This cancels any possible resistive path and, thus, inter-tactel crosstalk. For the tactels of the grounded row, resistance changes are turned into voltage variations by the transimpedance amplifiers. The amplifier output for the blue element in Figure 2.10 is exposed in Equation 2.1:

$$V_{OUT_{i,j}}(V) = \left(\frac{R_G}{R_{i,j}} + 1 \right) V_{REF} \quad (2.1)$$

where $R_{i,j}$ is the resistance of the tactel to be read. Note that, whereas $R_{i,j}$ depends exclusively on the pressure, R_G can be freely chosen to module the conversion gain.

The amplifiers outputs are connected to the analog channels of the PIC18F4680. They are multiplexed so that only the signal at the chosen channel passes to the microcontroller analog-to-digital converter (10 bit resolution for the A/D conversion). Note that when the tactel to digitize is not pressed $R_{i,j}$ is maximum, ideally infinite, so according to Equation 2.1, $V_{OUT_{i,j}}$ is equal to V_{REF} . Since $R_{i,j}$ is in the denominator, this voltage will be the minimum at the ADC input. For this reason, if V_{REF} is too high the dynamic range at the ADC input would be greatly reduced. It should not be too low either, since this could affected to the gain, being V_{REF} a multiplicative factor in the equation.

¹In reality, there is a small voltage difference between the terminals, but it is negligible in our application.

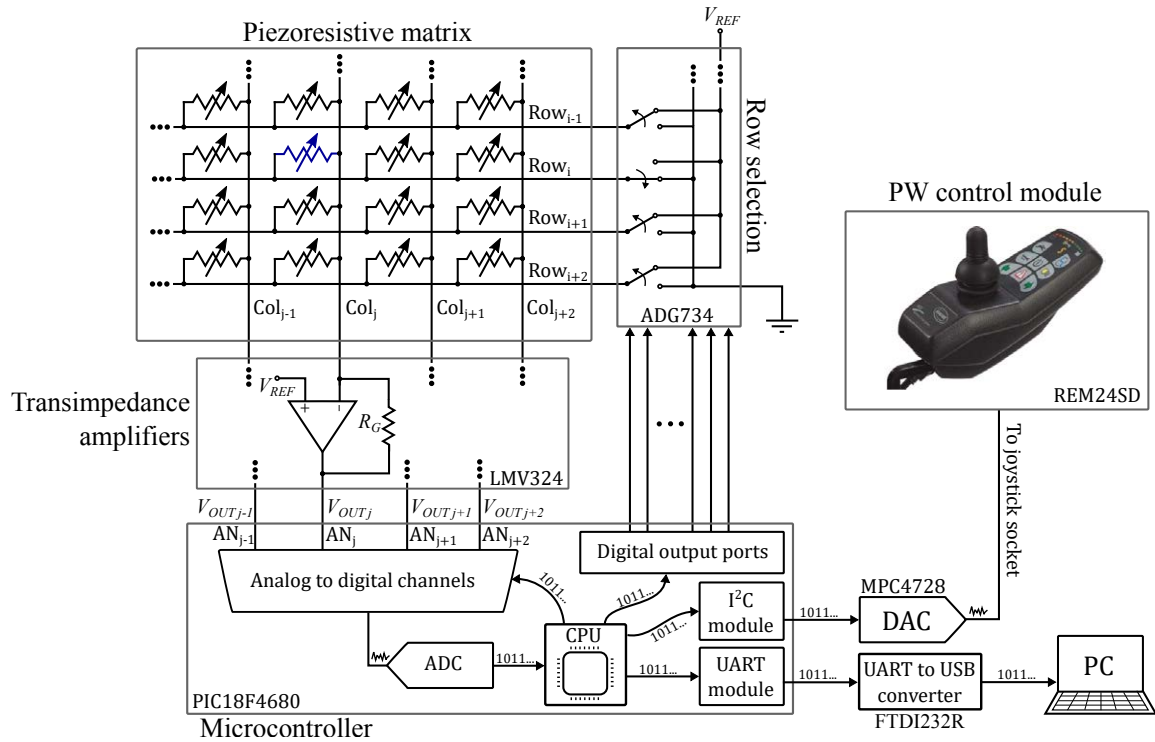


Fig. 2.10 Conditioning and control electronics schematic.

With the row of interest grounded, analog channels are one by one activated and all the columns of the latter are digitally converted. The procedure is repeated until the whole matrix is scanned and the digitized pressure map is available in the microcontroller memory. An algorithm analyzes it in order to extract the attendant driving intention. Once it is inferred, the PW speed is updated. As mentioned in the first section of this chapter, it is done through the joystick electronics. The joystick provides the PW control module with a set of analog signals that codify the PW speed at any moment. An external digital-to-analog converter (DAC) is used to carry out this function. The algorithm output is transferred via I²C bus to the DAC, whose outputs are connected directly to the joystick socket. The joystick emulation is addressed in the next point.

Moreover, an UART to USB converter has been added. This allows the board to send data to a computer via USB, what can be useful for further study. The described electronics is powered by the wheelchair batteries, through a voltage regulation.

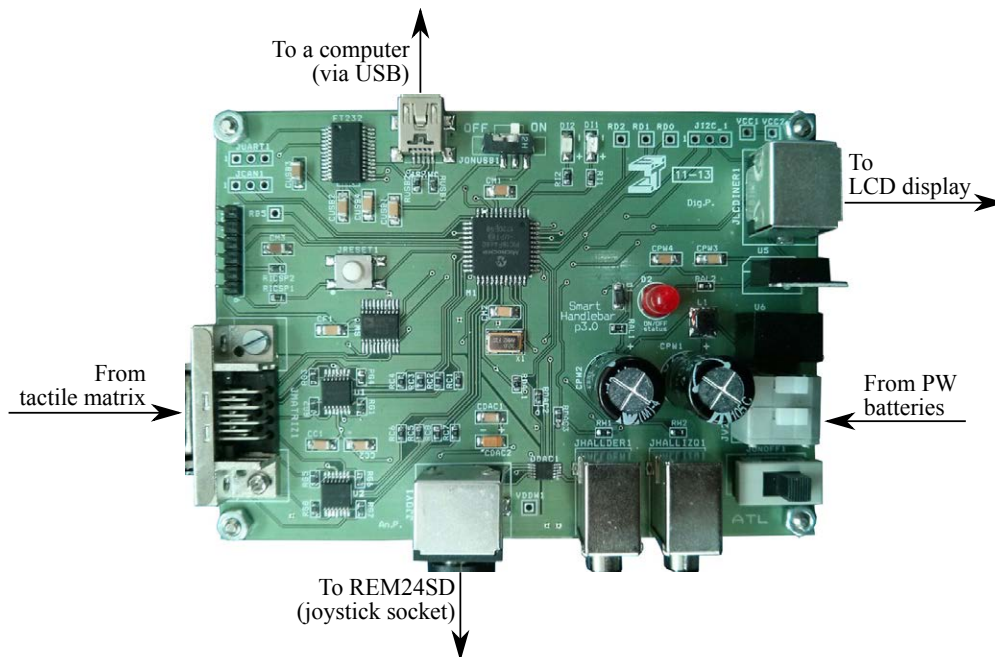


Fig. 2.11 Conditioning and control electronics implementation.

2.3.1 Joystick emulation

Two different wheelchairs have been used in this thesis. The first was the F35 by Sunrise Medical [104]. It was replaced by a Bora from Invacare [105] after suffering damages when it was being transported. The control solution both of them are equipped with is the DX System by the company Dynamic Controls [106]. This system integrates the power unit and the master control module (called DX Master Remote by the manufacturer). The first of them supplies with energy the wheel engines and the chair accessories that requires it (such as seat actuators, etc.). The other gives instructions via CAN bus to the former about how to perform its task, that is to say, which wheelchair parts has to be activated and when. The communications bus is closed and there is no information available about its content, so the specific commands in charge of movement are unknown. This way, it was necessary to explore other alternatives to make the PW move. Since the joystick is the accessory whose manipulation produces the PW movement, the chosen strategy was to study its outputs in order to emulate it in a reverse engineering process. The DX System supports several control modules; the one that our PW equips is the REM24SD [107]. It has to be opened to access to the joystick connections. There are six colored wires between the REM24SD board and the joystick. Forward, backward, right turn and left turn maneuvers were done while the evolution of the signal that each wire carries was studied. They vary between 0V and 5V according to the PW movement, concretely as exposed in Table 2.1.

Table 2.1 REM24SD - Joystick interface signals.

		Wires voltages (V)					
		V_{RED}	V_{BLACK}	V_{WHITE}	V_{BLUE}	V_{BROWN}	V_{YELLOW}
Maneuvers	<i>Stop</i>	5	0	2.5	2.5	2.5	2.5
	<i>Forward</i>	5	0	2.5	2.5	0 - 2.5	2.5 - 5
	<i>Backward</i>	5	0	2.5	2.5	2.5 - 5	0- 2.5
	<i>Left turn</i>	5	0	0 - 2.5	2.5 - 5	2.5	2.5
	<i>Right turn</i>	5	0	2.5 - 5	0 - 2.5	2.5	2.5

Voltage signals have been called by the color name of its associated wire. Two of them, V_{RED} and V_{BLACK} , do not change during the joystick operation. They are the supply voltage (5V) and ground (0V), respectively. The others can be grouped into two couples. V_{WHITE} and V_{BLUE} vary when turns are performed. In the absence of turns they remain at 2.5V, which is the half of the supply voltage. When the chair is turning to left, V_{BLUE} increases above that level. V_{WHITE} decreases under 2.5V in the same proportion. The bigger the distance to that voltage, the faster the turn is carried out. The limit is reached when V_{BLUE} is 5V and V_{WHITE} is 0V. With right turns, what happens is just the opposite. V_{BLUE} changes in the range from 2.5 to 0V and V_{WHITE} does it from 2.5 to 5V. The maximum turn speed is reached now when V_{BLUE} is 0V and V_{WHITE} is 5V. This way, it seems clear that these two signals control the turns speed and they depend on each other.

The same happens with V_{BROWN} and V_{YELLOW} and linear motion. When the PW moves forward, V_{YELLOW} rises above 2.5V. V_{BROWN} is reduced below 2.5V in the same amount that the previous one increases. If the PW moves backward, it is V_{BROWN} the signal that rises and V_{YELLOW} the one that decreases. Again, maximum speeds correspond with 0 and 5V and there is an interdependence between the signals.

In this manner, linear and turning speeds (v, ω) can be controlled by modifying, for example, V_{YELLOW} and V_{WHITE} , and the two others can be generated automatically according to Equations 2.2. The chosen speed control voltages may be named V_{linear} and $V_{angular}$ since they will be used to regulate the linear and angular speeds respectively.

$$\begin{aligned} V_{BROWN}(V) &= 5 - V_{YELLOW} \\ V_{BLUE}(V) &= 5 - V_{WHITE} \end{aligned} \quad (2.2)$$

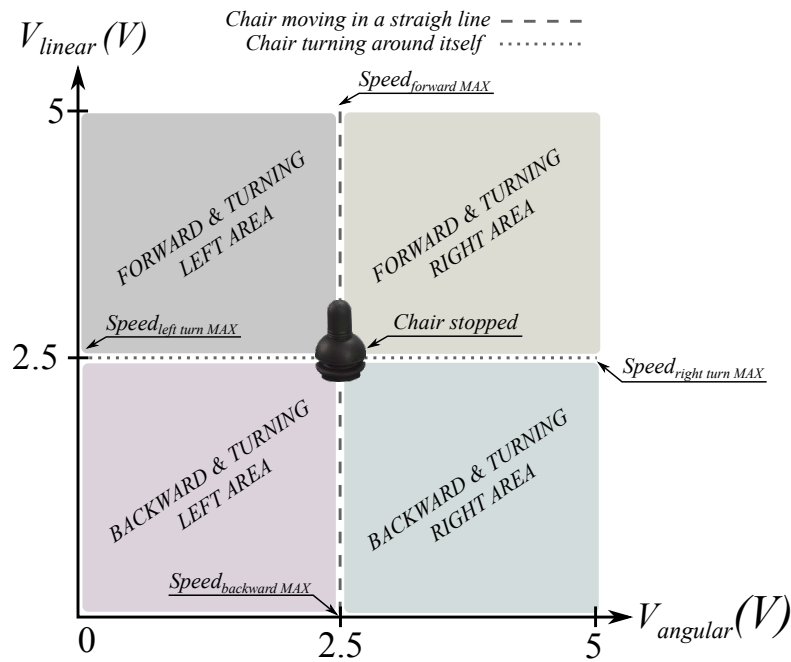


Fig. 2.12 PW speeds according to the control voltajes V_{linear} and $V_{angular}$ (previously named V_{WHITE} and V_{YELLOW} , respectively).

Figure 2.12 gives an overview. The PW movement can be seen as the sum of two components, linear and turn speed (see Figure 2.13), that are codified by two independent voltages. Note that when the speed voltages remain at 2.5V, both speeds are zero and the chair is stopped. If $V_{angular}$ is 2.5 and V_{linear} varies, the chair will move in a straight line, forwards or backwards depending on whether if the latter is bigger or smaller than 2.5V. If it is V_{linear} the one that remains at 2.5, the chair will turn around itself, clockwise if $V_{angular}$ is greater than 2.5V or counter-clockwise if it is smaller. When none of the signals are 2.5V, the chair moves forward or backwards and it turns at the same time. In light of the foregoing, angular and linear speeds can be expressed as:

$$\begin{aligned} v(m/s) &= G_{sens} (V_{linear} - 2.5) \\ \omega(rad/s) &= G_{sens} (V_{angular} - 2.5) \end{aligned} \quad (2.3)$$

where G_{sens} may be used to tune the sensitivity through a button of the REM24SD according to the assistant preferences.

As mentioned in the previous point, the PIC18F4680 executes an algorithm that determines the movement. Their outputs are the digital version of V_{linear} and $V_{angular}$. Both of them (and the two complementary analog signals) are generated by a DAC chip and wired into the joystick socket.

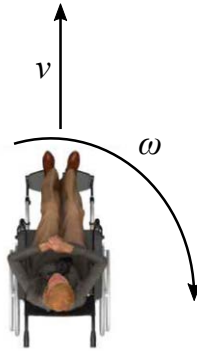


Fig. 2.13 PW movement is a composition of linear and angular speeds.

2.4 Preliminary analysis

Pressure data can be processed in several forms. A common way of processing the tactile images or map of forces in robotic manipulation tasks is the calculation of its center of mass (also known as center of pressure). The center of mass (*CoM*) of the tactile image provided by a sensor with $N \times M$ sensing units is defined as shown in Equations 2.4. It concentrates the data from all the tactels in a single spatial coordinate that provides information about how the pressure distribution is.

$$C_x = \frac{\sum_{x=1}^N \sum_{y=1}^M x \cdot p(x,y)}{\sum_{x=1}^M \sum_{y=1}^N p(x,y)} \quad (2.4)$$

$$C_y = \frac{\sum_{x=1}^N \sum_{y=1}^M y \cdot p(x,y)}{\sum_{x=1}^M \sum_{y=1}^N p(x,y)}$$

where x is the row number, y the column number, $p(x,y)$ the pressure value on the tactel indicated by the coordinates x and y , N and M are the tactile array dimensions and the point in coordinates (C_x, C_y) is the *CoM*.

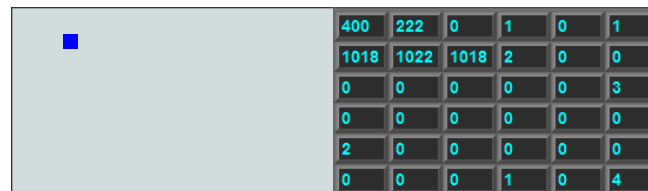


Fig. 2.14 Tactile image (right) and its center of mass (left) in one of the handles of the first prototype.

This parameter is proposed in this work as a way of processing the pressure map exerted by the user. By way of example, Figure 2.14 shows the resulting array from scanning the tactile cover of the first handlebar prototype and its corresponding center of mass. A preliminary analysis using this prototype consisted in studying how the *CoMs* of the tactile

images obtained by the left and the right handle changed over time when typical maneuvers were performed. It was observed that the *CoMs* shifts could be interpreted since some patterns were repeated according to the user driving intention. Figure 2.15 gathers an example of the *CoMs* displacements for four common maneuvers.

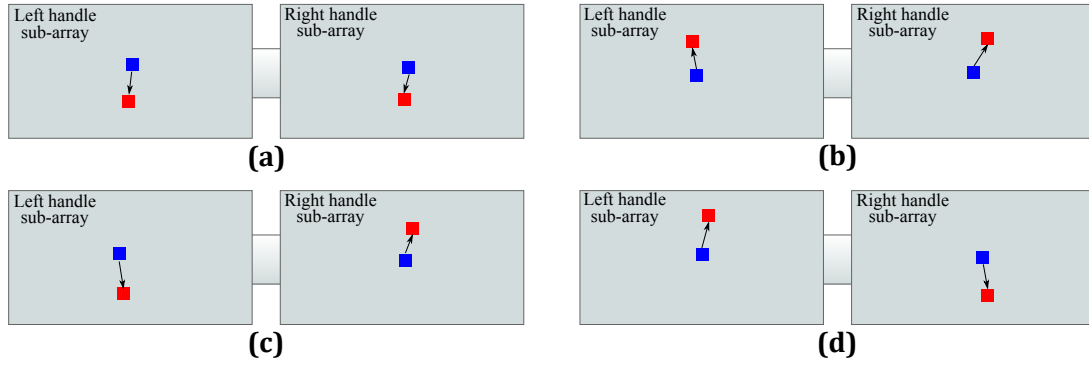


Fig. 2.15 Displacement of the *CoMs* under different maneuvers registered with the first prototype: (a) forward movement, (b) backward movement, (c) turn to the right and (d) turn to the left.

With the chair stopped, the handlebar was grasped and each of the four exercises described in the above figure were carried out. The blue square represents the initial *CoM*, i.e. the position of this parameter with the handles grasped but without exerting any additional force. The red square is the coordinate where the *CoM* moved once the force was exerted. It was observed that the *CoMs* extracted from both handles (CoM_R and CoM_L) varied mainly vertically. This was exploited in the development of the second prototype described in Section 2.2, where both handle tactile covers were built as linear arrays (x-axis was removed) and the spatial resolution along the y-axis was increased (see Figure 2.8). Note that, by eliminating the horizontal dimension, the calculation of the *CoM* in the second handlebar becomes simpler:

$$CoM = \frac{\sum_{y=1}^8 y \cdot p(y)}{\sum_{y=1}^8 p(y)} \quad (2.5)$$

where y and $p(y)$ are the position and the pressure value of the y^{th} tactel in the handle for which the *CoM* is being calculated. This is illustrated in Figure 2.16.

A testing algorithm based on the detected patterns was designed to check the feasibility of the proposal.

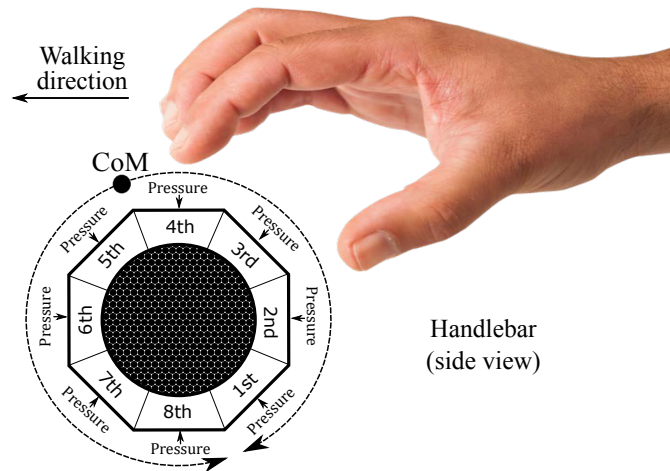


Fig. 2.16 CoM shift over the tactels group in the second prototype.

2.4.1 Testing algorithm

An algorithm was designed to check if PW movement could be generated according to the $CoMs$ shifts that were observed. It works as follows: when the user grasps the handlebar, CoM_L and CoM_R are computed and stored. They are considered the $CoMs$ in *rest condition* (CoM_{L_r}, CoM_{R_r}), that is to say, those with the user grasping the handles but with no intention of moving the PW. Their function is being used as initial references to determine if CoM_L and CoM_R in subsequent readings are shifted or not. There is a delay between the time the grip is detected and CoM_{L_r} and CoM_{R_r} are processed². This is due to the fact that the grip needs a little time to stabilize during which the $CoMs$ are temporarily varying. In addition, a dead band is defined around CoM_{L_r} and CoM_{R_r} (shaded area in Figure 2.17) so that, as long as the $CoMs$ are inside this area, they are considered to be in *rest condition*. This prevents little unintended displacements of the $CoMs$ from making the algorithm work improperly, due to electrical noise or mechanical vibrations.

In Figure 2.17, $CoM_{UP_{Min}}$ and $CoM_{Down_{Min}}$ represent the upper and lower dead band borders, respectively. $CoM_{UP_{Max}}$ and $CoM_{Down_{Max}}$ refer to the limits of the center of mass excursion during the driving and they were found heuristically in this algorithm. Taking into account the shifts shown in Figure 2.15 and the parameters described above, the classification of the user intention is carried out as Figures 2.18, 2.19 and 2.20 illustrate. The blue squares represent the centers of mass and the arrows indicate the range of possible displacement in which the intention of the user is considered. Note that the information of the centers of mass

²A message on the LCD indicates to the user that the rest condition reference parameters are being computed and driving is not yet allowed.

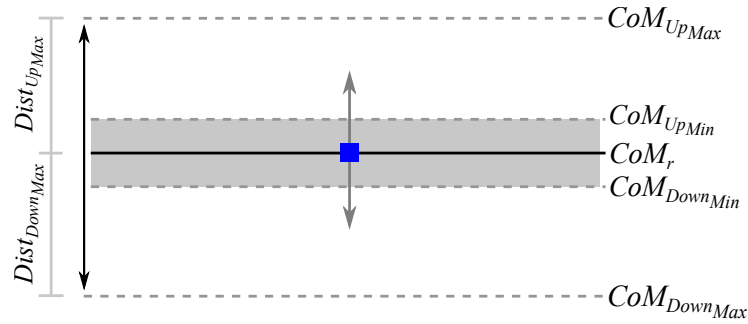


Fig. 2.17 Spatial parameters used by the testing algorithm.

of both hands is essential to identify the purpose of the user. Moreover, there is only one pattern identified with acceleration or deceleration (see Figure 2.18), while there are three patterns related to an intention to turn (see Figures 2.19 and 2.20). The reason is that the user can make a turn by changing the force exerted by both hands, or only that exerted by one hand. However, both hands are always used when an increment or decrement of the advance speed is desired. Note that each pattern is associated to only one purpose of the user. In the following the computation of the voltages V_{linear} and $V_{angular}$ that are required to activate the PW movement will be exposed.

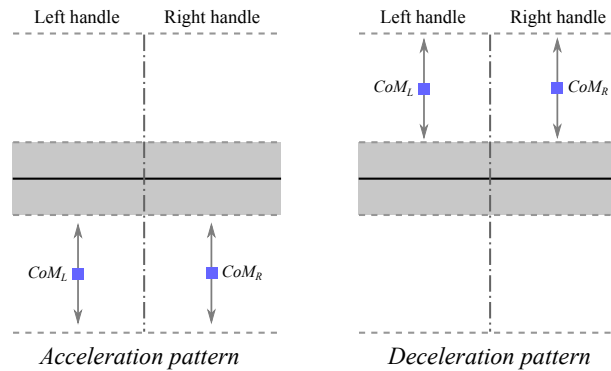


Fig. 2.18 Acceleration (left) and deceleration (right) patterns.

2.4.1.1 Acceleration/deceleration processing

Acceleration and deceleration processing is carried out when the patterns of Figure 2.18 are detected. If the acceleration (see Figure 2.18 left) or the deceleration (see Figure 2.18 right) patterns are recognized, the speed of advance of the wheelchair is calculated as:

$$V_{linear_n}(CoM_L, CoM_R) = \begin{cases} V_{linear_{n-1}} + \Delta_{Max} \cdot \Delta_{Acc}(CoM_L, CoM_R) & \text{if accel.} \\ V_{linear_{n-1}} - \Delta_{Max} \cdot \Delta_{Dec}(CoM_L, CoM_R) & \text{if decel.} \end{cases} \quad (2.6)$$

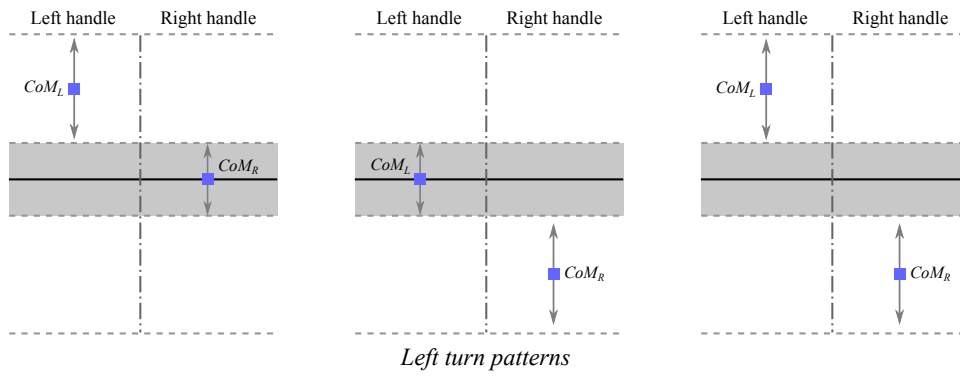


Fig. 2.19 Left turns patterns.

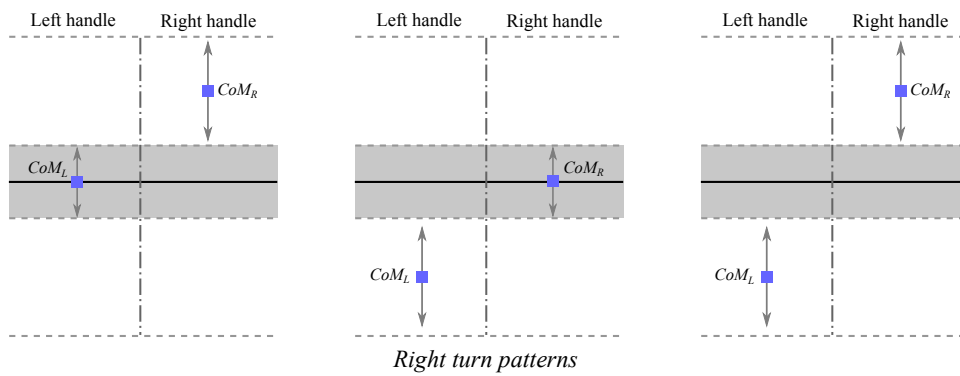


Fig. 2.20 Right turns patterns.

The subindex n refers to the computations that are made from the current tactile image whereas $n - 1$ is related to those parameters that were calculated using the image captured just before. Thus, $V_{linear_{n-1}}$ is the voltage responsible for the current forward/backward speed of the PW. V_{linear_n} is the voltage that will replace the latter. Δ_{Max} is the maximum increment of voltage allowed between consecutive tactile image readings. It determines therefore the maximum possible acceleration. Δ_{Acc} is given by:

$$\Delta_{Acc} = \frac{\left(CoM_{L_{DownMin}} + CoM_{R_{DownMin}} \right) - (CoM_L + CoM_R)}{\left(CoM_{L_{DownMin}} + CoM_{R_{DownMin}} \right) - \left(CoM_{L_{DownMax}} + CoM_{R_{DownMax}} \right)} \quad (2.7)$$

and Δ_{Dec} is obtained from the expression:

$$\Delta_{Dec} = \frac{(CoM_L + CoM_R) - \left(CoM_{LU_{PMin}} + CoM_{RU_{PMin}} \right)}{\left(CoM_{LU_{PMax}} + CoM_{RU_{PMax}} \right) - \left(CoM_{LU_{PMin}} + CoM_{RU_{PMin}} \right)} \quad (2.8)$$

Note that the change rate of V_{linear_n} is determined by Δ_{Acc} and Δ_{Dec} . These parameters are inside the interval $(0, 1]$ and depend on how far the centers of mass, CoM_L and CoM_R , are from the dead band limits. Thus, the largest increment of the current speed takes place when CoM_L reaches the value $CoM_{L_{DownMax}}$ and CoM_R the value $CoM_{R_{DownMax}}$, whereas the minimum increment happens when CoM_L is $CoM_{L_{DownMin}}$ and CoM_R is $CoM_{R_{DownMin}}$. The behavior is similar when the speed is decremented but now the change rate depends on the parameters $CoM_{LU_{PMax}}$, $CoM_{RU_{PMax}}$, $CoM_{LU_{PMin}}$ and $CoM_{RU_{PMin}}$ as the centers of mass shift toward their upper limits in this scenario. It is worth highlighting that the user does not have to exert any force in order to maintain a fixed linear speed. If the PW is moving in a straight line and the attendant is just holding the handles without exerting forces, the $CoMs$ will be inside the dead band and $V_{linear_n} = V_{linear_{n-1}}$. It is thought that it could be the most comfortable approach since the scenario in which the chair moves forward at a steady speed is the most frequent. Besides, if we recall the operation voltage ranges in Table 2.1, a deceleration pattern sustained over time could make that V_{linear_n} came back to 2.5V and the PW would stop. If the mentioned pattern persisted, the PW would start moving backwards. The same would happen with an acceleration pattern if the PW was initially going backwards.

2.4.1.2 Turn processing

A turn intention is detected if one of the patterns of Figures 2.19 and 2.20 is registered. In this case, the angular speed voltage is obtained by:

$$V_{angular}(CoM_L, CoM_R) = \begin{cases} \Delta_{T_{Max}} \cdot \Delta_L(CoM_L, CoM_R) & \text{if left turn} \\ \Delta_{T_{Max}} \cdot \Delta_R(CoM_L, CoM_R) & \text{if right turn} \end{cases} \quad (2.9)$$

where $\Delta_{T_{Max}}$ is the maximum allowed $V_{angular}$, that is to say, that for which the angular speed reaches its limit. Moreover, Δ_L and Δ_R are:

$$\Delta_L = \left(\frac{(CoM_L - CoM_R) - (CoM_{LUP_{Min}} - CoM_{RDown_{Min}})}{(CoM_{LUP_{Max}} - CoM_{RDown_{Max}}) - (CoM_{LUP_{Min}} - CoM_{RDown_{Min}})} \right)^2 \quad (2.10)$$

$$\Delta_R = \left(\frac{(CoM_R - CoM_L) - (CoM_{RUP_{Min}} - CoM_{LDown_{Min}})}{(CoM_{RUP_{Max}} - CoM_{LDown_{Max}}) - (CoM_{RUP_{Min}} - CoM_{LDown_{Min}})} \right)^2 \quad (2.11)$$

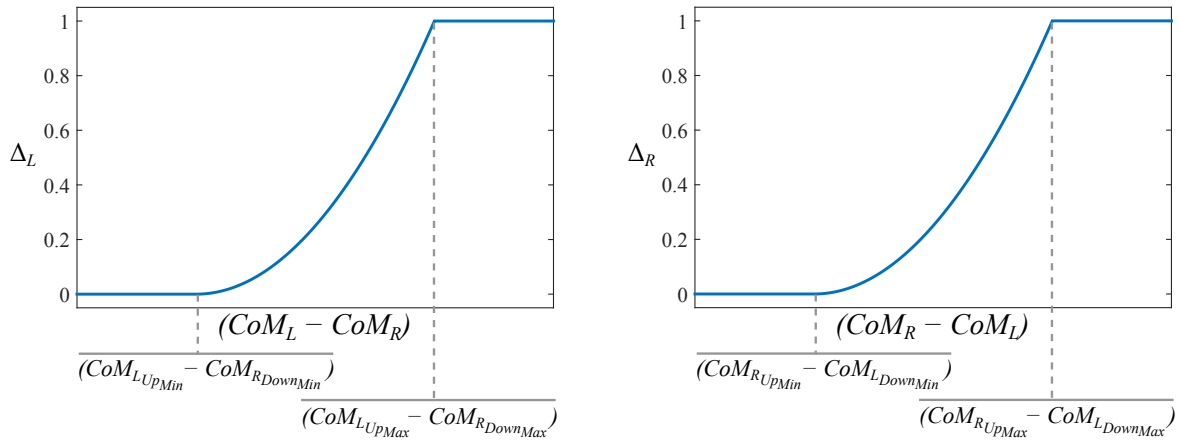


Fig. 2.21 Graphical representation of the parameters Δ_L (left) and Δ_R (right).

Δ_L and Δ_R are inside the interval $(0, 1]$ and they determine how tight the turn is. They are depicted in Figure 2.21, where their dependence on the Euclidean distance between CoM_L and CoM_R can be seen. This dependence follows a quadratic behavior to make the turns smoother (low pass filtering is also performed with the same goal). Note that the larger the distance $|CoM_R - CoM_L|$ the tighter the turn will be. Note also that $|CoM_R - CoM_L|$ is

smaller in the patterns of Figure 2.19 left and center and Figure 2.20 left and center, while the tightest turn is achieved with the patterns in Figures 2.19 and 2.20 right.

2.4.1.3 Linear speed correction

Note that, with the described approach, two different patterns can not happen at the same time. This way, it is possible that there is either an increment/reduction of the linear speed or a change in angular speed, but both of them cannot vary simultaneously. This can lead to the dangerous scenario in which a tight turn is made while the chair is moving forward at a high speed, what may cause that the PW collides with a wall or an object or make it even tip over. In order to avoid this situation, the maximum linear speed will depend on the current value of the angular speed. Once $V_{angular}$ is calculated, V_{linear} has to be adjusted according to the established limit. Figure 2.22 shows how the linear speed is rated to a value that depends on the turn speed. A sort of "safe operating" area is defined below the curve in Figure 2.22.

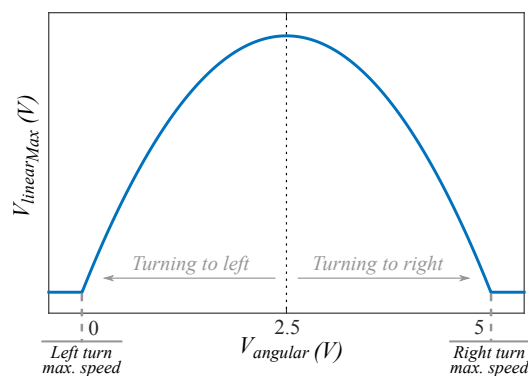


Fig. 2.22 V_{linear} limit modulation according to $V_{angular}$.

The final value of the linear speed is obtained from Equation 2.6 if this value is inside this area for a given turn speed. On the contrary, if this value is outside the safe operating area it is replaced by the rated value given by the curve in Figure 2.22.

2.4.2 Preliminary results

In order to test the feasibility of the proposal, six volunteers (aged between 33 and 51, average of 44.7) were asked to drive the chair grasping the handlebar and following the path shown in Figure 2.23. Its length is around 30 meters and a tape with a width of 5cm was used to mark it out on the ground. The microcontroller was executing the algorithm described in the previous subsection. Note that the path has tight turns to the left and right. The result of superimposing

a few selected frames shows the sequence of the movement along the path in Figure 2.24. Regarding the test participants, one of them had previous experience driving the PW with the implemented system. Two of them had driven the chair in different contexts a few times for approximately 15 minutes in total. The other three had no experience but they were allowed to follow the path twice before registering their performances. Figure 2.25 shows a photo of the experienced user driving on a ramp. The tests carried out by the participants, including that one going up the ramp, were recorded and they can be viewed in the section "Supplementary material" of [108].



Fig. 2.23 Preliminary test path.



Fig. 2.24 Participant following the path in the preliminary test.

Generally speaking, the users found the driving more or less comfortable and not difficult. Nevertheless, some flaws were reported:

1. Sometimes the system did not identify the participants driving intention through the patterns recognition. They had to release the handlebar and grasp it again to compute newly CoM_{L_r} and CoM_{R_r} , since they were not correct.



Fig. 2.25 Participant driving on a ramp with the handlebar mounted on a PW.

2. If the grasping was too loose, it was interpreted as if the user had released the handlebar and the chair stopped for safety reasons. After that and before driving could be continued, the reinitialization procedure took a few seconds, what was a bit confusing for some participants.
3. If the grasping was too tight, the output seemed to be saturated and the driving became more difficult. An artificially tight grip can make the driving impossible.
4. Sometimes there were little, sudden accelerations that could confuse some attendants and could be uncomfortable for the user seated on the chair.
5. The turn speed was occasionally perceived as excessive by one attendant.
6. The fact that no force is needed to keep the PW moving in a straight line seems to minimize the user sense of control and, sometimes, they may have the impression of being dragged by the PW instead of being them who control the driving.

Some of the reported weaknesses may be easily fixed by adjusting a few parameters of the algorithm. Others require a deeper study that leads to an improvement of the system control. The overall performance strongly depends on the "quality" of grasping, which is logical if we take into account the working principle of the device. This way, the process of stabilization of the centers of mass in order to obtain CoM_L and CoM_R , when the handlebar is just grasped should be definitely enhanced. At this time, it is slow and it is done in a quite arbitrary manner. Thus it would be worth analyzing in depth how the initial grasp takes place. On the other hand, it would be also advisable to study the user gripping force and how it affects to the $CoMs$ evolution when maneuvers are performed. It may be helpful in order to develop a system robust to its use by different attendants.

With respect to the point 6, it implies a change of the control algorithm used for generating the movement. With the algorithm described above, the participants needed to be instructed before driving the wheelchair with the tactile handlebar. Although this training was not extensive, it was still essential since the driving principle was not really the same of that in a regular handlebar. A linear movement based on momentary speed changes provoked by pushing or pulling turned out to be a little confusing. Moreover, the fact of having a non-zero constant linear speed just by holding the handles was as well confusing. All the aforementioned reduces the intuitiveness of the proposal, which is one of our key goals. In any case, it should be taken into account that the purpose of the proposed algorithm was to test the device potential capabilities as a driving interface and, indeed, all the volunteers completed successfully the test. The tactile handlebar seems to be a feasible alternative to the existing PW user interfaces although further research is necessary. The new approach will have to increase the feeling of being in control of the PW steering, what in turn will increase the comfort and users sense of security. In addition, haptic-based movement generation will be formulated so that very little training or directly no training is needed. It will require to deal with all the issues commented in this section.

3

Haptic-based driving control

"A user interface is like a joke. If you have to explain it, it's not that good."

— Martin LeBlanc

In Chapter 2, preliminary tests were carried out giving rise to series of key points that must be addressed to improve the usability of the haptic handlebar. In this chapter, they are studied in depth and some proposals are made. Firstly, an analysis of the forces and torques involved in the powered wheelchair driving is presented. An experiment is undergone using a force sensor to generate the control signals, with the purpose of identifying which variables extracted from the tactile handlebar are similar to the force and torque that control the PW driving. Based on the results of the latter, two variables are proposed. Furthermore, the effect of the user gripping force on the tactile handlebar parameters is analyzed. An experiment is realized and, as result, a method to correct this influence is given. The impact of the arrangement of the tactels inside the tactile array is also studied; the configuration with the best performance is selected. In addition, the handlebar grasp is addressed by exploring three aspects: the grip stabilization, the impact of the attendant height in this process and the

evolution of the centers of mass before the grip is steady. The latter analyses provide useful information aimed to enhance the system control. On the other side, a vibro-haptic feedback targeted to prevent high forces that lead to fatigue and overexertion is implemented. Finally, the proposed control variables are processed, considering what is presented throughout the chapter, to make them suitable to compute PW linear and angular speeds.

3.1 Haptic-based movement control based on force/torque analysis

The main aim of this section is to explore how the information extracted from the tactile handlebar may be processed, in order to achieve that our device can be operated as similar as possible as a regular handlebar. The first step is to describe what the interaction between an attendant and wheelchair is like. To this end, we will distinguish between pushing/pulling and turning maneuvers.

When caregivers push manual wheelchairs, and other similar ambulatory devices which are also manually propelled, they tend to lean on the handles, what produces a resultant force slightly downwards [109]. This contrasts with the fact that the greatest propulsion efficiency is reached when the whole force is directed forward. The origin of this phenomenon may lie in the use the body weight to help initiating movement when pushing a heavy load. In the case of a PW, engines are in charge of moving the chair and the existence of the downwards force component has not been yet studied. In fact, PW manufacturers do not always consider what research reports about the bio-mechanics of attendant - manual wheelchair interaction. For example, the authors of [109] found that the preferred handles height is in the region of 75% of shoulders height. However, a commercial PW as the F35 from Sunrise Medical (one of the models used in this thesis) allows a handles height range between 91 and 95cm. That height regulation makes that only attendants with a shoulders height in the interval 121-126cm can have the configuration the study in [109] points out. Despite of having a manual mode, PWs are not thought to be driven frequently in this way so it may be understandable that designers give priority to some aspects to the detriment of others.

With respect to turn maneuvers, the turning resistance may be seen as the torque needed to turn the wheelchair in its smallest circle, whose center is in the halfway between the two fixed rear wheels [109]. The handlebar center is located at approximately the same point, in a higher parallel plane x-y .

On the basis of the above and in the case of our device, pushing/pulling (P/P) assisted maneuvers are modeled as a force vector (F_y) in the plane parallel to the ground, i.e. in walking or forward direction. Turning operations are defined as the generation of a torque or turning moment (T_z) in the vertical axis located in the middle of the handlebar and perpendicular to the floor (see Figure 3.1). This was, for example, the approach that the authors of [65] followed to assist the driving of a supermarket trolley with a haptic handlebar. An experimental setup was designed in order to analyze the user - handlebar interaction while driving.

3.1.1 Experimental setup

The user interacts with the device by exerting a range of forces. Thus, the information that an analysis of the latter can provide is decisive. For this reason, another sensing device was added to the PW setup. It is the ATI Mini45 6-axis force/torque (F/T) and it was placed in the joint between the chair back frame and the center of the handlebar. This way, this high precision sensor can detect the forces and torques that are produced while maneuvering the PW through the handlebar and provide ground-truth measurements. Its other function is to generate control signals that can be used to activate the PW engines. Note that the PW driving is assisted through the F/T sensor outputs. Thus, the handlebar tactile sensors will be used exclusively to study the pressure exerted on them by the attendant during steering.

Figure 3.1 shows the experimental setup scheme. A computer has been introduced in order to ease the data acquisition and its analysis. It is in charge of gathering synchronously the pressure and the force/torque information from the tactile handlebar and the ATI Mini45 sensor, respectively. Besides, it updates the PW engines velocities at a rate of 60Hz. On the one hand, F_y and T_z are captured by the ATI Mini45 sensor and conditioned by the ATI FTIFPS1 amplifier. Afterward, the signals are digitized using the analog inputs of the multifunction card NI USB6009 from National Instruments. At the same time, the electronics described in Section 2.3 scans the handlebar tactile sensors and the microcontroller sends the data via UART-USB to the computer. F_y , T_z and pressure information are stored in the computer hard disc for further study.

On the other hand, before initiating the next reading, F_y and T_z are used by the application running on the computer to generate the voltages V_{linear} and $V_{angular}$ through the card NI USB6009. As the latter only has two DACs, an auxiliary circuit is placed between the NI USB6009 analog outputs and the joystick socket to generate the two extra complementary voltages needed (see Section 2.3.1). With this, the PW will move with linear and angular

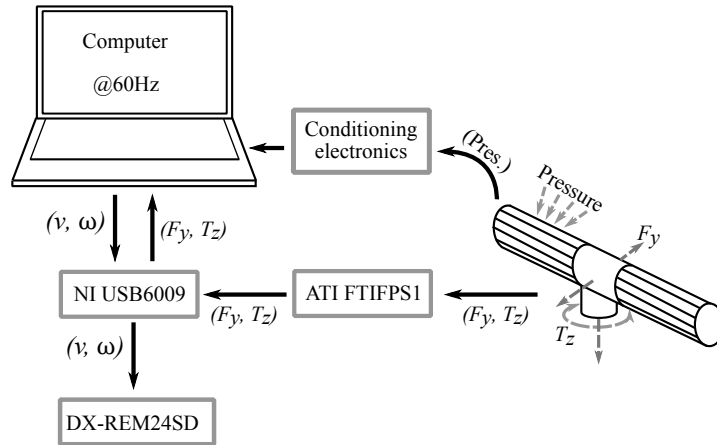


Fig. 3.1 Experimental setup scheme including a F/T sensor.

speeds that are proportional to the force in forward direction and the torque exerted on the handlebar during turns:

$$\begin{aligned} v &= G_{lin}F_y \\ \omega &= G_{ang}T_z \end{aligned} \quad (3.1)$$

where G_{lin} and G_{ang} are used to tune the sensitivity according to the assistant preferences.

The described setup enables the attendant to drive the PW using the handlebar in an intuitive way, as if it was a conventional one mounted in a non-motorized ambulatory device. However, it is worth noting that the F/T sensor will not be a permanent component of the system. Despite it could provided directly the signals needed to activate the PW, it has a high cost as mentioned in Chapter 1, with a price of several thousands of euros. Its use is exclusively aimed at research.

3.1.2 Experiment and results (E1)

In order to obtain the data involved in the PW driving an experiment (E1) was designed. Ten volunteers (P1-P10) with no previous experience with wheelchair driving and without any movement disorders took part in the test. They were between 24 and 63 years old, with an average age of 39,6. Given writing consent and complying with the ethical principles of the declaration of Helsinki at all times, they were asked to drive the wheelchair using the handlebar along the path showed in Figure 3.2. Marks on the ground and plastic cones were used to help the participants to follow the trajectory.

The path gathers, for about 25 meters, the typical maneuvers present in the normal usage of a handlebar. These are: several forward movements, two 90° turns, an open turn, a 180°

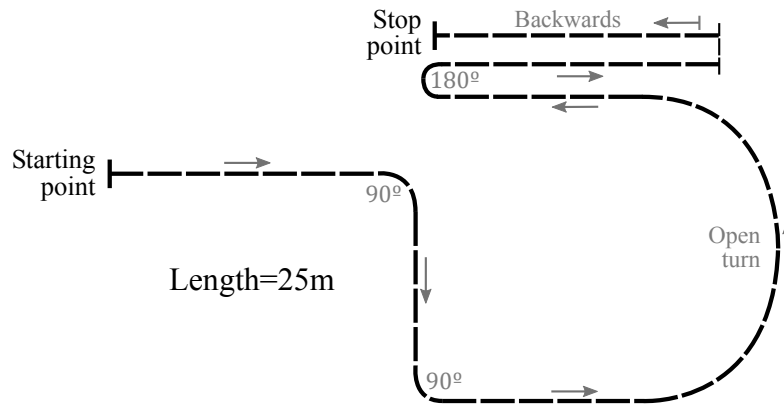


Fig. 3.2 Path of experiment E1.

turn around and a backward movement. Around one minute is required to cover the path length. It should be said that the participants were not aware of the experiment purpose. Two trials were carried out. The first one was used to familiarize the participants with the system and the path. During the second test F_y , T_z and the tactile output were registered as explained in the previous point. The volunteers did not receive any instruction at all about how to drive the PW with the developed device, so that their performance was based on their previous experience using handlebars.

The realization of the experimental setup can be observed in Figure 3.3. It is important to note that although nobody is seated on the chair during the experiment, the setup is still realistic. The weight of the setup as can be seen in the figure (PW frame, seat, batteries, etc.) is approximately the same of a conventional wheelchair with a person over 80kg on it. The seat was used to place the experiment hardware.

3.1.2.1 Force and torque analysis

The ATI Mini45 is a F/T 6-axis sensor, i.e. it provides the force and torque on the three spatial axes. It allows analyzing the interaction in each dimension. Not only the signals of interest, F_y and T_z , were influenced by the handlebar use (Figure 3.4 can help to visualize the framework). Firstly, there is a downward component of force (F_z). It was observed that the fact of just grasping the handlebar with the PW stopped produces a force sensor output in the vertical axis. It reflects that when a person grasps a handlebar he or she tends to lie his or her arms on the handles. When driving started, F_z varied around this downward component and these changes were similar to those of F_y . This effect also occurs when pushing manual wheelchairs as was mentioned in the first point of this section. Besides, F_z may be affected by the height of the user. Taking into account that the handles height was fixed, being the



Fig. 3.3 Experimental setup of E1.

same for all the participants of the test, it has been observed that F_z is clearly higher for the tall volunteers than for the shorter. On the one side, a higher value of the F_z offset when grabbing the handles may have its origin in the weight of the arms; taller people usually have larger and thus heavier arms than shorter.

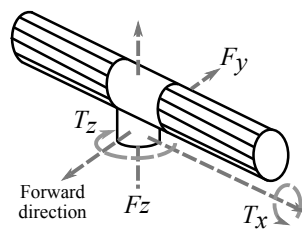


Fig. 3.4 Location of F_y , F_z , T_z and T_x .

On the other side, the greater variations of F_z while maneuvering may be explained by the angle formed by the user arms and the handlebar. The angle that taller attendants arms form with the forward direction plane when grasping the handles is higher than that formed by the arms of shorter ones. This way, it is more probable that the former exert a downward force component higher than the latter. Figure 3.5 illustrates this phenomenon. Abel et al. in [109] also point in this direction, this time analyzing the relationship between handles

and shoulders height while pushing a manual wheelchair. In fact, variations of F_z are much less similar to those in F_y for shorter participants, since in this case F_z is less modulated by driving.

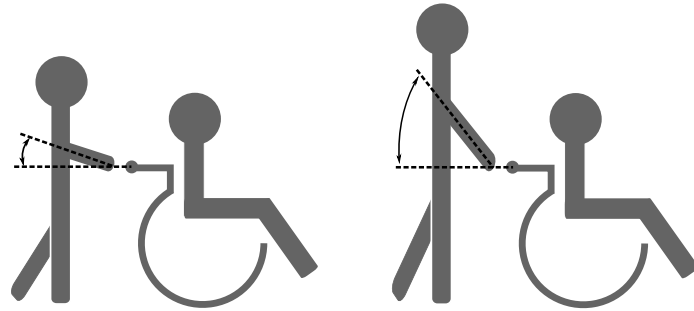


Fig. 3.5 Angle formed by the arms of shorter (left) and taller (right) attendants when grasping the handlebar.

F_y , by contrast, seems not be affected by the handlebar grasping, remaining at zero in this situation (see Figure 3.6); it only evolves following push and pull maneuvers. It is, therefore, confirmed as a good control variable to detect and quantify forward/backward movement intentions. Furthermore, the realization of the union between the F/T sensor and the chair frame bar (see Figure 3.3) makes that the torque in the axis defined by the frame bar, T_x , changes when pushing and pulling the handlebar. This T_x variation is similar to that in F_y for many users. Regarding rotations, as it was expected, T_z accurately represents the turns to left and to right. It is in addition not interfered by forward/backward movements.

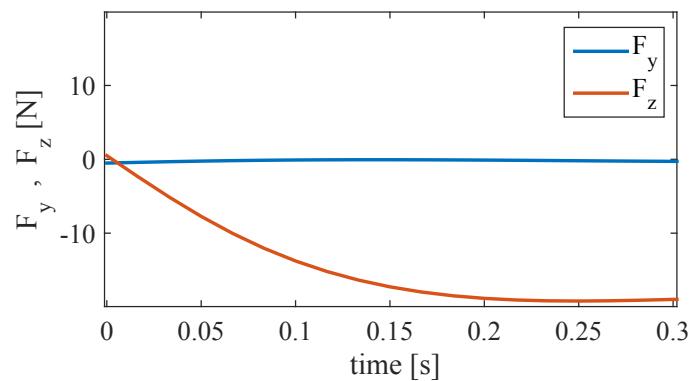


Fig. 3.6 F_y and F_z at the moment in which the handlebar is grasped.

It is also interesting to comment that sometimes the PW experienced some tugging while driving. The little sudden movements seemed to be modulated by the participant's gait. It may be related to linear speed gain. If it is too high, a push of the handlebar can cause that the chair moves forward faster than the person pace producing the jerks.

3.1.2.2 Proposed control variables

One of the main goals of this experiment was to study the force and torque involved in the handlebar maneuvering, together with the pressure variations exerted on the tactels of the handles. Since all the signals were captured synchronously, it is possible to try to identify if there is some kind of correspondence between those captured by the F/T sensor and the others obtained from the tactile sensors. If the processing of the pressure information provided variables similar to the those in charge of assisting the PW steering, F_y and T_z , it would be viable to implement an intuitive assisted driving, that allows operating as with a regular handlebar, based exclusively on the haptic handlebar.

Tactile images offer an independent variable per tactel, so that they are normally processed to obtain high level parameters that summarize the whole data set. In order to choose the most appropriate of them, it is necessary to take into account the different sources of error and how they affect to the calculated pressure parameters. Errors in tactile piezoresistive sensors arise mainly from the phenomena of hysteresis, drift and mismatching. Hysteresis was commented as one of the most common drawbacks of this kind of sensors in Chapter 1. It means that the tactels output under certain pressure depends on the previously exerted pressure. Drift can be described as the change of the tactels output over time, despite the exerted pressure does not vary. Finally, mismatching is due to the fact that tactels are physically different from each other, thus their outputs can be different under the same pressure. This happens both in our tactile arrays, where tactels have been designed with hand-made modifications, and in commercial high quality sensors based on piezoresistive matrix as, for example, the one of [110].

Manipulation or control tasks often are processed to obtain a few key parameters that can be further used as inputs. Different moments of the tactile image are computed with this purpose. For instance, an ellipsoid can be obtained from these moments. Its location, shape, size and orientation are similar to the contact properties of the object pressing on the tactels. The moments of the tactile image are calculated as Equation 3.2 shows.

$$M_{i,j} = \sum_{x=1}^N \sum_{y=1}^M x^i y^j p(x,y) \quad i, j > 0 \quad (3.2)$$

where $p(x,y)$ is the output of the tactel located at (x,y) , and N and M indicate the size of the sensor array (rows and columns).

Figure 3.7 shows the typical parameters of the ellipse that is used to describe objects in manipulation tasks. In the case of the example the object that presses against the tactels

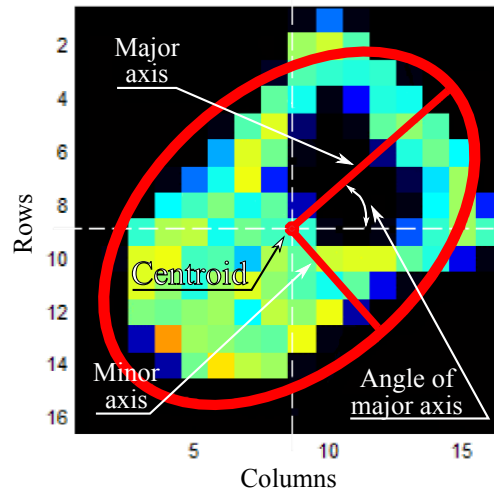


Fig. 3.7 Typical parameters of the ellipse that describes the object pressing on the tactels in manipulation tasks, in this case, a bottle opener (based on the Figure presented in [7]).

is a bottle opener. Note that the handlebar usage represents a different scenario. There is not an inanimate object interacting with the tactile sensors but the sensors are in a fixed configuration and the hands are exerting variable pressures. Since the tactile arrays resolution is low and one-dimensional, parameters as the ellipse axes or their angles make little sense. However, the centroid can provide useful information about the evolution of the pressure location on time. The centroid is calculated as shown in Equation 3.3, using the expression given in Equation 3.2:

$$X = \frac{M_{10}}{M_{00}}; \quad Y = \frac{M_{01}}{M_{00}} \quad (3.3)$$

with X and Y the horizontal and vertical coordinates of the centroid, respectively.

Note that, substituting the values of i and j of Equation 3.2 with the values given in the previous expression, it turns out that the centroid is none other than the center of mass presented in the Chapter 2 and whose mathematical form we already know. According to the conclusions reached by Sánchez-Durán et al. in [7], piezoresistive low cost sensors are good enough providing spatial distribution information whereas they are not the best option to provide contact forces. That means that relative high level parameters can be a good choice to process pressure data. Absolute variables as the aggregate output (sum of all tactels value) suffer considerably from hysteresis and drift.

This is quite logical if we look at definition of these sources of error. They affect to all the tactels to a greater or lesser extent so that there tends to be certain compensation in relative parameters. The typical hysteresis loop presents two different curves, one for ascending and other for descending pressures (Figure 3 in [7]). This way, in tactels suffering from hysteresis

the measured output for the same exerted pressure in two distinct moments between which there has been a pressure variation is:

$$p(x_i, y_j, t_k) = p(x_i, y_j, t_k - \Delta t) \pm \Delta P \quad (3.4)$$

where $p(x_i, y_j, t_k)$ is the pressure read on the tactel in coordinates (x_i, y_j) at the instant t_k and $p(x_i, y_j, t_k - \Delta t)$ is the output of the same tactel Δt seconds earlier for the same external pressure, having a pressure variation within the interval between both instants. ΔP is the increment/decrement modeled by the sensors hysteresis curve (the sign of the operation depends on whether the pressure variation has been ascending and after descending or vice versa).

The aggregate output (AO) when hysteresis is present, and using Equation 3.4, can be expressed as:

$$AO(t_k) = \sum_{x=1}^N \sum_{y=1}^M (p(x_i, y_j, t_k - \Delta t) \pm \Delta P) = AO(t_k - \Delta t) \pm (N \cdot M) \Delta P \quad (3.5)$$

Note that, assuming that all the tactels were affected by the error to the same extent, the hysteresis would have provoked a change of $(N \cdot M) \Delta P$ in the latter parameter. Looking at the effect of the same source of error on the centroid or center of mass, we have:

$$\begin{aligned} C_x(t_k) &= \frac{\sum_{x=1}^N \sum_{y=1}^M x \cdot (p(x, y, t_k - \Delta t) \pm \Delta P)}{\sum_{x=1}^M \sum_{y=1}^N p(x, y, t_k - \Delta t) \pm \Delta P} \\ C_y(t_k) &= \frac{\sum_{x=1}^N \sum_{y=1}^M y \cdot (p(x, y, t_k - \Delta t) \pm \Delta P)}{\sum_{x=1}^M \sum_{y=1}^N p(x, y, t_k - \Delta t) \pm \Delta P} \end{aligned} \quad (3.6)$$

In this case, the pressure increment/decrement, ΔP , is both in the numerator and the denominator. Thus, the error influence in the parameter is largely self-contained. It becomes clearer with a numeric example. Let us assume that the pressure on the array of one on the handles of the second prototype at the instant $(t_k - \Delta t)$ is $P(t_k - \Delta t) = [0 \ 1 \ 3 \ 3 \ 4 \ 3 \ 2 \ 0]$. For the latter read we have that $AO(t_k - \Delta t) = 16$ and $CoM(t_k - \Delta t) = 4.69$. After Δt seconds, the pressure on the contact tactels (from 2nd to 7th) increases by 2 units¹: $P(t_k) = [0 \ 3 \ 5 \ 5 \ 6 \ 5 \ 4 \ 0]$. This way, the updated parameters are $AO(t_k) = 28$ and $CoM(t_k) = 4.61$. As can be observed, AO has suffered a variation of 75% whereas the change in CoM has been of 1.71%. The experiment results presented in [7], Figure 6, also point in the same direction.

¹Note that in the example, for simplicity, units are not specified.

Note that the undesired effect of drift can be addressed through the same previous expressions and example, with the same consequences. The only difference is conceptual: although the sensor output changes, the external pressure does not change at no time between the instants $(t_k - \Delta t)$ and t_k .

There is also other considerations to take into account. Attendants are different from one another and they may behave diversely, so they could presumably grasp the handles with different forces. Parameters such as the CoM depend on the pressure distribution and do not represent the direct reflection of the pressure on the handles. This way, it is possible to obtain approximately the same CoM with different gripping forces. Note that, as showed in Equation 3.6 and the previous example, it is a parameter quite tolerant to pressure offset variations. It is, thereby appropriate to detect patterns and subtle changes and robust to the change of an user for other. Nevertheless, this alone is not sufficient as the main requirement that the chosen pressured-based control variables must meet is that they represent as reliably as possible the user intention.

In Section 3.1.2.1, we saw that PW driving maneuvers can be modeled by the couple formed by F_y and T_z . In this way, the pressure data analysis consisted in searching for those variables that show similarities with the mentioned force and torque. After assessing different manipulations of CoM , it was found the **sum** of the centers of mass of each handle (SUM_{CoM}) and their **subtraction** (SUB_{CoM}) were tightly coupled to F_y and T_z , respectively. Both parameters are computed as:

$$\begin{aligned} SUM_{CoM}(t) &= CoM_L(t) + CoM_R(t) \\ SUB_{CoM}(t) &= CoM_L(t) - CoM_R(t) \end{aligned} \quad (3.7)$$

where $CoM_L(t)$ is the center of mass calculated for the tactile array of the left handle and $CoM_R(t)$ is the same parameter for the array of the right handle.

The degree of coupling between the two pairs of variables was determined through the calculation of correlations for all the tests carried out by the volunteers. Previously, the four parameters involved in the analysis were low-pass filtered to remove possible noise and interferences. Besides, the initial and the final captured samples in which both centers of mass are not stable were discarded. These correspond to the very first moment in which the participant grasps the handlebar and to the instant when the user releases it at the end of test. Pearson coefficient ($r_{X,Y}$) was computed for the couples $\langle SUM_{CoM}, F_y \rangle$ and $\langle SUB_{CoM}, T_z \rangle$. It is a measure of the linear correlation between two variables. It varies in the interval $[-1, 1]$. A value of '1' means that there is total positive linear correlation, '-1' represents a total negative linear correlation and '0' the complete lack of linear correlation. The threshold above which

it is considered that there exists a strong correlation between the assessed variables may change from an area of science to other. In the field this work is developed, the threshold usually accepted is 0.7/-0.7. Hinkle et al. [111] propose the following rule of thumb for interpreting the size of the correlation coefficient:

Table 3.1 Rule of thumb for correlation interpretation.

Size of correlation	Interpretation
0.9 to 1 / -0.9 to -1	Very high positive/negative correlation
0.7 to 0.9 / -0.7 to -0.9	High positive/negative correlation
0.5 to 0.7 / -0.5 to -0.7	Moderate positive/negative correlation
0.3 to 0.5 / -0.3 to -0.5	Low positive/negative correlation
0 to 0.3 / 0 to -0.3	Negligible

The results obtained in the experiment for participants P1 to P5 are plotted in Figure 3.8 and the results for P6 to P10 in Figure 3.9. For their computation, the open source Matlab toolbox provided by the authors of [112] was used. Both figures show the link between the SUB_{CoM} and T_z (left column) and between SUM_{CoM} and F_y (right column). Besides, the simple linear regression has been depicted for every set of data. The calculated correlation coefficients for the first couple were: $r = 0.95(p < 0.001)$ [P1], $r = 0.84(p < 0.001)$ [P2], $r = 0.85(p < 0.001)$ [P3], $r = 0.88(p < 0.001)$ [P4], $r = 0.70(p < 0.001)$ [P5], $r = 0.80(p < 0.001)$ [P6], $r = 0.68(p < 0.001)$ [P7], $r = 0.67(p < 0.001)$ [P8], $r = 0.84(p < 0.001)$ [P9], $r = 0.82(p < 0.001)$ [P10]. The first order linear functions in these trends were $T_z = 0.17217SUB_{CoM} + 1.3989$ [P1], $T_z = 0.3148SUB_{CoM} + 1.2151$ [P2], $T_z = 0.59582SUB_{CoM} + 2.3231$ [P3], $T_z = 0.3947SUB_{CoM} + 1.7889$ [P4], $T_z = 0.50103SUB_{CoM} + 4.182$ [P5], $T_z = 0.55267SUB_{CoM} - 1.1027$ [P6], $T_z = 1.099SUB_{CoM} - 0.4982$ [P7], $T_z = 1.0459SUB_{CoM} + 5.2504$ [P8], $T_z = 0.60954SUB_{CoM} + 1.4806$ [P9] and $T_z = 0.44211SUB_{CoM} + 1.3992$ [P10]. Note that the higher point density is located at the central area of the graphs. This part corresponds to the absence of turns. Turns are temporary exercises during which samples are shifted from this area to one of the extremes of the chart, depending on whether the turn is to the left or to the right. Most of the time PW goes straight so it is foreseeable that points are concentrated in the central area.

Regarding the pair $\langle SUM_{CoM}, F_y \rangle$, the correlation coefficients were: $r = 0.91(p < 0.001)$ [P1], $r = 0.83(p < 0.001)$ [P2], $r = 0.77(p < 0.001)$ [P3], $r = 0.89(p < 0.001)$ [P4], $r = 0.71(p < 0.001)$ [P5], $r = 0.83(p < 0.001)$ [P6], $r = 0.56(p < 0.001)$ [P7], $r = 0.80(p < 0.001)$ [P8], $r = 0.78(p < 0.001)$ [P9] and $r = 0.85(p < 0.001)$ [P10], with the corresponding

first order linear functions: $F_y = 0.70353SUM_{CoM} - 87.691$ [P1], $F_y = 0.98466SUM_{CoM} - 113.06$ [P2], $F_y = 1.9257SUM_{CoM} - 266.37$ [P3], $F_y = 1.5108SUM_{CoM} - 218.59$ [P4], $F_y = 1.3854SUM_{CoM} - 198.8$ [P5], $F_y = 1.6081SUM_{CoM} - 206.18$ [P6], $F_y = 4.2626SUM_{CoM} - 653.25$ [P7], $F_y = 3.959SUM_{CoM} - 588.03$ [P8], $F_y = 2.1063SUM_{CoM} - 299.01$ [P9] and $F_y = 1.7871SUM_{CoM} - 223.17$ [P10]. In this case, the bulk of the samples are mainly concentrated at the bottom of the graph. Note that during the major part of the experiment, the PW is moving through the path with positive linear speed that is produced by pushing the handlebar. When pushing, CoM moves to the lower tactels of the tactile arrays (rear part of the handles, see Figure 2.16) so that their values are minimum. Consequently, the parameter SUM_{CoM} will be also minimum.

As can be observed, in the case of $\langle SUM_{CoM}, F_y \rangle$ the correlation was high positive for nine participants and moderate positive for one of them. Regarding $\langle SUB_{CoM}, T_z \rangle$, it was practically high positive for all the participants. Moreover, it was statistically significant for all the tests. This overall strong correlation implies a similarity between the involved variables that can be clearly observed in Figure 3.11. It depicts their evolution over time for one of the participants that had an average performance in the experiment, that is to say, it was neither the best nor the worst. As can be seen in the figure, the changes in the signals obtained by the ATI Mini45 (first plot and third plot, continuous line) are closely followed by the variables calculated from the centers of mass (second and forth plot, dashed line).

Although the results are generally solid, the seventh participant (P7) presents a correlation for $\langle SUM_{CoM}, F_y \rangle$ that, despite not being weak, is a little lower than for the others. It seems that, in his case, the cloud of points corresponding to the values captured by pulling the PW to go backwards² is a little unlinked to the rest of the samples. Figure 3.10 helps visualize the mismatching. Note that the first order function that fits in the test carried out by P7 deviates slightly from the data captured while pulling the handlebar, which affects to the linear relationship between the variables. This effect has not been observed so clearly in the rest of the tests, as can be checked in Figures 3.8 and 3.9.

Furthermore, it should be said that in the data of some of the participants it has been identified another little decoupling between F_y and SUM_{CoM} that may have reduced the correlation. It seems that SUM_{CoM} is slightly affected by turn maneuvers at certain times. The effect appears when the chair is going straight and some degree of turn is introduced. In order to keep a straight movement, attendants exert similar forces with both hands. When a turn component is incorporated, some of them reduce the pushing force of the left or right

² Maneuver during which both $CoMs$ move upwards through the area of the tactile arrays and F_y is greater than zero.)

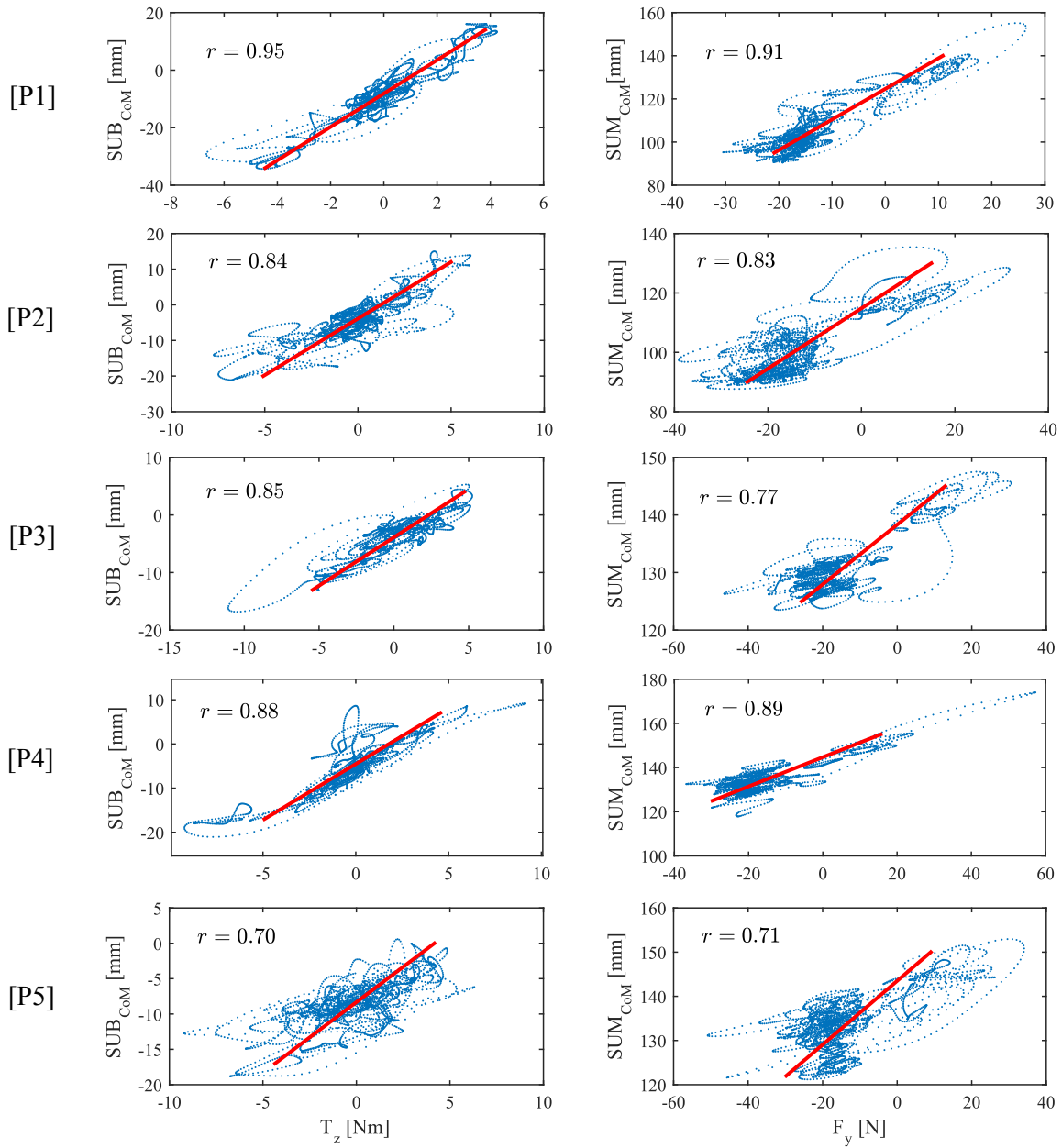


Fig. 3.8 Experiment results for participants P1-P5: coupling between the couples $\langle SUB_{CoM}, T_z \rangle$ (left column) and $\langle SUM_{CoM}, F_y \rangle$ (right column) with the corresponding first order linear functions superimposed.

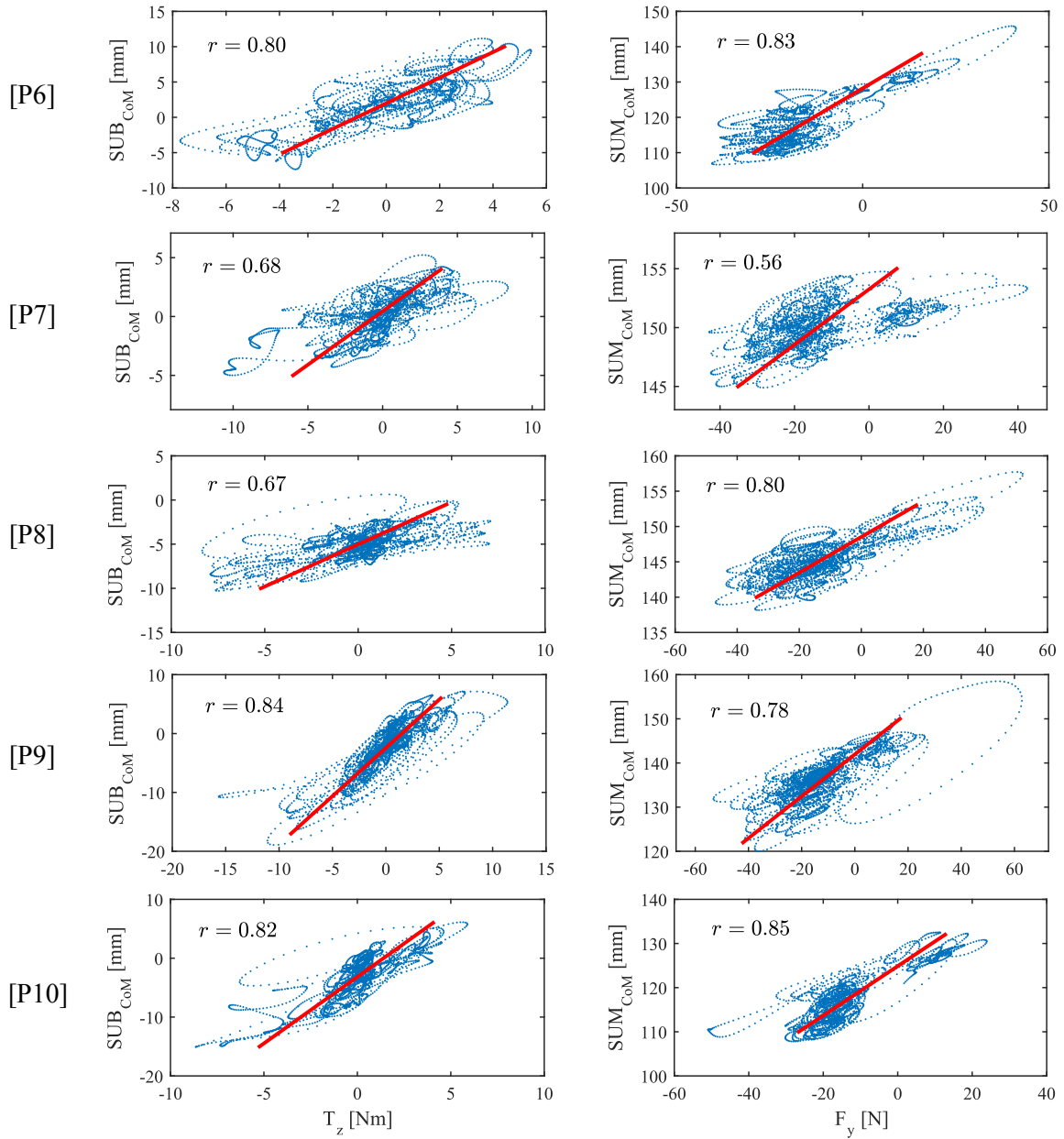


Fig. 3.9 Experiment results for participants P6-P10: coupling between the couples $\langle SUB_{CoM}, T_z \rangle$ (left column) and $\langle SUM_{CoM}, F_y \rangle$ (right column) with the corresponding first order linear functions superimposed.

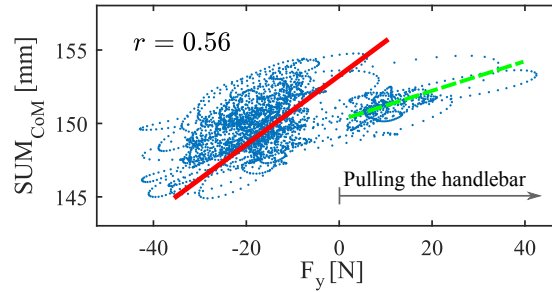


Fig. 3.10 SUM_{CoM} versus F_y for P7. The red line is computed from the data of P7 by linear regression. The green dashed line, which has a lower slope, fits better with the data captured during pulling maneuvers.

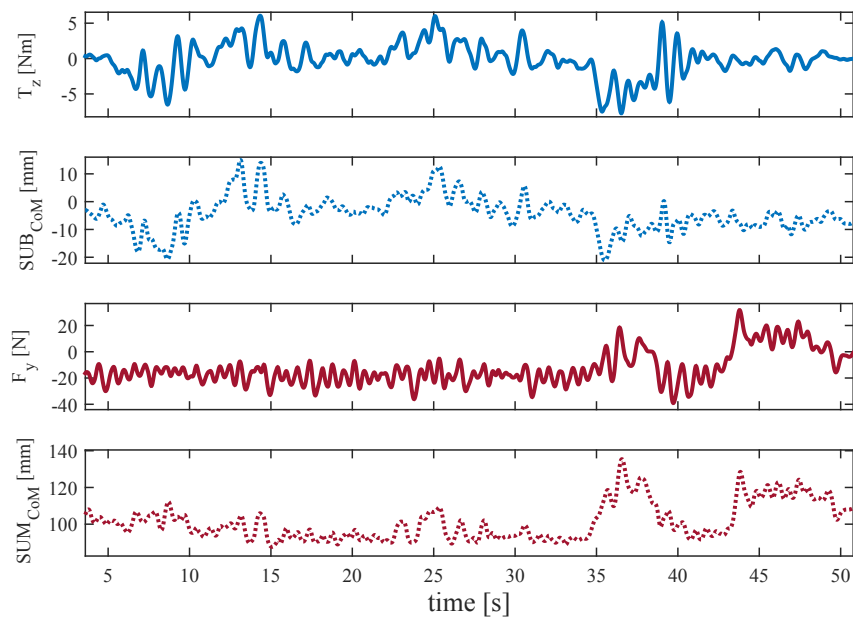


Fig. 3.11 T_z and F_y from the F/T sensor (first and third plot). SUB_{CoM} and SUM_{CoM} (second plot and fourth plot) obtained from processing of the pressure values.

hand (depending on whether the turn is to left or to right, respectively) whilst the force exerted by the other hand remain unchanged. When this happens, the force reduction of one of the hands impacts much more in CoM shifts than in F_y . This way, there is a little mismatch between F_y and SUM_{CoM} . This can clearly be seen in the data depicted in Figure 3.12, where the chair was moving straight, after that it was introduced a right turn and, just after, another to the left. The two dashed circles represent the time intervals in which the two turns are performed. Note that CoM_L remains unaltered during the right turn, i.e. the force exerted by the left arm does not change. However, CoM_R rises towards the rest condition, since very little force is exerted with this hand. With the turn to left happens the opposite. The force needed to carry out the maneuver is mostly exerted by the right arm whereas the left arm rests. Since SUM_{CoM} is the addition of both $CoMs$, it is affected by this asymmetry. However, F_y barely changes. If SUM_{CoM} were the variable that controls linear speed and this issue persisted, it could manifest itself as little unwanted linear speed drops during turns. Nonetheless, it should be taken into account that this effect was only observed for some of the participants and not in every turn maneuver so it should not be not be generalized in advance.

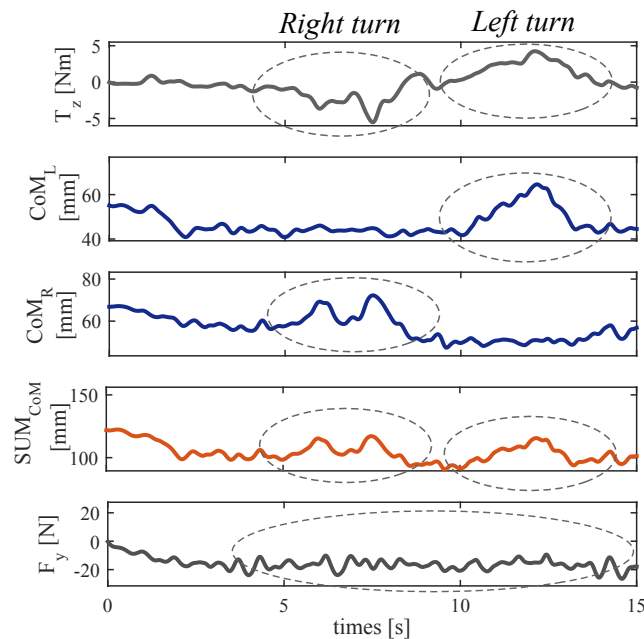


Fig. 3.12 From top to bottom: T_z , CoM_L , CoM_R , SUM_{CoM} and F_y . During the data acquisition the chair was moving ahead and, afterwards, a right and a left turns were introduced.

Notwithstanding the above, it should be borne in mind that we are working with persons who presents physical and behavioral differences. A range of parameters may influence the correlation: the fact of comparing outputs from sensors of different kind, the grip force or

the way of grasping the handlebar, among others. Although it seems that a deeper study could improve the case of moderate positive correlation of P7, the presented results are good enough to show that the substitution of the control inputs used to compute the wheelchair movement by those obtained from the tactile handlebar seems to be viable. Specifically, SUM_{CoM} detects and quantifies push and pull maneuvers and SUB_{CoM} does the same with turns.

In the following sections, several factors that impact on the control based on the previous variables will be presented. The identification of them helps improve the assistant driving experience.

3.2 Study of grip force effect

One of the issues detected as a result of the reports from the users that drove the chair with the control algorithm presented in Chapter 2 was that the force with which the handlebar is grasped during driving can affect the experience. Thus, a deeper study of this fact is interesting in order to improve the control. Excessive grip forces seem to saturate and block in some way the handlebar response. An initial step can be to determine the source of this effect, which could have either hardware or anatomic nature. On the one hand, the sensors can be reaching their saturation pressure so that their output remains invariable at its maximum. This way, there would be no CoM changes that resulted in effective driving maneuvers. On the other hand, the user gripping itself (how the contact between the hand surface and the tactile handlebar is) may be what limits the $CoMs$ range of excursion when grip force is high. Therefore, it is worth exploring whether the GF affects the proposed control variables of the previous section in one way or another.

3.2.1 Tactels response characterization

In order to study the tactels response, the handlebar was taken apart from the chair frame and introduced in a characterization platform as shown in Figure 3.13. The platform belongs to the laboratory of the research group EIS [113] and is composed of three stepper motors from Zaber Technologies, a high precision ATI Nano17 6-axis force/torque sensor, an acquisition card USB-6259 BNC by National Instruments and a conditioning electronics board designed by the group EIS. The three motors, that have a step length below $0.01\mu\text{m}$, are aligned with the spatial axes x , y and z . The z -motor (T-NA08A50) controls a plunger with a spring inside. Its function is to exert forces in z -axis. The ATI Nano17 is attached to the lower end of the

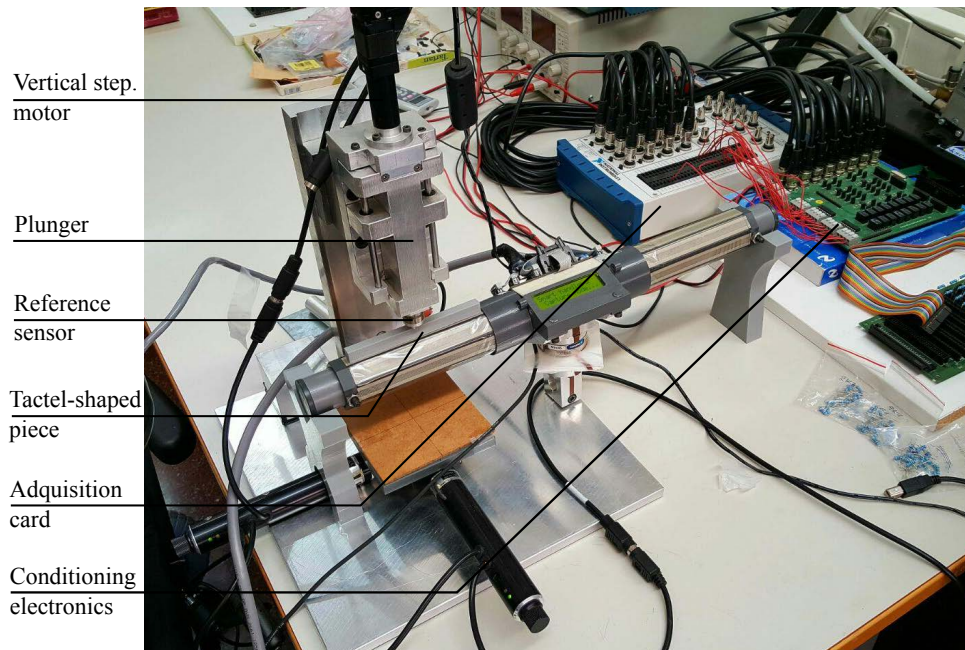


Fig. 3.13 Tactile handlebar in the characterization platform.

plunger so that it provides ground truth measurements of the force that is being applied. The described platform is managed with a computer to which the motors, the F/T sensor and the acquisition card are connected (further details can be found in [114]).

Due to the handlebar dimensions, two stands had to be 3D printed to place the center of the tactel to be characterized below the presser arm formed by the motor, the plunger and the F/T sensor. Besides, a custom plastic piece was designed so that the pressure could be exerted as uniformly as possible onto the tactel located at the top side of the left handle. In the upper side of the piece there was a little hole where the tip of the F/T sensor was fitted. Note that for simplicity reasons only one tactel is characterized. The tolerance between pressure sensors is a parameter normally given by the manufacturer. As said in Section 2.3, the A/D converter that translates pressure into digital information has a resolution of 10 bits. This way, the captured pressure is codified with values inside the range 0-1023 (this format will be named Digital Output Units, DOU). The test that was carried out consisted in pressing with growing force on the tactel surface up to it reached its maximum output. Afterward, the force was reduced until the exerted pressure was zero. During both ascending and descending excitation, measurements were taken at fixed increments/decrements of the tactel digital output. A little wait was introduced before making the measurement in order to let the output stabilize. The force with which the vertical stepper motor was pressing was captured by the ATI Nano17 sensor at the same time. Since the latter provides ground

truth data, its captures were used to build the characterization curve of the tactel of interest. Figure 3.14 depicts the information captured during the process of characterization.

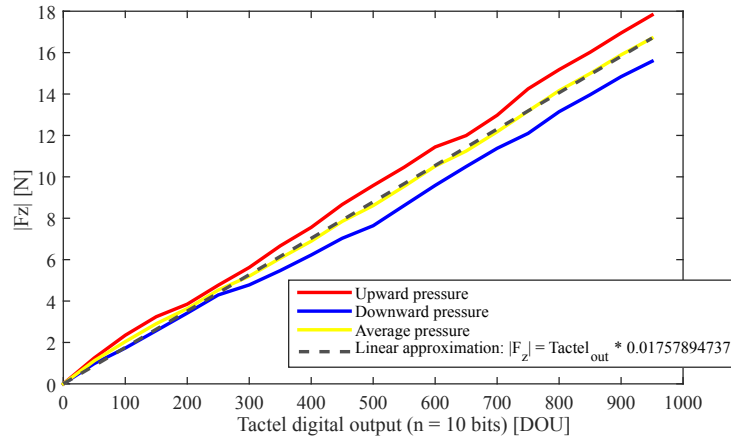


Fig. 3.14 Vertical axis: force captured by the ATI F/T Nano17. Horizontal axis: digitized pressure from the left top handlebar tactel. In red and blue sensors output for upward and downward force, respectively. In yellow the mean between the previous curves. The dashed line represents the linear approximation of this mean. According to the sensor reference, F_z decreases when pressing so the slope of the curve would be negative; this way, in order to facilitate the visualization, what is showed is the absolute value.

As can be noted, the curves originated by the rising (red) and the descendent (blue) pressure have slopes mildly different; this is caused by hysteresis. The more force is exerted, the more the behavior of the sensor is sensitive to this source of error. If the force is not high and its variations either, the effect of hysteresis can be considered negligible. In order to estimate the force that excites the tactels, the linear approximation of the mean between the red and blue curves in Figure 3.14 will be used (dashed line): $F_{tactel}(N) = 0.01757894737Tactel(DOU)$. The previous figure shows that the tactel response is linear in its operating range, which is approximately 0-18N. Above that level, it started becoming saturated and losing linearity.

3.2.2 Grip force impact on the coupling between the parameters extracted from the force sensor and those captured by the tactile handlebar

One way to estimate the gripping force as a single value could be to compute the mean force on the tactile handlebar when it is grasped:

$$GF = \frac{\sum_{x=1}^N \sum_{y=1}^M f(x,y)}{N \cdot M} \quad (3.8)$$

where $f(x,y)$ is the force on the tactel located at coordinates (x,y) (calculated using the expression in Figure 3.14), and N and M the number of rows and columns of the sensors array, respectively. In the case of the tactile handlebar, considering the structure in Figure 2.8, Equation 3.8 becomes:

$$GF = \frac{\sum_{x=1}^8 \sum_{y=1}^2 f(x,y)}{16} \quad (3.9)$$

If we look at the mean value of GF during the realization of the tests of the experiment E1 (presented in Section 3.1.2), the results are: $\overline{GF} = 3.47\text{N}[\text{P1}]$, $\overline{GF} = 6.53\text{N}[\text{P2}]$, $\overline{GF} = 14.01\text{N}[\text{P3}]$, $\overline{GF} = 7.9\text{N}[\text{P4}]$, $\overline{GF} = 12.15\text{N}[\text{P5}]$, $\overline{GF} = 10.73\text{N}[\text{P6}]$, $\overline{GF} = 17.07\text{N}[\text{P7}]$, $\overline{GF} = 15.72\text{N}[\text{P8}]$, $\overline{GF} = 12.57\text{N}[\text{P9}]$ and $\overline{GF} = 8.92\text{N}[\text{P10}]$. All of them are inside the tactels working range. It would be logical to think that the way GF is computed can lead to the situation in which some tactels present a low output and others are saturated; in this case, the value provided by the parameter GF would seem to be within the valid operating range and the saturation of some particular tactels would not be perceptible. This happens, indeed, in the case of [P7], for which sensor 4th (see Figure 2.16) is saturated during some time intervals. This tactel is practically entirely covered by the hand surface and it usually captures the higher pressures. Nevertheless, such high GF s as that from [P7] are rare cases and, even, it may be desirable to avoid them in order to prevent fatigue and overexertion (as will be shown in Section 3.5).

A question worth considering is if the attendant's GF affects the quality of the couplings presented in the Section 3.1.2.2, i.e., if GF impacts on how good SUM_{CoM} represents push/pull intentions and SUB_{CoM} represents turns intentions. A simple way to address this issue could be to check whether the correlations computed in the mentioned section increase or decrease when GF s raise or diminish or if these facts are not related at all. Figure 3.15 plots two charts with this aim. On the one hand, in their x-axis the participants' \overline{GF} s are listed in increasing order: $\overline{GF}s = (3.47[\text{P1}], 6.53[\text{P2}], 7.9[\text{P4}], 8.92[\text{P10}], 10.73[\text{P6}],$

12.15[P5], 12.57[P9], 14.01[P3], 15.72[P8], 17.07[P7]). On the other hand, y-axis gathers the correlations obtained for each participant: $r_{\langle SUM_{CoM}, F_y \rangle} = (0.91[P1], 0.83[P2], 0.89[P4], 0.85[P10], 0.83[P6], 0.71[P5], 0.78[P9], 0.77[P3], 0.80[P8], 0.56[P7])$ for the left chart, and $r_{\langle SUB_{CoM}, T_z \rangle} = (0.95[P1], 0.84[P2], 0.88[P4], 0.82[P10], 0.80[P6], 0.7[P5], 0.84[P9], 0.85[P3], 0.67[P8], 0.68[P7])$ for the right chart. This way, each point of the graphs is composed by the pair $(\overline{GF}, r_{\langle SUM_{CoM}, F_y \rangle})$ for Figure 3.15 left and $(\overline{GF}, r_{\langle SUB_{CoM}, T_z \rangle})$ for the same figure right. In addition to the graphical evaluation, it can be useful to see how much the evolution of the two pairs of vectors is correlated. In this case, besides Pearson correlation, Spearman's rank-order correlation ($\rho_{X,Y}$) is computed. It is a measurement of the monotonicity between two variables.

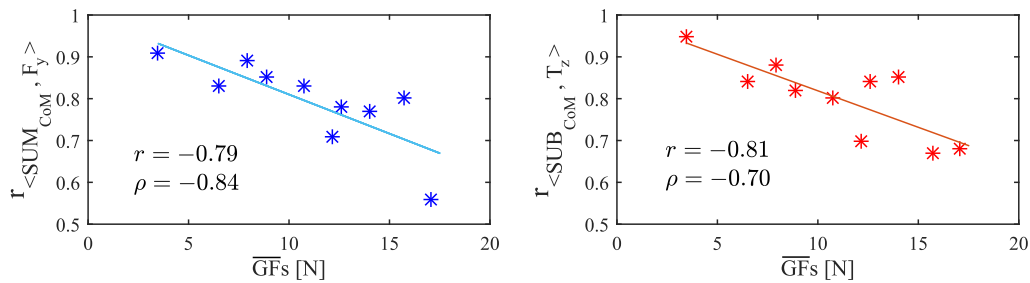


Fig. 3.15 GF 's effect on the couplings between $\langle SUM_{CoM}, F_y \rangle$ and $\langle SUB_{CoM}, T_z \rangle$ (1st order functions superimposed).

As Figure 3.15 shows, despite not having a large number of samples, the impact of the GF on the linkage between F_y , T_z and the proposed control variables is quite clear. Pearson and Spearman's rank-order correlation coefficients are: $r = -0.79$ ($p = 0.0064$), $\rho = -0.84$ ($p = 0.0024$) for GF and $r_{\langle SUM_{CoM}, F_y \rangle}$ and $r = -0.81$ ($p = 0.0048$), $\rho = -0.70$ ($p = 0.03$) for the same variable and $r_{\langle SUB_{CoM}, T_z \rangle}$. The value of the coefficients imply a high negative correlation of both types Pearson and Spearman's rank-order. This fact reveals the existence of an strongly monotonic and linear relationship between the degree of coupling of the two pair of variables and the exerted GF . This way, higher gripping forces presumably lead to a worse control of the device and, therefore, to a poorer driving experience.

3.2.3 Grip force impact on $CoMs$ excursion (E2)

As said at the beginning of this section, during the preliminary test explained in Chapter 2, certain lack of response was perceived when high grip forces were exerted. It probably has to do with a reduction of the excursion of the centers of mass. $CoMs$ ' excursion could be defined as the maximum distance that $CoMs$ can cover through the sensors arrays while

using the tactile handlebar. An experiment (**E2**) was designed to analyze if the gripping force affects the CoM excursion and limits it somehow. Figure 3.16 shows the experimental setup scheme. The handlebar was fixed to a support clamped to a laboratory table. Pressure data from tactels and F_y and T_z from the F/T sensor were gathered by a computer at 60Hz. Seven volunteers (P1-P7) from 21 to 32 with a mean age of 26.9 years took part in this study after agreement and informed consent. They were given instructions to realize a set of maneuvers (see Figure 3.17). Firstly, they would grasp the handlebar and perform the following sequence:

1) Rest condition (R.C.)³ → push → rest condition → pull → rest condition.

They had to keep the current condition (push, rest or pull) at least for one second before changing to the next state. After this first test, they were asked to carry out a new sequence:

2) Rest condition → left turn → rest condition → right turn → rest condition.

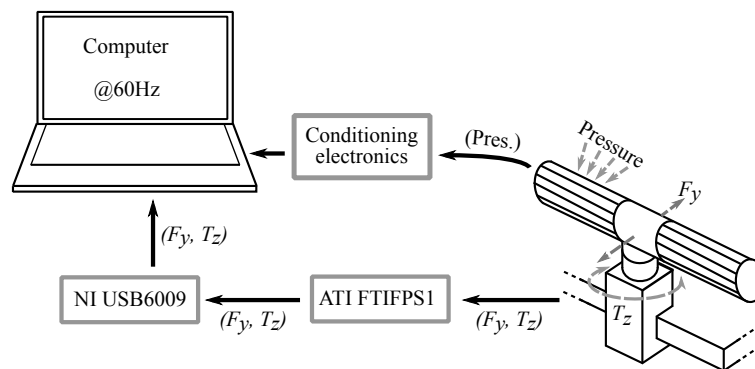


Fig. 3.16 Experimental setup scheme of E2. The handlebar is fixed to a laboratory table.

The described sequences were repeated three times, each with a different gripping force: grasping the handlebar weakly, in a normal⁴ way and strongly. "Weakly", "normal" and "strongly" are subjective terms and, for example, what is a weak grasping for an user can be strong for another. The purpose of giving the participants these commands was to ensure the availability of the typical maneuvers carried out with different gripping forces by the same person, in the same conditions. Considering the three kinds of grips for both types of maneuvers, there are forty-two tests, twenty-one for push/pull exercises and another twenty-one for turns. All of them were low-pass filtered to reduce noise.

Figures from 3.18 to 3.20 show the data collected for every participant during the sequence of push/pull maneuvers. Moreover, data captured for the sequence of turn maneuvers are plotted in Figures from 3.21 to 3.23. Note that there are four graphs per participant. For the

³Let us remind that it consists in just keeping the handles grasped.

⁴They grasped the handles in a way they considered normal or natural.

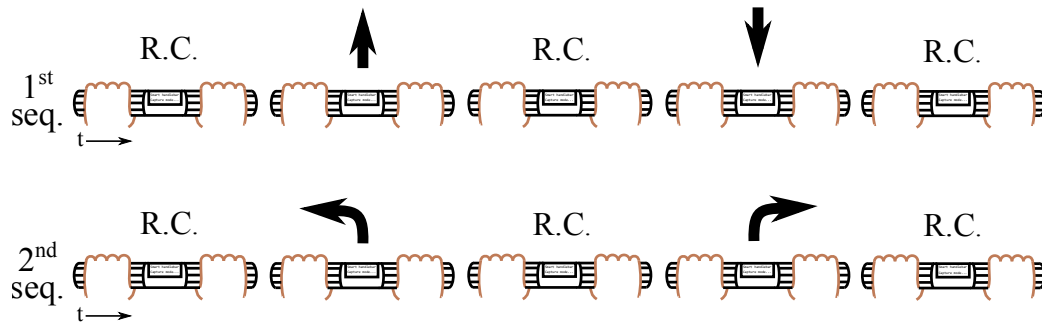


Fig. 3.17 During the 1st sequence P/P maneuvers are exerted (top). In the 2nd sequence, turns are performed (bottom).

first kind of series (Fig. 3.18 - 3.20), the upper two represent in y -axis the variation of the center of mass of each hand, CoM_L and CoM_R , with respect to F_y , in x -axis. $CoMs$ appear normalized so that they are expressed in tactel coordinates⁵. The lower two are the linear approximation of the two previous functions. Regarding the second sequence (Fig. 3.21 - 3.23), the presented information is the same of the previous case but changing F_y by T_z .

Note that in most of the upper charts of the figures, there is a group of samples around the vertical line of $F_y = 0$ and $T_z = 0$. These are the $CoMs$ associated to the very first moments in which the hands begin to wrap the tactels and, in this experiment, they should be ignored since the handlebar is not yet firmly grasped during their computation. Although they are displayed in the charts, they are not used in the calculations. Besides, due to the position of the F/T reference sensor in the experimental setup of E2, F_y appears inverted with respect to how it was shown in the results of the experiment E1 (Figures 3.8 and 3.9). In spite of not being a key issue, it has to be taken into account if both charts are compared.

Pearson and Spearman's rank-order correlation coefficients were calculated to assess the degree of linear and monotonic coupling between the center of mass of each hand (CoM_L and CoM_R) and F_y , for the 1st sequence of maneuvers, and T_z for the 2nd sequence. The values of the coefficients can be consulted in Tables A.1 and A.2, in Appendix A. Correlation is strong for most of the tests. This already happened with the control variables SUM_{CoM} and SUB_{CoM} so, despite not being strictly necessary from the mathematical point of view, it seems a quite natural consequence.

Figures 3.18-3.23 help understand the way the GF impacts on the $CoMs$ excursion. The 1st order functions obtained by linear regression present a slope that clearly decreases as the grip passes from "weak" to "normal" and from "normal" to "strong", both for the push/pull

⁵For example, if the normalized CoM value is '3', it means that this parameter is located on the 3rd tactel of the tactile array (see Figure 2.16), or in other words, the tactel with the coordinate $y = 3$ (see Equation 2.5)

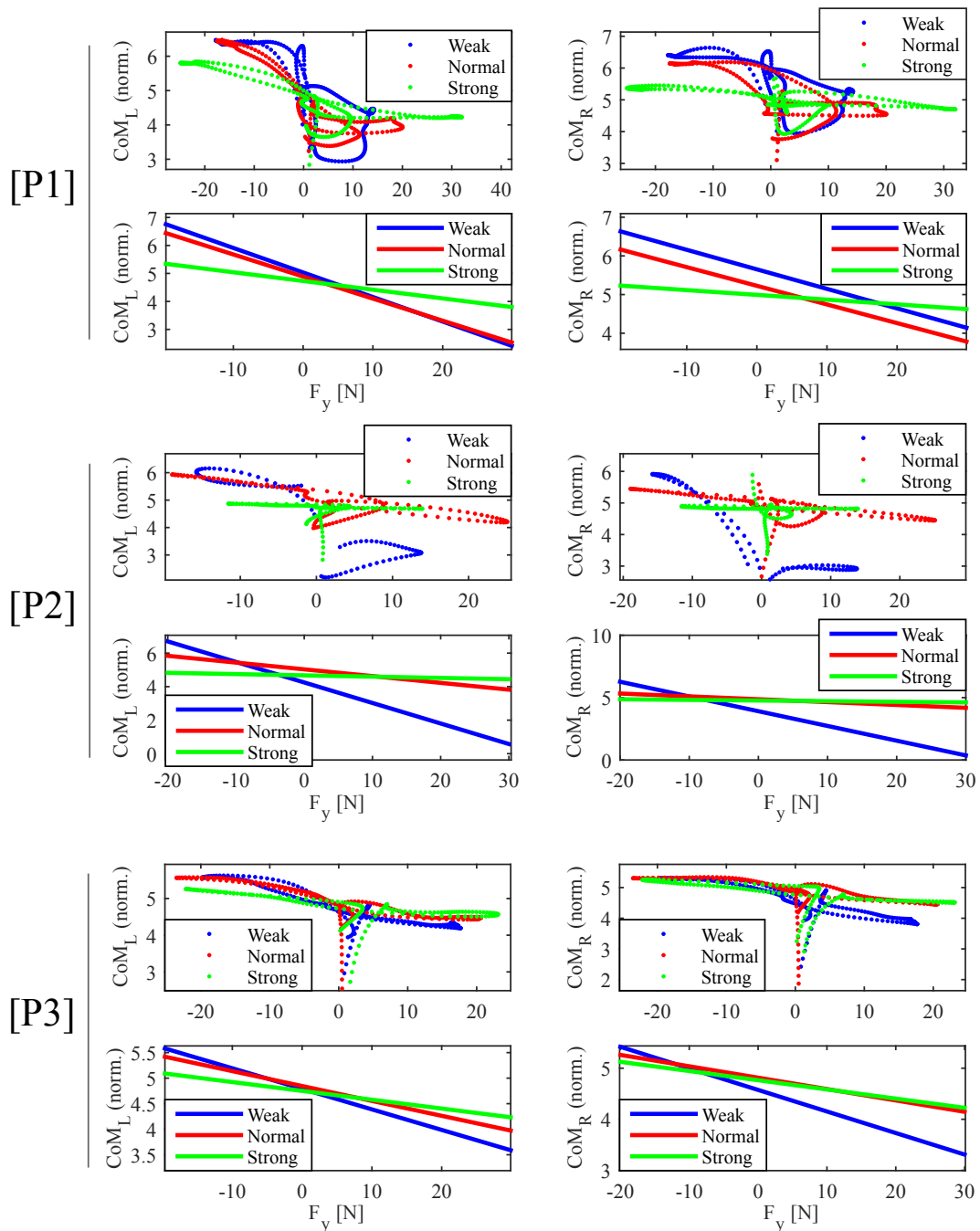


Fig. 3.18 Participants P1-P3: CoM_L and CoM_R versus F_y (upper graphs) during P/P maneuvers (1st sequence). Linear approximations (lower graphs). The

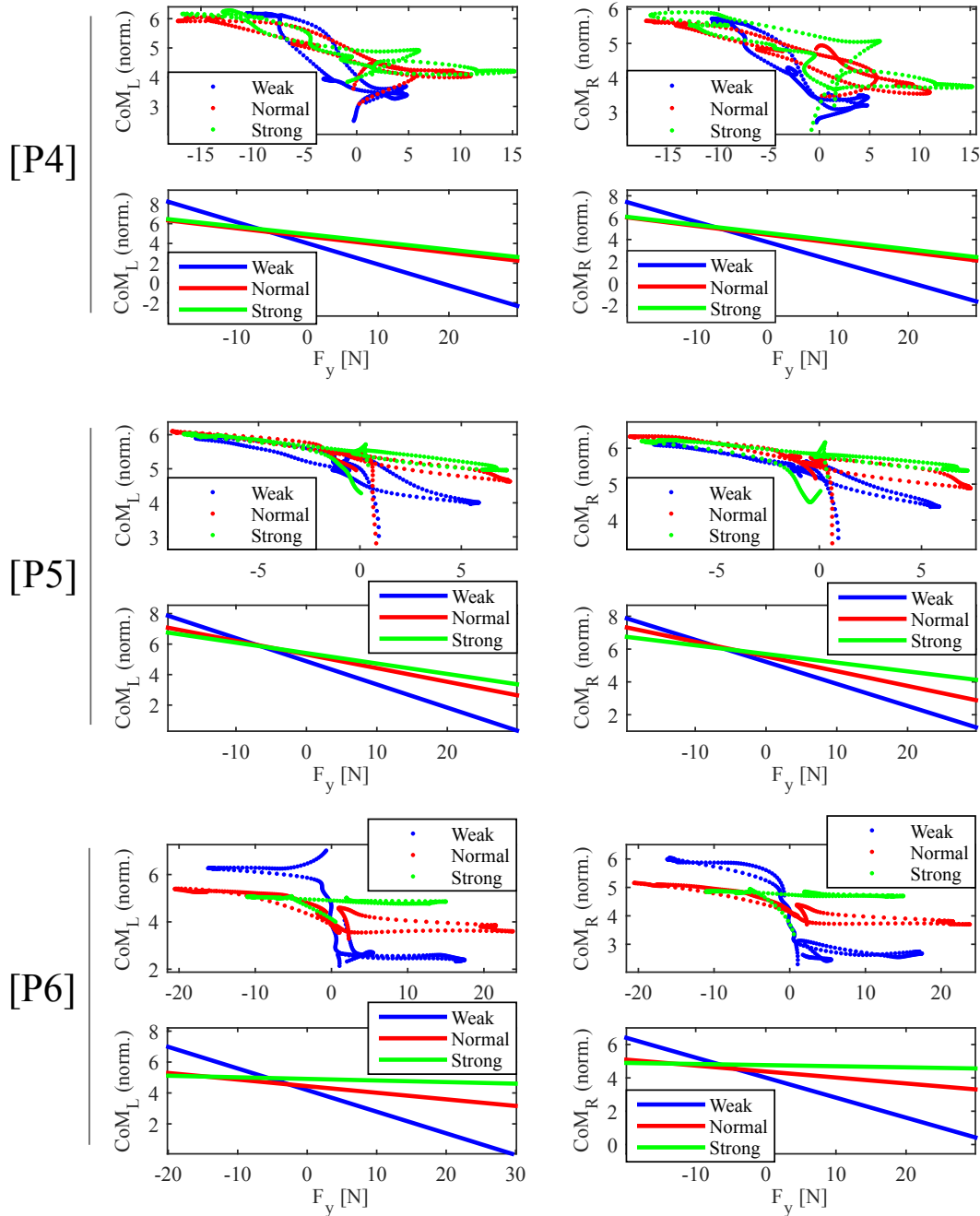


Fig. 3.19 Participants P4-P6: CoM_L and CoM_R versus F_y (upper graphs) during push/pull maneuvers (1st sequence). Linear approximations (lower graphs).

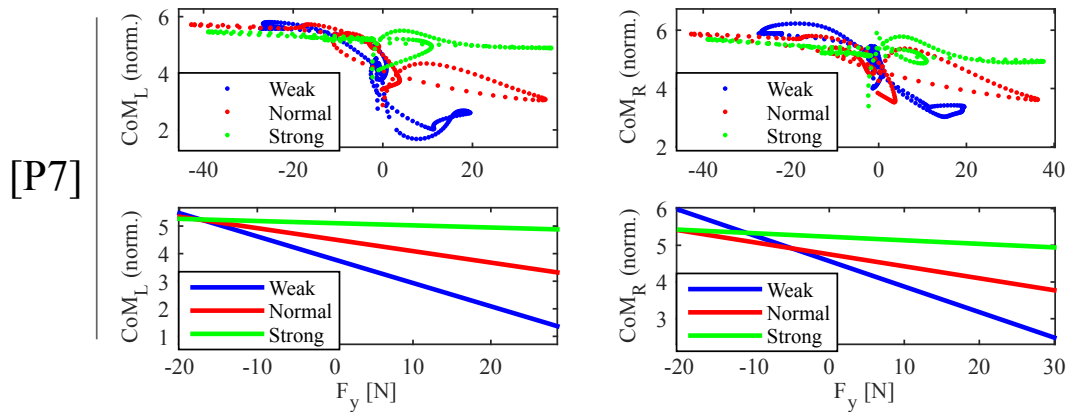


Fig. 3.20 Participant P7: CoM_L and CoM_R versus F_y (upper graphs) during push/pull maneuvers (1st sequence). Linear approximations (lower graphs).

and for the turn sequences. This is a phenomenon that affects all the tests performed by the participants so that it could be reasonable to think that the higher the gripping force, the lower the CoM excursion is. An analysis of the GF evolution and the tactels response could throw some light on the causes behind this effect. As said before, the parameter GF quantifies the force exerted when grasping the handles. Hence, it can be as well altered as the steering is carried out (see Equation 3.9 to remember how it is calculated). This effect is more accentuated in this experiment, in which the handlebar does not rotate around its axis nor moves forward or backward, since the participants exert forces on an immobile structure (there is no movement as response to force stimuli). We could consider that the GF is formed by two components: the force exerted to keep the handlebar grasped and that applied when making maneuvers.

Given the above, what has been observed seems to suggest that the higher GF , the higher the component of the parameter due exclusively to the grip is and the lower the part that correspond to the maneuver itself. Figure 3.24 shows this: the lower two chart display T_z (in blue) and the GF on the handlebar (GF_{HB} , in red) and they belong to the sequence of turns of one participant who was applying a "weak" grip. The GF component due to force exerted during the left and right turns is well visible just by comparing the variations in time of the pressure-based parameter (dashed rectangles) and the ATI Mini45 torque output. In the two central graphs, that correspond to the "normal" grip exercise of the same subject, the influence of the maneuvers in GF is still perceptible, although the "offset" caused by the grasp is higher. Finally, the two uppers correspond to the performance of the same sequence, this time with a "strong" grip. As can be seen, GF is mostly provoked by the handle grasp;

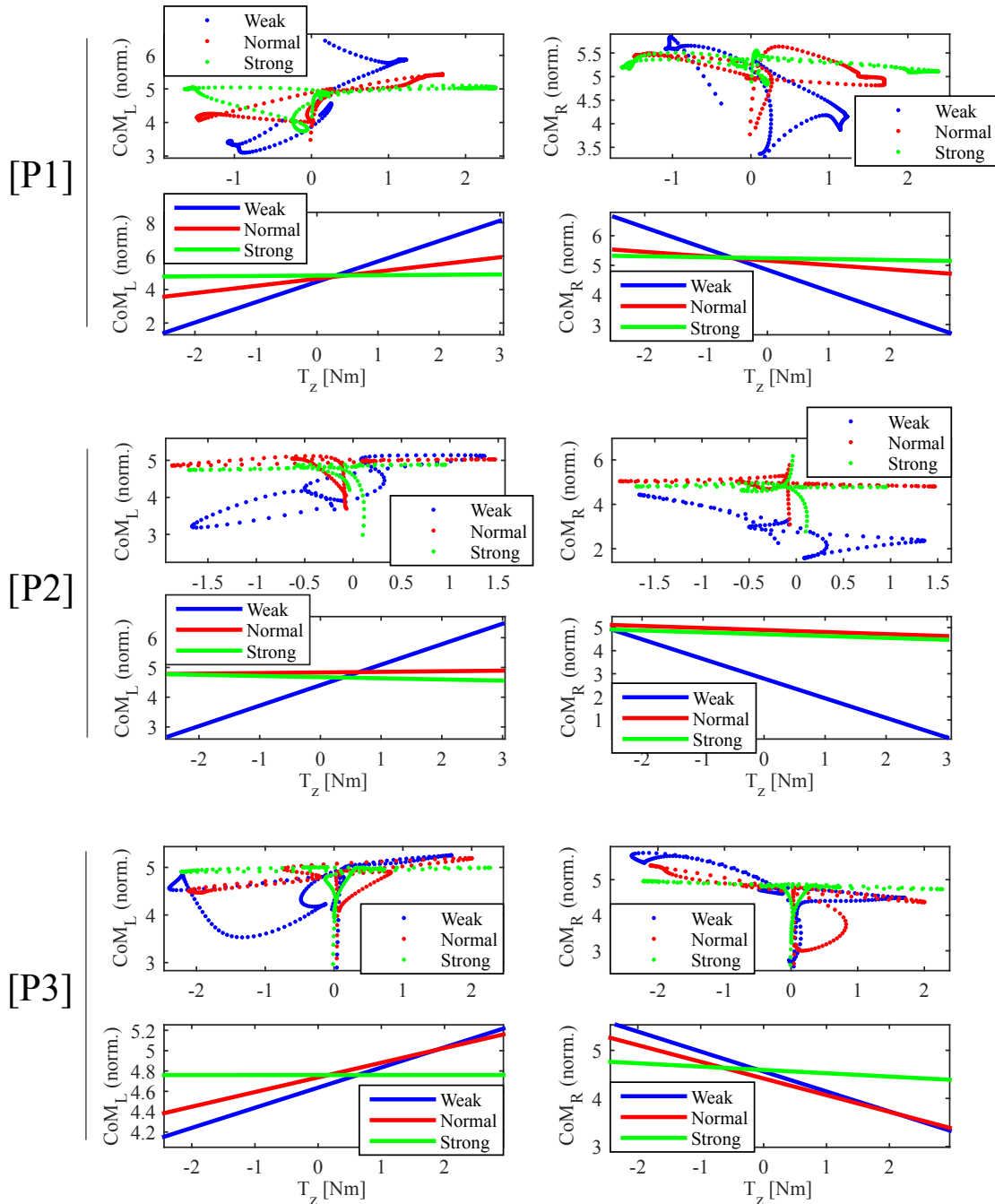


Fig. 3.21 Participants P1-P3: CoM_L and CoM_R versus T_z (upper graphs) during turn maneuvers (2nd sequence). Linear approximations (lower graphs). The

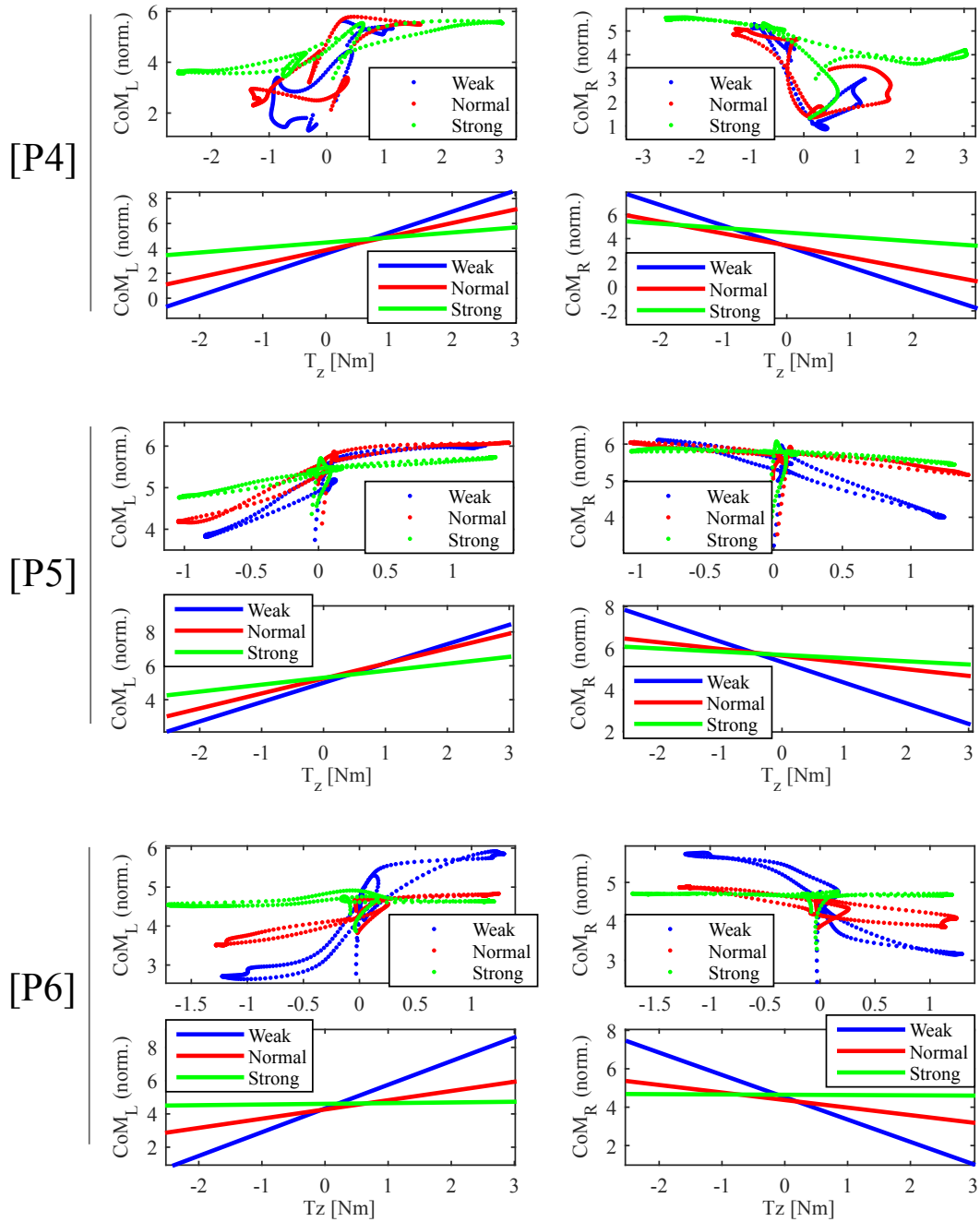


Fig. 3.22 Participants P4-P6: CoM_L and CoM_R versus T_z (upper graphs) during turn maneuvers (2nd sequence). Linear approximations (lower graphs).

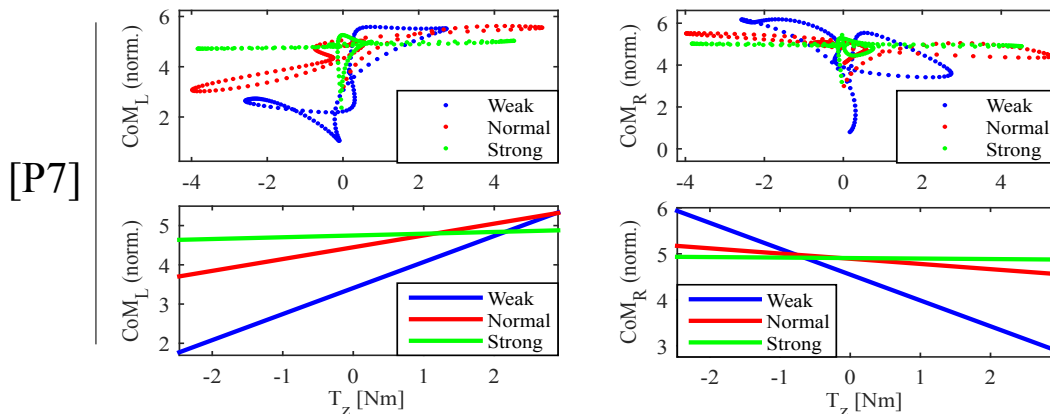


Fig. 3.23 Participant P7: CoM_L and CoM_R versus T_z (upper graphs) during turn maneuvers (2nd sequence). Linear approximations (lower graphs).

it is flat a considerable part of the time and is almost unaffected by the turns exercises. As shown in the figure, the CoM excursion has gone down from 53.04mm to 21.36mm, and from 21.36mm to 6.54mm as the GF increased.

Another consequence of high gripping forces is the saturation of the pressure sensors. During the tests of E2, some tactels reached saturation. Those that did it firstly were the 4th and the 5th of the tactile array (see Figure 2.16). In the tests in which the participants applied "weak" grip force none of the tactels reached that condition. In some of those with "normal" grip force, the 4th and the 5th started being saturated for two participants. In one test also the 7th was in this condition. When they were said to exert "strong" grip force, the output of some of the tactels appeared saturated in all the trials. In the worst case, this output was saturated for up to five tactels. In the test in which the tactile sensor was less saturated, the output of three tactels presented this condition.

As said, the saturation of the tactels response makes their output constant, and prevent the pressure variation applied while performing maneuvers from being captured by the system. A tactile output that does not change results in an immobile center of mass. This way, saturation can be considered with certainty one of the causes behind the CoM excursion reduction. Nevertheless, it must be borne in mind that, as showed in Figures 3.18-3.23, the excursion also decreases when switching from "weak" to "normal" grip. In fact, for the example of Figure 3.24, this parameter has been halved when passing from the lower to the central graphs. For this case, the tactels response during the "normal" grip exercise was that showed in Figure 3.25.

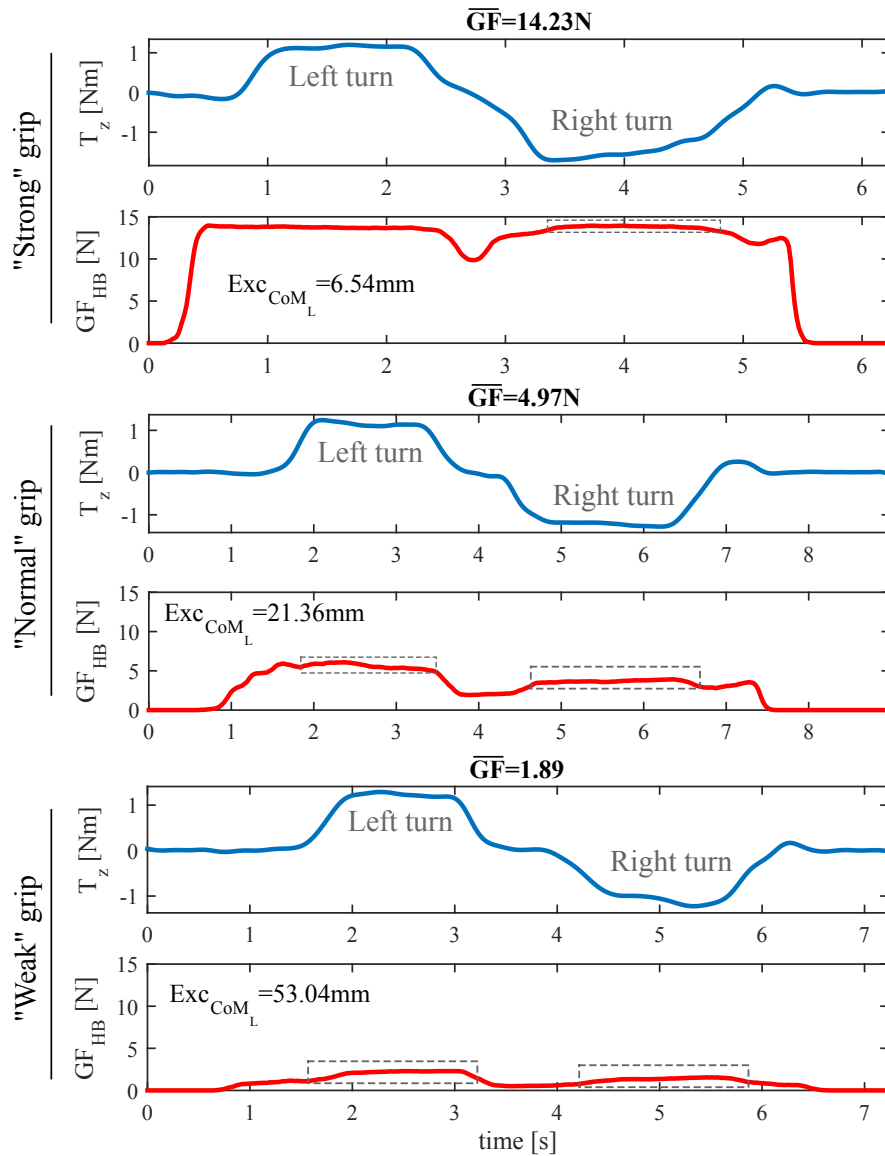


Fig. 3.24 From top to bottom: T_z and GF_{HB} during the performance of the sequence of turns of E2 by one average participant for "strong", "normal" and "weak" grip.

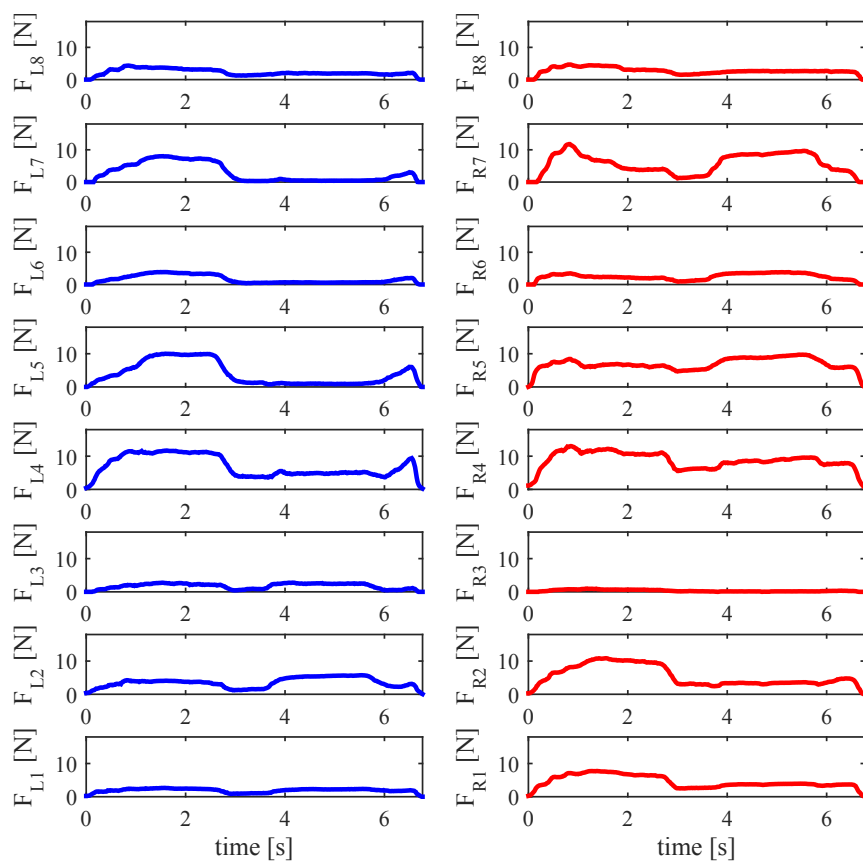


Fig. 3.25 Output of the tactels of the left (in blue) and right (in red) handles during the "normal" grip exercise plotted in Figure 3.24.

As observed, all of them are far from reaching saturation and, therefore, the tactual saturation can not be the only explanation for the effect that is being studied. What the data seems to show is that the lack of excursion could also have an anatomic nature. In other words, as hands increase the gripping force, they would experience a growing loss of their capacity to introduce pressure variations. This way, the force component responsible for performing maneuvers decreases as that used to keep the handles grasped increases.

3.2.3.1 Correction of GF effect on $CoMs$ excursion

The direct consequence of the behavior explained above is that the output of the system is affected by the GF in terms of the powered wheelchair linear and angular speeds. Attendants who tend to grasp stronger will need to push, pull or turn stronger than those who grasp weaker in order to get the same speeds. Thus, it is necessary to add some kind of correction that minimizes this adverse effect. A way to proceed could consist in making the output gain dependent of the GF . For that purpose, the data from experiment E2 can be used.

Following this approach, all the tests belonging to the 1st and 2nd sequences were classified into several groups or categories according to the mean gripping force (\overline{GF}) exerted during the whole of their performance. The groups, whose lower and upper limits are expressed in tactual digital output units⁶, were:

- G_1 for the interval 0-100 (0-1.76N)
- G_2 for 100-200 (1.76-3.52N)
- G_3 for 200-300 (3.52-5.27N)
- G_4 for 300-400 (5.27-7.03N)
- G_5 for 400-600 (7.03-10.54N)
- G_6 for \overline{GF} s above 600 (10.54N)

This way, if four tests had \overline{GF} s of 0.67N, 1.81N, 2.83N and 13.60N, the first would be in G_1 , the second and the third in G_2 and the fourth in G_6 . The groups were made separately for the tests of the 1st (G_{PP}) and the 2nd (G_T)⁷ sequence of E2, for which the maneuvers involved were pushing/pulling and turns, respectively. As seen in Figures 3.18-3.23, 1st order

⁶The conversion from DOU to Newtons can be done with the expression introduced in section 3.2.1.

⁷'PP' stands for "push/pull" whereas 'T' comes from "turns".

functions were calculated as linear approximations of each test result. These functions can be expressed as:

$$\begin{aligned} CoM_{PP_{L_{LIN}}} &= aF_y + b \\ CoM_{PP_{R_{LIN}}} &= cF_y + d \end{aligned} \quad (3.10)$$

for the sequence of push/pull maneuvers, and:

$$\begin{aligned} CoM_{T_{L_{LIN}}} &= eT_z + f \\ CoM_{T_{R_{LIN}}} &= gT_z + h \end{aligned} \quad (3.11)$$

for the sequence of turns. a, b, c, d, e, f, g and h are constants.

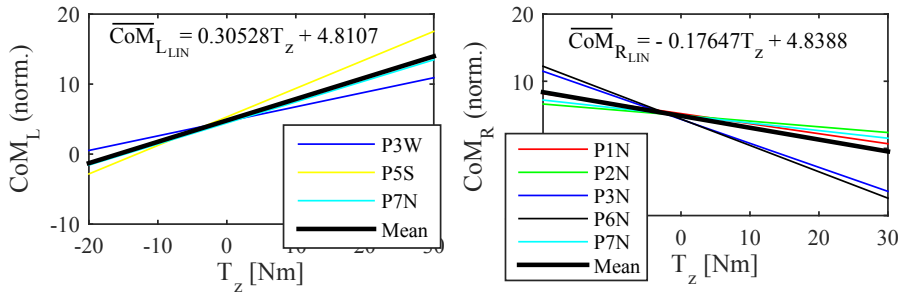


Fig. 3.26 1st order approximations for the tests included in the category G_{T_3} and mean of these functions (thicker line in black) for the left and the right handle.

Figure 3.26 displays, for example, the linear approximations of the tests inside G_{T_3} , which includes the trials from the sequence of turns with a \overline{GF} between 200(3.52N) and 300(5.27N). Specifically, G_{T_3} contains for CoM_L the tests from the participants P3, P5 and P7, whose intention was applying a "weak", "strong" and "normal" gripping force, respectively. For the CoM_R , tests from P1, P2, P3, P6 and P7 are in this category, all of them corresponding to "normal" gripping force exercises. The thicker black line in both graphs represents the mean of the linear functions of the category G_{T_3} . This mean is indeed used as a way to summarize the information provided by the trials included in each category. It can be computed as shown in Equations 3.12 and 3.13.

$$\begin{aligned} \overline{CoM}_{L_{LIN}G_{PPj}} &= \frac{\sum_{i=1}^N CoM_{PP_{L_{LIN}i}}}{N} = F_y \frac{\sum_{i=1}^N a_i}{N} + \frac{\sum_{i=1}^N b_i}{N} = \bar{a}F_y + \bar{b} \\ \overline{CoM}_{R_{LIN}G_{PPj}} &= \frac{\sum_{i=1}^N CoM_{PP_{R_{LIN}i}}}{N} = F_y \frac{\sum_{i=1}^N c_i}{N} + \frac{\sum_{i=1}^N d_i}{N} = \bar{c}F_y + \bar{d} \end{aligned} \quad (3.12)$$

$$\begin{aligned}\overline{CoM}_{LLING_{T_j}} &= \frac{\sum_{i=1}^N CoM_{T_{LLIN_i}}}{N} = T_z \frac{\sum_{i=1}^N e_i}{N} + \frac{\sum_{i=1}^N f_i}{N} = \bar{e}T_z + \bar{f} \\ \overline{CoM}_{RLING_{T_j}} &= \frac{\sum_{i=1}^N CoM_{T_{RLIN_i}}}{N} = T_z \frac{\sum_{i=1}^N g_i}{N} + \frac{\sum_{i=1}^N h_i}{N} = \bar{g}T_z + \bar{h}\end{aligned}\quad (3.13)$$

where N is the number of tests of the group G_{PP_j} (Eq 3.12) or G_{T_j} (Eq 3.13); i refers to each particular test belonging to G_{PP_j} (Eq 3.12) or G_{T_j} (Eq 3.13). $CoM_{PP_{LLIN_i}}$, $CoM_{PP_{RLIN_i}}$, $CoM_{T_{LLIN_i}}$ and $CoM_{T_{RLIN_i}}$ are computed using the expressions in Equations 3.10 and 3.11.

Table 3.2 Gradients of the mean of the linear functions for the tests in the categories associated with push/pull maneuvers (second column for CoM_L and third for CoM_R). Gradient of SUM_{CoM} computed from the latter (fourth column). Accumulated $m_{SUM_{CoM}}$ decline (fifth row).

Category (\overline{GF})	\bar{a}	\bar{c}	$m_{SUM_{CoM}} (\bar{a} + \bar{c})$	$dec_{G_{PP1} \rightarrow G_{PP1+i}}$
G_{PP1} (0-100)	-0.1323	-0.1459	-0.2782	-
G_{PP2} (100-200)	-0.0670	-0.1201	-0.1871	1.487
G_{PP3} (200-300)	-0.0547	-0.0600	-0.1147	2.426
G_{PP4} (300-400)	-0.0405	-0.0390	-0.0795	3.500
G_{PP5} (400-600)	-0.0295	-0.0196	-0.0491	5.661
G_{PP6} (600+)	-0.0111	-0.0098	-0.0209	13.325

Table 3.3 Gradients of the mean of the linear functions for the tests in the categories associated with turns maneuvers (second column for CoM_L and third for CoM_R). Gradient of SUB_{CoM} computed from the latter (fourth column). Accumulated $m_{SUB_{CoM}}$ decline (fifth row).

Category (\overline{GF})	\bar{e}	\bar{g}	$m_{SUB_{CoM}} (\bar{e} - \bar{g})$	$dec_{G_{T1} \rightarrow G_{T1+i}}$
G_{T1} (0-100)	1.0470	-1.0525	2.0995	-
G_{T2} (100-200)	0.4729	-0.6288	1.1017	1.906
G_{T3} (200-300)	0.3053	-0.1765	0.4818	4.358
G_{T4} (300-400)	0.1429	-0.1547	0.2975	7.057
G_{T5} (400-600)	0.0320	-0.0390	0.0711	29.547
G_{T6} (600+)	0.0296	-0.0293	0.0589	35.642

On the other hand, Tables 3.2 and 3.3 list the gradients of the mean functions calculated for the groups G_{PP1} - G_{PP6} and G_{T1} - G_{T6} , computed as showed in Equations 3.12 and 3.13. Moreover, from the latter, the mean slope of the parameters SUM_{CoM} and SUB_{CoM} have also been computed. Since $SUM_{CoM} = CoM_L + CoM_R$ and $SUB_{CoM} = CoM_L - CoM_R$, these variables are affected by the dependance of CoM on F_y and T_z in Equations 3.10 and 3.11.

From the expression of SUM_{CoM} and SUB_{CoM} and using the latter equations, the slope or gradient of both parameter can be obtained as:

$$\begin{aligned} m_{SUM_{CoM}} &= a + c \\ m_{SUB_{CoM}} &= e - g \end{aligned} \quad (3.14)$$

Finally, the last columns of each table show how $m_{SUM_{CoM}}$ and $m_{SUB_{CoM}}$ decrease as switching from one category to the other with higher GF . The comparisons between the slopes are made with respect to the first groups, G_{PP1} and G_{T1} , which present the highest value of this parameter. For example, looking at the third row of Table 3.2, $dec_{G_{PP1} \rightarrow G_{PP3}}$ is $-0.2782 / -0.1147 = 2.426$; in other words, $m_{SUM_{CoM_{G_{PP3}}}}$ would have to be multiplied by $dec_{G_{PP1} \rightarrow G_{PP3}}$ in order to be equal to $m_{SUM_{CoM_{G_{PP1}}}}$. These values are used to build the variable gain curves, that are shown in Figure 3.27.

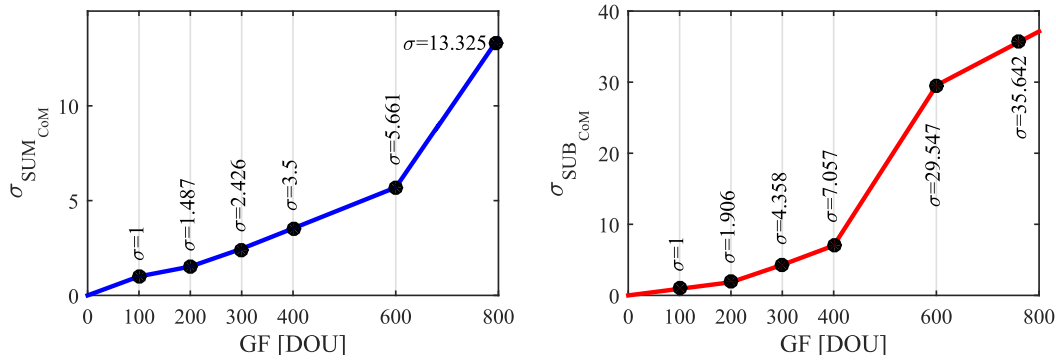


Fig. 3.27 Gripping force-dependent gain functions for SUM_{CoM} (left) and SUB_{CoM} (right).

The left chart shows $\sigma_{SUM_{CoM}}$, that is the gain function for the parameter SUM_{CoM} . In the right part the variable gain for SUB_{CoM} , $\sigma_{SUB_{CoM}}$, is plotted. Note that for the upper values of the first groups, G_{PP1} and G_{T1} , there is no amplification ($\sigma = 1$). Besides, from these points to zero, both functions introduce an attenuation whose purpose is to reduce linear and angular speeds until a minimum level of GF is reached. It prevents very weak and not firm grips from causing unexpected and unsafe PW movements. The remaining part of the curves, that with $GF > 100$, has been built by linear interpolation between the values of the parameters $dec_{G_{PP1} \rightarrow G_{PP1+i}}$ and $dec_{G_{T1} \rightarrow G_{T1+i}}$. Note that G_{PP6} and G_{T6} have lower (600) but not upper limit. The upper GF values used in the interpolation for these groups come from to the tests that presented the maximum \overline{GF} (794DOU in push/pull sequence and 761DOU in turns sequence).

The above provides a method to mitigate the effect of GF on the $CoMs$ excursion. Lower CoM excursions provoked by higher GFs are compensated with a greater amplification intro-

duced by $\sigma_{SUM_{CoM}}$ and $\sigma_{SUB_{CoM}}$. Therefore, the effect of increasing GF on the slope of the control parameters is minimized. Their slope after the correction is shown in Equation 3.15:

$$\begin{aligned} m_{SUM_{CoM}_{corrected}} &= \sigma_{SUM_{CoM}} \cdot m_{SUM_{CoM}} \\ m_{SUB_{CoM}_{corrected}} &= \sigma_{SUB_{CoM}} \cdot m_{SUB_{CoM}} \end{aligned} \quad (3.15)$$

3.3 Study of the effect of the arrangement of the tactile array (E3)

Wider CoM excursions result in a bigger range of variation of the variables SUM_{CoM} and SUB_{CoM} , which in turn allows assistants to have a larger control of the device. The arrangement of the tactels inside the tactile cover was shown in Chapter 2, Figure 2.16 left. $CoMs$ are calculated as was shown in Equation 2.5. In the latter, the variable y represents the position of each tactel in the array, what depends on the organization that has been considered to compute the CoM . This is not trivial or irrelevant. For a particular tactile image, if the tactel that is taken as the beginning of the array ($y = 1$) changes, the resulting CoM also varies. Table 3.4 help clarify this fact. The first column gathers the values of y in Equation 2.5. The following columns list the correspondence between each value of y and a real tactel of the handle. Looking at Figure 2.16, we can see that the second column, *arrangement A*, represents the "original" configuration, i.e. that that has been used so far. *Arrangement B* consists in rotating anticlockwise the tactels order one position. In *arrangement C*, the tactels configuration has been rotated anticlockwise two positions with respect to *arrangement A* and so on. Considering CoM_A , CoM_B and CoM_C the centers of mass computed for these three tactels configurations, it is possible that $CoM_A \neq CoM_B \neq CoM_C$ even when the same tactile image has been used for all of them.

The original configuration proposed in Figure 2.16 makes the $CoMs$ decrease when the handles are pushed (they move towards tactels for which y is low) and increase when they are pulled ($CoMs$ move to tactels with high y), providing a good identification of the performed maneuvers (as showed in Section 3.1.2.2). Nonetheless, the results that can be obtained by choosing other array arrangements were not explored.

An experiment (**E3**) was designed to explore the influence of changes in the array configuration in the parameters of interest. The experimental setup was very similar to that of Figure 3.16 for the experiment E2, but with the difference that the handlebar was fixed to a PW. Twelve participants took part in the experiment after agreement and informed consent, and without knowledge of its purpose. They were between 26 and 63 years old, with a mean

Table 3.4 Example of different arrangements of the tactile array. From one to the next, the beginning of the array is rotated one position. y refers to the variable of Equation 2.5.

y	Arr. A	Arr. B	Arr. C	Arr. D	Arr. E	Arr. F	Arr. G	Arr. H
1	1st	2nd	3rd	4th	5th	6th	7th	8th
2	2nd	3rd	4th	5th	6th	7th	8th	1st
3	3rd	4th	5th	6th	7th	8th	1st	2nd
4	4th	5th	6th	7th	8th	1st	2nd	3rd
5	5th	6th	7th	8th	1st	2nd	3rd	4th
6	6th	7th	8th	1st	2nd	3rd	4th	5th
7	7th	8th	1st	2nd	3rd	4th	5th	6th
8	8th	1st	2nd	3rd	4th	5th	6th	7th

age of 38.6 years. They were asked to carry out twice each of the sequences presented in the experiment E2 (see Figure 3.17). Moreover, they would do it with the handlebar adjusted at the minimum ($h_1 = 98.5\text{cm}$) and maximum ($h_2 = 108\text{cm}$) height allowed by the settings of the used PW (F35 by Sunrise Medical). They were not given any specification about how to grasp the handlebar. The total number of performed tests was forty-eight for the each handlebar height (twenty-four tests for the sequence of push/pull maneuvers and another twenty-four for the sequence of turns). All of them were filtered in order to reduce noise before being analyzed.

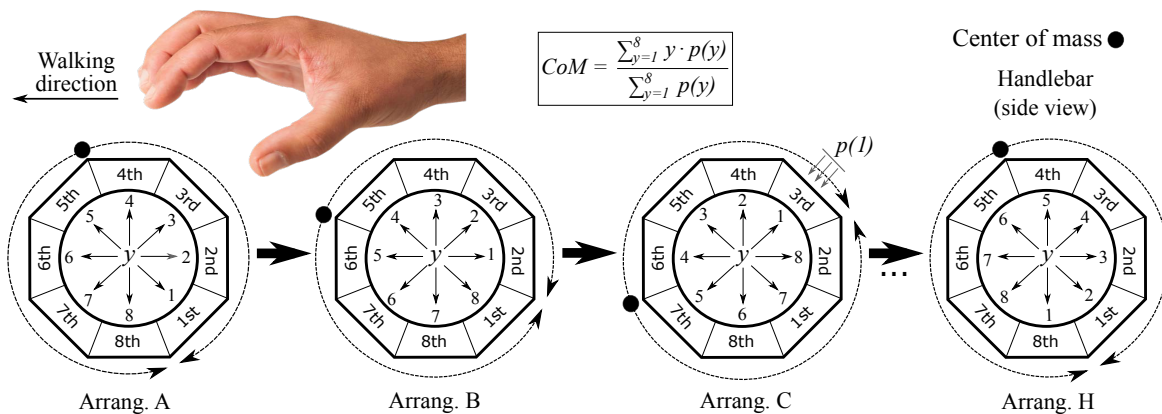


Fig. 3.28 Tactels arrangements for the calculation of the CoM of the tests from the experiment E3.

For every trial, the CoM of the left and the right handle was computed eight times, using the eight different tactels configurations presented in Table 3.4. The correspondence between the values of the variable y and the real tactels that they refer to can be better seen with the help of Figure 3.28. Excursion was calculated for CoM_A , CoM_B , CoM_C , CoM_D , CoM_E ,

CoM_F , CoM_G and CoM_H (the subindex represents the tactels arrangement for which the CoM is calculated). In Tables A.3- A.6 (Appendix A), the tactel arrangements that produced the maximum CoM excursion are given in the columns labeled $Arr_{1^{a}Exc}$. On the other hand, values in column $Arr_{2^{a}Exc}$ represent the tactels configurations whose CoM excursion was the second highest. In both columns, the normalized⁸ excursions are showed in brackets. Tables A.3 and A.4 list the results for height h_1 and tables A.5 and A.6 for h_2 . Figures 3.29-3.34 can help assess which arrangements provide a larger value of this parameter. They are made from the data of the previous tables.

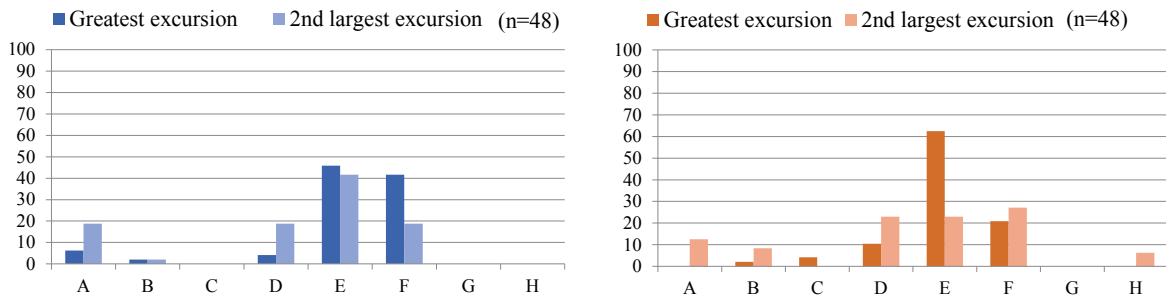


Fig. 3.29 Percentage of times that each tactel arrangement led to the maximum excursion (left chart - deeper blue for left handle, right chart - deeper orange for right handle). Percentage of times that each tactel arrangement led to the second largest excursion (left chart - lighter blue for left handle, right chart - lighter orange for right handle). All the test carried out with a handlebar height of h_1 were included.

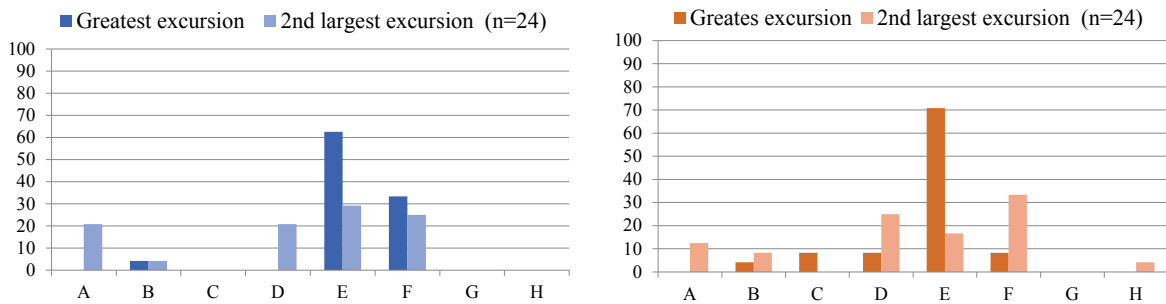


Fig. 3.30 Percentage of times that each tactel arrangement led to the maximum excursion (left chart - deeper blue for left handle, right chart - deeper orange for right handle). Percentage of times that each tactel arrangement led to the second largest excursion (left chart - lighter blue for left handle, right chart - lighter orange for right handle). Only the test carried out during the sequence of P/P maneuvers were included (height= h_1).

Figure 3.29 includes all the tests performed with the handlebar adjusted at h_1 . As can be seen, the tactels configuration for which CoM was the largest in a higher percentage of times

⁸They are expressed in terms of number of tactels. For example, if the normalized value is '2', it means that the CoM moves a maximum distance of two tactels in the array.

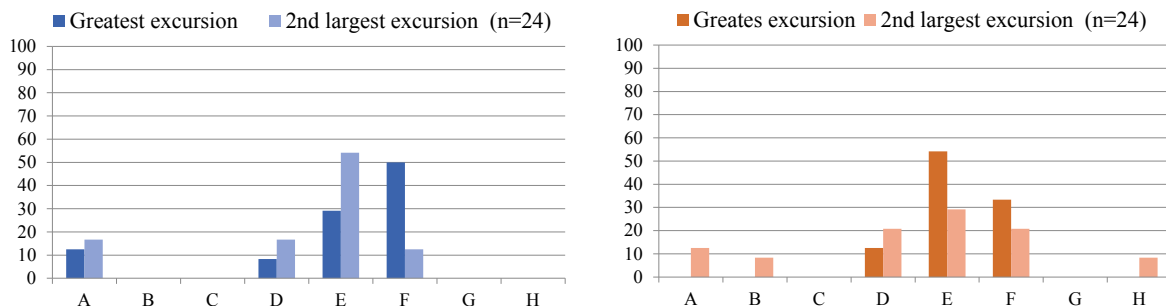


Fig. 3.31 Percentage of times that each tactel arrangement led to the maximum excursion (left chart - deeper blue for left handle, right chart - deeper orange for right handle). Percentage of times that each tactel arrangement led to the second largest excursion (left chart - lighter blue for left handle, right chart - lighter orange for right handle). Only the test carried out during the sequence of turns maneuvers were included (height= h_1).

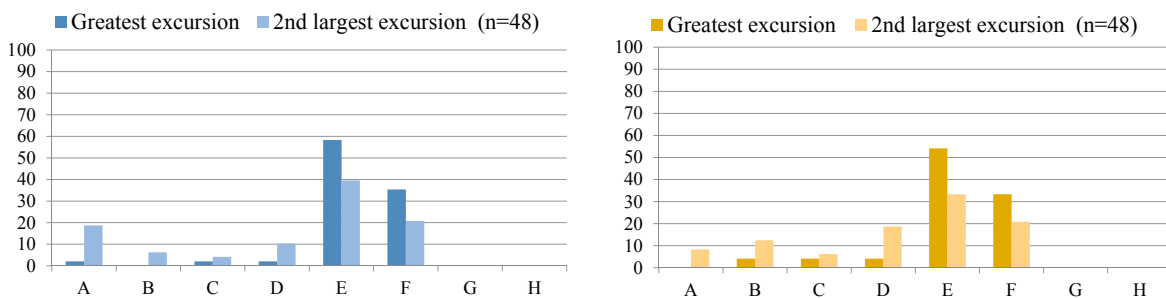


Fig. 3.32 Percentage of times that each tactel arrangement led to the maximum excursion (left chart - deeper blue for left handle, right chart - deeper yellow for right handle). Percentage of times that each tactel arrangement led to the second largest excursion (left chart - lighter blue for left handle, right chart - lighter yellow for right handle). All the test carried out with a handlebar height of h_2 were included.

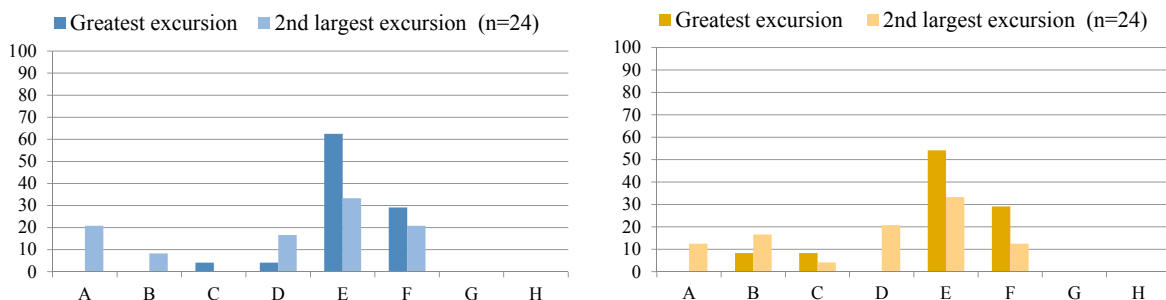


Fig. 3.33 Percentage of times that each tactel arrangement led to the maximum excursion (left chart - deeper blue for left handle, right chart - deeper yellow for right handle). Percentage of times that each tactel arrangement led to the second largest excursion (left chart - lighter blue for left handle, right chart - lighter yellow for right handle). Only the test carried out during the sequence of P/P maneuvers were included (height= h_2).



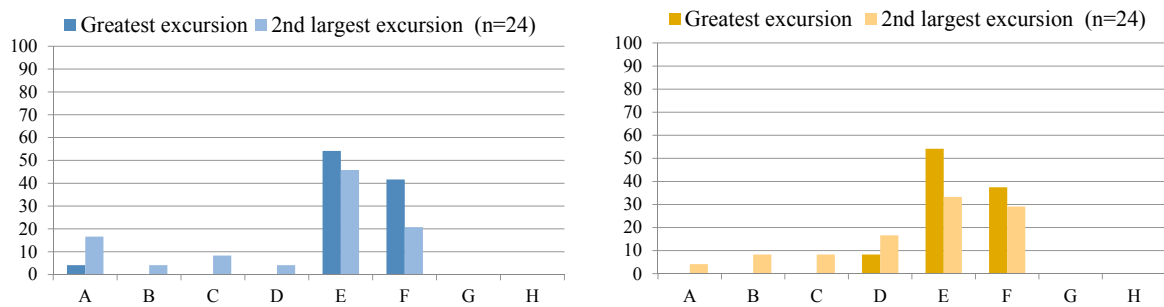


Fig. 3.34 Percentage of times that each tactel arrangement led to the maximum excursion (left chart - deeper blue for left handle, right chart - deeper yellow for right handle). Percentage of times that each tactel arrangement led to the second largest excursion (left chart - lighter blue for left handle, right chart - lighter yellow for right handle). Only the test carried out during the sequence of turns maneuvers were included (height= h_2).

was *arrang. E* (45.83% for the left and 62.5% for the right handle). The second configuration that stands above the rest is *arrang. F* (41.67% for CoM_L and 20.83% for CoM_R). The advantage of *arrang. E* is clear in all the trials, above all for the results computed from CoM_R (right charts in Figures 3.30 and 3.31). The only exception is the case of the results computed for the left handle in the tests performing turning maneuvers (see Figure 3.31 left). In this case, it was *arrang. F* that produced the best excursion (50% of times). However, for this particular category, *arrang. E* was the second configuration producing the highest value (21.17% of times) and the first leading to the second largest excursion (54.17% of times, lighter blue bar).

The tendency is the same if we look at the tests carried out at a height of h_2 (see Figures 3.32-3.34). The prevalence of *arrang. E* as that leading to the maximum excursion is clear (58.3% and 54.17% of times for CoM_L and CoM_R , respectively). Besides, the configuration with the second highest percentage of times producing the largest excursion is also *arrang. F* (35.42% and 33.3% of cases for CoM_L and CoM_R , respectively). The main difference between the results obtained for h_1 and those obtained for h_2 seems to lie in the fact that, at a height of h_2 , the behavior of both handles in terms of CoM excursion is much more symmetric. With the handlebar at h_2 the peculiarity found for the CoM_L excursion during turns commented in the previous paragraph (*arrang. F* was better than *arrang. E* in one of the graphs) is not observed. The absence of more significant dissimilarities may be due to the fact that, in spite of being the maximum range of adjustment that the PW allowed, the difference between the two heights, h_1 and h_2 , is not very large.

The data show that selecting the area marked in Figure 3.35 left (approximately where *arrang. E* and *F* have their tactel with $y = 1$) as the beginning of the tactile array can be appropriate to have good CoM excursions. In fact, the results of the experiments show that

the *arrangement E* is the best to compute *CoMs*. It is not only the tactels configuration that produced the biggest excursion more often but, in the majority of cases in which other arrangement achieved this goal, *arrang. E* led to the second largest excursion (see lighter color bars in the previous diagrams). Nevertheless, the latter would be a good choice only if the couplings between the control variables and F_y and T_z showed by the results of experiment E1 were not affected. This way, it seems pertinent to recalculate correlations of E1 with the new arrangement of tactels. For the pair SUB_{CoM} and T_z , the new results⁹ are: $r = 0.95$ [P1], $r = 0.94$ [P2], $r = 0.91$ [P3], $r = 0.94$ [P4], $r = 0.79$ [P5], $r = 0.89$ [P6], $r = 0.82$ [P7], $r = 0.40$ [P8], $r = 0.83$ [P9], $r = 0.90$ [P10]. For the couple formed by SUM_{CoM} and F_y they are: $r = 0.91$ [P1], $r = 0.92$ [P2], $r = 0.91$ [P3], $r = 0.88$ [P4], $r = 0.74$ [P5], $r = 0.86$ [P6], $r = 0.85$ [P7], $r = 0.81$ [P8], $r = 0.59$ [P9], $r = 0.81$ [P10]. As observed, although there are isolated cases in which the correlation has decreased, for most of them this parameter has increased providing quite better results. In view of the results, the more appropriate approach seems to be use a configuration of tactels as that of *arrangement E* as option by default (see Figure 3.35 right). Future calculations, unless otherwise indicated, will be done with this tactel organization. Nevertheless, the fact that some couplings are worse may suggest that, although there is one arrangement suitable for the majority of users, it may not be "universal". This way, it is possible that it has to be adapted from time to time to concrete attendants. Lastly, as the new tactels arrangement is a 180° rotation of the previous used configuration (*arrang. A*), the *CoM* evolution while carrying out maneuvers has been vertically reflected with respect to previous one. It just involves that the changes of the control variables related to maneuvers are now made in the opposite direction. For example, pushes will now cause *CoM* increments and pulls *CoM* reductions.

3.4 Study of the handlebar grasp (E4)

It is well known that, in order to provide reliable information, sensors are subjected to a process of calibration. This way, their output is compensated so that it is zero in the absence of external stimuli. Obviously, calibration requires to know previously which the output is when there is no input.

In the case of the tactile handlebar we may consider that a *dynamic calibration* takes place. As explained before, the key parameter in our system is not the pressure itself but how it varies, specifically, the evolution of the *CoM*. This way, we need to know an initial

⁹Note that P1-P10 refer to the participants of E1 and not to those who took part in the experiment presented in this section, E3.

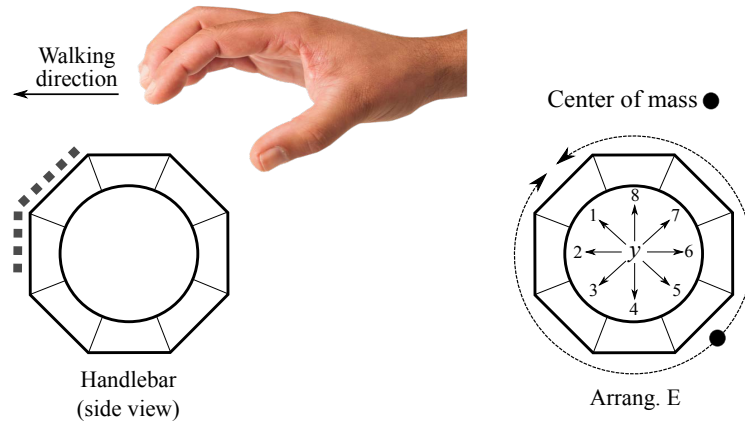


Fig. 3.35 Area that produces biggest CoM excursions when selected as origin of the tactile array (dashed line, left). Arrangement chosen as new tactel configuration by default (right).

reference of the CoM values in order to make measurements that can be used by the control algorithm. In the tactile handlebar, the starting scenario is not that in which there is not pressure, but that in which the handlebar has just been grasped. Each time this situation is detected a process of recalibration begins. The initial state of reference that will be used to compute the subsequent CoM variations corresponds to that with the handlebar grasped without exerting additional forces with the intention of carrying out a maneuver. This state was previously called "rest condition".

As explained in previous sections, the control parameters are based on the addition and subtraction of the centers of mass of each handle. In accordance with the above, in order to detect the assistant's intention, it is a prerequisite to know the value of the $CoMs$ when *there is no intention*. In Chapter 2, the center of mass in this situation was named CoM_r . This way, CoM_r must be subtracted from the center of mass obtained from the captured tactile image so that it can be used to determine the caregiver's wishes:

$$CoM = CoM_{measured} - CoM_r \quad (3.16)$$

where $CoM_{measured}$ is the center of mass computed for the measured tactile image. In the same way, the control variables in rest condition can be expressed as:

$$\begin{aligned} SUM_{CoM_r} &= CoM_{L_r} + CoM_{R_r} \\ SUB_{CoM_r} &= CoM_{L_r} - CoM_{R_r} \end{aligned} \quad (3.17)$$

Thus, when they are computed for attendant's intention recognition they have the form:

$$\begin{aligned} SUM_{CoM} &= (CoM_{L_{measured}} - CoM_{L_r}) + (CoM_{R_{measured}} - CoM_{R_r}) \\ SUB_{CoM} &= (CoM_{L_{measured}} - CoM_{L_r}) - (CoM_{R_{measured}} - CoM_{R_r}) \end{aligned} \quad (3.18)$$

Or expressed in a shorter way:

$$\begin{aligned} SUM_{CoM} &= SUM_{CoM_{measured}} - SUM_{CoM_r} \\ SUB_{CoM} &= SUB_{CoM_{measured}} - SUB_{CoM_r} \end{aligned} \quad (3.19)$$

The correct assessment of the value of CoM_r is hence essential. It is the reference from which driving intention is detected and measured. When the handlebar is just grasped, during the time in which the grip is not still steady, the $CoMs$ take transient values. A waiting time is introduced in order to ensure that this momentary regime is over and rest condition state has been reached. CoM_{L_r} and CoM_{R_r} are stored after this waiting period. A mistake in the choice of the waiting time can have two consequences. On the one side, if it is too short, the stored CoM_{s_r} may correspond to transient values of the CoM so they will not be well established. This leads to a system malfunction and, thereby, an erratic and unmanageable driving. On the other side, if the time is too long, the CoM stabilization process can be perceived by the attendant as contrived and uncomfortable. This is the case of the preliminary results shown at the end of Chapter 2. When the participants grasped the handlebar they had to wait several seconds before they could start driving the PW, what they reported as a little confusing. At that time, the length of the waiting time was chosen heuristically.

In the light of the above, it is worthwhile to analyze how the grasping process takes place. Gathering experimental data of the grasping process and analyzing it can help determine a suitable waiting time. In addition, it could contribute to find out if there exists some kind of pattern in the transient regime of CoM that goes from the moment when the grip is detected until its stabilization.

An experiment was conducted (E4) with this purpose. Forty-two participants from 20 to 64 and a mean age of 34.3 years participated in it after agreement and informed consent. They ignored the purpose of the study. The handlebar was attached to the rear part of the frame of a PW (Bora by Invacare) at a height of 108.5cm. The custom conditioning electronics presented in Section 2.3 was in charge of scanning the tactile arrays and sending the data to a computer at a rate of 60Hz (see Figure 3.36). The PW was mechanically braked so that it was immobile. The participants were asked to stand behind the chair at such a distance that they considered natural and comfortable. They were said to grasp the handlebar after received

a spoken command. They would keep it grasped until they heard another command, then they would release it. They would perform this exercise twice. Regarding the grip, they should do it without exerting any special force beyond what is necessary to keep it grasped steadily. As an example, they were told to imagine that they were stopped at a traffic light while driving the PW, waiting to cross the street. This way, they would keep the handlebar grasped but would not exert push/pull or turn forces because they are just waiting the traffic light to be green.

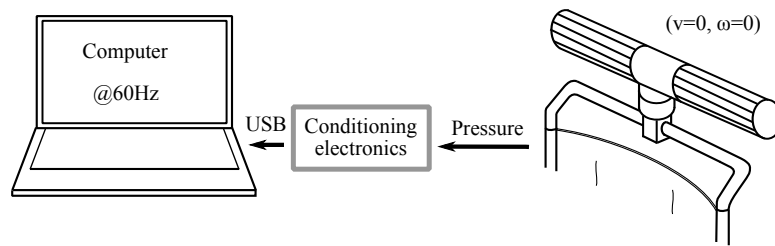


Fig. 3.36 Scheme of experimental setup of the E4.

Eighty four trials were realized. In the data analysis, the threshold of GF above which it was considered that a grasping process were taking place was 0.03N ($t=0$). Three seconds after this force threshold is reached ($t=3\text{s}$), the grip was considered stable. It was a time long enough to have a stable CoM , as observed experimentally.

3.4.1 Grip stabilization

In order to assess how long it takes to stabilize the grip for each participant, it is necessary to define the circumstances according to which this condition is reached. During an interval of time that goes from $t=3\text{s}$ to the moment before the participants received the signal to release the handlebar, the variability of the centers of mass including the data from all the tests was studied (this time span will be identified by the subindex $t>3$). As said before, all the grips were considered already stabilized within this time interval. The obtained results are showed in Table 3.5.

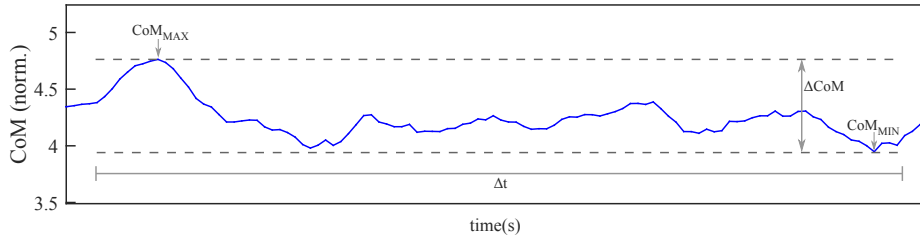
Δ_{CoM} refers to the maximum variation of the CoM during the specified time interval, i.e. $CoM_{MAX} - CoM_{MIN}$ (see Figure 3.37). The first row contains the value of $\Delta_{CoM_{t>3}}$ from the test for which it was maximum, the second row the value from the test for which it was minimum, and the third and fourth are the mean and standard deviation of this parameter when it is computed for the eighty-four trials. One possible way to estimate how much time is needed to reach the stable state could be to calculate how long it takes for the CoM variation to be within an specified range. The length of this range is a design choice. If it is too narrow

Table 3.5 Variability of CoM in rest condition: statistical measures.

	$\Delta CoM_{L_{t>3}}$	$\Delta CoM_{R_{t>3}}$
Param.	Value (norm.)	Value (norm.)
Max.	0.3699	0.3307
Min.	0.0189	0.0185
Mean	0.1118	0.0918
Std. Dev.	0.0720	0.0546

(n = 84)

it can lead to too short waiting times and if it is very wide to too long waiting times, with the consequences already explained.

**Fig. 3.37** Visual example of the parameter ΔCoM .

In this experiment, the chosen range was:

$$\Delta CoM_{stab.} = \bar{\Delta CoM}_{t>3} + 2s_{\Delta CoM_{t>3}} \quad (3.20)$$

where $\bar{\Delta CoM}_{t>3}$ is the mean and $s_{\Delta CoM_{t>3}}$ the standard deviation of $\Delta CoM_{t>3}$, both shown in Table 3.5.

Statistically speaking, given that the distribution of the variable $\Delta CoM_{t>3}$ is approximately normal, around the 95% of the tests would have a value of this parameter inside the chosen limits. Once the threshold of CoM variation below which the grip is considered stable ($\Delta CoM_{stab.}$) was selected, the time needed to reach it was computed. On average, it was $t_{L_{stab}} = 0.69s$ and $t_{R_{stab}} = 0.73s$, times for CoM_L and CoM_R respectively¹⁰.

From the previous results, the following procedure is proposed for the initial grasp of the handle. Once the onset of the grasp is detected, a waiting time of 0.7s is introduced ($t_{L_{stab}} = 0.69s$ and $t_{R_{stab}} = 0.73s$, so it can be a valid number). Then, ΔCoM is checked before

¹⁰Other values of $\Delta CoM_{stab.}$ were tested, but the result was similar in terms of driving experience whereas times of CoM stabilization were longer. For example, for $\Delta CoM_{stab.} = \bar{\Delta CoM}_{t>3}$, $t_{L_{stab}}$ and $t_{R_{stab}}$ were 1.94 and 2.04 seconds. Adding one $s_{\Delta CoM_{t>3}}$ to the latter, the times were 1.14 and 1.24 seconds.

storing CoM_{L_r} and CoM_{R_r} , to rule out the possibility that the user has exerted an sudden change of force at the last moment. If it is within the limits, the centers of mass in rest condition are saved.

Other option may consist in assessing the stabilization of the $CoMs$ by monitoring if Δ_{CoM} is confined within $\Delta_{CoM_{stab.}}$, instead of introduced an initial waiting time. This way, the condition $\Delta_{CoM} \leq \Delta_{CoM_{stab.}}$ would be periodically checked until it is fulfilled. In that moment, the $CoMs$ may be considered stabilized and CoM_{L_r} and CoM_{R_r} be stored. Both solutions provide similar results with regard to the driving experience, although the first proposal seemed to be more accurate in the trials. Whatever option is selected, just after saving the $CoMs$ of reference an audible signal is emitted to indicate to the assistant that he or she can start driving.

3.4.2 Influence of attendant's height

In the first section of this chapter, it was commented that the authors of [109] found that the height of the caregiver affected the interaction between he or she and a manual wheelchair, when the latter was propelled. Similarly, given that a good number of volunteers participated in experiment E4, the obtained data could be used to explore if their height has any influence on our system. With this purpose, the participants were asked for their height. They went from 1.58m to 1.95m, with a mean of 1.76m. As was illustrated in Figure 3.5, the angle formed by the arms of the attendants when grasping the handlebar varies with this characteristic. This may affect the centers of mass in rest condition. Figure 3.38 plots CoM_{L_r} and CoM_{R_r} versus heights of the participants of the experiment.

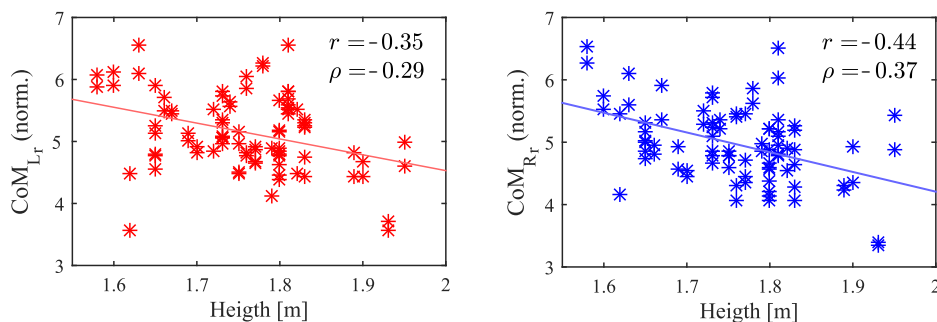


Fig. 3.38 Link between the centers of mass with stabilized grip and the attendants' height. Corresponding 1st order functions superimposed.

Pearson correlation and Spearman's rank order correlation coefficients were computed. They are $r = -0.35$ ($p = 0.0011$) and $\rho = -0.29$ ($p = 0.0087$) for the left handle and

$r = -0.44(p < 0.001)$ and $\rho = -0.37(p < 0.001)$ for the right handle. The results show coefficients slightly low but not negligible. Besides, all of them were found statistically significant. It seems that the CoM_{s_r} tend to increase or decrease as the heights are lower or higher, respectively. Some statistical measures of this parameter are listed in Table 3.6.

Table 3.6 CoM_s of reference from the participants of E4: statistical measures.

	CoM_{L_r}	CoM_{R_r}
Param.	Value (norm.)	Value (norm.)
Max.	6.5539	6.5370
Min.	3.5609	3.3489
Mean	5.1482	4.9729
Std. Dev.	0.6217	0.6106

($n = 84$)

The tendency that Figure 3.38 seems to outline, including the variation of the angle formed by the user's arm and the handlebar, is depicted in Figure 3.39. To put it another way, different users' heights may be translated into displacements CoM_{s_r} around the handlebar axis. One might well wonder why the correlations are not stronger. A possible answer may lie in the angle formed by the forearm and the closed hand through the wrist joint.

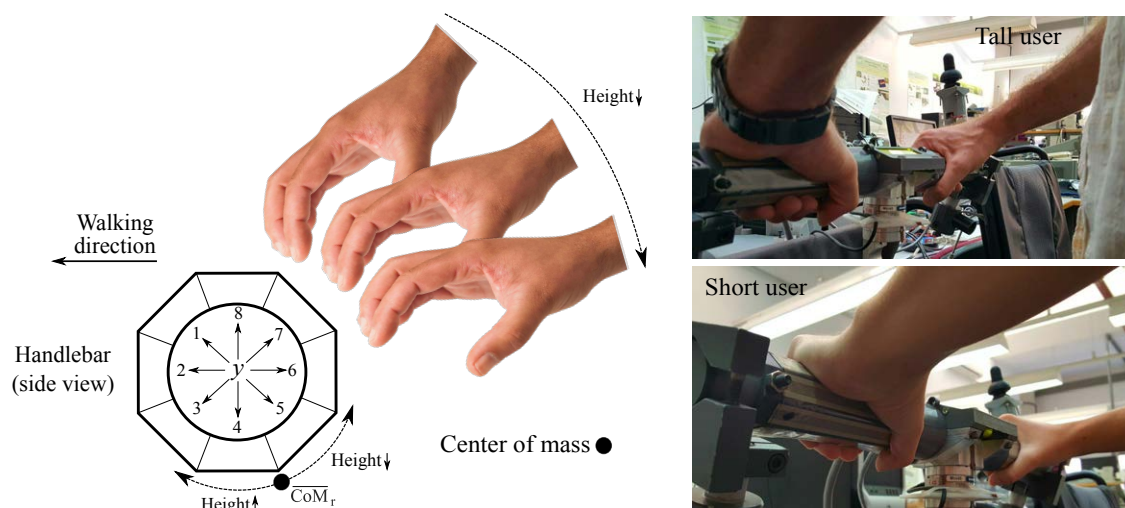


Fig. 3.39 Tendency of CoM_r evolution as the height of the attendant changes (left). Grips from a taller (top right) and a shorter user (bottom right).

This angle is almost zero for many users. However, it is significant for other people as shown in Figure 3.40. When this angle is not negligible, it has an effect on the CoM_{s_r} which is similar to that caused by the variation of the assistant height. In this way, tall attendants

with handle grips as that of Figure 3.40 center will have values of CoM_{s_r} similar to those from a shorter person whose handle grip has a zero angle. The opposite happens with short attendants for which the handle grip is like the example of Figure 3.40 right. Their CoM_{s_r} will be close to those from taller people with a grip with zero angle. This phenomenon may be one of the causes behind the outliers in Figure 3.38, which have a direct impact on the correlation values.

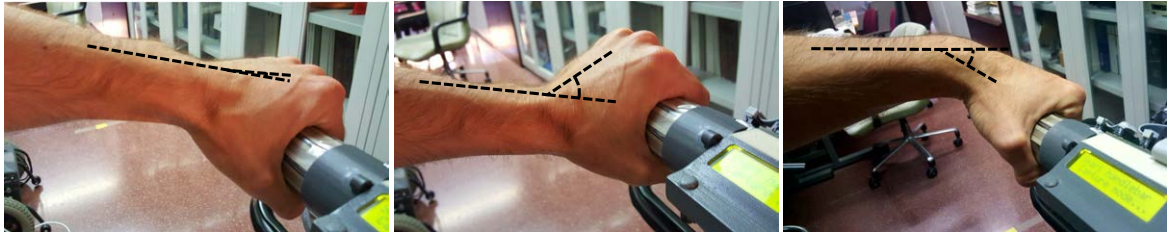


Fig. 3.40 Handle grip with an angle between the forearm and the closed hand that is almost zero (left). Handle grips for which the angle is significant in both directions (center and right).

Another observed fact is that the same attendant does not grasp the handles always in the same way. Between the first and the second test repetition, the participants were asked to walk away from the PW and to get close to it again. The aim of this instruction was to "reset" their posture behind the PW and thus to analyze if there was any change in the grip in terms of stabilization.

Table 3.7 Difference in the parameter CoM_r in two consecutive grips of the same participant: statistical measures.

	$ CoM_{L_{r_k}} - CoM_{L_{r_{k+1}}} $	$ CoM_{R_{r_k}} - CoM_{R_{r_{k+1}}} $
Param.	Value (norm.)	Value (norm.)
Max.	1.038	1.3055
Min.	0.0077	0.0048
Mean	0.2584	0.257
Std. Dev.	0.2711	0.2518

($n = 84$)

As can be seen in Table 3.7, the mean difference of the variable CoM_r for two grips of the same person is around one quarter of tactel. However, the results present a large dispersion. Whereas there are participants for which the CoM_{s_r} stabilized almost in the same point in both grasps, the difference exceeds a distance of one tactel for others. Besides, the standard deviation is equal or larger than the mean, depending on the handle. Since the height is a

fixed factor, what could be happening in the case in which this difference is large is that the same participant may be grasping with different fist-forearm angles.

Another interesting point consists in exploring a possible relationship between the gripping force and the height of the attendant. Some statistical measures from the sample of the experiment are showed in Table 3.8.

Table 3.8 Gripping force exerted for the participants of E4, once the grip is steady: statistical measures.

	GF_L	GF_R
Param.	Value (N)	Value (N)
Max.	14.0566	12.8744
Min.	0.6219	0.5933
Mean	3.8490	4.2767
Std. Dev.	2.4464	2.4509

($n = 84$)

The sample presents a large range, with a peak of 14N, in the case of the left handle, and minimum values near 0.5N. The mean GF exerted by the participants of E4 when grasping the handlebar is around 4N, which is far from the maximum values. This could be an indication that the data are positively skewed. It is confirmed when the median and mode are calculated (mode < median < mean for both left and right handles). Some works have shown that the hand size is directly related to the person's height [115]. Others even propose the hand size as a parameter based on which the height could be estimated [116, 117]. One might think that the GF may be higher for bigger hands; they cover more tactile area than those that are smaller. Since the taller the people, the larger their hands are, it would imply the existence of a link between the height and the GF . In order to assess this possible coupling, both parameters from the participants of E4 are plotted together in Figure 3.41. Besides, Pearson correlation and Spearman's rank order correlation coefficients are computed.

The values obtained from the calculations are: $r = 0.14$ ($p > 0.05$) and $\rho = 0.12$ ($p > 0.05$) for the left handle and $r = 0.17$ ($p > 0.05$) and $\rho = -0.10$ ($p > 0.05$) for right handle. As seen, both types of correlation are negligible (see Table 3.1 in Section 3.1.2.2). Moreover, none of the four results were found statistically significant. The consequence of the latter numbers is clear: according to the sample of E4, there is no relationship between the GF in rest condition and the attendant's height.

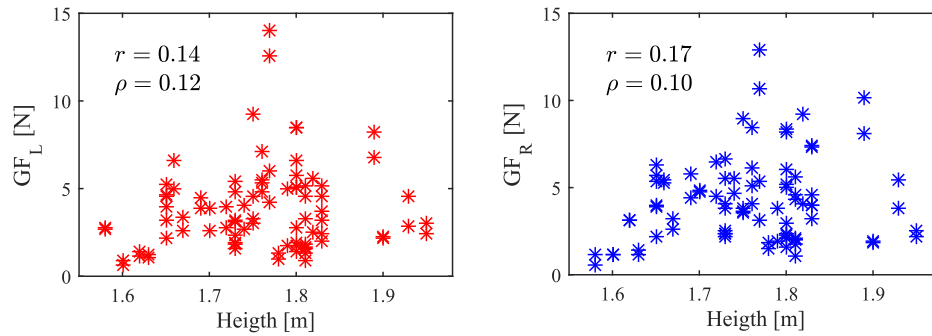


Fig. 3.41 Gripping force versus height from participants of E4.

3.4.3 *CoM* evolution during the grasp onset

So far, the focus has mostly been on the process of stabilization of the *CoMs* once the handles are grasped. As said, it is of crucial importance to take the correct values of CoM_{Lr} and CoM_{Rr} , since they are the references to distinguish the rest condition from that in which maneuvers are being performed. Well-chosen $CoMs_r$ ensure reliable SUM_{CoM} and SUB_{CoM} control variables. The used strategy has been centered on the detection of the situation for which the *CoMs* variation does not exceed certain limits. This way, the evolution of the *CoMs* before reaching that condition has been ignored and discarded. This section examines how the grasp is made from the very moment in which the hands make contact with the handlebar.

Figure 3.42 plots some examples of the *CoM* variation from the moment in which the grasp starts taking place. In order to understand the meaning of the values of *CoM* shown in the y-axis it is convenient to have in mind their correspondence with the spatial coordinates of the tactile sensor (see, for example, Figure 3.39 left). As can be observed, what seems to be a pattern has been found in the evolution of *CoM*. To better follow the graphs of Figure 3.42, it is advisable to take into account the hand contact area when the handle is grasped. The lighter part of Figure 3.43 left represents the area of the hand that presses against the tactels. The limits can move slightly from one person to another, above all those of the top and bottom parts. On the right side of this figure, there are examples of six different people grasping the left handle in rest condition. In the photos, a black circle signals the tactel with the spatial coordinate¹¹ $y = 5$. The variations of the *CoM* in each of the graphs of Figure 3.42 occur because all the points of the hand area highlighted in Figure 3.43 do not make contact with the handle at the same time. This way, for a certain period of time there is a situation in which some tactels are pressed and others are not yet; besides the output of the pressed tactels

¹¹Remember that tactels *arrang. E* is now used.

is varying. All this causes displacements of the centers of mass. Since the curve depicted in the twenty-four graphs of the mentioned figure is similar to that found in many more cases (approximately 80% of the tests), there are reasons to think that there is an underlying pattern or tendency.

According to the graphs, the first computed *CoMs* are around the tactels with coordinates $y \in [5, 6.5]$. Those values are in a local minimum from which the curves begin to increase¹². After that, a local maximum is eventually reached. From the latter, the *CoMs* begin to decrease and finally they stabilize. There are some instances, as CoM_{R9} , CoM_{R10} , CoM_{L9} or CoM_{R12} , for which the fall ends with a little rebound before starting stabilizing. In order to explain how the grasp takes place, it is interesting to match the mentioned parts of the curve with the pressure that the different areas of the hand exert. Figure 3.44 is helpful in this regard. In this figure, the grasping process has been represented, starting from a situation in which there is no contact between the tactels and the hand (step [1]) and ending with a grasp with a *CoM* on the road to its stabilization (step [6]). Moreover, the represented *CoM* has all the characteristics previously mentioned: a starting minimum, and local maximum, a fall and a little rebound (it is, indeed, the onset of CoM_{R9} of Figure 3.42). The *CoM* value at $t = 0$ corresponds to the area of the tactile array that makes contact with the hand firstly. The minimum in the graph is related to the contact of the area formed by the right side of the palm and the base of the thumb¹³ with the tactels of the rear part of the handle, as indicated in the figure (step [2]). Afterwards, the upper half of the palm starts making contact with the tactels that present the higher values of y , what produces a shift of the center of mass towards them and, therefore, an increment of its value (step [3]). Note that in those tests that do not present a starting minimum *CoM* (e.g. CoM_{L9} in Figure 3.42), the first contact is made between the upper palm area and the higher tactels, and step [2] does not take place. As the fingers start surrounding the handle, tactels with y around the values 1-3 begin to register pressure (step [4]). This causes a fall of the *CoM*, which had reached its highest value in the previous step. In some tests, at this point the *CoM* slope decreases little by little until being practically zero as the *CoM* stabilizes. Others presents a rebound as depicted in

¹²Note, however, that there are some exceptions as CoM_{L2} , CoM_{L9} or CoM_{R7} , that do not seem to behave in the same way. As explained, when data of E4 were captured, a threshold of $GF = 0.03N$ was set to detect the grip onset. Therefore, the *CoMs* relating to the grasps with a GF below the latter are not showed in the graphs. Having a look at the evolution of CoM_{L2} and CoM_{R7} during the time before the GF threshold is reached, a starting local minimum is also found; it is 6.44 for CoM_{L2} and 5.31 for CoM_{R7} . The case of CoM_{L9} is different. No matter how far we step back in time towards smaller GF s, it starts from a local maximum. Note that in the three previous examples, the center of mass produced by the other hand (CoM_{R2} , CoM_{R9} and CoM_{L7}) does begin with a minimum, as observed in the most of the tests.

¹³The explanation is made considering the hand in the figure, which is the right. What is going to be said is also valid for the left hand, taking into account that both hands are symmetrical.

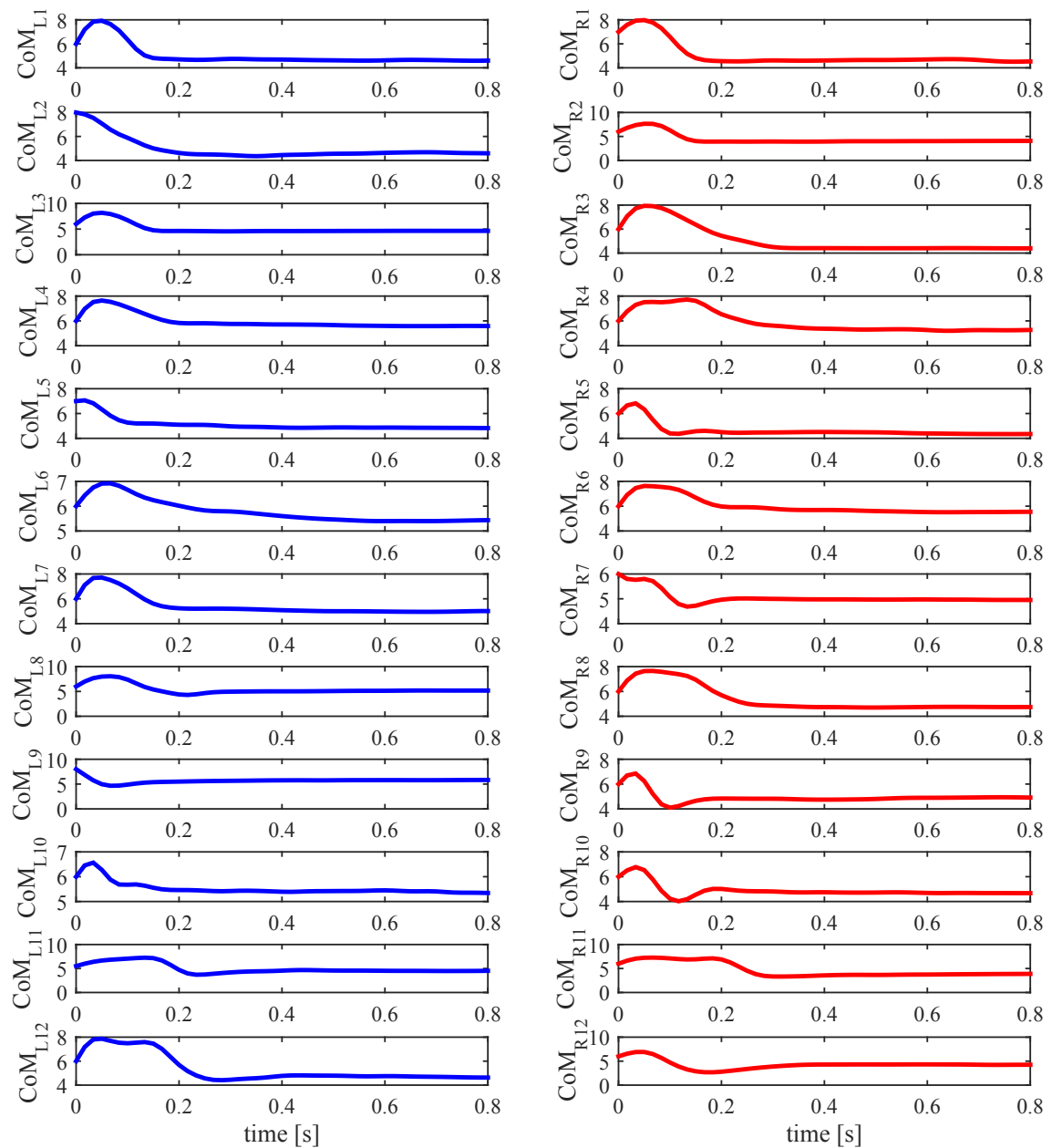


Fig. 3.42 Twelve examples, extracted from the data of E4, of the evolution of CoM_L (left) and CoM_R (right) when the handlebar is just grasped. The parameters are normalized to be expressed in tactels coordinates.

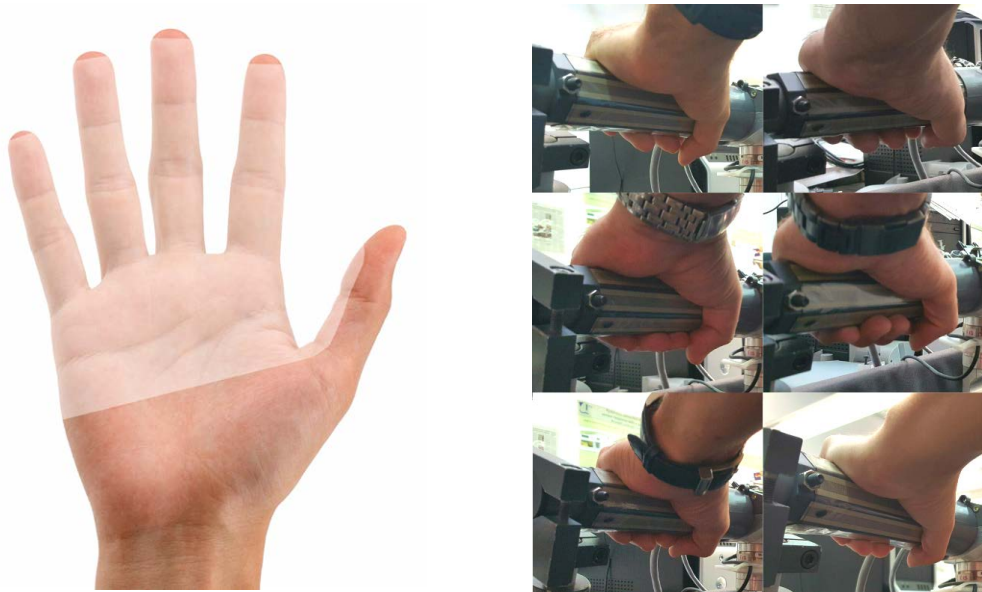


Fig. 3.43 Hand surface in contact with the handles when they are grasped (lighter area in left). Six people grasping the left handle in rest condition (right). The photos have been taken from the rear, in a point between the handlebar and the person.

steps [5] and [6]. It may suggest that some people, maybe as a reflex action, tend to exert what seems a fast "recognition" grip. Once the grasped surface is "scanned", some of them release slightly the grip reducing the GF (further details will be given later). Note that, as showed in Figure 3.43, when the handle is grasped the hand surface pressing on the front tactels is larger than that pressing on the tactels located at the rear side. This way, when the GF increases, the output from the front tactels is greater and the CoM tends to move towards them, experimenting a little decline (these tactels are in the interval around $y \in [1 - 4]$). The opposite happens when the GF decreases, i.e. CoM moves towards the rear part (y is around 5-8) and its value increases.

Note that the process that takes place during the rebound shown in steps [5] and [6] appears to be involuntary and occurs quite quickly. For some of the participants what happens is that illustrated in Figure 3.45: the GF reaches a peak while the CoM is in the valley of the rebound. After that, the CoM begins to increase up to its steady value whereas the GF decreases until a level that the person feels natural or convenient. According to the captured data, this happens when the rebounds occurs in the range $t = 200 - 500ms$ approximately. When the phenomenon takes place before and in a smaller time interval, as is the case of Figure 3.44, no notable changes in GF are observed. In some of the tests it seems that the GF growth rate changes during the rebound, but it has been observed in few cases so no

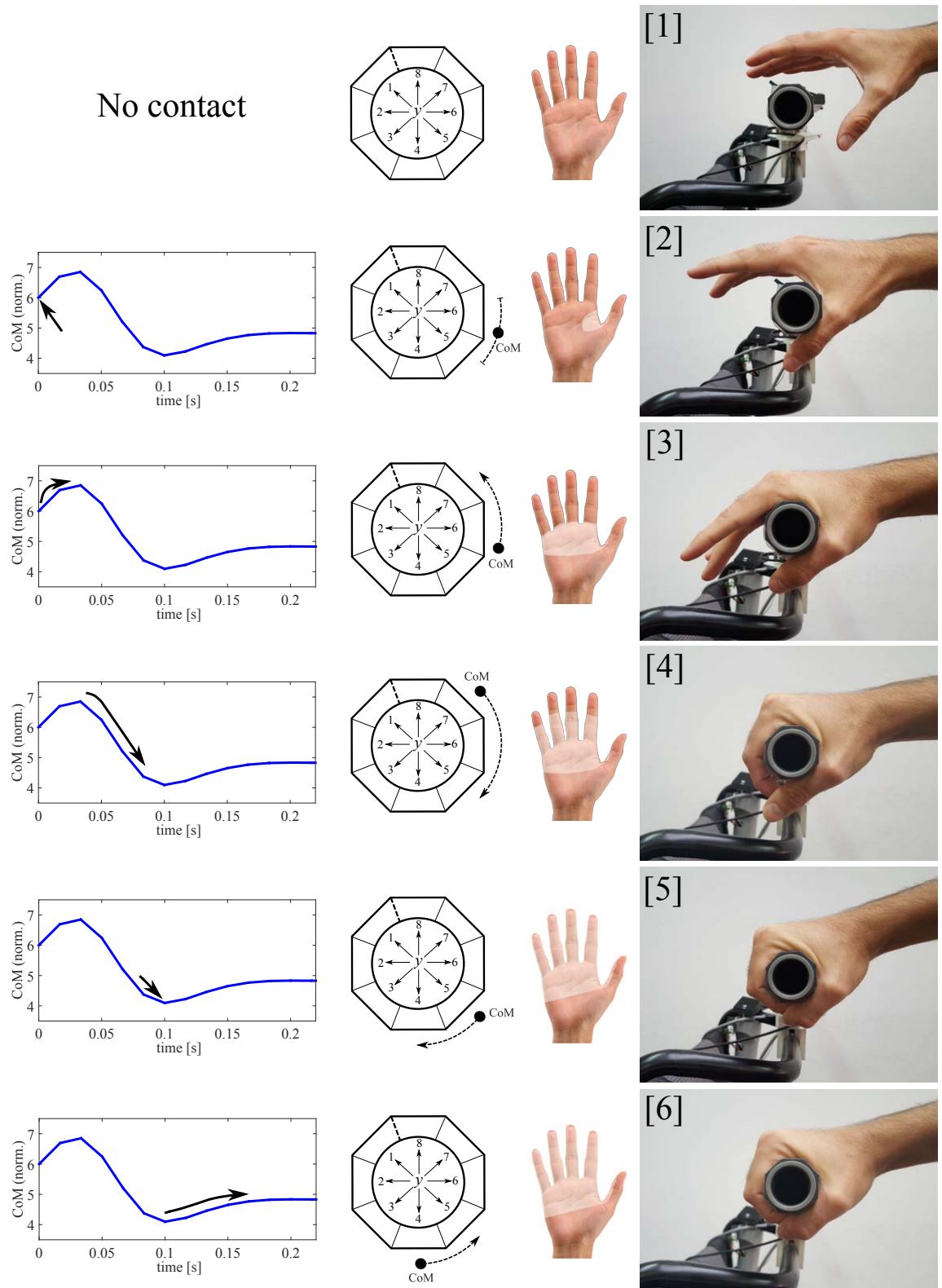


Fig. 3.44 Process of the handlebar grasp (ordered from top to bottom). The lighter area in the open hand represents the contact with the handle in each step ([1]-[6]).

conclusion can be drawn. Perhaps, a higher time resolution would be required for a detailed analysis of these instances.

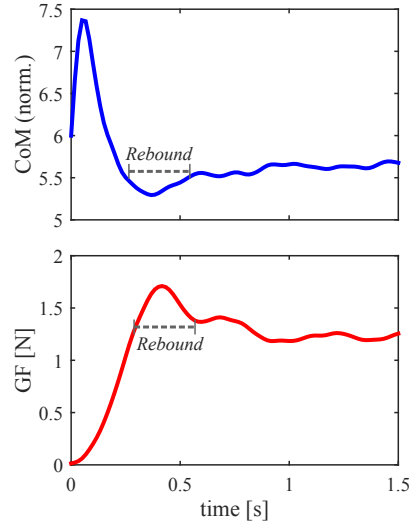


Fig. 3.45 *CoM* (top) and *GF* (bottom) from a test in which there is a rebound.

Regardless of whether the grasp presents the rebound of the steps [5] and [6], all the tests experience eventually a decline of *GF*, as the *CoM* stabilizes and the person "feels" that the grip is firm. As said, the pattern (with its subtle variations) has been seen in the 80% of the tests of E4, maybe more with a reduction of the *GF* threshold used to detect contact. This way, its identification could be useful to distinguish if a just made contact comes from a hand grip or it has been caused by an object or a person with an intention distinct from grasping. A complementary method to check if the handlebar continues to be grasped is to analyze if certain front and rear tactels measure a pressure above a threshold. A correct grasp has to excite the front tactels with the fingers little, ring, middle and index and the rear tactels with part of the palm and the beginning of the thumb. The fact that these regions of tactels are not activated at the same time is an indication that other kind of contact is being made and the chair would stop. This prevents the PW from moving when an attendant is, for example, just leaning his or her forearms on the handlebar to rest. It would also stop the PW if the attendant releases the handles. As design choice, we could decide, for example, that the chair continues to move if one of the handles is released. This can be the case in which the attendant releases one handle to see the time in his or her wristwatch.

On another note, the results of E4 can be utilized to study the process of the handlebar release. As explained previously, during the experiment the participants received a signal to release the handlebar. This way, the evolution of the *CoM* during this action has also been captured. Figure 3.47 shows the curves for some of the tests. As can be seen, the behavior

of CoM when the handles are released is basically symmetric with respect to that observed when the handlebar was grasped (see Figure 3.42). This means that the release takes place in reverse order to that showed in Figure 3.44, i.e. following the steps from [6] to [1]. In contrast to what happened to some tests during the grasp, no clear relationship has been seen between the rebound that some of the trials present and the GF .

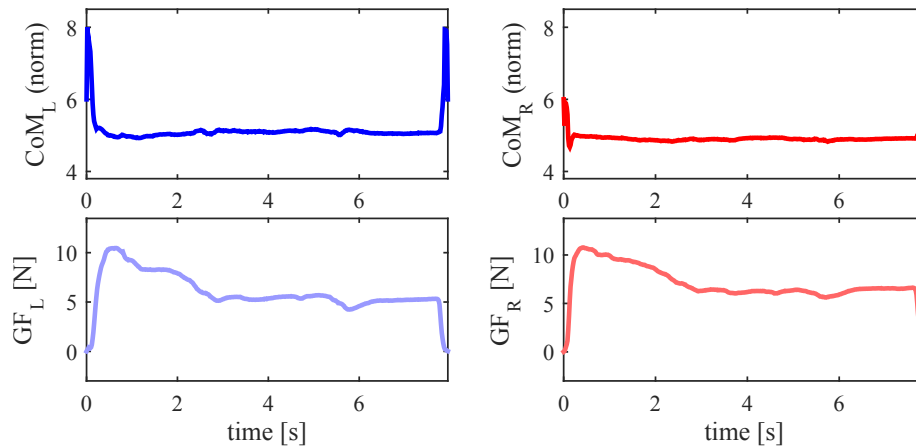


Fig. 3.46 Evolution of the pairs CoM_L and GF_L (left side, top and bottom respectively) and CoM_R and GF_R (right side, top and bottom respectively) during a performance of E4.

As a final remark, the data from E4 have showed something that had been already mentioned in Section 3.1.2.2. The CoM is a parameter more robust than others, as for example, the GF . During the experiment, in many trials, once the CoM had already stabilized, the GF continued to vary and took considerably longer to reach the stabilization. Furthermore, the former was quite insensitive to the changes of the latter. Figure 3.46 depicts an example of this. With this regard, Appendix D was added to the document. It includes the discussion about a related proposal, in which the gripping force is used as control variable to identify the user intention in a haptic bicycle-type handlebar. The experiment the authors carried out is replicated and their proposal is assessed with the data extracted from experiment E1.

3.5 Vibro-haptic feedback to prevent overexertion

As seen in previous sections, there are some cases of the performed experiments in which the participants exerted such gripping forces that several tactels became saturated. In others, we have seen people whose grip produced forces near 15N (see Figure 3.41), even in rest condition, for which the mean is around 4N. One possible way to adequately process such gripping forces lies in the reconfiguration of the conditioning electronics. This would modify

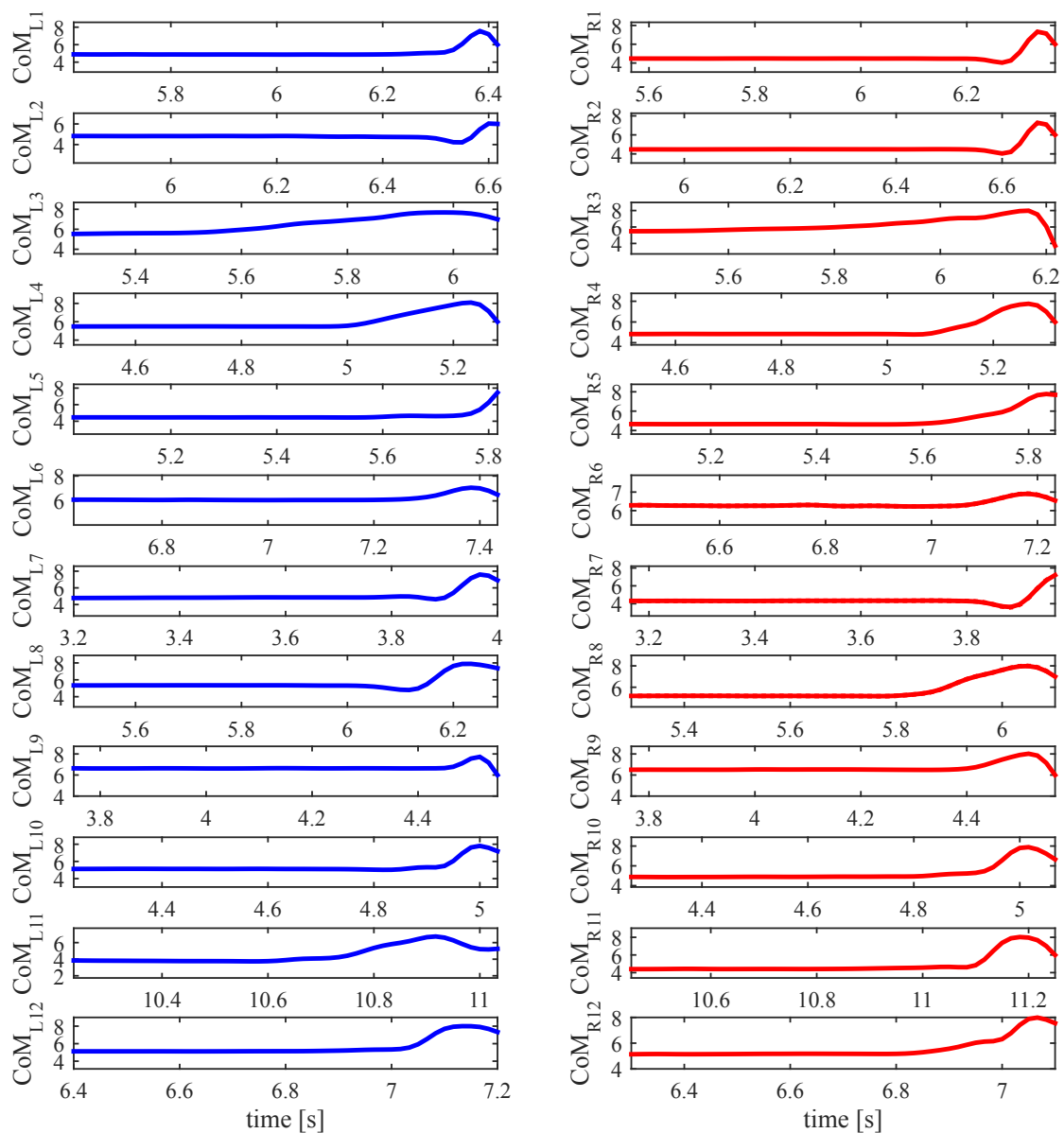


Fig. 3.47 Twelve examples, extracted from the data of E4, of the evolution of CoM_L (left) and CoM_R (right) when the handlebar is released. The parameters are normalized to be expressed in number of tactels.

the operating curve of the tactels output so that it would reach saturation at higher pressures. Nonetheless, it should also be taken into consideration that an extension of the readable force range can lead to a loss of linearity in the response to the higher forces. Besides, if the average force while using the handlebar is low, an increment of the dynamic range of the input force makes the resolution decrease for most users. This is important if small force changes have to be detected. Another undesirable effect was briefly mentioned in Section 3.4.3. The hand surface does not contact uniformly throughout the whole tactile handle cover. The area pressing on the front part is greater than that pressing on the rear, so that when an attendant increases the force of his or her grip it has a bigger effect on the front tactels. It has been already showed that the *CoM* is quite robust to *GF* variations and, in fact, this effect is very limited once the grasp is firm. However, there are occasions where, in spite of being infrequent, a relevant increment of the *GF* can produce a variation of the *CoM* that starts being identified by the system as a maneuver. In these cases, the PW moves slightly backwards (the *CoMs* move towards the front tactels experiencing a decline, SUM_{CoM} decreased and a little pull maneuver is detected). Moreover, it was explained in Section 3.2.3 that the gripping force may be seen as the sum of two components, one due to the grip itself and other related to maneuvers exertion. When *GF* is excessive, the second component is masked by the first. In this case, the compensation introduced with $\sigma_{SUB_{CoM}}$ and $\sigma_{SUM_{CoM}}$ starts being ineffective and driving becomes erratic.

High gripping forces are not only unsuitable because they can produce a malfunction of the device, but they are also inadequate from the assistant's point of view. The main objective of the proposed system is to assist the caregiver, to free this person from the heavy task that propelling a wheelchair involves. There is no sense in making use of a device with this functionality by exerting a high and unnecessary force. High gripping forces lead to overexertion and fatigue, precisely what our device intends to avoid. At this point, one interesting question may arise: why do some of the participants exert such forces? A lot of experiments, like those presented in this document, require volunteers for who the device to test is unfamiliar. This is a measure aimed to avoid biases and to obtain data as reliable as possible. This way, for the cases we have seen so far, it was the first time that the participants interacted with the device or the setup. However, during the development of a system like this, many informal experiments and trials are carried out. Thus, there was a group of people who had tested the handlebar more than once, some of them in several occasions. When the handlebar was used by them, it was observed that the *GF* remained at low levels. In order to study this tendency, some of the participants that took part in the previous formal experiments were asked to use freely the system, i.e. to drive for a while carrying out the maneuvers they wished. After few trials, they seemed to start feeling comfortable with the

device so that the same tendency was observed for most of them: the GF decreased. After asking them about their feelings and sensations driving the device, the following conclusion was reached: the PW with all the experimental setup (computer, conditioning electronics, wires, sensors and amplifier, acquisition card, etc.) seems to have a "complex", "contrived", "risky to drive" and "heavy" appearance. This may cause that, during the first contact, some participants tend to be "too cautious" and, in a way, they may have the feeling of having to struggle against the device instead of cooperating with it. It should be borne in mind that the current version of the system is a prototype for research purposes, hence it may look bulky and cumbersome (future versions will cope with the mentioned issue). The participant of E4 whose gripping force was the highest (14.07N and 12.87N for right and left handle, respectively) was asked to drive the PW freely for approximately one and a half minute. Figure 3.48 shows the captured $CoMs$ and GFs . As can be observed, the mean GF falls down to 5.5N (left) and 5.8N (right). The fall is quite clear in the chart of GF_R , for which from $t=4s$ the parameter remains most of the time in the range of 3-4.5N. Note that there is a drop of approximately 10N with respect to when the same volunteer participated in E4.

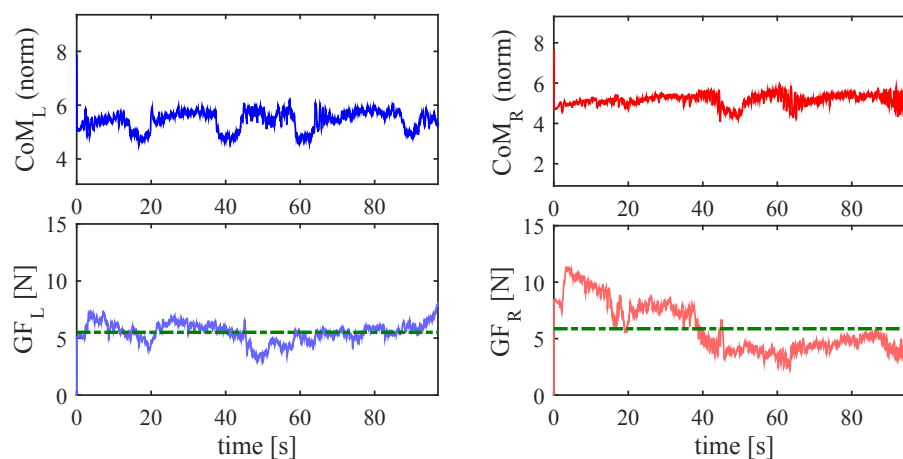


Fig. 3.48 Evolution of the pairs CoM_L and GF_L (left side, top and bottom) and CoM_R and GF_R (right side, top and bottom) during the driving of the PW by the participant of E4 whose GF was the highest. The dashed line represents the mean GF .

In view of the above, it seems a good idea to add some kind of feedback to warn the assistant when he or she exerts an excessive gripping force. This would prevent him or her, mainly during the first uses, from overexertion. Over time, as the attendant becomes familiar with the haptic handlebar, the warnings would decrease and, eventually, they would be no longer required and would not occur. Vibrations are widely used as notification signal in haptic support systems [118]. A warning system based on vibrations allows an inconspicuous and effective communication that is only perceived by the person who grasps the handlebar. This is valuable for the AT users, which have a preference for discreet devices [119–121]. An

audio signal does not have this characteristic and visually displaying a message on the LCD may be missed by the user. Two DC vibration motors [122] have been used to implement a vibro-haptic feedback. They incorporate a small unbalanced mass in their axis to produce vibrations while rotating. The motors have been attached to 3D printed pieces that are inserted into the both handlebar ends (see Figure 3.49).



Fig. 3.49 Vibration motor and piece where it is placed (left). The whole set inserted in the left handle end (right).

The circuit designed to generate the vibration is depicted in Figure 3.50. A HMPS-A42 NPN bipolar transistor is in charge of activating the motor. Its base is wired to a digital output of the acquisition card NI USB6009, that turns on and off the element. A capacitor and a diode have been placed in parallel with the engine, which is quite delicate, as protective components. When current flows through the motor, it produces a vibration that is transmitted through the plastic piece to the handle.

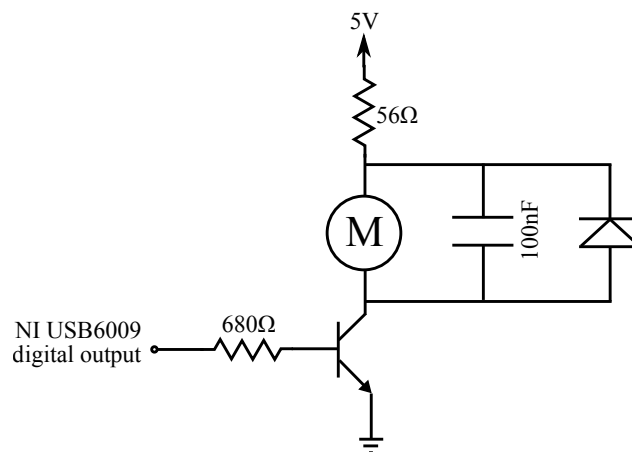


Fig. 3.50 Schematic of the motor activation circuit.

3.6 Processing of control parameters based on CoM

As explained in previous sections, the force (F_y) and torque (T_z) exerted while driving show a strong link with two variables obtained from the $CoMs$. This coupling, assessed by Pearson correlation, has proven to be highly linear. Therefore, the two proposed control variables (SUB_{CoM} and SUM_{CoM}) detect and quantify push/pull maneuvers an turns, in a similar way as force and torque signals do it. However, they are affected by some factors that have been previously reported in this document. This way, a processing is required in order to make the variables usable to generate linear and angular speeds. The result of this processing is depicted in Figures 3.51 and 3.52. F_{yCoM} and T_{zCoM} are the parameters obtained after adding some corrections to SUB_{CoM} and SUM_{CoM} . Note that their name is based on the similarity with the force and torque regarding maneuvering control, but they are not an estimation of these magnitudes.

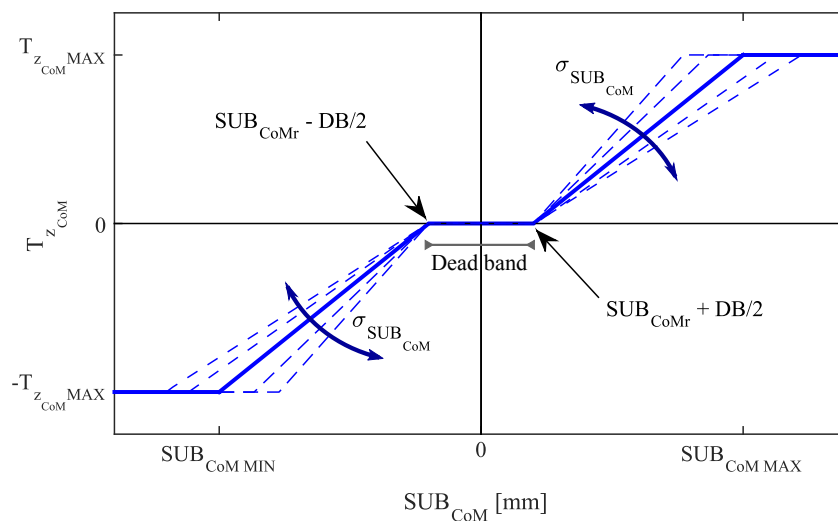


Fig. 3.51 Processing of SUB_{CoM} to estimate turns.

As can be observed in the figures, both $\sigma_{SUB_{CoM}}$ and $\sigma_{SUM_{CoM}}$ module the gradient of the functions. Let us remind that these two parameters depend on the gripping force (see Section 3.2.3.1), so that the higher the GF the greater the slope of the functions is. Both coefficients are updated with the GF associated to each captured tactile image. Thus, the functions $F_{yCoM}(SUM_{CoM})$ and $T_{zCoM}(SUB_{CoM})$ are recalculated as new samples from the tactile handlebar are received. $\sigma_{SUB_{CoM}}$ and $\sigma_{SUM_{CoM}}$ may be seen as gains which make the driving sensation of the users whose grip is stronger as similar as possible to that of those who grasp weaker. $F_{yCoM}MAX$ and $T_{zCoM}MAX$ are the values for which the maximum linear and angular speeds are reached.

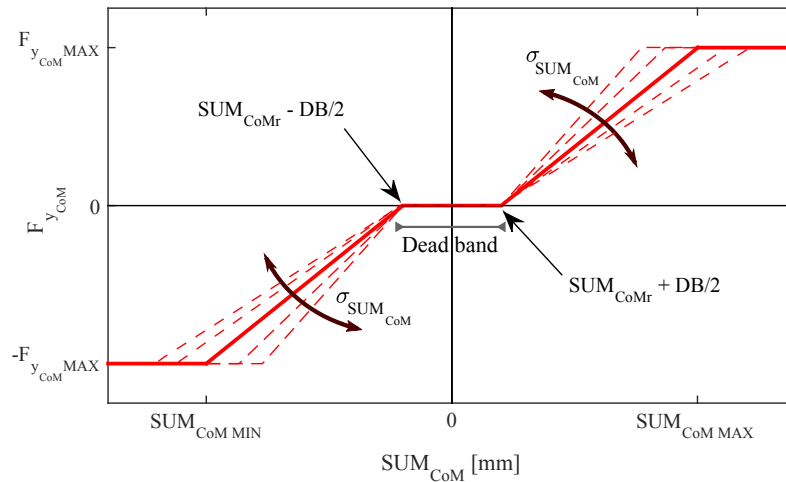


Fig. 3.52 Processing of SUM_{CoM} to estimate forward and backward motion.

The zero value of SUB_{CoM} and SUM_{CoM} corresponds to those pressure maps for which the sum and the subtraction of the $CoMs$ are equal to SUB_{CoM_r} and SUM_{CoM_r} (see Equation 3.19). The previous values are related to the $CoMs$ of reference, i.e. those stored when the handlebar is grasped, once the grip is steady and the $CoMs$ are stabilized. However, the centers of mass are not static but they present small variations even in rest condition. This may produce the detection of a non-zero $F_{y_{CoM}}$ and $T_{z_{CoM}}$, which would result in small and undesired PW movements. As with the testing algorithm presented in Chapter 2, a dead band centered in $SUM_{CoM} = 0$ and $SUB_{CoM} = 0$ has been introduced. This way, the fluctuations around SUB_{CoM_r} and SUM_{CoM_r} will be ignored and $F_{y_{CoM}}$ and $T_{z_{CoM}}$ will continue to be zero.

Moreover, the dead band has a variable width. This feature was introduced because, when the attendant stopped the chair after being driving, sometimes it experienced some little jerks. It is due to the fact that when the user stops the PW and stays in rest condition, although he or she is not exerting maneuver related forces, the grasp may be slightly different from that when the handlebar was grasped initially. This produces that the $CoMs$ do not reach the values of reference computed in the grasp onset (CoM_{L_r} and CoM_{R_r}) and their fluctuations can make SUM_{CoM} or SUB_{CoM} fall out of the dead band. This situation is illustrated in Figure 3.53 left. As showed in the example, after stopping, the $SUM_{CoM_{measured}}$ in rest condition is a little larger than SUM_{CoM_r} ($SUM_{CoM} > 0$, see Equation 3.19). This difference is big enough to produce that some of the values surpass the dead band right limit.

In order to avoid this effect, when SUM_{CoM} enters the dead band, the latter is immediately broadened. In this manner, the possible difference between $SUM_{CoM_{measured}}$ and SUM_{CoM_r} when the user stops remains within the boundaries of the band. This case is depicted in Figure 3.53 right. Thereafter, when the attendant starts driving again the band is shortened

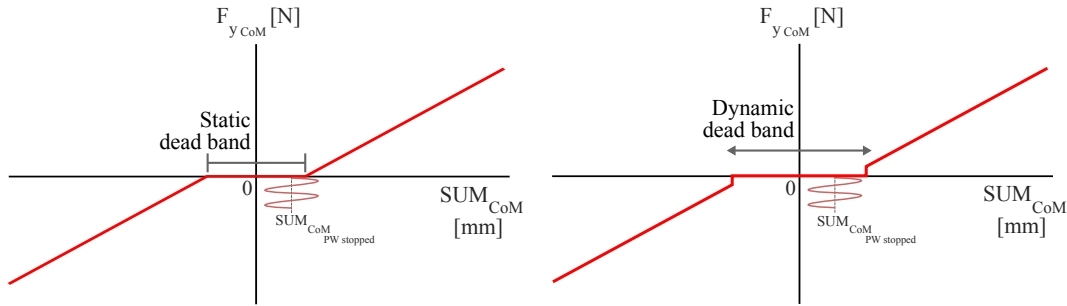


Fig. 3.53 Static and dynamic dead bands (left and right).

and returns to its original width. Hence the dynamic range while performing maneuvers is not affected¹⁴.

After the above processing, the linear and angular speeds are calculated in a similar way to that shown in Equation 3.1. The main difference is that now, instead of using the force and torque provided by the F/T sensor, the parameters used are F_{yCoM} and T_{zCoM} (see Equation 3.21).

$$\begin{aligned} v &= G_{lin} F_{yCoM} \\ \omega &= G_{ang} T_{zCoM} \end{aligned} \quad (3.21)$$

where G_{lin} and G_{ang} can be used to tune the sensitivity according to each assistant preferences.

The last correction affects the linear and angular speeds and it has to do with the dissimilarity between the left and right handles. Tactile sensors suffer from mismatching since tactels behave slightly different. This source of error is present in the handlebar tactile sensor of our prototype. As discussed in Section 3.1.2.2, parameters as the center of mass processes tactile images as a whole, what makes them quite robust to this kind of flaws. However, there are certain situations in which the mismatching has to be taken into account and its undesired effects have to be corrected. Figure 3.54 and 3.55 help understand it. The former depicts three different scenarios. That on the left corresponds to the rest condition ($CoMs = CoMs_r$), so no movement is produced. According to that in the center, the PW would be turning around itself. Note that the $CoMs$ have moved the same distance (Δ) in opposite directions, so that $SUB_{CoM} \neq 0$ ($\omega \neq 0$) and $SUM_{CoM} = 0$ ($v = 0$). In the third scenario, the PW would be moving straight. Both $CoMs$ have moved upwards the distance Λ , so $SUB_{CoM} = 0$ ($\omega = 0$) and $SUM_{CoM} \neq 0$ ($v \neq 0$).

Nevertheless, the previous figure depicts an ideal situation. As explained above, tactile handles do not have exactly the same response even if their inputs are identical. Moreover,

¹⁴Only the initial push that resumes driving has to be a little stronger, although the difference is hardly perceptible.

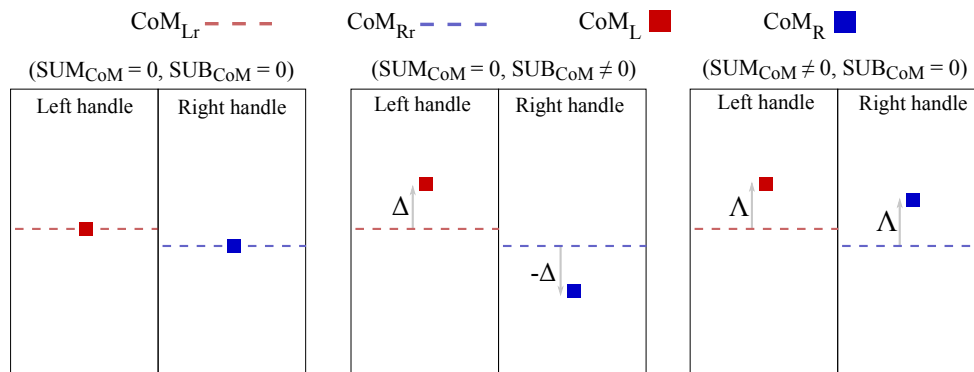


Fig. 3.54 Ideal scenarios in which the PW is stopped, turning around itself and moving straight (from left to right).

the captured force maps are exerted by persons who may not exert the exact same force with both hands. This way, the asymmetries inherent to the human being are added to the sensors mismatching causing the effect showed in Figure 3.55. The range of displacement of the centers of mass of both handles differs. Besides, this divergence increases as maneuvers become more pronounced. The central scenario in Figure 3.55 represents the case of a user who tries to turn around himself or herself, exerting pressure maps whose centers of mass left and right have moved different distances. It makes that $SUM_{CoM} = \delta$ and not zero, what produces a non negligible linear speed. This is specially dangerous because, often, tight turns are performed in narrow spaces: avoiding obstacles in a room, turning around in a corridor, etc. A non desired and unexpected linear speed can originate a collision with a wall, a table, etc. In fact, this effect was observed during some trials. Some volunteers had problems realizing turns in a narrow corridor and they reported that the PW moved forward in an unforeseen way.

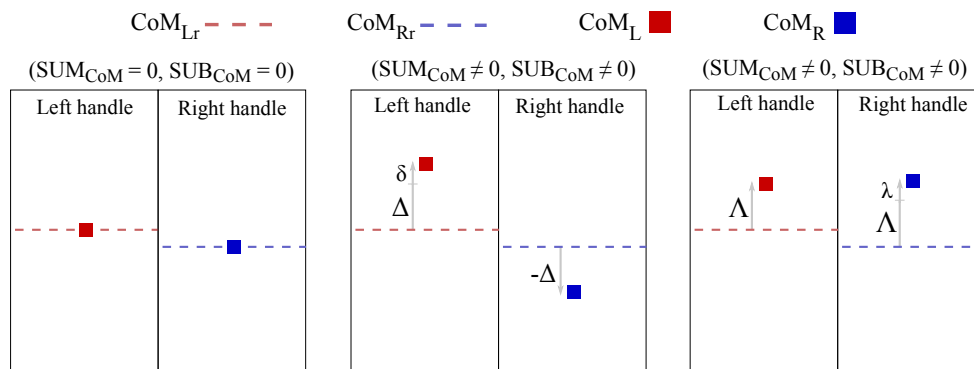


Fig. 3.55 Real scenarios with the PW stopped, performing a turn around the PW vertical axis and performing a pushing maneuver (from left to right).

Regarding the third scenario, it is also possible that both $CoMs$ move distinct lengths when pushing the chair. As with SUM_{CoM} , the asymmetry would cause that SUB_{CoM} was not zero but λ . This may introduce a small angular speed. Unlike the previous case, according to that observed experimentally, it does not seem to be problematic. Note that the PW assistant is *another element* in the control loop. What may be happening is that the user is compensating unconsciously these little deviations by exerting a slightly larger force with one arm than with the other when the trajectory is not totally straight. Another explanation may be that the component λ has such size that the non-zero SUB_{CoM} is inside the dead band of function T_{zCoM} and, therefore, it does not cause turning movement.

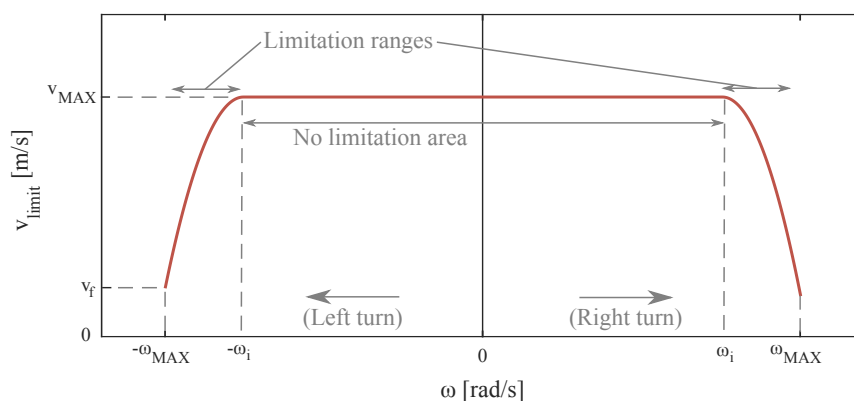


Fig. 3.56 Linear speed limitation based on angular speed.

On the basis of the above, since the hazardous situation seems to lie in tight turns, a linear speed limitation has been added when they take place. Figure 3.56 illustrates the correction. v_{limit} is a function that represents the maximum linear speed allowed at any time. As showed, linear speed remains unchanged during the most part of the turning range. It is only when angular speed is near its maximum, what represents a tight turn, that the linear speed is limited. Note that a small linear speed (v_f) is allowed even at ω_{MAX} . This is because an entire cancellation of the linear speed was perceived as if the PW became suddenly stuck, what was awkward. The left and right limitation curves are defined by the expression given in Equation 3.22.

$$v_{limit_{rangeL/R}} = \frac{(v_f - v_{MAX})}{(\omega_i - \omega_{MAX})^2} (\omega + \omega_i)^2 + v_{MAX} \quad (3.22)$$

where v_f is the lowest limit of the linear speed, v_{MAX} the maximum allowed value of this parameter, ω_i and $-\omega_i$ the angular speeds from which the limitation ranges begin and ω_{MAX} the maximum angular speed (see Figure 3.56).

* * *

After having added to the system control all the measures proposed throughout the different sections included in this chapter, the haptic handlebar must be evaluated. For this purpose, an controlled experiment is presented in the next chapter.



UNIVERSIDAD
DE MÁLAGA

4

Haptic handlebar evaluation

"The strongest arguments prove nothing so long as the conclusions are not verified by experience. Experimental science is the queen of sciences and the goal of all speculation."

— Roger Bacon

In Chapter 2, the implementation of the handlebar was described and the first tests were carried out. The results of the latter gave rise to a deeper study of the system in Chapter 3. According to the conclusions drawn a control was proposed. Now, in this chapter the system is going to be evaluated with a formal controlled experiment. It comprises two different parts: the first of them is aimed to extract objective data about the driving. The other has the purpose of gathering the subjective perception of the attendants when driving using the system. In the process, the haptic handlebar is compared to other common commercial device that performs the same function.

4.1 Haptic handlebar and attendant joystick comparison (E5)

One way to evaluate the device proposed in this manuscript is to compare it, in a controlled experiment, with other assistive system which is currently a commercial alternative. As explained in Chapter 1, the most common option that fully assists the caregiver in the PW driving is the attendant joystick. This way, a joystick was added to the upper-rear part of the chair frame, that is where these tools are usually located. It is connected to the joystick socket of the PW control module. With this modification, the PW can be dually driven either with the haptic handlebar or with the attendant joystick. At this point it is crucial, not only to assess the performance of both devices from an objective and rigorous standpoint, but also to extract and take into consideration the subjective perception and the opinion of the participants. With this purpose, an experiment (E5) was designed. It consists of two parts, one targeted at measuring and comparing the driving performance when both devices are used (E5.1), and other focused on the volunteers driving sensation (E5.2). Ten people (P1-P10) took part in this experiment, given writing consent and complying with the declaration of Helsinki at all times. Their ages were collected in the second part of the experiment and they will be showed together with the results of this part. They were not aware of the experiment target.

4.1.1 Assessment of driving performance (E5.1)

4.1.1.1 Experimental setup

The first part required the design and implementation of a new experimental setup. A first step has been already commented. A joystick was added to the setup allowing the PW to be steered with it. Switching from the handlebar to the joystick and vice versa was just made by changing the cable that was connected to the PW control module. In order to assess both systems driving capacities a path of 35 meter was designed. It combines straight lines and soft turnings with challenging curves. It can be seen in Figure 4.1.

A yellow tape with a width of 5cm was used to mark out the trajectory to be followed by the participants. In order to extract precise and reliable data, it was necessary to provide the persons who were to drive the PW with a mechanism that allowed them to know how their performance was being. This way, they could correct the trajectory deviations. A laser pointer was added to the setup with this purpose. It was placed in a platform attached to the

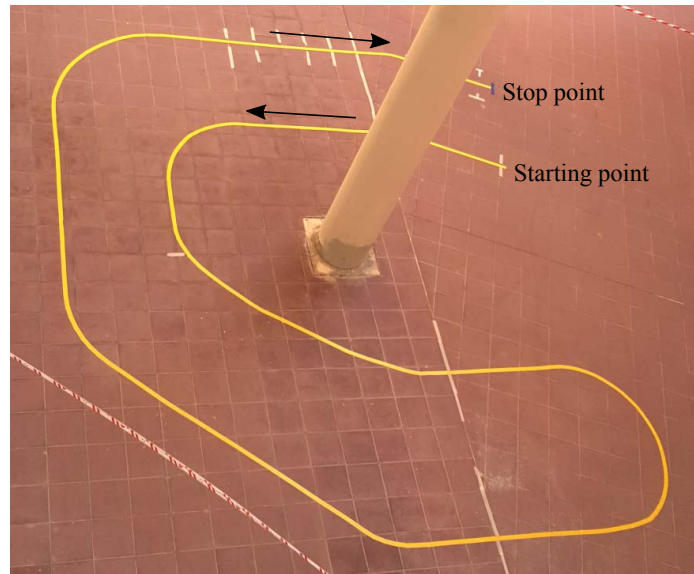


Fig. 4.1 Path of experiment E5.

PW seat pointing to the ground. As a result, a circular light was seen on the floor just before the chair, aligned with the middle point between the two wheels. The participants were said to keep the laser beam circular light inside the tape while driving. This way if they saw that the light came out of the tape surface, a correction could be made. The experimental setup is shown in Figure 4.2. Only the new elements with respect to the setup in Figure 3.3 have been labeled.

A camera, Pro 9000 by Logitech, was also added to the setup. It was attached to the same structure of the laser pointer in the PW seat. As with the latter it was pointing to the ground. Connected to a computer, it captured the piece of floor just before the chair. Its function was to record the tests carried out by the participants. The videos would be used to measure to what extent they followed the path. Figure 4.3 shows the camera and laser pointer on the chair seat. The reflection of the laser on the tape is displayed on the right, as was seen by the participants.

E5.1 involved two different trials so that, apart from that explained above, another location was used. It was a corridor and a research laboratory. Figure 4.4 depicts the maneuvers to carry out in this place, with the most important distances and sizes. Its use will be explained in the next subsection.

4.1.1.2 Protocol and methods

As said before, the experiment E5.1 comprised two distinct trials:



Fig. 4.2 Experimental setup of E5.

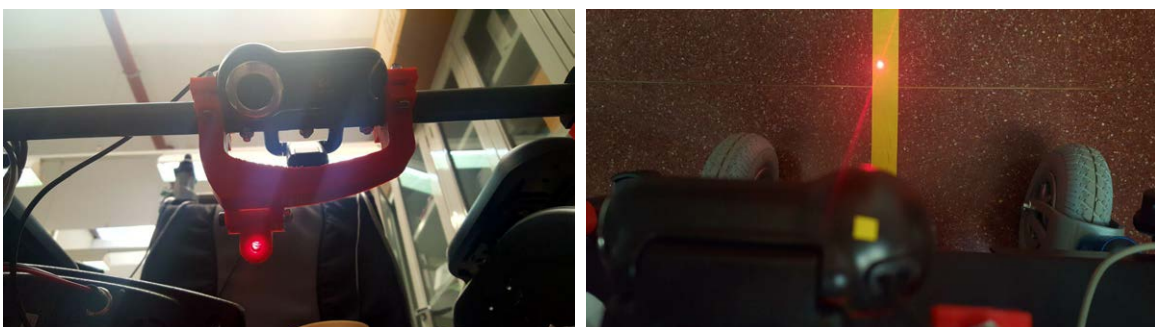


Fig. 4.3 Laser pointer and cam attached to the PW seat, from below (left). The same structure from above (right). The laser circular reflection is visible on the tape.

1. The first was that realized where Figure 4.1 depicts. The marked path is on the ground floor of a university building, that is a quite ample space. Before capturing their performance following the path, the participants were allowed to drive around freely with both devices, about two minutes with each of them. This intended to emulate a real life situation, concretely the experience of driving the PW in an open space with few obstacles. They drove as they wished, performing different maneuvers. During this time, the haptic handlebar settings were adapted to the person who did not fit in the default configuration. Few changes were made. The adjustments were basically handlebar sensitivity, tactels arrangement (see Section 3.3) and handlebar height. The attendant joystick was entirely controlled by the PW firmware, which is specially designed for that. After that, the participants were asked to follow the path on the ground, keeping the laser light into the tape to the possible extent but driving as natural as they could. They were not given any instruction about speed or time limitations. They performed the test with one of the devices, and with the other afterwards. After realizing the test one time, they may have learned slightly the maneuvers that they were going to perform during the second trial. Although the driving device is different, this could favor a better performance in the second test and distort the results. This way, half of the participants started using the attendant joystick and the other half started with the haptic handlebar.
2. Thereafter, the volunteers were moved to an indoor location of the same facility to perform the second trial. It is showed in Figure 4.4. Here, the environment comprises a corridor and a laboratory. If we compare the size of the PW and the available room, we see that the setup implies driving in narrow spaces. The aim was to emulate a daily life driving activity in enclosed and confined places such as the inside of a house, a supermarket, etc. The test consisted in entering the laboratory from the corridor through the door, turning to the left and, once reached certain point, driving backwards arriving at the stop point after turning right¹. The only marks on the ground were those to indicate the starting and stop points and that where the movement had to be switched from forwards to backwards. Again, the participants did not receive instructions about speed or time, but only about driving as naturally as possible avoiding colliding with the obstacles (walls and table). If they collided they could correct the trajectory as many times as necessary. As with the previous path, half of volunteers started the test with the joystick and the other half with the handlebar. The number of collisions made with each driving interface was registered.

¹The PW is turning to the left. It is right from the point of view of the attendant, who is walking backward.

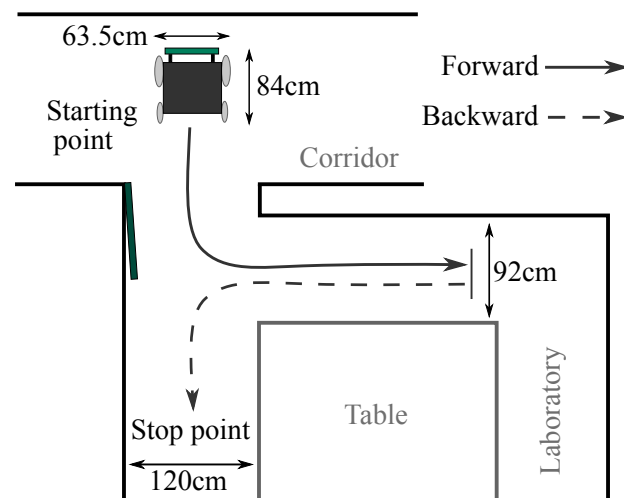


Fig. 4.4 Corridor and laboratory used in the first part of the experiment E5. Continuous and dashed lines refer to the PW going forward and backward, respectively.

Regarding the data handling, the videos recorded following the path were processed in Matlab with color-based segmentation, using K-means clustering [123]. The laser and camera were oriented in such a way that the light circle appeared in the upper part of the videos, in a fixed position. It made the processing lighter since only a few of the upper lines of each frame were necessary in the computation. Figure 4.5 shows an example of color-based segmentation applied to a frame. From top to bottom, we can see how the algorithm distinguishes the color of the tape and the laser light from the rest of elements of the image, mainly floor tiles and dirt. Once the tape (target trajectory) and the laser light (actual trajectory) are isolated in an image, the error can be computed. The distance between the tape and the laser point is measured in number of pixels, and after, translated into centimeters, since the scale pixel-to-meters is known.

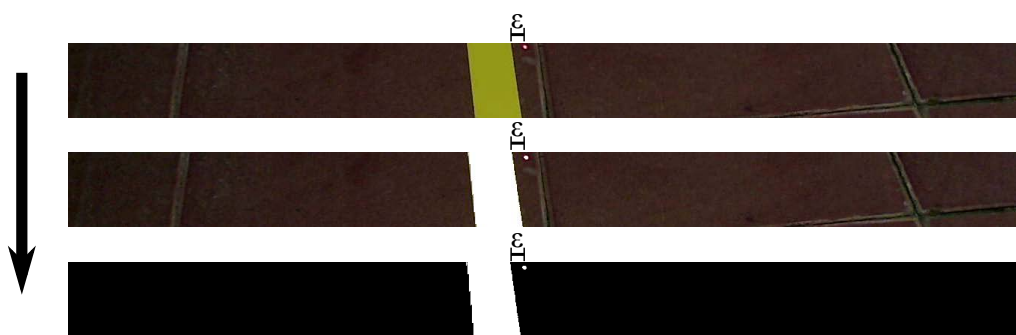


Fig. 4.5 Example of the color-based segmentation in the video processing of experiment E5.1.

In Figure 4.6, we can see the result of processing the first eighty frames of one of the tests. The frame rate of the video was 15fps, so only a simple division is required to convert

to time units. On the upper part, red and yellow curves refer to the left and right tape borders. The dashed line represents the laser light used as reference to guide the participants. It is a constant since the light is always in the same location in the videos and it is the tape what appears varying as the participant drives. Below, the trajectory error is showed. Note that, as long as the dashed line is between the red and the yellow curve (thus the light is inside the tape area), the error is zero.

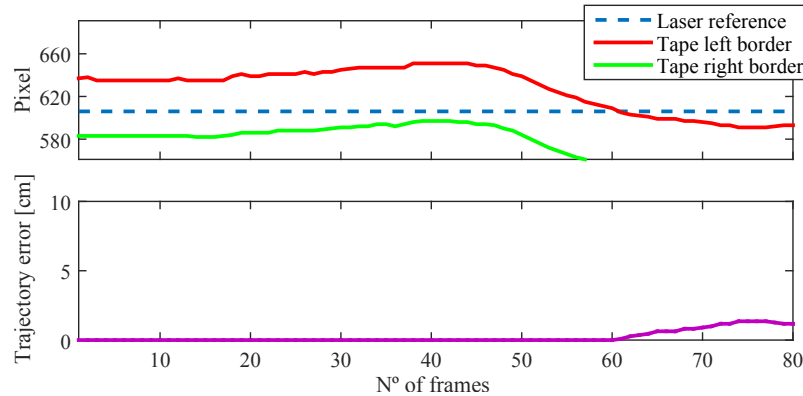


Fig. 4.6 Graphical representation of the tape borders detection for the first 80 frames of one test (top). The dashed line refers to the laser light position. Distance from the reference laser light to the tape (bottom).

4.1.1.3 Results

The trajectory errors registered for both devices during the first trial of E5.1 are depicted in Figures 4.7 and 4.8. The biggest errors correspond to the first left turn and the subsequent right turn (see Figure 4.1). They are tight and there hardly are straight segments between them. The first right turn is specially challenging and appears as a peak error in some of the charts as those from P2, P3 or P4.

Since it is difficult to come to firm conclusions by using the latter figures, some parameters have been calculated from the experimental data. They are the following: mean trajectory error (\overline{Error}), maximum trajectory error ($Error_{MAX}$), test duration and product between the mean trajectory error and the duration of each test ($\overline{Error} \cdot Duration$). The values of each of them are listed in Tables A.7 and A.8, in Appendix A. The diagrams of Figure 4.9 have been built from those tables and ease the visual comparison of the obtained values for the attendant joystick and the haptic handlebar.

All of them are aimed to measure the performance of the volunteers when driving with one interface and the other. The mean error is a good variable to assess how accurate the

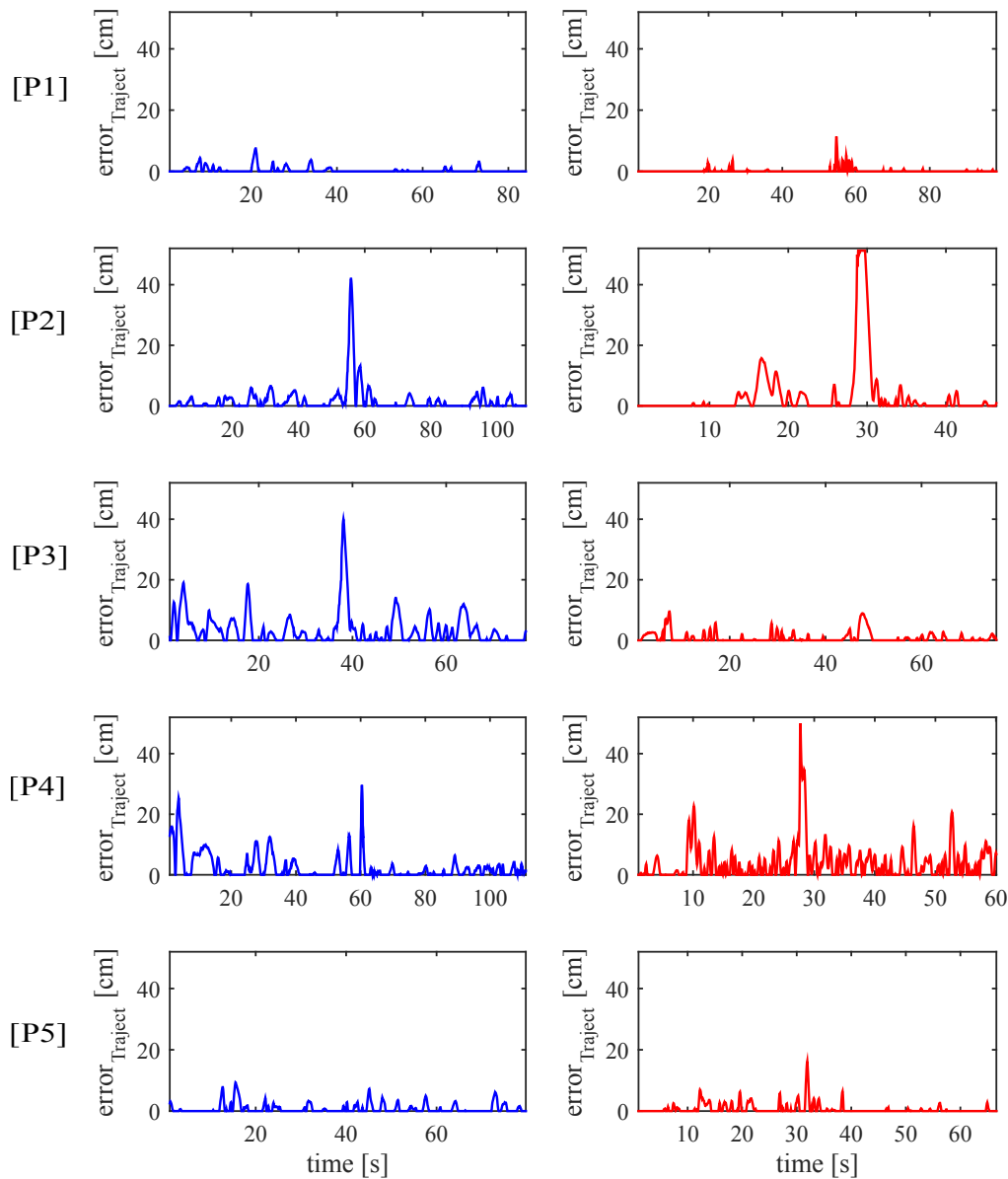


Fig. 4.7 Trajectory error for participants P1-P5 in experiment E5.1 using the attendant joystick (left, in blue) and the haptic handlebar (right, in red).

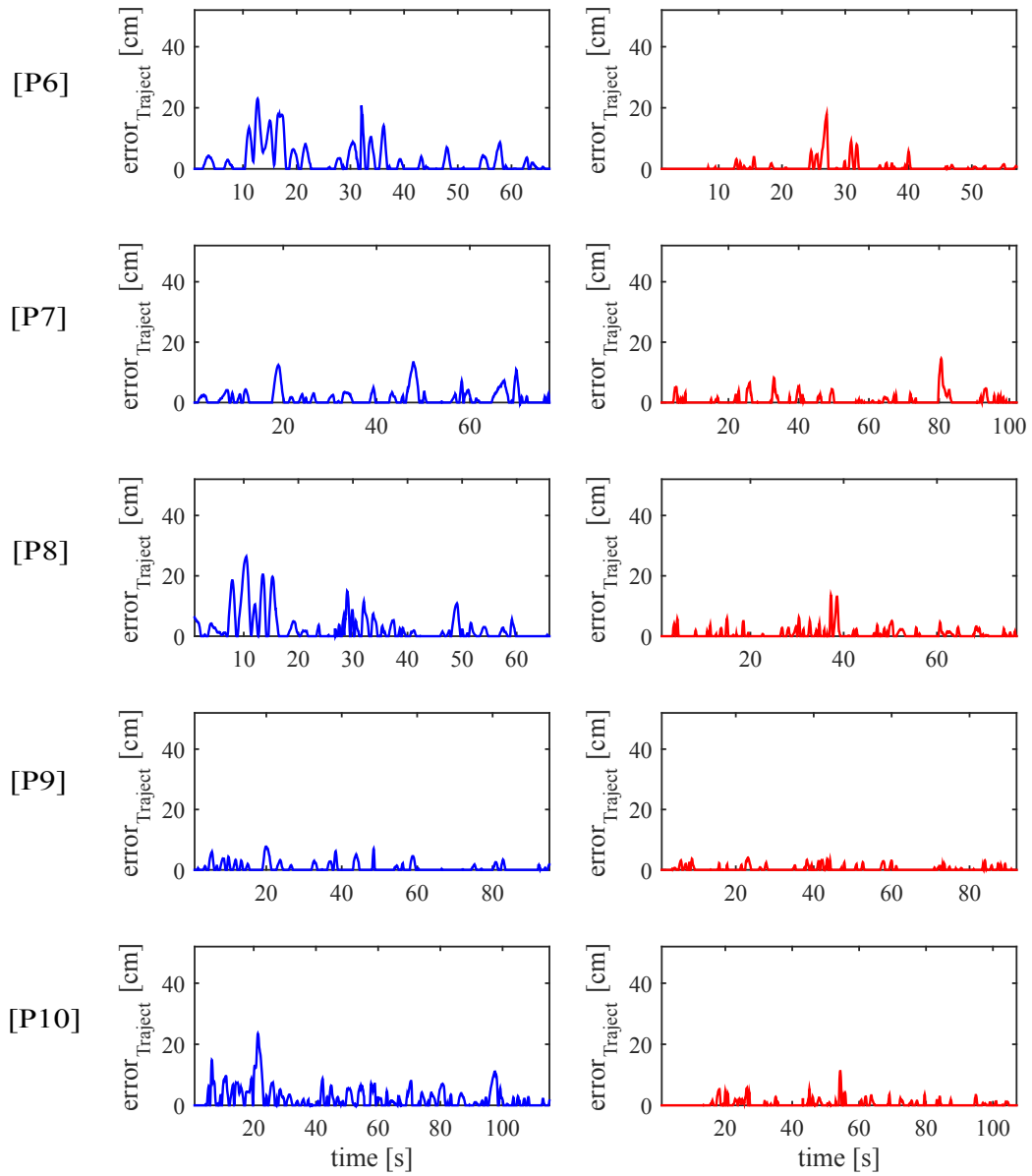


Fig. 4.8 Trajectory error for participants P6-P10 in experiment E5.1 using the attendant joystick (left, in blue) and the haptic handlebar (right, in red).

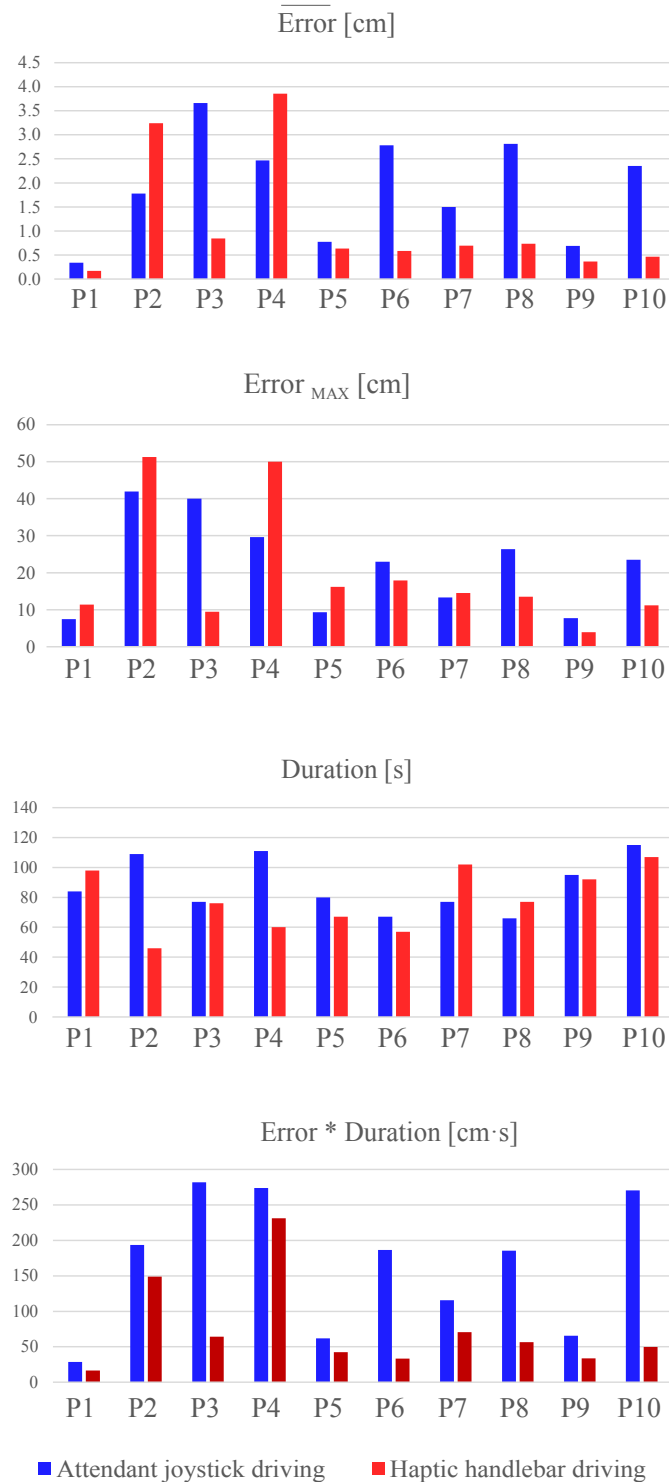


Fig. 4.9 From top to bottom: mean trajectory error, maximum trajectory error, test duration, product of mean trajectory error by test duration. The results for the attendant joystick are showed in blue and those for the haptic handlebar in red.

trajectory tracking was (Figure 4.9 top). As can be observed, \overline{Error} shows better numbers for the haptic handlebar than for the joystick in 80% of the tests. Besides, the difference is considerably large in four of the ten tests. Below, in the same figure, we see that in the case of $Error_{MAX}$ the values are more similar. The maximum error was caused by the use of the handlebar in half of the tests and using the joystick in the other half. However, the importance of this parameter is relative. A particular volunteer may produce a large deviation at some point and still have a good performance, if we look at the driving during the whole test. The bar chart below that of $Error_{MAX}$ gathers the test durations, i.e. how much time the participants needed to complete the full path. The required time was longer for the handlebar driving in three of the ten tests. Hence seven participants spent more time following the path when they used the joystick. Finally, in Figure 4.9 bottom, the bar diagram shows the product $\overline{Error} \cdot Duration$. This parameter is interesting since, the trajectory error and the test duration may be linked. That is to say, if a participant spends much more time undergoing the test with one of the devices than with the other, the error will be probably smaller with the first than with the second. This way, this parameter combines the error and the trial duration so that the latter point is taken into consideration. High values suggest that either long time was used to carry out the test, or the error made was large or both causes at the same time. On the contrary, behind low values may lie either small errors, or little times or the two previous cases at the same time. In order to distinguish each particular case, \overline{Error} and duration diagrams are helpful. As observed, the results provided by this parameter are better for the handlebar than for the joystick in all the tests. Focusing on the \overline{Error} chart (top), P2 and P4 were the only two subjects that made a bigger error with the handlebar than with the joystick. However, as said, they got a better $\overline{Error} \cdot Duration$ for the handlebar use. Looking at the $Duration$ bars we find that it could be well due to that fact that they spent about twice the time performing the experiment when the joystick than with the handlebar.

Concerning the handlebar system configuration, participants P4 and P6 found more comfortable to drive the PW when tactels arrangements D and F were selected (see Table 3.4 in Section 3.3). Note that they consist in rotating one tactel clockwise and anticlockwise, respectively, the arrangement by default (E), that was preferred by the rest of participants. Besides, these two persons reported to have noticed an asymmetry when pushing and pulling. The effort needed to make the PW go backwards was higher than that to make the PW go forward. The remaining modifications were slight variations of the linear and angular speeds gains. Some participants as P2 experienced little jerks at the beginning of the test, when his driving was still a little hesitant. It became steadier afterwards. It seems that when tugs appeared, they were modulated by the attendant's gait.

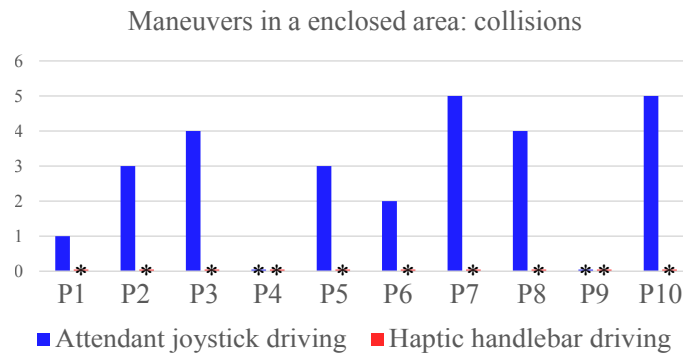


Fig. 4.10 Number of collisions during driving in the second location with the attendant joystick (in blue) and with the haptic handlebar (in red) (* represents zero collisions).

Regarding the second trial carried out in the location of Figure 4.4, as explained, collisions with the environment were registered when both interfaces were used. The results are depicted in Figure 4.10. Collisions took place between the PW and either the walls or the laboratory table. As showed, no impacts occurred when the haptic handlebar was used, in none of the tests. Only in two of the ten tests, there were not impacts when driving with the joystick. In the remaining eight tests, there were between one to five collisions. They occurred mainly in turns while going forward and backward. The backward maneuver was significantly difficult for the most of the volunteers. Note that, although time information is not displayed, impacts normally lead to delays and longer times. When the PW collided with an obstacle, it had to be moved away from the latter to resume the march. This process took time. So, driving with the handlebar was faster on more occasions. On the other side, although there were no collisions, some users realized some of the maneuvers with the handlebar producing little tugs, in little discrete movements that are not common in a natural driving.

As seen throughout the section, the haptic handlebar driving provides better results than that using the attendant joystick. These are objective results, which are really valuable. However, the participants perceptions have not been yet considered. The next section will be aimed at it.

4.1.2 Gathering of participants perception (E5.2)

In order to collect the opinions and perceptions of the ten participants, they were asked to fill a form just after taking part in the experiment E5.1. They could spend as much time as they needed. The form was implemented with the tool Google Forms and was filled in the same laboratory where the second part of E5.1 took place. The questionnaire was anonymous

and the computer screen was placed in such a way that it was not visible for the experiment organizers.

The form consisted of two parts. The first was composed of questions about the driving experience using the haptic handlebar and the attendant joystick. The same questions were asked for both devices. The type of questionnaire chosen to present the distinct selectable answers was the Likert scale [124, 125]. It has proven to be a good tool to gather the opinion of respondents [126, 127]. This way, for every question the participants were given several possible answers that were ordered gradually, from left to right. The number of options was seven and only one of them could be selected. An odd number has been chosen in order to provide the surveyed with a central neutral choice. It reduces the bias by allowing truly neutral people to express themselves honestly without forcing them to decide on one of the sides [128]. After each question, there was a text entry box in case they wished to justify or expand their response.

4.1.2.1 Form questions

The content of the form was the following²:

Q1. *With respect to its use, how do you consider the haptic handlebar / attendant joystick?*

- 1) Very difficult
- 2) Difficult
- 3) Rather difficult
- 4) Neither easy nor difficult
- 5) Rather easy
- 6) Easy
- 7) Very easy

Q2. *Concerning comfort, how do you consider the haptic handlebar / attendant joystick?*

- 1) Very uncomfortable
- 2) Uncomfortable
- 3) Rather uncomfortable

²Actually, what is showed is its translation into English. The original form was in Spanish, the home language of the respondents.

- 4) Neither comfortable nor uncomfortable
- 5) Rather comfortable
- 6) Comfortable
- 7) Very comfortable

Q3. *How much training do you consider is needed to use the haptic handlebar / attendant joystick?*

- 1) Too much
- 2) A lot
- 3) Quite a lot
- 4) Neither too much nor too little
- 5) Little
- 6) Very little
- 7) None

Q4. *Regarding its usefulness, how do you consider the haptic handlebar / attendant joystick?*

- 1) Very useless
- 2) Useless
- 3) Rather useless
- 4) Neither useful nor useless
- 5) Rather useful
- 6) Useful
- 7) Very useful

Q5. *With respect to safety, how do you consider the haptic handlebar / attendant joystick?*

- 1) Very insecure
- 2) Insecure
- 3) Rather insecure
- 4) Neither safe nor insecure
- 5) Rather safe

- 6) Safe
- 7) Very safe

Q6. *Concerning physical and mental fatigue, how do you consider the haptic handlebar / attendant joystick?*

- 1) Very tiring
- 2) Tiring
- 3) Rather tiring
- 4) Neither effortless nor tiring
- 5) Rather effortless
- 6) Effortless
- 7) Very effortless

The second part of the survey comprised a few personal questions:

a) *Had you used a joystick before performing the experiment (videogames, machine operating, etc.)?*

- 1) Yes
- 2) No

b) *Had you used a device similar to the haptic handlebar before taking part in the experiment?*

- 1) Yes
- 2) No

c) *Are you familiar with the role of wheelchair assistant?*

- 1) Yes
- 2) No

d) *How old are you?*

- 1) 25-30
- 2) 30-35

- 3) 35-40
- 4) 40-45
- 5) 45-50
- 6) 50-55
- 7) 55-60
- 8) 60-65

e) *Leave, if you wish, an additional comment about your experience after having driven with both devices.*

4.1.2.2 Form responses

Below, in Figure 4.11, a summary of the responses to the form questions is given. Note that, since it was anonymous, it is not possible to know the correspondence between each participant (P1-P10) and each set of answers (R1-R10). At the end of Appendix A, all the responses from every volunteer can be consulted together with the commentaries they left, if they did it. The seven responses available for each question are numbered from the most negative (1) to the most positive impression (7). This way, the higher the number of the chosen option, the better the respondent's opinion is and, conversely, the lower the number associated to the answer, the worse is the participant's perception. The central answer (4) indicates neutrality. Some parameters have been calculated for the groups of responses to each question. They are listed in Table 4.1. The *median* (\tilde{x}) has been used as measure of the central tendency [129]. In addition, the Mann–Whitney test *U* – *value* has been computed to assess the statistical significance when comparing the groups of responses given to the same question referring to the attendant joystick and to the haptic handlebar. Finally, another parameter has been computed to evaluate the perception of both devices (*Pe*). It takes into account the number of times that each option (1-7) has been selected as answer to a particular question, so that it gives an overall picture of the participants' perception for each assessed aspect. It is calculated as:

$$Pe_{i_{AJ/HH}} = \frac{\sum_{j=1}^7 n_{A_j} \cdot j}{\sum_{j=1}^7 n_{A_j}} \quad (4.1)$$

where i refers to asked question (Q1-Q6). n_{A_j} represents the number of times that certain option, A_j , has been selected by the respondents when answering the question Q_i . j varies in the interval [1-7], since seven options are always given. n_{A_j} is within the range [0-10], as there are ten participants. Note that Pe varies in the range [1-7]. *AJ* and *HH* means attendant joystick and haptic handlebar, respectively.

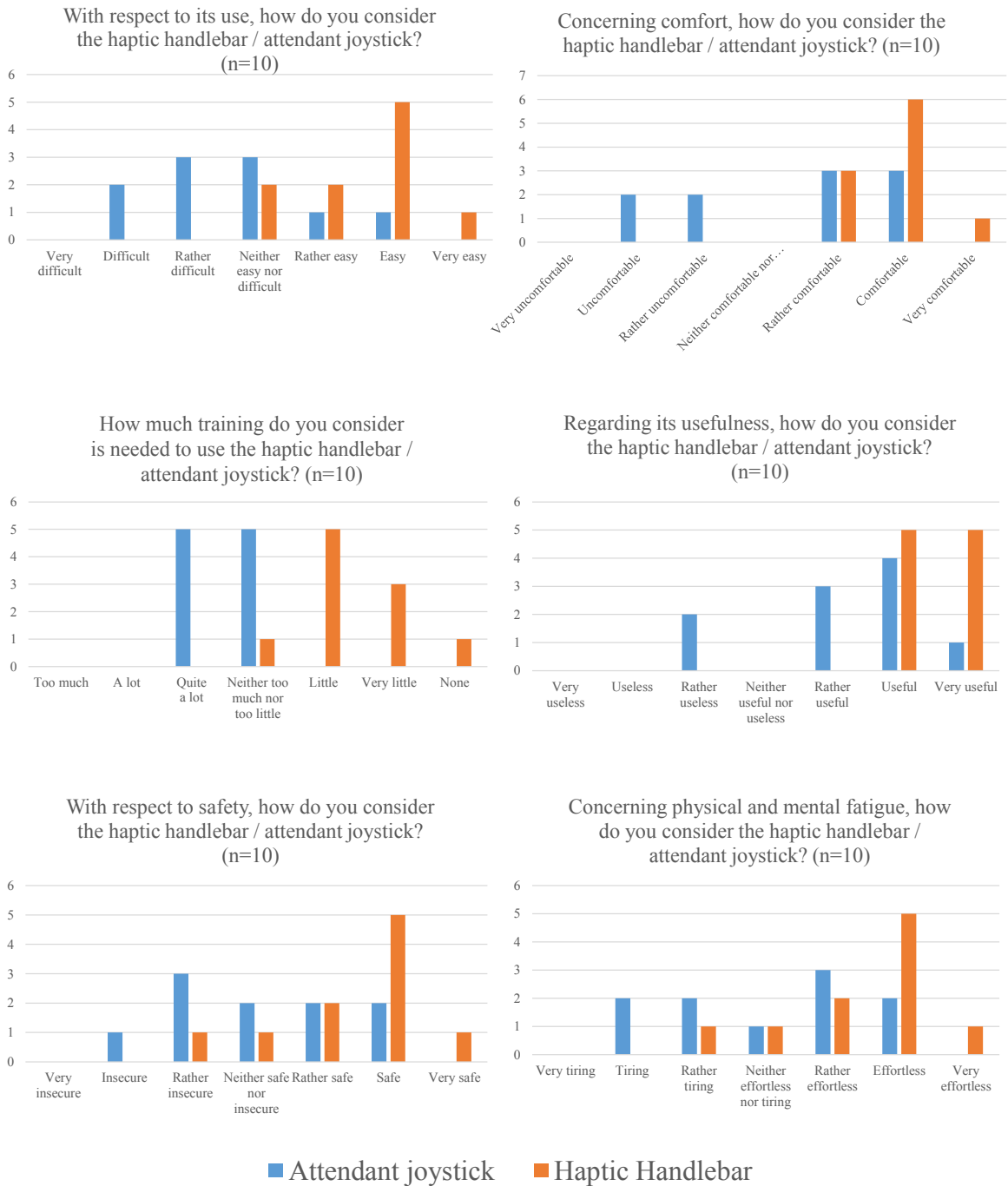


Fig. 4.11 Participants’ opinion about different aspects of the driving with both devices: ease of use (top-left), comfort (top-right), training (center-left), usefulness (center-right), safety (bottom-left) and fatigue (bottom-right).



Table 4.1 Pe coefficient, $Median (\tilde{x})$ and $U - value$ of Mann-Whitney Test (one-tailed, with $U_{critical_{p<0.05}} = 27$) for the Likert scale results of the questionnaire.

		Pe	\tilde{x}	$U - value$
Q1. Ease of use	<i>Attendant Joystick</i>	3.6	3.5	12.5
	<i>Haptic Handlebar</i>	5.5	6	
Q2. Comfort	<i>Attendant Joystick</i>	4.3	5	22.5
	<i>Haptic Handlebar</i>	5.8	6	
Q3. Required training	<i>Attendant Joystick</i>	3.5	3.5	2.5
	<i>Haptic Handlebar</i>	5.4	5	
Q4. Usefulness	<i>Attendant Joystick</i>	5.2	5.5	17.5
	<i>Haptic Handlebar</i>	6.5	6.5	
Q5. Safety	<i>Attendant Joystick</i>	4.1	4	23.5
	<i>Haptic Handlebar</i>	5.4	6	
Q6. Fatigue	<i>Attendant Joystick</i>	4.1	4.5	24.5
	<i>Haptic Handlebar</i>	5.4	6	

Pe, \tilde{x} perception reference: 1 (Negative) \leftarrow 4 (Neutral) \rightarrow 7 (Positive)

$Pe_{i_{AJ}}$ and $Pe_{i_{HH}}$ are useful to compare both driving interfaces. In line with the above, if their value is below 4, the global perception is *negative*. If it is around 4, the opinion about the device tends to be *neutral*. Finally, above 4 the perception of the driving system starts being *positive*. In the top part of Figure 4.11, we can see what the participants think about the ease of use of both devices. Some of them find the joystick kind of difficult to use, with $Pe_{1_{AJ}} = 3.6$ and $\tilde{x}_{1_{AJ}} = 3.5$. Only two participants think that this device is rather easy or easy to use. In general, they consider the handlebar easy to use, $Pe_{1_{HH}} = 5.5$ and $\tilde{x}_{1_{HH}} = 6$. None of the subjects answered with a negative option (1-3) with respect to the use of this device. Regarding comfort, we see that the opinions about the haptic handlebar are considerably positive ($Pe_{2_{HH}} = 5.8$ and $\tilde{x}_{2_{HH}} = 6$, with all the answers between 5 and 7). The attendant joystick acceptance in terms of comfort has been quite neutral looking at $Pe_{2_{AJ}} = 4.3$, or moderately positive considering $\tilde{x}_{2_{AJ}} = 5$. Four participants have a perception moderately negative and six moderately positive. With respect to the amount of training required to use properly the driving interfaces, half of the volunteers are neutral (4) whereas the other half have the impression that quite a lot training is needed to use the joystick, $Pe_{3_{AJ}} = 3.5$ and $\tilde{x}_{3_{AJ}} = 3.5$. The handlebar is perceived as an interface for which not much training is required, $Pe_{3_{HH}} = 5.4$ and $\tilde{x}_{3_{HH}} = 5$. Concerning the question geared to finding out what users think of the usefulness of both devices, the result is quite significant since both parameters represents a quite positive trend: $Pe_{4_{AJ}} = 5.2$, $\tilde{x}_{4_{AJ}} = 5.5$, $Pe_{4_{HH}} = 6.5$ and $\tilde{x}_{4_{HH}} = 6.5$. It

may indicate they perceive the assistance of the PW driving as useful and, in this direction, any help is appreciated. Regarding the sense of safety, the thoughts about the attendant joystick are mainly neutral, $Pe_{5_{AJ}} = 4.1$ and $\tilde{x}_{5_{AJ}} = 4$, and negative and positive opinions are compensated. If the joystick is not moved the PW is stopped, but if it is pressed there is no way of knowing whether it has been activated involuntarily or by a blow with an object, what may be perceived as risky. Sense of security is greater with the haptic handlebar, $Pe_{5_{HH}} = 5.4$ and $\tilde{x}_{5_{HH}} = 6$, which automatically stops the PW if the user releases the handlebar. Finally, at the bottom, the last question is aimed at the fatigue produced by driving. Regarding the use of the joystick, the overall sensation is neutral, $Pe_{6_{AJ}} = 4.1$ and $\tilde{x}_{6_{AJ}} = 4.5$, with positive and negative opinions in equal numbers. The handlebar is seen more or less as an effortless device, $Pe_{6_{HH}} = 5.4$ and $\tilde{x}_{6_{HH}} = 6$. Furthermore, all the results of comparing the answers given to the questions regarding the joystick and the handlebar use with the Mann-Whitney U Test are statistically significant (the critical value of U at $p < 0.05$ is 27).

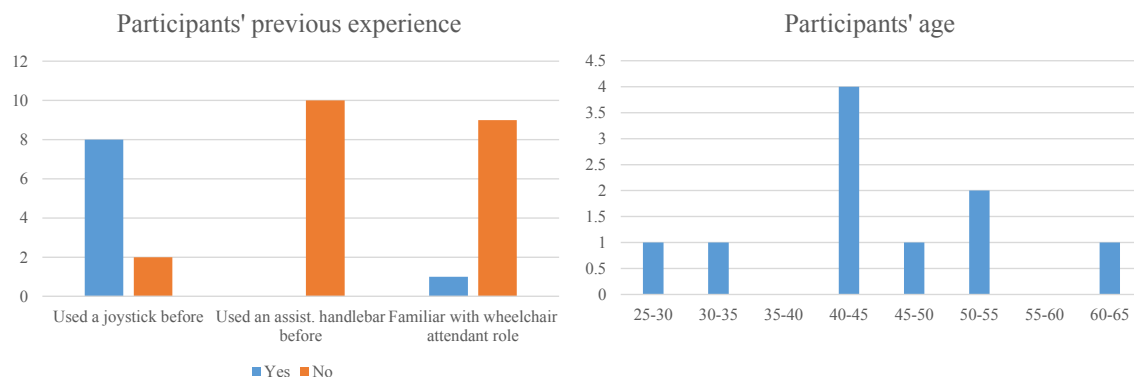


Fig. 4.12 Participants' previous experience with a joystick, an assistive handlebar and wheelchair attendant role (left). Participant's ages (right).

Figure 4.12 summarizes the answers to the personal questions asked to the participants. On the left, we see that the most of them had used a joystick before and none a handlebar providing powered assistance (it goes without saying that they had used a regular handlebar formerly). One volunteer had previous experience in tasks of caregiving people who use a wheelchair. On the right, we can see that a wide age-range has been covered.

The commentaries left by the participants highlighted the ease of use of the haptic handlebar: "*With a little practice, it's easy to control the movement*", "*After using it a little, it is easy to handle*", "*It's easy to adapt to the device*", etc. Also its usefulness: "*It greatly reduces the effort that has to be made in order to move and steer the chair*" or "*This device has really ample possibilities*". Others may seem to be negative, like the following about safety: "*Mainly during the learning period [it is rather insecure]. With practice, it gets safer*". Or this one speaking of fatigue: "*It can be rather tiring in the beginning when you*

are focused on the handlebar. After getting used to it a little, it's not tiring at all." However, when they say "the learning period" or "the beginning" they are referring to *their* learning period that was no more than some minutes, as explained previously. If only some minutes of driving are needed in order that the system becomes safer or effortless, we can see that the message that we can extract from the commentaries is quite optimistic. There are also some commentary that may help improving the haptic handlebar and that will be discussed in the next section.

Regarding the comments about the joystick, those about its use are, for example: "*It is operated with only one hand, what I found more complicated and less natural than the handlebar use*" or "*The lateral movements are abrupt and it is difficult to follow a specific trajectory because of the zigzag. Only the forward movements are steady*". They transmit lack of intuitiveness and difficulty in the maneuverability. With respect to comfort, they continue in the same vein: "*It is more easy to accommodate and to steer grasping the handlebar than grasping the joystick*", "*The hand posture is not very natural*". In general, they reflect that training is needed: "*It requires much more training than the handlebar*" or "*The backward driving is difficult and it requires considerable training*". They also highlight the superiority of the handlebar in safety terms: "*(...) I think that the handlebar monitors in a better way what the attendant is doing [in order to avoid risks]. Besides, the handlebar has a softer response to certain kind of maneuvers*". As seen and as is logical, the commentaries are on the same line as the rest of results of the experiment.

4.2 Discussion

In this chapter, an experiment composed of two parts has been presented. The first of them, E5.1, was aimed to compare as objectively as possible two assistive driving devices, such as the attendant joystick and haptic handlebar presented in this document. The experiment has provided generally better numbers for the handlebar in each of the computed parameters. This device has also obtained a much better performance maneuvering in an enclosed space, location in which the joystick has proven to be an unwise option (as reported in the literature cited in Chapter 1). The second part of the experiment, E5.2, was designed to gather the subjective perception of the participants when they used both devices. Again, the haptic handlebar has showed better results than the attendant joystick in all the assessed aspects, with $Pe_{i_{HH}} > Pe_{i_{AJ}}$ and $\tilde{x}_{i_{HH}} > \tilde{x}_{i_{AJ}}$ for all of them.

In addition to proving the superiority of the haptic handlebar as driving interface, the experiment has provided useful information that can be useful for the improvement of the

latter. As commented, two participants did not drive the PW properly through the handlebar when the tactel arrangement E was selected, what indicates that, although it may be valid for a large number of users, it is not an "universal" option. This possibility was previously suggested in Section 3.3. Besides, an asymmetry was found by these two participants, who needed to make a bigger effort when going backwards than when going forward. This may suggest that, among the eight available arrangements there would be none that totally fixed with their *grasping* characteristics. With a higher tactel resolution, there would be a larger set of tactel arrangements, what may allow a finer tuning. If the problem was not solved after increasing the tactel resolution, other options could be assessed. It may open the door, for example, to the possibility of using two tactels arrangements and, therefore, two $CoMs$ per hand, one that provided good response for forward and other that did it for backward maneuvering. The evaluation of which weight to give to each CoM could be studied with techniques as, for instance, fuzzy logic. Another simpler solution could consist in, if the asymmetry is recognizable by the system and it is only a problem of gain (the linear correlation is preserved), assigning different gains to forward and backward maneuvers. If we look back, we can recall that the same asymmetry commented above was already observed in the case of volunteer P7, in the experiment E1 (see Figure 3.10, in Chapter 3), for which the gradient of the function $SUM_{CoM}(F_y)$ was substantially different in forward and backward maneuvers.

Furthermore, although it has been enhanced, the starting phase of $CoMs$ stabilization is still perceived as contrived by some users, as this commentary shows: "[...] *the system is a little slow at first, when you have to wait to hear the sound signal*³. *What if I need to move the chair quickly to avoid an obstacle heading towards us?*". Note that this volunteer reflects on the hazardous scenario in which the PW has to be moved while the $CoMs$ are stabilizing. It suggests that a secondary "basic" control that allows a range of limited movements (perhaps, moving forward or backward a little) and does not depend on the $CoMs$ could be implemented. It may be used in case of emergency or to move the PW without the purpose of driving it (for example, if it is stopped and is an obstacle in the trajectory of another person).

On the other hand, some jerks and tugs have appeared in some cases in the beginning of the driving and when realizing fine maneuvers. They seem to be related to a hesitant and halting driving, above all when the user is not familiar with the system and he or she seems insecure. This phenomenon tends to be less present in more experienced users. Either way, it is worth studying the possibility of the implementation of some corrective mechanism that module the response of the system according to the driving circumstances, for example,

³Let us remind that an audible signal is emitted when the dynamic calibration process ends (see Section 3.4.1).

canceling the gait modulated effect or smoothing the system output when fine maneuvers are detected.

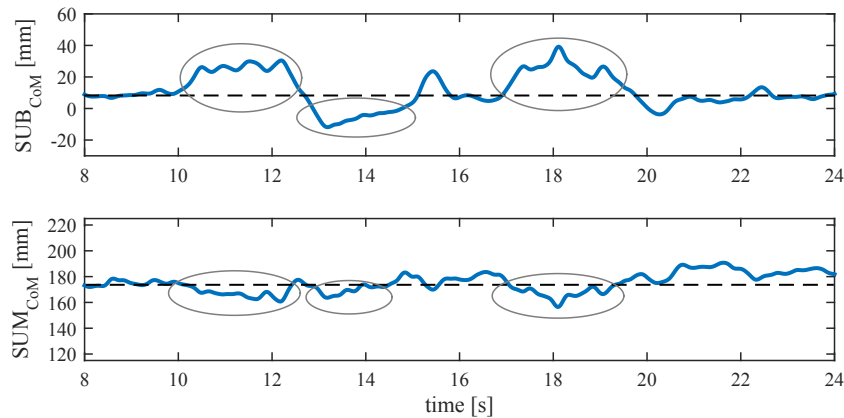


Fig. 4.13 Evolution of SUB_{CoM} , the dashed line represents the absence of turns (top). Evolution of SUM_{CoM} , the dashed line represents a constant forward speed (bottom).

On a separate issue, in Chapter 3, an interference between the parameters SUB_{CoM} and SUM_{CoM} was reported in some of the tests of E1. Figure 3.12 illustrated it. In that case, the system was controlled by the F/T sensor output. The same has been observed in some test of E5.1, this time using the tactile handlebar as control element. This inference is depicted in Figure 4.13. As can be seen, the turns observed in SUB_{CoM} (marked with ellipses in Figure 4.13 top) have certain impact on SUM_{CoM} (the same figure bottom). However, none of the participants have reported discomfort while driving in situations in which this interference may be taking place. It may suggest that either the effect is weak and difficult to notice or its repercussion is not totally negative and the little decrement of linear speed is not inconvenient when turning. In any case, further study would be necessary to draw more robust conclusions about this issue.

5

Haptic interface in another assistive systems

The most important thing about a technology is how it changes people.

— Jaron Lanier

In the introductory chapter, in Section 1.3, it was explained that the cost issue inherent to force sensors is shared by a large range of assistive devices, specially those that require a haptic interface to be used. This way, if the proposal that has been presented in the previous chapters of this thesis could be extended to other assistive systems, the mentioned drawback may be overcome. Since we thought that it deserved further study, a first step is taken in this direction in this chapter. Specifically, a haptic cane handle has been designed and implemented. Its performance is tested through an experiment after being attached to an instrumented cane; the *CoM* has happened to be again an useful parameter. Finally, the results are presented and discussed.

5.1 Instrumented cane (E6)

As said before, among of all the possible assistive tools, we decided to start with one of the most common and simplest: the cane. Canes increase balance and provide sensory feedback from the ground [130]. They are usually prescribed to avoid falls in the elderly [131]. They also allow post-stroke patients to have a safer gait and rehabilitation [132–134]. Both of them are cases in which a monitoring of the cane usage is necessary. In the elderly, monitoring may help avoid misuses that lead to accidents [135]. It is also useful in the recovery process of post-stroke individuals, since it provides data that can be used to improve the physical therapy [133]. To monitor the cane use, it has to be instrumented. That is to say, it must be equipped with sensors that are the elements in charge of capturing the information. Research has been dedicated to the development of this kind of canes. For example, a force sensor was attached to a cane shaft in order to measure interaction force in [136]. The device was used together with a treadmill in a virtual reality setup for rehabilitation. Instrumentations based on embedded sensors and processing units have been proposed in order to extend monitoring to day-to-day activities. This is the case of [137], where the applied force and the cane orientation are measured. A load cell and a 3-axis accelerometer are used for this purpose. A microcontroller acquires these data and provides audio feedback to let the users know about how they are using the cane for bearing their weights. Cane orientation and applied load force are also relevant parameters in the case of instrumented active canes [26, 24].

Our proposal consisted in conveying the idea of the tactile handlebar to the cane handle and exploring what information related to the cane usage it was able to provide. With this purpose, a first prototype was implemented. In the following, details of the prototype, experiments and results are provided.

5.1.1 Tactile cane handle

The implementation of the tactile handle can be seen in Figure 5.1 right. The base structure was a parallelepiped-shaped handle built in plastic. The same cost-effective commercial FSR sensors [91] that were used in the first tactile handlebar prototype were chosen to form the tactels. As in that case, their output is less sensitive and linear when placed on a rough surface. Thus, in order to have a good performance, they must lie on a flat surface [103]. This constraint explains the square profile of the handle. The FSR sensors covered the four sides of the latter, so that there were five of them in the top and lateral sides and three on the bottom. There were only three on this side because it is where the clamping screw to

attach the handle to the cane shaft was placed. Therefore, there was less space available. The eighteen tactels were interconnected forming a matrix of four rows by five columns (Figure 5.1 left). Note that, as said, in the lower face the number of columns is reduced to three. As in the case of the tactile handlebar, the matrix configuration is optimal since it minimizes the resources needed to address and digitize the tactels. Moreover, soft pads were placed on the active area of the FSR sensors to enhance the response by concentrating the force. Finally, the whole structure was covered with a layer of foam to make the grasp more comfortable. The dimensions of the resulting parallelepiped are 23mm×23mm×151mm.

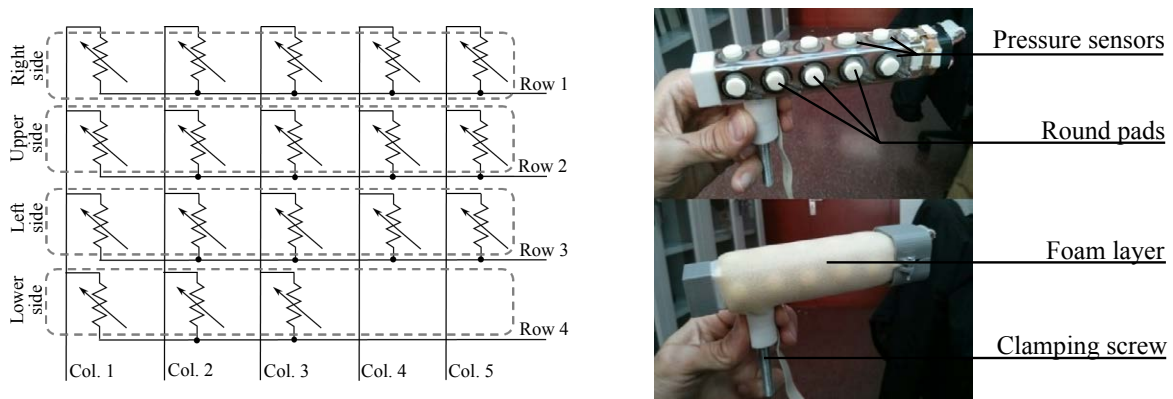


Fig. 5.1 Tactile cane handle schematic (left). Handle implementation (right).

The conditioning electronics is based again on a PIC18F4680, which has a wide range of input/output interfaces and a considerable number of Analog-to-Digital (AD) channels at an affordable price. Figure 5.2 shows the circuit scheme. As can be observed it is similar to that of the tactile handlebar (Section 2.3). The columns of the FSR matrix are wired to the AD channels of the microcontroller through transimpedance amplifiers. The rows are connected to analog switches controlled by generic digital input/output ports of the PIC. These activate the switches in order to ground the row that is going to be read and to connect the others to a reference voltage (V_{REF}). Note that the output of the amplifier for the chosen tactel can be calculated as shown in Equation 2.1. Besides, the feedback resistance, R_G , is implemented with a potentiometer so the gain of every column can be tuned independently. The output for the rest of the tactels will be zero as the voltage in their both terminals is the same, V_{REF} , due to the virtual short in the amplifier inputs. Once the voltage V_{OUT} has been digitized for every tactel, the information is ready to be sent to other devices through two communication interfaces: via UART-USB or via I2C. For the latter, a level conversion has been added so that it can communicate with, for example, Arduino boards. The implementation of the conditioning electronics in a PCB can be seen in Figure 5.3.

In order to analyze the prototype possibilities an experiment (**E6**) was designed. It is explained in the next sections.

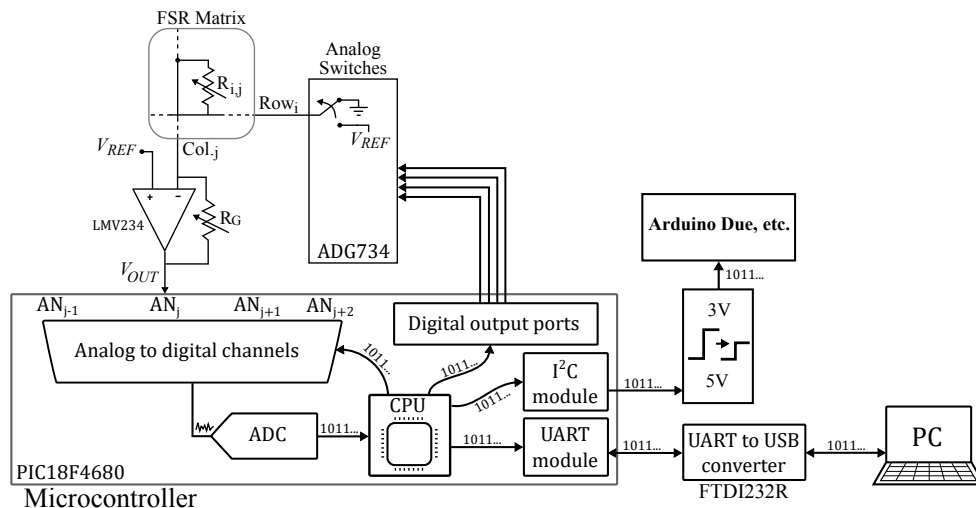


Fig. 5.2 Cane handle conditioning electronics scheme.

5.1.2 Experimental setup

The prototype was intended to be attached to an instrumented cane, so one of this kind was used in the experiment. It was built with an orthopedic cane from which the original handle was removed. Its height could be adjusted to fit each user. With the purpose of obtaining ground truth measurements, two more sensors were added. The first of them was an inertial measurement unit (IMU). It measured the cane pitch angle in the walking direction. It is the angle with respect to the vertical in the sagittal plane. In order to get the cane orientation an AHRS algorithm was running on the module. An Arduino Due board gathered the data from the IMU.

The other sensor was a Force/Torque ATI Mini45. It is the same that was used in the setup of the haptic handlebar experiments (Figure 3.3). It was placed in the middle of the cane shaft, so that it was divided in two segments joined by the F/T sensor. The experimental setup is showed in Figure 5.4 left. The F/T ATI Mini45 obtained the load force in the cane axis, F_z , i.e. that exerted by the cane user when leaning on it. The force sensor was connected to its amplifier (ATI FTIFPS1), which output was read by the National Instruments USB-6211 acquisition card. This card was connected to a personal computer to provide force data. All the data were synchronously acquired at a rate of 40Hz. The parameters captured by the two sensing devices and the tactile handle are showed in Figure 5.4 right.

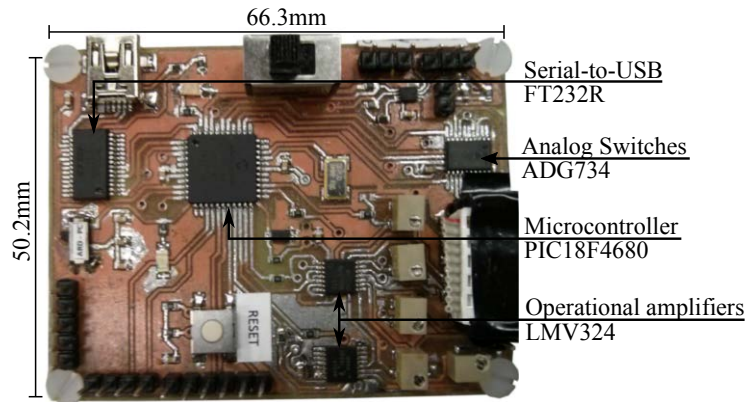


Fig. 5.3 Cane handle conditioning electronics board.

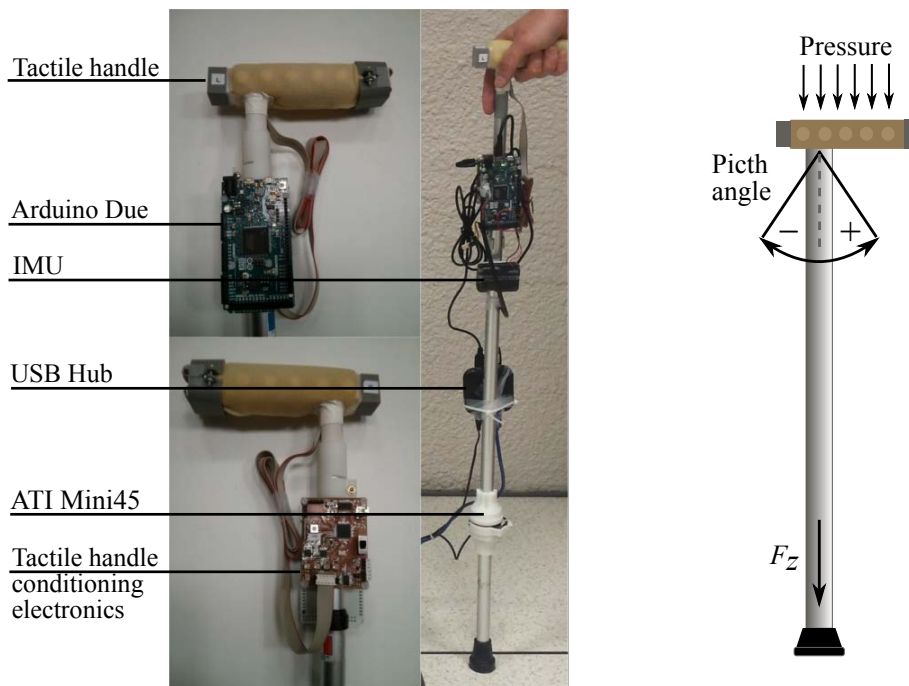


Fig. 5.4 Experimental setup of E6.

5.1.3 Protocol and methods

Ten healthy volunteers (P1-P10) with an average age of 25.3 years old (min:21, max:32) were selected to participate in the experiments. They were equipped with a knee brace and a modified sole in order to simulate walking impairment [138]. All the subjects gave written informed consent. The experiment met the ethical principles of the declaration of Helsinki. The participants were asked to walk for a distance of 5.5m using the cane, at their preferred speed. Each subject underwent four trials. The subjects were naive about the purpose of the experiments.

During the experiment, the pitch angle, the force sensor measurements and the tactile array data from the handle were captured as detailed above. As seen in Chapter 3, an useful way to process maps of pressures is by computing their center of mass or center of pressure. For the case of the cane handle it was calculated separately for each side, as Equation 5.1 shows.

$$CoM_{side} = \frac{\sum_{y=1}^5 y \cdot p(y)}{\sum_{y=1}^5 p(y)} \quad (5.1)$$

where y and $p(y)$ are the position and the pressure value of the y^{th} tactel of the array indicated by the subindex $side$. Note that, actually, for the lower side y varies from 1 to 3 (not to 5).

Figure 5.5 depicts an example of a pressure map from the cane handle and may help understand the previous expression.

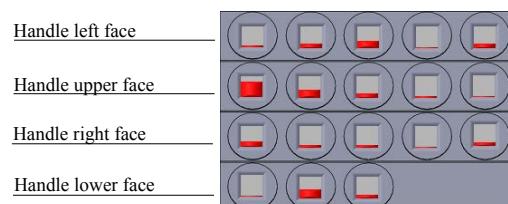


Fig. 5.5 Pressure map obtained from the tactile handle.

As with the tactile handlebar, the cane handle can also provide information about the grip pressure. Again, this can be estimated either in a global way, that is to say, including all the tactels or considering each row separately. Thus, the component of the grip pressure in one row of the FSR matrix could be calculated as the mean pressure on that side of the handle (see Equation 5.2).

$$\bar{P}_{side} = \frac{\sum_{y=1}^5 y \cdot p(y)}{5} \quad (5.2)$$

where, as with Equation 5.1, y is within [1,3] for the lower side .

We hypothesized that cane orientation angle was correlated with the center of mass of the pressure sensors equipping the handle upper side, i.e. that computed using Equation 5.1 where *side* refers to the upper face of the handle, CoM_U (see Figure 5.5). We also conjectured that a coupling may exist between the load force exerted on the cane when walking and the mean pressure on the upper side of the handle. The latter parameter is calculated with Equation 5.2, taking again the handle upper face, \bar{P}_U . For each trial, the data corresponding to the first and the last walking steps were removed from the four parameters. They were considered as transients and not representative of steady gait. The noise of the force sensor data was removed using zero phase low-pass filtering (a forward reverse processing was implemented). Each subject mean behavior was then computed considering his or her four trials. As the subject velocity across the trials could vary slightly, the completion of the task did not take necessarily the same amount of time. This made that each trial had a different number of samples. The mean duration of the four trials was taken as a basis. CoM_U , \bar{P}_U , load force (F_z) and pitch angle variables were then interpolated or extrapolated to fit the chosen duration. Thereafter, the mean CoM_U , \bar{P}_U , F_z and pitch angle trajectories were finally computed. Lastly, in order to assess the associations between the two pairs of variables, $\langle CoM_U, Pitch \rangle$ and $\langle \bar{P}_U, F_z \rangle$, Pearson and Spearman's rank-order correlation coefficients were computed for each participant.

5.1.4 Results

The obtained Pearson correlation coefficients for $\langle CoM_U, Pitch \rangle$ were: $r = 0.89$ [P1], $r = 0.94$ [P2], $r = 0.78$ [P3], $r = 0.97$ [P4], $r = 0.85$ [P5], $r = 0.95$ [P6], $r = 0.97$ [P7], $r = 0.86$ [P8], $r = 0.85$ [P9] and $r = 0.77$ [P10]. The Spearman's rank-order coefficients for the same pair of parameters were: $\rho = 0.86$ [P1], $\rho = 0.95$ [P2], $\rho = 0.72$ [P3], $\rho = 0.97$ [P4], $\rho = 0.84$ [P5], $\rho = 0.94$ [P6], $\rho = 0.97$ [P7], $\rho = 0.88$ [P8], $\rho = 0.81$ [P9] and $\rho = 0.76$ [P10]. As can be seen, Pearson numbers show a very high correlation in four tests and a high correlation in the rest (see Table 3.1). If we look at Spearman coefficients what happens is exactly the same. The linear regression functions that fitted with each of the tests were: $Pitch = 84.201CoM_U + 206.84$ [P1], $Pitch = 17.464CoM_U + 41.249$ [P2], $Pitch = 67.683CoM_U + 112.61$ [P3], $Pitch = 21.922CoM_U + 55.449$ [P4], $Pitch = 41.448CoM_U + 100.98$ [P5], $Pitch = 24.276CoM_U + 55.602$ [P6], $Pitch = 21.914CoM_U + 43.132$ [P7], $Pitch = 29.229CoM_U + 66.729$ [P8], $Pitch = 26.562CoM_U + 41.096$ [P9] and $Pitch = 77.724CoM_U + 106.11$ [P10].

The results obtained for the couple formed by \bar{P}_U and F_z computing Pearson correlation were: $r = -0.98$ [P1], $r = -0.95$ [P2], $r = -0.96$ [P3], $r = -0.96$ [P4], $r = -0.95$ [P5],

$r = -0.96$ [P6], $r = -0.96$ [P7], $r = -0.95$ [P8], $r = -0.95$ [P9] and $r = -0.94$ [P10]. The Spearman coefficients coefficients were: $\rho = -0.93$ [P1], $\rho = -0.92$ [P2], $\rho = -0.97$ [P3], $\rho = -0.94$ [P4], $\rho = -0.94$ [P5], $\rho = -0.93$ [P6], $\rho = -0.94$ [P7], $\rho = -0.92$ [P8], $\rho = -0.88$ [P9] and $\rho = -0.93$ [P10]. Analyzing the previous numbers, we see that regarding Pearson correlation all the coefficients represent a very high negative correlation. In the case of the Spearman results, nine of them lead to a very high negative and one to a high negative correlation. The linear functions computed for the previous coupling were: $F_z = -0.0577\bar{P}_U + 7.1396$ [P1], $F_z = -0.083\bar{P}_U + 3.3471$ [P2], $F_z = -0.0631\bar{P}_U + 6.1159$ [P3], $F_z = -0.037314\bar{P}_U + 5.4194$ [P4], $F_z = -0.071135\bar{P}_U + 20.175$ [P5], $F_z = -0.040969\bar{P}_U + 9.4888$ [P6], $F_z = -0.0569\bar{P}_U + 2.6507$ [P7], $F_z = -0.0651\bar{P}_U + 7.6922$ [P8], $F_z = -0.04976\bar{P}_U + 3.963$ [P9] and $F_z = -0.086121\bar{P}_U + 6.1022$ [P10]. Besides, all of the assessed duos were found statistically significant ($p < 0.001$). Figure 5.6 and 5.7 depict the previous link between both pairs of variables for each participant.

To illustrate the reported results, the data from participant P8 (which may be representative of the group, not being the best nor the worse) are taken as an example. Figure 5.8 shows the mean F_z and the mean pitch angle trajectory measured by the ground truth sensors F/T ATI Mini45 and the IMU. In dashed line we see the estimations of the latter using the parameters obtained from the tactile cane handle. Linear functions given above for P8 and shown in red in Figure 5.7 were used for the computation. Note that time numbers are not given. As explained, the showed chart was built as the mean of four trials that were interpolated or extrapolated to fit a particular duration, so time units do not represent a real trajectory time and are not relevant. The periodicity of the signals in Figure 5.8 may suggest that both the pitch cane angle and the load force are likely to be related to the gait pattern. This is useful since registering the variability of the gait (stride to stride) over a period of time has proven to be an effective fall predictor [139].

5.2 Discussion

The results show a certainly good association between CoM_U , \bar{P}_U and respectively the cane pitch angle and the load force. The observations were in line with the intuition. Indeed the only way to cancel partially the variations of CoM_U , while rotating the cane around its tip, is to move the whole arm in order to keep the hand inner surface parallel to the handle. This movement is not natural. Moving naturally and comfortably implies a change of CoM_U . The correlation between \bar{P}_U and the load force F_z is intuitive since force and pressure are two related physical variables. Note that, in the presented results only the upper five tactels

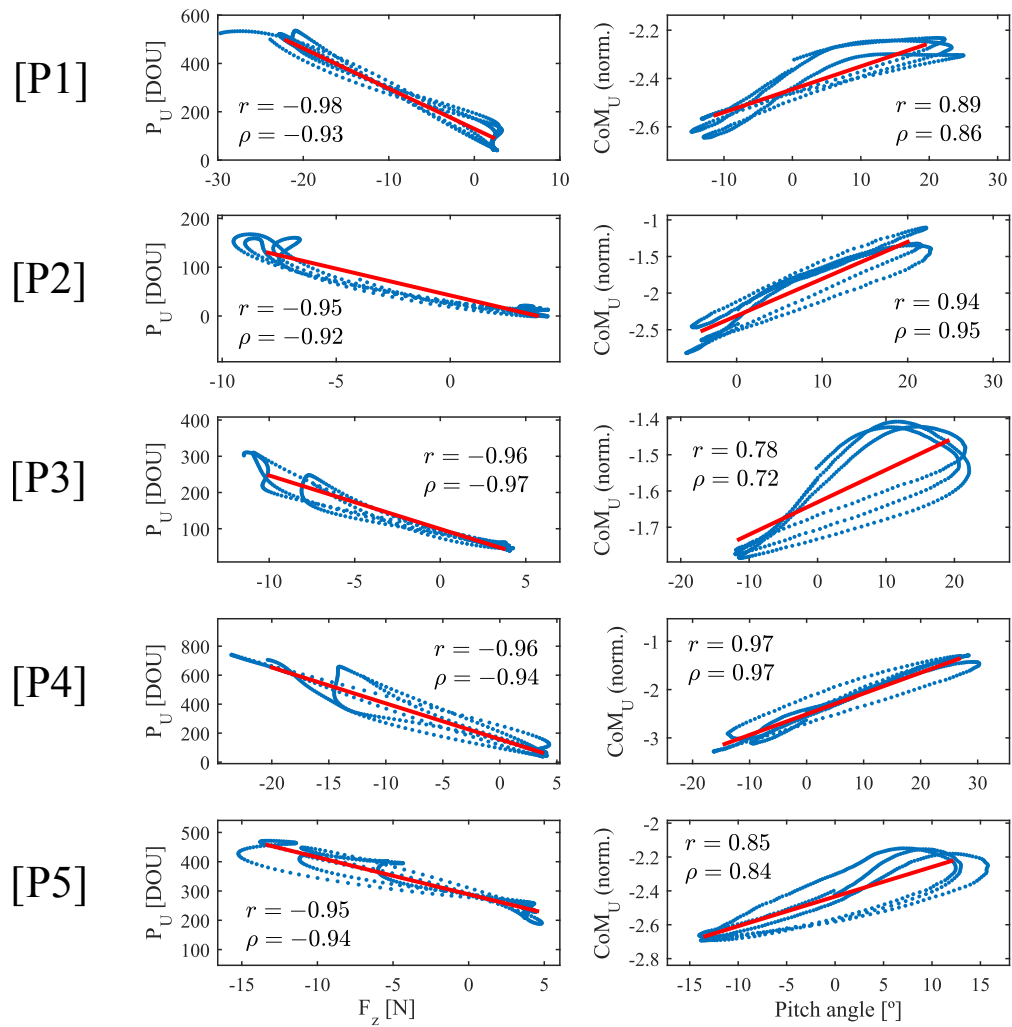


Fig. 5.6 Experiment results for participants P1-P5: coupling between the couples $\langle \bar{P}_U, F_z \rangle$ (left column) and $\langle CoM_U, Pitch \rangle$ (right column) with the corresponding first order linear functions superimposed.

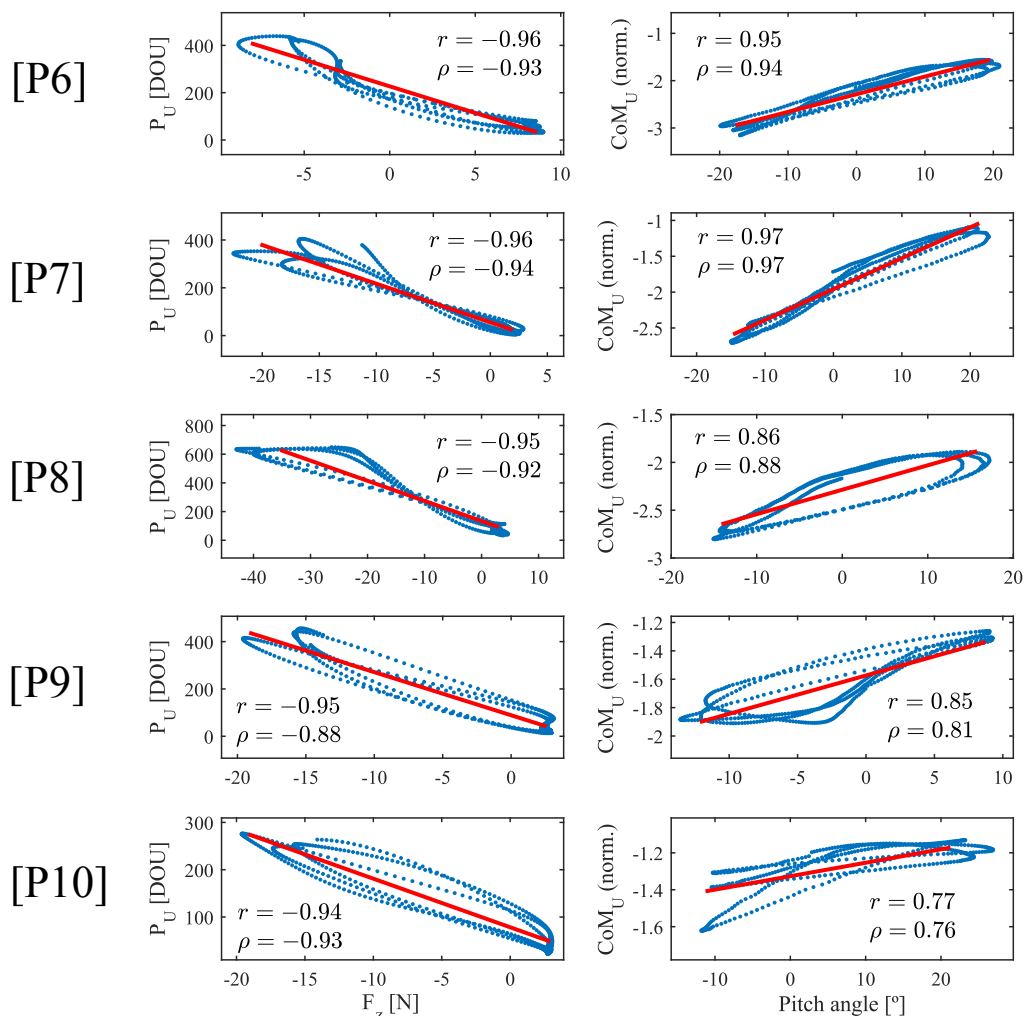


Fig. 5.7 Experiment results for participants P6-P10: coupling between the couples $\langle \bar{P}_U, F_z \rangle$ (left column) and $\langle CoM_U, Pitch \rangle$ (right column) with the corresponding first order linear functions superimposed.

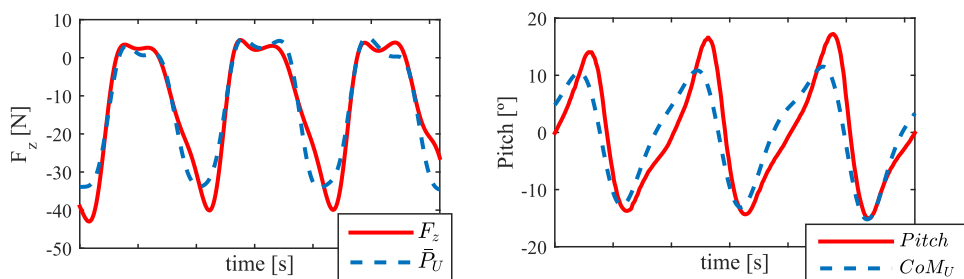


Fig. 5.8 Test of P8: on the left, mean F_z measured by the ATI Mini45 sensor (red) and estimation using the parameter \bar{P}_U (blue dashed line). On the right, mean pitch angle trajectory (red) captured by the IMU and its estimation based on the CoM_U (blue dashed line).

were used. Other combinations involving all the tactels, assessing each side of the handle independently, taking the distinct faces in pairs, only three of them, etc. were evaluated. However, in all those cases, the results were worse than those showed above. This is quite positive, since it means that only five FSR sensors have been needed to provide these good estimations of load force and cane orientation. This is only a first step and there is much room for improvement. On the one hand, a second prototype that equips only an array of tactels exposed on the upper side of the handle may be developed. The electronics may be miniaturized and wireless communication implemented. Another option could be to store the data locally in a memory card to be further analyzed. It would allow an autonomous utilization of the cane out of the health center. It would be also appropriate to enhance the ergonomics of the handle, considering what research has reported in this line. Besides, a deeper study of the information extracted from the handle may provide either another useful variables or good ideas for using those showed. On the other hand, given the good results shown, the extension to other assistive systems that incorporate handles as haptic interface could be planned. Robotic walkers, as those cited in Section 1.3, have handles on which the user leans as happens with the cane. In addition, their handles are also used to maneuver the device, in a manner similar to the way the PW handlebar operates. Walkers may be therefore also good candidates to test the proposal.



UNIVERSIDAD
DE MÁLAGA

6

Conclusions and future work

"The joy of discovery is certainly the liveliest that the mind of man can ever feel."

— Claude Bernard

6.1 Conclusions

The work developed in this thesis presents a haptic interface to be used in ambulatory assistive devices. It is based on tactile sensors, that represent a cost-effective technology and seem to be promising candidates to replace force sensors in this kind of human-machine interaction. This study covers the design, implementation, analysis and evaluation of the proposal in a particular application: a haptic handlebar aimed to assist the driving of wheelchairs. It is intended to be used in powered chairs by attendants whose tasks involve the care of a person with reduced mobility, either if they are relatives or professional caregivers. Furthermore, the work has been extended to other assistive device: a haptic handle has been proposed to be attached to a cane to collect data about its use.

After the previous general description, the main conclusions of this work are listed below:

- After reviewing the existing situation of people who suffer from mobility incapacity and require a wheelchair and the aid of a caregiver to move around, it was found that the duties of the latter involve heavy tasks that eventually trigger injuries. The *assistance of the assistant* has been often left aside even when there is evidence that it is necessary. The study of the state of the art showed that a large number of assistive ambulatory devices provided by research are based on force sensors. These are costly and, therefore, they reduce the possibility for the different devices to reach the market. In this way, a haptic handlebar that allow powered wheelchairs attendants to steer intuitively and effortless was proposed. It is based on tactile sensors, which are cost-effective.
- The implementation of the haptic handlebar was presented and the system architecture in which it is included was described. Two prototypes were developed taking into consideration both pressure sensors size constraints and the effect of the handles geometry on physical magnitudes such as the gripping force. Besides, the sensors arrangement was configured in form of matrix, what minimizes the resources required for addressing. Conditioning and control electronics was also proposed. It was based on a microcontroller, which is a low cost solution. Reverse engineering was used to find how the outputs of the joystick that the chair incorporates control its movement. The previous analysis resulted in the strategy that was used to control the movement. Specifically, the haptic handlebar electronics provides the same outputs as the joystick, so that the proposed assistive device is directly connected to the wheelchair joystick socket.
- A first control algorithm was proposed to test the system and a preliminary experiment was undertaken. The reports of the participants were used to detect the main flaws of the device and to identify the work lines to follow. In particular, driving difficulties were related to excessive gripping forces, the initial calibration was perceived as contrived and the intuitiveness of the proposal needed to be enhanced.
- According to the latter reports, the realization of an improved haptic-based driving control was explored:
 - An experimental setup including a force/torque sensor to provide ground-truth measurements was implemented. After analyzing the forces and torques involved in the driving process, two control variables were proposed. They are based

- on the centers of mass computed for the left and the right handle. They are highly correlated with the force and torque exerted during push/pull and turning maneuvers, respectively. This way, they can be used to identify and quantify the user intention and to activate the wheelchair engines accordingly.
- The effect of the gripping force on the system control was studied. To this end, the tactels response was previously characterized. It was found that increasing gripping forces worsen the capacity of the control variables to predict the driving caregiver intention. Besides, high gripping forces also reduce the dynamic range of the control parameters so a method was proposed to correct this influence.
 - The impact that the tactels arrangement inside the matrix has on the control was also explored. It was discovered that there are configurations better than others regarding the performance of the control variables. The different tactels arrangements were assessed and the configuration with better results in most of the cases was proposed as default option.
 - The study of the handlebar grasp was also addressed. The analysis of the grip stabilization helped establish time parameters to compute the handlebar dynamic calibration when it is grasped. The influence of the attendant height in this process was also studied. As a result, it was found that not only the height but also the angle formed by the forearm and the hand may impact on the reference center of mass computed for the calibration.
 - Finally, a vibro-haptic feedback mechanism was added with the purpose of preventing fatigue and overexertion. This way, when the gripping force exerted by attendant exceeds certain threshold, the handlebar vibrates to warn him or her that keeping that situation is not advisable. At the same time, the performance of the system is improved by avoiding high gripping forces.
- The haptic handlebar, incorporating all that was explained above, was evaluated in a controlled experiment. Besides, it was compared with the attendant joystick, other assistive device that also provides fully driving assistance. For this purpose the experiment was divided in two parts.
 - The first of them was aimed to acquire objective data of the wheelchair driving using both devices. This way, the participants followed a path trying to keep a laser light inside a tape that marked the target trajectory on the ground. The error between the actual and the target path was computed. They also steered the wheelchair in a enclosed space such as a laboratory. The collisions with the environment were registered.

- The other part was focused on gathering the subjective perception of the attendants when driving as well as their opinion about the devices. In this way, after the completion of the first part, they filled a form with questions about different aspects of their driving experience.
- The evaluation showed better results for the haptic handlebar than for the attendant joystick in all the categories assessed. Besides, the perception of the users was also more positive in the case of the haptic handlebar, that scored well in aspects as ease of use, intuitiveness, comfort, usefulness or safety. This way, the device which is the main contribution of this thesis seems to be a viable alternative to assist attendants whose functions imply caring people in wheelchairs. It fulfills the three goals set in Chapter 1: to be intuitive, to provide complete steering assistance and to be cost-effective. Nonetheless, some flaws were detected. They will be discussed in the next section.
- Lastly, the idea of the haptic interface was extended to an instrumented cane. A haptic handle was designed, implemented and attached to a cane. An experiment was carried out to study if the tactile handle may provide information about the cane use. It was found that two parameters extracted from the haptic handle correlated strongly with the pitch angle and the load force on the cane axis while using the cane. Thus, the haptic handle may be useful to help health care professionals to improve physical therapies based on the monitoring of the parameters provided by the device.

6.2 Ongoing and future work

Most of the possible work lines which arise after the development of this work are related to different issues detected in the realized experiments. Others are improvements that may as well be assessed.

Firstly, a version of the handlebar with higher resolution may be implemented. It would allow the study of the case of those attendants for which none of the tactels configurations available entirely fitted with their grasping characteristics. With eight tactels, the rotation angle of the elements coordinates between an arrangement and the next is 45° (see Figure 6.1), which may be considered a not very precise adjustment. A larger number of elements could allow a finer tuning.

A first step was taken in this direction in the research group. New versions of tactile handles equipping tactile sensors with higher spatial resolution are being developed. Besides,

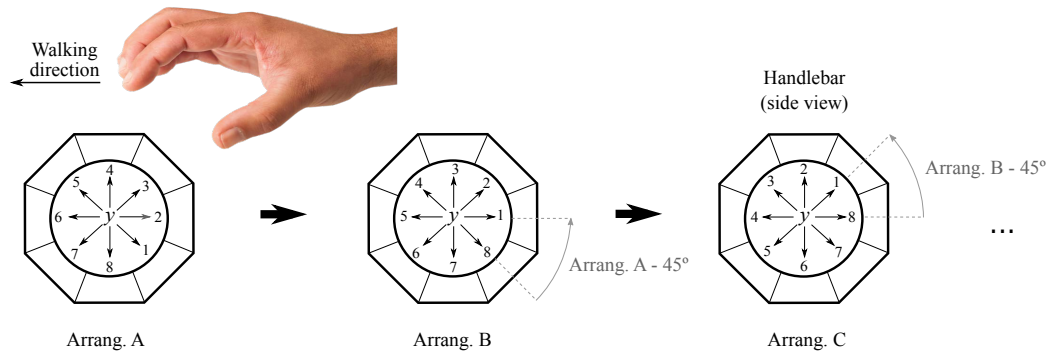


Fig. 6.1 With the current prototype, a rotation of 45° in the coordinates of the elements takes place between one tactels arrangement and the next.

the tactile sensors are being also made in the laboratory with piezoresistive materials, what makes the proposal even cheaper. Figure 6.2 shows a new handle that doubles the spatial resolution of those used in this work¹.

In addition to increasing the resolution, it would be interesting to explore some method that provided automatically the most suitable configuration for each attendant. One first approximation could involve a calibration that consisted in grasping the handlebar and carrying out basic and short maneuvers with the chair stopped: pushing (a), pulling (b), turning to the right (c) and to the left (d). The output that those inputs should produce is already known: $v > 0$ (a), $v < 0$ (b), $\omega > 0$ (c) and $\omega < 0$ (d). The algorithm could calculate virtually the linear and angular speeds using the *CoM*-based control parameters, but computing them once for each tactels arrangement (note that the *CoMs* depend on the selected tactel configuration as shown in Section 3.3). This way, the arrangement that produces an output more in line with that expected could be chosen. This information may be stored in an user profile.



Fig. 6.2 Tactile handle equipping 16 tactels. At the bottom, the electrodes are covered with a piezoresistive sheet.

¹The handle is composed of two parts, an upper and a lower half. In the photos, the upper half is shown.

Besides, more research could be aimed at the grip stabilization. The waiting time to stabilize the grip is perceived as contrived by some users, so a faster way of computing the reference parameters may be a substantial improvement. Again, user profiles could help. It should not be troublesome since the number of attendants that assist a person is often small. The user profile could support a history log of the reference parameters computed for the attendant in previous driving experiences. By having a set of predefined parameters, the waiting time before starting driving may be shorter. This information is easy to store, for example, in the flash memory that microcontrollers incorporate.

On the other hand, as the reader must have already noted, proportional control has been chosen to manage the system. No other controllers have been assessed. The main reason for this lies in the assistive ambulatory device used in this thesis. Powered wheelchairs are equipped with electronics that runs a firmware developed by the manufacturer. This firmware deals with all the tasks that the wheelchair management requires. One of them is the engines activation and the generation of motion. The strategy of the joystick emulation has been highly practical, but has made the PW firmware be a given part of the system control. It could be considered as transparent but it would be a significant simplification. In fact, it has been observed that it smooths in a quite evident way the movement produced by the joystick. The manufacturer was contacted in order to obtain detailed information about the PW operating. However, that provided only referred to the joystick interface. This way, a possible measure to take could involve the direct managing of the engines activation. It would remove the proprietary firmware processing from our control loop and it would allow different controls to be assessed in a proper way.

If the previous suggestion were carried out, admittance control may be a good candidate to test. It has been successfully used in many examples of rehabilitation and assistance research [26, 101, 140–143]. This model is defined as a transfer function in which the forces and torques exerted by the users are the input and the reference velocity of the ambulatory device is the output (see Equation 6.1).

$$G(s) = \frac{V(s)}{F(s)} = \frac{1}{Ms + B} \quad (6.1)$$

where M and B are respectively the mass and damping parameters.

The proposal of the authors of [142] is especially interesting. They implemented a walking aid robot for which they used a variable admittance control whose configuration depends on the velocity. The participants of the experiment performed in this study reported that they preferred to *feel* the device slower and steadier at the beginning and the end

of the motion, and light and responsive when they were moving faster. This way, the authors proposed a variable dumping model that met this requirement. This approach could be assessed in our system. In Chapter 4, the experiment E5.1 showed that some users experienced tugs when realizing precise and slow maneuvers in an enclosed space. Maybe, with a system less responsive in this situation, the tugs would be reduced or eliminated. In open spaces, speeds are higher and it is good to have a fast response. Thus, it might be worth exploring the proposal in [142].

The same authors used in [142] a F/T sensor along with odometry to study the user gait. They estimated parameters such as the gait frequency or the stride length from the power spectrum. As said in several sections of this document, the PW movement were modulated by the gait for some users. This way, little jerks appeared. Some ways of compensating this effect may be studied if their characteristics are known. For this reason, the haptic handlebar output could be analyzed in order to extract gait information.

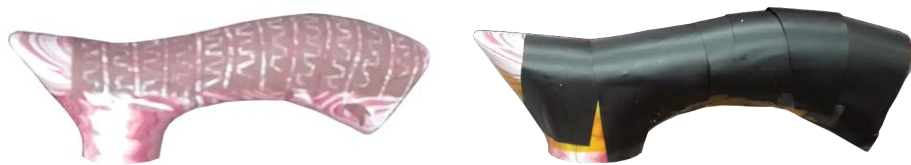


Fig. 6.3 Tactile cane handle. On the right, the tactels electrodes are exposed. On the left, they have been covered with piezoresistive sheets for testing purposes.

Lastly, regarding the haptic cane handle presented in Chapter 5, one of the main findings was that only a linear array is necessary to provide information about the pitch angle and the load force. This way, its implementation could be cheaper than that shown in this work. Considering the latter, new models are being studied in the research group (see Figure 6.3). The parallelepiped shaped handle has been replaced by a large-circumference handle, that has been reported in the literature as that preferred by the users [144]. As with the handle of Figure 6.2, the tactile sensor has been made in our laboratory. It allows to use more ergonomic shapes by removing the requirement of the FSR commercial sensors according to which a flat base surface is needed [103]. A Bluetooth module has also been added to send the data to a computer. In addition, the new cane handle has eleven tactels, that is more than twice the number of elements of the prototype of Chapter 5. Both handles, the one of Figure 6.2 and that of Figure 6.3, are currently being tested.



UNIVERSIDAD
DE MÁLAGA

References

- [1] B. C. Gulack, B. Hale, W. D. White, R. E. Moon, and E. Bennett-Guerrero, "Marriage and mortality after noncardiac surgery," *Journal of Surgical Research*, vol. 210, no. Supplement C, pp. 152 – 158, 2017. [Online]. Available: <http://www.sciencedirect.com/science/article/pii/S0022480416304772>
- [2] X.-K. He, Z.-H. Lin, Y. Qian, D. Xia, P. Jin, and L.-M. Sun, "Marital status and survival in patients with primary liver cancer," *Oncotarget*, vol. 8, no. 39, p. 64954, 2017.
- [3] "'The health advantages of marriage". Harvard Medical School. Harvard Health Publishing," 2016, URL: <https://www.health.harvard.edu/blog/the-health-advantages-of-marriage-2016113010667> [accessed: August, 2017].
- [4] M. D. Wulf, "Predicted population pyramid for Western Europe in 2030," 2017, URL: <http://www.populationpyramid.net/western-europe/2030/> [accessed: February, 2017].
- [5] "Interlink Electronics. FSR@400 Series. Data sheet." 2011, URL: http://www.interlinkelectronics.com/datasheets/Datasheet_FSR.pdf [accessed: June, 2017].
- [6] C. S. Edgren, R. G. Radwin, and C. B. Irwin, "Grip force vectors for varying handle diameters and hand sizes," *Human Factors*, vol. 46, no. 2, pp. 244–251, 2004, pMID: 15359674. [Online]. Available: <http://dx.doi.org/10.1518/hfes.46.2.244.37337>
- [7] J. A. Sánchez-Durán, J. A. Hidalgo-López, J. Castellanos-Ramos, s. Oballe-Peinado, and F. Vidal-Verdú, "Influence of errors in tactile sensors on some high level parameters used for manipulation with robotic hands," *Sensors*, vol. 15, no. 8, pp. 20409–20435, 2015. [Online]. Available: <http://www.mdpi.com/1424-8220/15/8/20409>
- [8] K. Yamada, K. Ohara, A. Ichikawa, and T. Fukuda, "User intention estimation by grip sensor for cane-type walking support robot," in *2016 International Symposium on Micro-NanoMechatronics and Human Science (MHS)*, Nov 2016, pp. 1–3.
- [9] "World Population Prospects: The 2015 Revision," *United Nations. Department of Economic and Social Affairs, Population Division*, 2015, URL: https://esa.un.org/unpd/wpp/publications/files/key_findings_wpp_2015.pdf [accessed: April, 2017].
- [10] "World Health Organization. What are the public health implications of global ageing?" 2011, URL: <http://www.who.int/features/qa/42/en/> [accessed: April, 2017].

- [11] “Population ageing in Europe: facts, implications and policies,” *European Union, Directorate General for Research and Innovation Socioeconomic sciences and humanities*, 2014, URL: https://ec.europa.eu/research/social-sciences/pdf/policy_reviews/kina26426enc.pdf [accessed: January, 2016].
- [12] B. A. Hawkins, “Aging well: Toward a way of life for all people,” *Preventing Chronic Disease*, vol. 2, no. 3, p. A03, July 2005.
- [13] “European Disability Strategy 2010-2020: A Renewed Commitment to a Barrier-Free Europe,” *COMMUNICATION FROM THE COMMISSION TO THE EUROPEAN PARLIAMENT, THE COUNCIL, THE EUROPEAN ECONOMIC AND SOCIAL COMMITTEE AND THE COMMITTEE OF THE REGIONS*, 2010, URL: <http://eur-lex.europa.eu/LexUriServ/LexUriServ.do?uri=COM:2010:0636:FIN:en:PDF> [accessed: April, 2017].
- [14] “Disability statistics - barriers to social integration,” *EUROSTAT: Statistic explained*, 2015, URL: http://ec.europa.eu/eurostat/statistics-explained/index.php/Disability_statistics_-_barriers_to_social_integration [accessed: April, 2017].
- [15] W. S. Harwin, J. L. Patton, and V. R. Edgerton, “Challenges and opportunities for robot-mediated neurorehabilitation,” *Proceedings of the IEEE*, vol. 94, no. 9, pp. 1717–1726, Sept 2006.
- [16] “International Campaign for Cures of Spinal Cord Injury Paralysis,” 2017, URL: <http://campaignforcure.org/> [accessed: April, 2017].
- [17] C. Cans, J. D. la Cruz, and M.-A. Mermet, “Epidemiology of cerebral palsy,” *Paediatrics and Child Health*, vol. 18, no. 9, pp. 393–398, September 2008.
- [18] M. Rantakokko, M. Mänty, and T. Rantanen, “Mobility decline in old age,” *Exercise and Sport Sciences Reviews*, vol. 41, no. 1, pp. 19–25, 2013.
- [19] A. S. Buchman, P. A. Boyle, S. E. Leurgans, L. L. Barnes, and D. A. Bennett, “Cognitive function is associated with the development of mobility impairments in community-dwelling elders,” *The American Journal of Geriatric Psychiatry*, vol. 6, no. 19, pp. 571–580, June 2011.
- [20] L. Robinson, G. Gibson, A. Kingston, L. Newton, G. Pritchard, T. Finch, and K. Brittain, “Assistive technologies in caring for the oldest old: a review of current practice and future directions,” *Future Medicine*, vol. 4, no. 9, pp. 365–375, August 2013.
- [21] “Assistive Technology Industry Association,” 2017, URL: <https://www.atia.org/at-resources/what-is-at/> [accessed: March, 2017].
- [22] E. de Sousa Leite, T. P. Rodrigues, M. do Carmo Andrade Duarte de Farias, M. A. S. P. Moreira, G. K. G. D. Bittencourt, F. B. de Oliveira, C. A. Simpson, and A. O. Silva, “Influence of assistive technology for the maintenance of the functionality of elderly people: an integrative review,” *International Archives of Medicine*, vol. 9, 2016. [Online]. Available: <http://imed.pub/ojs/index.php/iam/article/view/1501>

- [23] C. A. Cifuentes and A. Frizera, *Assistive Devices for Human Mobility and Gait Rehabilitation*. Cham: Springer International Publishing, 2016, pp. 1–15. [Online]. Available: http://dx.doi.org/10.1007/978-3-319-34063-0_1
- [24] R. Ady, W. Bachta, and P. Bidaud, “Development and control of a one-wheel telescopic active cane,” in *5th IEEE RAS/EMBS International Conference on Biomedical Robotics and Biomechatronics*, Aug 2014, pp. 461–466.
- [25] I. Shim and J. Yoon, “A robotic cane based on interactive technology,” in *IECON 02 [Industrial Electronics Society, IEEE 2002 28th Annual Conference of the]*, vol. 3, November 2002, pp. 2249–2254 vol.3.
- [26] S. H. Pyo, M. G. Oh, and J. W. Yoon, “Development of an active haptic cane for gait rehabilitation,” in *2015 IEEE International Conference on Robotics and Automation (ICRA)*, May 2015, pp. 4464–4469.
- [27] V. Pasqui, L. Saint-Bauzel, C. Zonga *et al.*, “Projet MIRAS : Multimodal interactive robot for assistance in strolling,” *Technologies pour la santé et l’autonomie*, vol. 33, no. 2, p. 165–172, April 2012.
- [28] J. Shin, D. Itten, A. Rusakov, and B. Meyer, “Smartwalker: Towards an intelligent robotic walker for the elderly,” in *Intelligent Environments (IE), 2015 International Conference on*, July 2015, pp. 9–16.
- [29] A. Morris, R. Donamukkala, A. Kapuria, A. Steinfeld, J. T. Matthews, J. Dunbar-Jacob, and S. Thrun, “A robotic walker that provides guidance,” in *Robotics and Automation, 2003. Proceedings. ICRA '03. IEEE International Conference on*, vol. 1, September 2003, pp. 25–30 vol.1.
- [30] K.-T. Yu, C.-P. Lam, M.-F. Chang, W.-H. Mou, S. H. Tseng, and L. C. Fu, “An interactive robotic walker for assisting elderly mobility in senior care unit,” in *2010 IEEE Workshop on Advanced Robotics and its Social Impacts*, October 2010, pp. 24–29.
- [31] M. W. Brault, “Americans with disabilities: 2010,” *Household Economic Studies*, pp. 70–131, July 2012.
- [32] “Euobserver. disability in figures,” 2012, URL: <https://euobserver.com/disability/118249> [accessed: April, 2017].
- [33] A. Brandt, S. Iwarsson, and A. Stähle, “Older people’s use of powered wheelchairs for activity and participation,” *Journal of Rehabilitation Medicine*, vol. 36, no. 2, pp. 70–77, March 2004.
- [34] I.-H. Tsai, D. E. Graves, and C.-H. Lai, “The association of assistive mobility devices and social participation in people with spinal cord injuries,” *Spinal Cord*, no. 52, pp. 209–215, January 2014.
- [35] M. L. S. Rose and P. M. Ferguson-Pell, “Wheelchair provision for people with spinal cord injury: 1,” *British Journal of Therapy and Rehabilitation*, vol. 9, no. 10, pp. 391–400, 2002. [Online]. Available: <http://dx.doi.org/10.12968/bjtr.2002.9.10.13675>

- [36] L. Fehr, W. Langbein, and S. Skaar, "Adequacy of power wheelchair control interfaces for persons with severe disabilities: a clinical survey," *Journal of Rehabilitation Research and Development*, vol. 37, no. 3, pp. 353–360, May/June 2000.
- [37] C. Torkia, D. Reid, N. Korner-Bitensky, D. Kairy, P. W. Rushton, L. Demers, and P. S. Archambault, "Power wheelchair driving challenges in the community: a users' perspective," *Disability and Rehabilitation: Assistive Technology*, vol. 10, no. 3, pp. 211–215, 2015. [Online]. Available: <http://dx.doi.org/10.3109/17483107.2014.898159>
- [38] G. Lee, K. Kim, and J. Kim, "Development of hands-free wheelchair device based on head movement and bio-signal for quadriplegic patients," *International Journal of Precision Engineering and Manufacturing*, vol. 17, no. 3, pp. 363–369, 2016. [Online]. Available: <http://dx.doi.org/10.1007/s12541-016-0045-5>
- [39] S. Yokota, H. Hashimoto, D. Chugo, Y. Ohyama, J. She, and H. Kobayashi, "Supporting technology for wheelchair users," in *Inclusive Society: Health and Wellbeing in the Community, and Care at Home: 11th International Conference on Smart Homes and Health Telematics, ICOST 2013, Singapore, June 19-21, 2013, Proceedings*, vol. 7910. Springer, 2013, p. 118.
- [40] H. Seki and S. Tadakuma, "Straight and circular road driving control for power assisted wheelchair based on fuzzy algorithm," in *IECON 2006 - 32nd Annual Conference on IEEE Industrial Electronics*, Nov 2006, pp. 3898–3903.
- [41] B. E. Dicianno, D. M. Spaeth, R. A. Cooper, S. G. Fitzgerald, M. L. Boninger, and K. W. Brown, "Force control strategies while driving electric powered wheelchairs with isometric and movement-sensing joysticks," *IEEE Transactions on Neural Systems and Rehabilitation Engineering*, vol. 15, no. 1, pp. 144–150, March 2007.
- [42] R. S. Rao, R. Seliktar, and T. Rahman, "Evaluation of an isometric and a position joystick in a target acquisition task for individuals with cerebral palsy," *IEEE Transactions on Rehabilitation Engineering*, vol. 8, no. 1, pp. 118–125, Mar 2000.
- [43] R. K. Megalingam, V. Rangan, S. Krishnan, and A. B. E. Alinkeezhil, "Ir sensor-based gesture control wheelchair for stroke and sci patients," *IEEE Sensors Journal*, vol. 16, no. 17, pp. 6755–6765, Sept 2016.
- [44] A. Fattouh, M. Sahnoun, and G. Bourhis, "Force feedback joystick control of a powered wheelchair: preliminary study," in *2004 IEEE International Conference on Systems, Man and Cybernetics (IEEE Cat. No.04CH37583)*, vol. 3, Oct 2004, pp. 2640–2645 vol.3.
- [45] A. Hadj-Abdelkader, B. Cherki, and G. Bourhis, "Powered wheelchair driving using a 3d haptic device," in *2015 International Conference on Virtual Rehabilitation (ICVR)*, June 2015, pp. 106–114.
- [46] V. K. Narayanan, F. Pasteau, M. Marchal, A. Krupa, and M. Babel, "Vision-based adaptive assistance and haptic guidance for safe wheelchair corridor following," *Computer Vision and Image Understanding*, vol. 149, pp. 171 – 185, 2016. [Online]. Available: <http://www.sciencedirect.com/science/article/pii/S1077314216000539>

- [47] Sugihara, Keisuke, Fujimoto, Shinsaku, and Yoshida, Koji, "Development of electric wheelchair with input of force feedback joystick," *MATEC Web of Conferences*, vol. 51, p. 02008, 2016. [Online]. Available: <https://doi.org/10.1051/mateconf/20165102008>
- [48] S. Kamiuchi and S. Maeyama, "A novel human interface of an omni-directional wheelchair," in *RO-MAN 2004. 13th IEEE International Workshop on Robot and Human Interactive Communication (IEEE Catalog No.04TH8759)*, Sept 2004, pp. 101–106.
- [49] A. Z. Neto, A. Mesquita, M. M. Spindola, and M. Magnani, "Prototype of a wheelchair controlled by cervical movements," in *2014 IEEE International Conference on Bioinformatics and Bioengineering*, Nov 2014, pp. 134–140.
- [50] N. Peixoto, H. Nik, and H. Charkhkar, "Voice controlled wheelchairs: fine control by humming," *Computer methods and programs in biomedicine*, vol. 1, no. 112, pp. 156–165, October 2013.
- [51] J. C. Garcia, M. Marron, J. Ureña, and D. Gualda, "Intelligent wheelchairs: Filling the gap between labs and people," *ASSISTIVE TECHNOLOGY RESEARCH SERIES*, no. 33, pp. 202–209, September 2013.
- [52] F. G. Wood, "The meaning of caregiving," *Rehabilitation Nursing*, vol. 16, no. 4, pp. 195–198, July-August 1991.
- [53] A. R. BROWN and G. P. MULLEY, "Injuries sustained by caregivers of disabled elderly people," *Age and Ageing*, vol. 26, no. 1, p. 21, 1997. [Online]. Available: [+http://dx.doi.org/10.1093/ageing/26.1.21](http://dx.doi.org/10.1093/ageing/26.1.21)
- [54] J. Roberts, H. Young, K. Andrew, A. McAlpine, and J. Hogg, "The needs of carers who push wheelchairs," *Journal of Integrated Care*, vol. 20, no. 1, pp. 23–34, 2012. [Online]. Available: <http://dx.doi.org/10.1108/14769011211202265>
- [55] F. Stewart and E. Patterson, "Caring in scotland: Analysis of existing data sources on unpaid carers in scotland," *Scottish Government. Social Research. Edinburgh*, July 2010.
- [56] C. S. Kim, D. Lee, and M. K. Chung, "Effects of ramp slope on usability when a wheelchair is propelled by attendant," *Proceedings of the Human Factors and Ergonomics Society Annual Meeting*, vol. 56, no. 1, pp. 629–633, 2012. [Online]. Available: <http://dx.doi.org/10.1177/1071181312561131>
- [57] L. Demers, M. J. Fuhrer, J. Jutai, J. Lenker, M. Depa, and F. D. Ruyter, "A conceptual framework of outcomes for caregivers of assistive technology users," *American journal of physical medicine and rehabilitation*, vol. 8, no. 88, pp. 645–655, August 2009.
- [58] "Rehabilitation technology information service. wheelchair eligibility criteria," 2017, URL: <http://www.retis.scot.nhs.uk/wheelchaircriteria.html> [accessed: April, 2017].
- [59] "Dynamic Controls. DX2 Compact Attendant Remote Module," 2017, URL: <https://dynamiccontrols.com/en/mobility-product-users/products/dx2/secondary-remotes> [accessed: January, 2017].

- [60] G. Lacey and S. MacNamara, "User involvement in the design and evaluation of a smart mobility aid," *Journal of rehabilitation research and development*, vol. 37, no. 6, p. 709, 2000.
- [61] "Rascal Mobility. Rascal We Go 250," 2017, URL: <http://www.electricmobility.co.uk/products/rascal-wego-250/24/> [accessed: December, 2016].
- [62] "Alber. Viamobil and Viamobil Eco," 2017, URL: <https://www.alber.de/en/products/push-brake-aids.html> [accessed: December, 2016].
- [63] T. Suzuki, H. Uchiyama, C. Holloway, and N. Tyler, "Assisting control for attendant propelled wheelchair based on force velocity relationship," in *2012 Annual International Conference of the IEEE Engineering in Medicine and Biology Society*, Aug 2012, pp. 3073–3076.
- [64] A. Kakimoto, H. Matsuda, and Y. Sekiguchi, "Development of power-assisted attendant-propelled wheelchair," in *Engineering in Medicine and Biology Society, 1997. Proceedings of the 19th Annual International Conference of the IEEE*, vol. 4, Oct 1997, pp. 1875–1876 vol.4.
- [65] M. Gollér, T. Kerscher, M. Ziegenmeyer, A. Rönnau, J. Zöllner, and R. Dillman, "Haptic control for the interactive behavior operated shopping trolley inbot," in *Proceedings of the New Frontiers in Human-Robot. Interaction Symposium at the Artificial Intelligence and Simulation of Behaviour (AISB)*, April 2009.
- [66] A. Green, C. Bogdan, J. Falb, D. Ertl, K. S. Eklundh, and H. Kaindl, "Deliverable d7.5, report on evaluation of the robot trolley," CommRob Consortium, Tech. Rep., Jun. 2010.
- [67] H. Kitagawa, K. Terashima, T. Miyoshi, J. Urbano, and S. Nishisaka, "Power assist system for omni-directional transport wheelchair using fuzzy reasoning," in *Proceedings of the 2004 IEEE International Conference on Control Applications, 2004.*, vol. 1, Sept 2004, pp. 123–130 Vol.1.
- [68] C. Zhu, M. Oda, M. Yoshioka, T. Nishikawa, S. Shimazu, and X. Luo, "Admittance control based walking support and power assistance of an omnidirectional wheelchair typed robot," in *2010 IEEE International Conference on Robotics and Biomimetics*, Dec 2010, pp. 381–386.
- [69] J. Miyata, Y. Kaida, and T. Murakami, " v - ϕ -coordinate-based power-assist control of electric wheelchair for a caregiver," *IEEE Transactions on Industrial Electronics*, vol. 55, no. 6, pp. 2517–2524, June 2008.
- [70] S. Tashiro and T. Murakami, "Step passage control of a power-assisted wheelchair for a caregiver," *IEEE Transactions on Industrial Electronics*, vol. 55, no. 4, pp. 1715–1721, April 2008.
- [71] S. Katsura and K. Ohnishi, "A wheelchair type mobile robot taking environmental disturbance into account," in *7th International Workshop on Advanced Motion Control. Proceedings (Cat. No.02TH8623)*, 2002, pp. 500–505.

- [72] T. B. Sheridan, "Human and machine haptics in historical perspective," in *Workshop on Human and Machine Haptics*, 1997.
- [73] R. S. Dahiya, G. Metta, M. Valle, and G. Sandini, "Tactile sensing - from humans to humanoids," *IEEE Transactions on Robotics*, vol. 26, no. 1, pp. 1–20, Feb 2010.
- [74] R. S. Dahiya, P. Mittendorf, M. Valle, G. Cheng, and V. J. Lumelsky, "Directions toward effective utilization of tactile skin: A review," *IEEE Sensors Journal*, vol. 13, no. 11, pp. 4121–4138, Nov 2013.
- [75] H. Xie, H. Liu, L. D. Seneviratne, and K. Althoefer, "An optical tactile array probe head for tissue palpation during minimally invasive surgery," *IEEE Sensors Journal*, vol. 14, no. 9, pp. 3283–3291, Sept 2014.
- [76] S. Zhao, D. Parks, and C. Liu, "A medical tactile sensor for measuring tissue hardness in robotic surgical tools," in *2011 16th International Solid-State Sensors, Actuators and Microsystems Conference*, June 2011, pp. 2843–2846.
- [77] M. Kalantari, M. Ramezanifard, R. Ahmadi, J. Dargahi, and J. Kovecses, "Design, fabrication, and testing of a piezoresistive hardness sensor in minimally invasive surgery," in *2010 IEEE Haptics Symposium*, March 2010, pp. 431–437.
- [78] Y. Hu, R. B. Katragadda, H. Tu, Q. Zheng, Y. Li, and Y. Xu, "Bioinspired 3-d tactile sensor for minimally invasive surgery," *Journal of Microelectromechanical Systems*, vol. 19, no. 6, pp. 1400–1408, Dec 2010.
- [79] H. Xie, H. Liu, S. Luo, L. D. Seneviratne, and K. Althoefer, "Fiber optics tactile array probe for tissue palpation during minimally invasive surgery," in *2013 IEEE/RSJ International Conference on Intelligent Robots and Systems*, Nov 2013, pp. 2539–2544.
- [80] W. Feng, S. Guo, C. Chi, H. Wang, K. Wang, and X. Ye, "Realization of a catheter driving mechanism with micro tactile sensor for intravascular neurosurgery," in *2006 IEEE International Conference on Robotics and Biomimetics*, Dec 2006, pp. 1628–1633.
- [81] M. Tanaka, C. Ji-Young, S. Chonan, and Y. Tanahashi, "Tactile sensor system for detection of prostate cancer and hypertrophy," in *2005 IEEE International Conference on Information Acquisition*, June 2005, pp. 6 pp.–.
- [82] Q. Peng, S. Omata, D. M. Peehl, and C. E. Constantinou, "Stiffness mapping prostate biopsy samples using a tactile sensor," in *2011 Annual International Conference of the IEEE Engineering in Medicine and Biology Society*, Aug 2011, pp. 8515–8518.
- [83] T. Salo, K. U. Kirstein, J. Sedivy, J. Grunenfelder, T. Vancura, G. Zund, and H. Baltes, "Continuous blood pressure monitoring utilizing a cmos tactile sensor," in *The 26th Annual International Conference of the IEEE Engineering in Medicine and Biology Society*, vol. 1, Sept 2004, pp. 23 226–23 229.
- [84] Z. Zhen, Q. Jinwu, Z. Yanan, and S. Linyong, "A new navigation method for intelligent colonoscope," in *2007 IEEE/ICME International Conference on Complex Medical Engineering*, May 2007, pp. 31–34.

- [85] C. H. Chuang, K. F. Lu, and J. L. Mu, “Flexible tactile sensor attached to laparoscope for mechanical characteristics of soft materials and tissues,” in *2013 Transducers Eurosensors XXVII: The 17th International Conference on Solid-State Sensors, Actuators and Microsystems (TRANSDUCERS EUROSENSORS XXVII)*, June 2013, pp. 2169–2172.
- [86] C. H. Chuang, T. H. Li, I. C. Chou, and Y. J. Teng, “Piezoelectric tactile sensor for submucosal tumor hardness detection in endoscopy,” in *2015 Transducers - 2015 18th International Conference on Solid-State Sensors, Actuators and Microsystems (TRANSDUCERS)*, June 2015, pp. 871–875.
- [87] A. Saha, A. Konar, R. Burman, and A. K. Nagar, “Eeg analysis for cognitive failure detection in driving using neuro-evolutionary synergism,” in *2014 International Joint Conference on Neural Networks (IJCNN)*, July 2014, pp. 2108–2115.
- [88] B. Robins and K. Dautenhahn, “Tactile interactions with a humanoid robot: Novel play scenario implementations with children with autism,” *International Journal of Social Robotics*, vol. 6, no. 3, pp. 397–415, 2014. [Online]. Available: <http://dx.doi.org/10.1007/s12369-014-0228-0>
- [89] N. Vuillerme, O. Chenu, N. Pinsault, A. Moreau-Gaudry, A. Fleury, J. Demongeot, and Y. Payan, “Pressure sensor-based tongue-placed electrotactile biofeedback for balance improvement - biomedical application to prevent pressure sores formation and falls,” in *2007 29th Annual International Conference of the IEEE Engineering in Medicine and Biology Society*, Aug 2007, pp. 6113–6116.
- [90] M. I. Tiwana, S. J. Redmond, and N. H. Lovell, “A review of tactile sensing technologies with applications in biomedical engineering,” *Sensors and Actuators A: Physical*, vol. 179, pp. 17 – 31, 2012. [Online]. Available: <http://www.sciencedirect.com/science/article/pii/S0924424712001641>
- [91] “Interlink Electronics. FSR402®,” 2011, URL: <http://www.interlinkelectronics.com/FSR402.php> [accessed: April, 2017].
- [92] “Interlink Electronics. FSR408®,” 2011, URL: <http://www.interlinkelectronics.com/FSR408.php> [accessed: December, 2016].
- [93] C. Valadão, T. Bastos, A. Frizera, and R. Carelli, “Towards a smart walker controller for physiotherapy and rehabilitation purposes,” in *2014 IEEE 23rd International Symposium on Industrial Electronics (ISIE)*, June 2014, pp. 1578–1583.
- [94] M. Martins, C. P. Santos, A. Frizera, A. Matias, T. Pereira, M. Cotter, and F. Pereira, “Smart walker use for ataxia’s rehabilitation: Case study,” in *2015 IEEE International Conference on Rehabilitation Robotics (ICORR)*, Aug 2015, pp. 852–857.
- [95] P. Médéric, V. Pasqui, F. Plumet, and P. Bidaud, “Elderly people sit to stand transfer experimental analysis,” *Climbing and Walking Robots*, pp. 953–960, 2006.
- [96] P. Di, J. Huang, S. Nakagawa, K. Sekiyama, and T. Fukuda, “Fall detection for elderly by using an intelligent cane robot based on center of pressure (cop) stability theory,” in *2014 International Symposium on Micro-NanoMechatronics and Human Science (MHS)*, Nov 2014, pp. 1–4.

- [97] P. Di, K. Sekiyama, J. Huang, S. Nakagawa, F. Chen, and T. Fukuda, "Real time posture control for stability improvement of intelligent cane robot," in *2012 International Symposium on Micro-NanoMechatronics and Human Science (MHS)*, Nov 2012, pp. 346–351.
- [98] Q. Yan, J. Huang, and Z. Luo, "Human-robot coordination stability for fall detection and prevention using cane robot," in *2016 International Symposium on Micro-NanoMechatronics and Human Science (MHS)*, Nov 2016, pp. 1–7.
- [99] P. Di, Y. Hasegawa, S. Nakagawa, K. Sekiyama, T. Fukuda, J. Huang, and Q. Huang, "Fall detection and prevention control using walking-aid cane robot," *IEEE/ASME Transactions on Mechatronics*, vol. 21, no. 2, pp. 625–637, April 2016.
- [100] S. Nakagawa, P. D, J. Huang, K. Sekiyama, and T. Fukuda, "Control of intelligent cane robot considering usage of ordinary cane," in *2013 IEEE RO-MAN*, Aug 2013, pp. 762–767.
- [101] K. Wakita, J. Huang, P. Di, K. Sekiyama, and T. Fukuda, "Human-walking-intention-based motion control of an omnidirectional-type cane robot," *IEEE/ASME TRANSACTIONS ON MECHATRONICS*, vol. 18, no. 1, pp. 285–296, February 2013.
- [102] F. Vidal-Verdú, Ó. Oballe-Peinado, J. A. Sánchez-Durán, J. Castellanos-Ramos, and R. Navas-González, "Three realizations and comparison of hardware for piezoresistive tactile sensors," *Sensors*, vol. 11, no. 3, pp. 3249–3266, 2011.
- [103] F. Vidal-Verdú, M. J. Barquero, J. Castellanos-Ramos, R. Navas-González, J. A. Sánchez, J. Serón, and A. García-Cerezo, "A large area tactile sensor patch based on commercial force sensors," *Sensors*, vol. 11, no. 12, p. 5489–5507, May 2011. [Online]. Available: <http://dx.doi.org/10.3390/s110505489>
- [104] "Sunrise Medical. F35 powered wheelchair," 2014, URL: <http://www.sunrisemedical.es/sillas-de-ruedas/quickie/silla-electrica-plegable-f35-r2> [accessed: June, 2017].
- [105] "Invacare. Bora powered wheelchair," 2015, URL: https://www.ortopediamimas.com/index.php?controller=attachment&id_attachment=7443 [accessed: June, 2017].
- [106] "Dynamic Controls. DX System," 2015, URL: <https://dynamiccontrols.com/en/designers-and-manufacturers/products/dx> [accessed: June, 2017].
- [107] "Invacare (Dynamic Controls). REM24SD," 2017, URL: http://www.invacare.co.uk/sites/uk/files/product_documents/388a37873ef7f7ee34fc042a50cebf7c4707b4e9_55c4b17852dccba2348b4579.pdf [accessed: June, 2017].
- [108] A. Trujillo-León and F. Vidal-Verdú, "Driving interface based on tactile sensors for electric wheelchairs or trolleys," *Sensors*, vol. 14, no. 2, pp. 2644–2662, 2014. [Online]. Available: <http://www.mdpi.com/1424-8220/14/2/2644>
- [109] E. W. Abel and T. G. Frank, "The design of attendant propelled wheelchairs," *Prosthetics and Orthotics International*, vol. 15, no. 1, pp. 38–45, 1991, PMID: 1857639. [Online]. Available: <http://dx.doi.org/10.3109/03093649109164273>

- [110] “Tekscan™. I-Scan System,” 2017, URL: <https://www.tekscan.com/products-solutions/systems/i-scan-system> [accessed: June, 2017].
- [111] D. E. Hinkle, W. Wiersma, and S. G. Jurs, *Applied Statistics for the Behavioral Sciences*, 5th ed. Houghton Mifflin, 2002.
- [112] C. Pernet, R. Wilcox, and G. Rousselet, “Robust correlation analyses: False positive and power validation using a new open source matlab toolbox,” *Frontiers in Psychology*, vol. 3, p. 606, 2013. [Online]. Available: <http://journal.frontiersin.org/article/10.3389/fpsyg.2012.00606>
- [113] “Research group: Electronics for Instrumentation and Systems. University of Málaga, Spain,” 2017, URL: <http://www.eis.uma.es/> [accessed: July, 2017].
- [114] J. C. Ramos, “Caracterización, Modelado y Diseño de Sensores Táctiles Piezorresistivos (in spanish),” Ph.D. dissertation, Departamento de Electrónica. Universidad de Málaga, November 2015.
- [115] P. K. Pawar and A. Dadhich, “Study of correlation between human height and foot length in residents of mumbai,” *International Journal of Biological and Medical Research*, vol. 3, no. 3, pp. 2232–2235, 2012.
- [116] A. Ibegbu, E. David, W. Hamman, U. Umana, and S. Musa, “Hand length as a determinat of height in school children,” *Advances in Life Sciences*, vol. 5, no. 1, pp. 12–17, 2015.
- [117] R. Guerra, I. Fonseca, F. Pichel, M. Restivo, and T. Amaral, “Hand length as an alternative measurement of height,” *European journal of clinical nutrition*, vol. 68, no. 2, p. 229, 2014.
- [118] S. Petermeijer, D. Abbink, M. Mulder, and J. de Winter, “The effect of haptic support systems on driver performance: A literature survey,” *IEEE Transactions on Haptics*, vol. 8, no. 4, pp. 467–479, 2015.
- [119] L. Robinson, K. Brittain, S. Lindsay, D. Jackson, and P. Olivier, “Keeping in touch everyday (kite) project: developing assistive technologies with people with dementia and their carers to promote independence,” *International Psychogeriatrics*, vol. 21, no. 3, p. 494–502, 2009.
- [120] M. A. Hersh, “The design and evaluation of assistive technology products and devices part 1: Design,” *International Encyclopedia of rehabilitation*, 2010.
- [121] J. Stewart, S. Bauman, M. Escobar, J. Hilden, K. Bihani, and M. W. Newman, “Accessible contextual information for urban orientation,” in *Proceedings of the 10th International Conference on Ubiquitous Computing*, ser. UbiComp ’08. New York, NY, USA: ACM, 2008, pp. 332–335. [Online]. Available: <http://doi.acm.org/10.1145/1409635.1409679>
- [122] “Fadisel. Vibration motor C-6070,” 2017, URL: <http://fadisel.com/docs/c-6070-3.pdf> [accessed: June, 2017].

- [123] “MathWorks. Documentation: Color-Based Segmentation Using K-Means Clustering,” 2017, URL: <https://es.mathworks.com/help/images/examples/color-based-segmentation-using-k-means-clustering.html> [accessed: July, 2017].
- [124] “SimplyPsychology. Likert scale,” 2017, URL: <https://www.simplypsychology.org/likert-scale.html> [accessed: June, 2017].
- [125] “SurveyMonkey. What is a Likert scale?” 2017, URL: <https://www.surveymonkey.com/mp/likert-scale/> [accessed: June, 2017].
- [126] H. Schuman and S. Presser, *Questions and answers in attitude surveys: Experiments on question form, wording, and context*. Sage, 1996.
- [127] W. Saris, M. Revilla, J. A. Krosnick, and E. M. Shaeffer, “Comparing questions with agree/disagree response options to questions with item-specific response options,” in *Survey Research Methods*, vol. 4, no. 1, 2010, pp. 61–79.
- [128] “FluidSurveys UNIVERSITY. Odd or Even? The Ongoing Debate of Neutral Rating Scales,” 2017, URL: <http://fluidsurveys.com/university/odds-evens-ongoing-debate-rating-scale/> [accessed: June, 2017].
- [129] S. Jamieson *et al.*, “Likert scales: how to (ab) use them,” *Medical education*, vol. 38, no. 12, pp. 1217–1218, 2004.
- [130] J. E. Edelstein, “Assistive devices for ambulation,” *Physical Medicine and Rehabilitation Clinics of North America*, vol. 24, no. 2, pp. 291 – 303, 2013, ambulation in Adults with Central Neurologic Disorders. [Online]. Available: <http://www.sciencedirect.com/science/article/pii/S1047965112001325>
- [131] W. C. Mann, C. Llanes, M. D. Justiss, and M. Tomita, “Frail older adults’ self-report of their most important assistive device,” *OTJR: Occupation, Participation and Health*, vol. 24, no. 1, pp. 4–12, 2004. [Online]. Available: <https://doi.org/10.1177/153944920402400102>
- [132] M. Murray, A. Seireg, and R. Scholz, “A survey of the time, magnitude and orientation of forces applied to walking sticks by disabled men.” *American Journal of Physical Medicine & Rehabilitation*, vol. 48, no. 1, pp. 1–13, 1969.
- [133] C.-L. Chen, H.-C. Chen, M.-K. Wong, F.-T. Tang, and R.-S. Chen, “Temporal stride and force analysis of cane-assisted gait in people with hemiplegic stroke,” *Archives of Physical Medicine and Rehabilitation*, vol. 82, no. 1, pp. 43 – 48, 2001. [Online]. Available: <http://www.sciencedirect.com/science/article/pii/S0003999301269937>
- [134] G. U. Sorrento, P. S. Archambault, and J. Fung, “The effects of a robot-controlled haptic leash compared with an instrumented cane on gait and posture in post-stroke and older adults,” in *2017 International Conference on Virtual Rehabilitation (ICVR)*, June 2017, pp. 1–7.
- [135] H. H. Liu, J. Eaves, W. Wang, J. Womack, and P. Bullock, “Assessment of canes used by older adults in senior living communities,” *Archives of gerontology and geriatrics*, vol. 52, no. 3, pp. 299–303, 2011.

- [136] C. Perez, A. Oates, L. Hughey, and J. Fung, "Development of a force-sensing cane instrumented within a treadmill-based virtual reality locomotor system," in *2009 Virtual Rehabilitation International Conference*, June 2009, pp. 154–159.
- [137] J. Mercado, G. Chu, E. J. Imperial, K. G. Monje, R. M. Pabustan, and A. Silverio, "Smart cane: Instrumentation of a quad cane with audio-feedback monitoring system for partial weight-bearing support," in *2014 IEEE International Symposium on Bioelectronics and Bioinformatics (IEEE ISBB 2014)*, April 2014, pp. 1–4.
- [138] M. Ackermann and W. Schiehlen, "Dynamic analysis of human gait disorder and metabolic cost estimation," *Archive of Applied Mechanics*, vol. 75, no. 10, pp. 569–594, 2006.
- [139] J. M. Hausdorff, H. K. Edelberg, M. E. Gudkowicz, M. A. F. Singh, and J. Y. Wei, "The relationship between gait changes and falls," *Journal of the American Geriatrics Society*, vol. 45, no. 11, pp. 1406–1406, 1997. [Online]. Available: <http://dx.doi.org/10.1111/j.1532-5415.1997.tb02944.x>
- [140] A. Yurkewich, S. F. Atashzar, A. Ayad, and R. V. Patel, "A six-degree-of-freedom robotic system for lower extremity rehabilitation," in *2015 IEEE International Conference on Rehabilitation Robotics (ICORR)*, Aug 2015, pp. 810–815.
- [141] K. Gui, H. Liu, and D. Zhang, "Towards multimodal human-robot interaction to enhance active participation of users in gait rehabilitation," *IEEE Transactions on Neural Systems and Rehabilitation Engineering*, vol. PP, no. 99, pp. 1–1, 2017.
- [142] M. Spenko, H. Yu, and S. Dubowsky, "Robotic personal aids for mobility and monitoring for the elderly," *IEEE Transactions on Neural Systems and Rehabilitation Engineering*, vol. 14, no. 3, pp. 344–351, Sept 2006.
- [143] H. Yu, M. Spenko, and S. Dubowsky, "An adaptive shared control system for an intelligent mobility aid for the elderly," *Autonomous Robots*, vol. 15, no. 1, pp. 53–66, Jul 2003. [Online]. Available: <https://doi.org/10.1023/A:1024488717009>
- [144] R. F. Edlich, C. Hartigan, R. F. Morgan, F. P. Hunter Jr, R. E. Shotwell, and J. G. Thacker, "Ergonomics of support cane handles." *Journal of Burn Care & Research*, vol. 8, no. 2, pp. 150–154, 1987.
- [145] J. Gonzalez, A. J. Muaeoz, C. Galindo, J. A. Fernandez-Madrigal, and J. L. Blanco, "A description of the sena robotic wheelchair," in *MELECON 2006 - 2006 IEEE Mediterranean Electrotechnical Conference*, May 2006, pp. 437–440.
- [146] J.-A. Fernández-Madrigal, *Simultaneous Localization and Mapping for Mobile Robots: Introduction and Methods: Introduction and Methods*. IGI Global, 2012.
- [147] S. Katsura and K. Ohnishi, "Human cooperative wheelchair for haptic interaction based on dual compliance control," *IEEE Transactions on Industrial Electronics*, vol. 51, no. 1, pp. 221–228, Feb 2004.
- [148] X. Yun and Y. Yamamoto, "Internal dynamics of a wheeled mobile robot," in *Intelligent Robots and Systems '93, IROS '93. Proceedings of the 1993 IEEE/RSJ International Conference on*, vol. 2, Jul 1993, pp. 1288–1294 vol.2.

- [149] C. C. Macadam, "Understanding and modeling the human driver," *Vehicle System Dynamics*, vol. 40, no. 1-3, pp. 101–134, 2003. [Online]. Available: <http://www.tandfonline.com/doi/abs/10.1076/vesd.40.1.101.15875>
- [150] "LMV3xx Low-Voltage Rail-to-Rail Output Operational Amplifiers. Texas Instruments," 2017, URL: <http://www.ti.com/lit/ds/symlink/lmv324.pdf> [accessed: July, 2017].
- [151] S. O. Onyango, Y. Hamam, K. Djouani, B. Daachi, and N. Steyn, "A driving behaviour model of electrical wheelchair users," *Computational intelligence and neuroscience*, vol. 2016, 2016.
- [152] K.-T. Nam, D.-J. Jang, Y. C. Kim, Y. Heo, and E.-P. Hong, "A study of a handrim-activated power-assist wheelchair based on a non-contact torque sensor," *Sensors*, vol. 16, no. 8, p. 1251, 2016.



UNIVERSIDAD
DE MÁLAGA

Appendix A

Extension of experiments results

This appendix collects some of the data obtained from the different experiments carried out in the development of this thesis and that were not include in the main body of the document. They are additional data that are not crucial to follow the explanations and whose inclusion in the text may have made the reading more difficult.

Specifically, those results that can be consulted in this section are the following:

Correlation coefficients for E2 tests: Tables A.1 and A.2 list the Pearson and Spearman's rank-order correlation coefficients calculated in the experiment E2. As said in Section 3.2.3, they assess the degree of linear and monotonic coupling between the centers of mass CoM_L and CoM_R and F_y , for the 1st sequence (push/pull), and T_z for the 2nd sequence of maneuvers (turns). "Wk", "Nm" and "Str" are the short forms of "Weak", "Normal" and "Strong". Remember that they were subjective terms and do not necessarily represent low or high forces.

Excursion of centers of mass of E3 tests: In the experiment E3, the excursion of the $CoMs$ considering eight different tactels arrangements (from A to H) were computed. In Tables A.3, A.4, A.5 and A.6, the tactel arrangements that produced the maximum CoM excursion are given in the columns labeled $Arr_{1^{a}Exc}$. On the other hand, values in column $Arr_{2^{a}Exc}$ are those tactels configurations whose CoM excursion was the second highest. The value of the excursion is shown between brackets (normalized, in number of tactels).

Trajectory errors of E5.1 tests: The first trial of E5.1 was used to extract objective measurements of the participants' performance following the path. These are presented in Tables A.7 and A.8 (for the joystick and the handlebar, respectively) and are: mean error, maximum error, test duration, product of mean error by test duration (from 2nd to 5th column).

Table A.1 Pearson (r) and Spearman's rank-order (ρ) correlation coefficients for the pair of variables formed by the center of mass of each hand (CoM_L/CoM_R) and F_y during the 1st sequence of maneuvers (push/pull) of the experiment E2. They are classified by the type grip that the participant intended to perform ('weak', 'normal' and 'strong').

Participant		$r_{<CoM_L, F_y>}$	$\rho_{<CoM_L, F_y>}$	$r_{<CoM_R, F_y>}$	$\rho_{<CoM_R, F_y>}$	$GF_L[N]$	$GF_R[N]$
P1	<i>Wk.</i>	-0.64	-0.70	-0.45	-0.66	1.42	2.15
	<i>Nm.</i>	-0.92	-0.92	-0.83	-0.75	2.18	3.65
	<i>Str.</i>	-0.91	-0.91	-0.86	-0.87	4.75	7.76
P2	<i>Wk.</i>	-0.77	-0.84	-0.69	-0.48	0.57	0.93
	<i>Nm.</i>	-0.96	-0.97	-0.91	-0.93	5.29	9.36
	<i>Str.</i>	-0.89	-0.92	-0.34	-0.37	13.77	14.14
P3	<i>Wk.</i>	-0.96	-0.95	-0.96	-0.97	5.50	5.47
	<i>Nm.</i>	-0.97	-0.96	-0.95	-0.96	9.37	8.34
	<i>Str.</i>	-0.97	-0.96	-0.95	-0.97	11.25	10.56
P4	<i>Wk.</i>	-0.92	-0.92	-0.93	-0.89	0.75	0.69
	<i>Nm.</i>	-0.96	-0.94	-0.97	-0.97	2.98	3.19
	<i>Str.</i>	-0.92	-0.91	-0.86	-0.83	4.49	4.01
P5	<i>Wk.</i>	-0.95	-0.91	-0.96	-0.92	0.95	1.07
	<i>Nm.</i>	-0.99	-0.97	-0.97	-0.95	2.12	2.48
	<i>Str.</i>	-0.99	-0.96	-0.96	-0.90	3.27	4.45
P6	<i>Wk.</i>	-0.86	-0.89	-0.91	-0.94	1.16	2.21
	<i>Nm.</i>	-0.88	-0.87	-0.94	-0.96	3.48	6.59
	<i>Str.</i>	-0.94	-0.82	-0.95	-0.86	13.33	14.53
P7	<i>Wk.</i>	-0.92	-0.85	-0.94	-0.93	1.21	1.92
	<i>Nm.</i>	-0.90	-0.95	-0.89	-0.90	3.10	3.37
	<i>Str.</i>	-0.77	-0.79	-0.75	-0.74	11.80	11.78

Table A.2 Pearson (r) and Spearman's rank-order (ρ) correlation coefficients for the pair of variables formed by the center of mass of each hand (CoM_L/CoM_R) and T_z during the 2nd sequence of maneuvers (turns) of the experiment E2. They are classified by the type grip that the participant intended to perform ('weak', 'normal' and 'strong').

Participant		$r_{<CoM_L, T_z>}$	$\rho_{<CoM_L, T_z>}$	$r_{<CoM_R, T_z>}$	$\rho_{<CoM_R, T_z>}$	GF_L [N]	GF_R [N]
P1	<i>Wk.</i>	0.87	0.75	-0.63	-0.66	0.83	1.78
	<i>Nm.</i>	0.92	0.90	-0.76	-0.71	2.40	3.59
	<i>Str.</i>	0.09	0.24	-0.40	-0.32	8.56	11.02
P2	<i>Wk.</i>	0.89	0.88	-0.83	-0.83	0.84	1.81
	<i>Nm.</i>	0.58	0.50	-0.82	-0.91	2.40	3.60
	<i>Str.</i>	0.87	0.83	-0.30	-0.60	8.31	10.78
P3	<i>Wk.</i>	0.56	0.66	-0.90	-0.88	3.63	2.83
	<i>Nm.</i>	0.93	0.91	-0.90	-0.96	6.49	3.97
	<i>Str.</i>	0.30	0.33	-0.94	-0.90	12.66	13.48
P4	<i>Wk.</i>	0.83	0.75	-0.80	-0.78	0.21	0.36
	<i>Nm.</i>	0.84	0.78	-0.74	-0.78	0.50	0.67
	<i>Str.</i>	0.93	0.91	-0.74	-0.85	1.46	2.18
P5	<i>Wk.</i>	0.93	0.97	-0.96	-0.96	0.98	1.47
	<i>Nm.</i>	0.94	0.97	-0.97	-0.94	1.91	2.93
	<i>Str.</i>	0.95	0.99	-0.92	-0.93	4.85	5.92
P6	<i>Wk.</i>	0.96	0.97	-0.97	-0.98	0.78	1.89
	<i>Nm.</i>	0.96	0.98	-0.95	-0.92	3.32	4.97
	<i>Str.</i>	0.49	0.62	-0.44	-0.58	12.51	14.23
P7	<i>Wk.</i>	0.70	0.58	-0.82	-0.82	1.19	1.11
	<i>Nm.</i>	0.93	0.93	-0.72	-0.89	3.61	4.25
	<i>Str.</i>	0.80	0.91	-0.41	-0.48	12.78	13.60

Table A.3 Participants P1-P6: arrangements of tactels for which the CoM excursion was maximum (Arr_{1^aExc}) and those for which it was the second largest (Arr_{2^aExc}). In parentheses, the normalized value of the calculated excursion. PP1 and PP2 refer to the two tests of P/P maneuvers whereas T1 and T2 are related to the two tests in which turns were performed. The height of the handlebar for these data was h_1 .

Participant	Test	CoM_L		CoM_R	
		Arr_{1^aExc}	Arr_{2^aExc}	Arr_{1^aExc}	Arr_{2^aExc}
P1	PP1	E (2.4485)	A (1.9827)	E (1.7465)	D (1.2007)
	PP2	E (2.7445)	A (2.0026)	E (2.182)	D (1.4942)
	T1	A (1.9118)	E (1.8525)	E (2.1293)	D (1.7183)
	T2	F (2.9598)	A (2.9549)	E (2.5516)	D (2.1496)
P2	PP1	E (3.2349)	F (3.1911)	E (2.9061)	F (2.4126)
	PP2	F (3.6815)	E (3.4767)	E (3.0186)	F (2.9077)
	T1	F (4.11)	E (3.8315)	F (2.6041)	E (2.4232)
	T2	F (3.6863)	E (3.423)	F (3.0297)	E (2.924)
P3	PP1	E (2.8751)	F (2.3118)	D (2.3398)	E (2.0784)
	PP2	E (2.9336)	F (2.6579)	E (3.0332)	F (2.4098)
	T1	F (3.1093)	E (2.7359)	E (2.902)	F (2.8382)
	T2	E (4.0414)	F (2.9879)	D (3.8009)	E (3.1792)
P4	PP1	E (2.0752)	A (1.5625)	E (2.2062)	D (2.1211)
	PP2	E (1.8405)	D (1.4541)	E (2.4838)	D (1.9301)
	T1	E (1.5984)	A (1.5815)	D (1.9412)	F (1.847)
	T2	A (1.9372)	E (1.825)	D (2.7784)	E (2.4218)
P5	PP1	F (1.0308)	B (0.91866)	C (1.0101)	E (0.86322)
	PP2	B (1.2037)	F (1.1372)	B (1.1448)	F (1.0574)
	T1	A (1.7157)	E (1.5474)	E (1.673)	A (1.2064)
	T2	D (2.9143)	E (2.6243)	E (1.4665)	A (1.0659)
P6	PP1	E (2.8724)	A (2.1368)	E (3.5736)	A (2.6046)
	PP2	F (2.5427)	E (2.3854)	E (2.9548)	B (1.9777)
	T1	F (2.377)	E (2.1049)	E (2.8801)	F (2.1041)
	T2	E (2.3488)	D (1.7285)	E (2.5182)	F (2.0325)

$$(h_1 = 98.5cm)$$

Table A.4 Participants P7-P12: arrangements of tactels for which the CoM excursion was maximum (Arr_{1^aExc}) and those for which it was the second largest (Arr_{2^aExc}). In parentheses, the normalized value of the calculated excursion. PP1 and PP2 refer to the two tests of P/P maneuvers whereas T1 and T2 are related to the two tests in which turns were performed. The height of the handlebar for these data was h_1 .

Participant	Test	CoM_L		CoM_R	
		Arr_{1^aExc}	Arr_{2^aExc}	Arr_{1^aExc}	Arr_{2^aExc}
P7	PP1	F (3.6349)	E (2.164)	F (2.8672)	E (2.546)
	PP2	F (4.0076)	E (3.5265)	E (2.7008)	F (2.3122)
	T1	F (4.1434)	E (3.5655)	F (3.8429)	E (2.8892)
	T2	F (3.4056)	E (3.156)	F (2.8463)	E (2.6749)
P8	PP1	E (3.4182)	D (3.317)	D (3.4368)	E (3.1404)
	PP2	E (3.3483)	F (2.6802)	C (2.2948)	D (2.2632)
	T1	D (2.8584)	F (2.7887)	F (3.4077)	D (2.7681)
	T2	F (2.9713)	D (2.1469)	F (2.5015)	F (1.4996)
P9	PP1	E (3.5084)	A (2.7535)	E (3.4341)	A (2.7076)
	PP2	F (3.3362)	E (2.5915)	E (3.5834)	F (2.3285)
	T1	F (3.6195)	E (3.3579)	E (3.1958)	F (2.4647)
	T2	F (4.0019)	E (3.3616)	E (3.8346)	F (3.2702)
P10	PP1	E (2.6878)	D (2.3444)	E (2.7606)	A (1.5379)
	PP2	E (2.4464)	D (2.0653)	E (2.0525)	F (1.3162)
	T1	E (2.8041)	D (2.1494)	E (2.4522)	D (1.2683)
	T2	E (2.1309)	D (2.1172)	E (2.8089)	A (1.6374)
P11	PP1	F (1.2259)	E (1.1914)	E (1.0797)	F (0.97412)
	PP2	F (1.0806)	E (0.9143)	F(1.0795)	B (1.0789)
	T1	F (1.6118)	E (1.1466)	F (1.3581)	B (1.034)
	T2	F (2.1849)	A (1.5457)	F (2.2436)	E (2.2152)
P12	PP1	E (1.9253)	F (1.3056)	E (1.3939)	F (1.0865)
	PP2	E (3.573)	D 1.929)	E (3.0318)	D (1.4821)
	T1	E (4.5732)	F (3.8674)	E (3.5834)	D (2.6238)
	T2	E (4.1966)	A (2.7681)	E (3.6436)	B (1.6914)

$$(h_1 = 98.5cm)$$

Table A.5 Participants P1-P6: arrangements of tactels for which the CoM excursion was maximum (Arr_{1^aExc}) and those for which it was the second largest (Arr_{2^aExc}). In parentheses, the normalized value of the calculated excursion. PP1 and PP2 refer to the two tests of P/P maneuvers whereas T1 and T2 are related to the two tests in which turns were performed. The height of the handlebar for these data was h_2 .

Participant	Test	CoM_L		CoM_R	
		Arr_{1^aExc}	Arr_{2^aExc}	Arr_{1^aExc}	Arr_{2^aExc}
P1	PP1	E (3.1955)	A (2.6868)	E (2.7604)	A (1.9244)
	PP2	E (2.8837)	A (2.1904)	E (2.3674)	D (1.902)
	T1	A(2.5457)	E (2.2535)	E (2.547)	D (1.7558)
	T2	E (2.9403)	A (2.9206)	E (3.088)	D (1.795)
P2	PP1	F (3.2079)	E (2.3124)	F (2.5252)	E (2.2044)
	PP2	F (3.9904)	E (2.9618)	F (2.5933)	E (2.2317)
	T1	E (4.0155)	F (3.7899)	F (2.8603)	E (2.2674)
	T2	E (4.2802)	F (4.0123)	F (2.7513)	E (2.4625)
P3	PP1	E (5.8942)	F (4.6163)	E (5.757)	F (4.0099)
	PP2	F (4.3263)	E (3.4694)	F (2.9851)	E (2.6972)
	T1	F (3.816)	E (2.8607)	E (3.2368)	F (3.056)
	T2	F (3.4109)	E (3.13)	E (5.2442)	F (3.8464)
P4	PP1	E (2.6049)	F (1.8309)	E (2.3481)	D (1.753)
	PP2	E (2.1635)	F (1.8767)	E (2.1276)	D (1.5182)
	T1	E (2.1989)	A (1.869)	D (2.5586)	E (2.5303)
	T2	E (2.1527)	A (2.0058)	E (2.5058)	D (2.3535)
P5	PP1	C (1.3488)	D(1.2855)	B (1.5031)	C(1.4375)
	PP2	E (1.7724)	B (1.3495)	C (2.3412)	D (2.1792)
	T1	E (1.6134)	C (1.4724)	D (1.3291)	C (1.2791)
	T2	E (1.8817)	C (1.5269)	E (1.5975)	C (1.5673)
P6	PP1	E (3.022)	A (2.1522)	E (3.0956)	B (2.2453)
	PP2	E (2.1265)	B (1.8475)	E (2.3617)	B (1.8077)
	T1	E (3.3191)	F (3.039)	E (2.9429)	F (1.9715)
	T2	E (2.0757)	B (2.0321)	E (2.4514)	F (1.5174)

($h_2 = 108cm$)

Table A.6 Participants P7-P12: arrangements of tactels for which the CoM excursion was maximum (Arr_{1^aExc}) and those for which it was the second largest (Arr_{2^aExc}). In parentheses, the normalized value of the calculated excursion. PP1 and PP2 refer to the two tests of P/P maneuvers whereas T1 and T2 are related to the two tests in which turns were performed. The height of the handlebar for these data was h_2 .

Participant	Test	CoM_L		CoM_R	
		Arr_{1^aExc}	Arr_{2^aExc}	Arr_{1^aExc}	Arr_{2^aExc}
P7	PP1	F (4.2313)	E (2.1988)	F (2.8366)	E (1.5596)
	PP2	F (4.1002)	E (2.2356)	F (3.0317)	E (2.3042)
	T1	F (3.2103)	E (2.3594)	F (3.2718)	E (2.2753)
	T2	F (4.5338)	E (2.0249)	F (3.9787)	E (3.3151)
P8	PP1	E (3.2005)	A (2.3863)	F (2.0692)	E (2.0394)
	PP2	E (4.2182)	D (3.491)	E (2.8583)	B (2.5598)
	T1	F (3.0649)	E (2.0428)	F (2.1713)	E (1.4549)
	T2	F (4.1132)	E (1.8745)	F (2.3548)	D (1.3629)
P9	PP1	E (2.6126)	A (2.3355)	E (2.8858)	A (2.1474)
	PP2	E (3.6626)	F (2.634)	E (3.34)	F (2.7385)
	T1	F (3.0792)	E (3.0597)	E (4.6579)	F (3.1962)
	T2	F (3.1962)	E (2.718)	F (3.7518)	E (3.5067)
P10	PP1	E (3.2441)	D (2.6393)	E (2.4978)	A (1.3381)
	PP2	D (2.5994)	E (2.4933)	E (2.8377)	B (1.4978)
	T1	E (3.1802)	A (2.0865)	E (2.7584)	A (1.2146)
	T2	E (2.856)	D (2.4264)	E (2.7396)	B (1.2926)
P11	PP1	F (3.2441)	E (2.6393)	B (2.4978)	E (1.3381)
	PP2	F (1.7136)	E (1.3873)	F (1.5589)	E (1.5271)
	T1	F (2.1344)	E (1.3689)	F (1.7171)	B (1.3998)
	T2	F (1.9932)	E (1.2567)	F (1.689)	E (1.4945)
P12	PP1	E (2.2649)	D (1.7723)	E (1.6108)	D (1.5475)
	PP2	E (2.2933)	F (1.6749)	C (1.4525)	F (1.0858)
	T1	E (3.5029)	F (2.7148)	E (2.914)	F (2.8817)
	T2	E (4.9669)	F (4.8531)	E (5.7163)	F (4.1613)

($h_2 = 108cm$)

Table A.7 Parameters from the tests of the experiment E5.1 for the attendant joystick driving. From left to right: mean and maximum trajectory errors, test duration, mean trajectory error and test duration product. The last row gathers the mean of all the latter parameters considering all the tests.

Participant	Attendant joystick			
	\overline{Error} [cm]	$Error_{MAX}$ [cm]	$Duration$ [s]	$\overline{Error} \cdot Durat$
P1	0.342	7.498	84.000	28.693
P2	1.776	41.966	109.000	193.628
P3	3.660	40.021	77.000	281.782
P 4	2.467	29.659	111.000	273.859
P5	0.773	9.351	80.000	61.858
P6	2.781	22.971	67.000	186.320
P7	1.501	13.342	77.000	115.539
P8	2.810	26.373	66.000	185.434
P9	0.689	7.713	95.000	65.454
P10	2.353	23.489	115.000	270.549
All tests mean	1.915	22.238	88.100	166.311

Table A.8 Same parameters of those explained for Table A.7, this time for the haptic handlebar.

Participant	Haptic handlebar			
	\overline{Error} [cm]	$Error_{MAX}$ [cm]	$Duration$ [s]	$\overline{Error} \cdot Durat$
P1	0.169	11.396	98.000	16.601
P2	3.239	51.239	46.000	149.008
P3	0.847	9.500	76.000	64.401
P 4	3.854	49.990	60.000	231.252
P5	0.635	16.221	67.000	42.564
P6	0.585	17.941	57.000	33.336
P7	0.694	14.546	102.000	70.786
P8	0.735	13.554	77.000	56.593
P9	0.366	3.924	92.000	33.705
P10	0.467	11.193	107.000	49.943
All tests mean	1.159	19.950	78.200	74.819

Responses to form of E5.2: the subjective perception of the use of both the haptic handlebar and the attendant joystick and the opinion of the participants were collected through a questionnaire. Here the answers can be consulted.

Note that the answers of the respondents R1 to R10 are not necessary linked to the participants P1 to P10, since the form was anonymous. When a respondent has left an additional comment¹, it appears just after the answer he or she selected.

Questions focusing on the haptic handlebar:

Q1. *With respect to its use, how do you consider the haptic handlebar?*

- R1. 6) Easy
- R2. 4) Neither easy nor difficult
- R3. 6) Easy. *"With a little practice, it's easy to control the movement."*
- R4. 4) Neither easy nor difficult
- R5. 6) Easy
- R6. 7) Very easy
- R7. 5) Rather easy
- R8. 6) Easy. *"After using it a little, it is easy to handle."*
- R9. 6) Easy. *"Not the first time but it is easy after using it a little."*
- R10. 5) Rather easy

Q2. *Concerning comfort, how do you consider the haptic handlebar?*

- R1. 6) Comfortable
- R2. 5) Rather comfortable
- R3. 6) Comfortable. *"Once you've learned how to handle it, you just must guide the movement."*
- R4. 5) Rather comfortable
- R5. 6) Comfortable
- R6. 6) Comfortable
- R7. 6) Comfortable
- R8. 7) Very comfortable. *"If the height is adequate, it is really easy to use it."*

¹Original comments were given in Spanish. In the document they have been translated into English.

R9. 6) Comfortable

R10. 5) Rather comfortable

Q3. *How much training do you consider is needed to use the haptic handlebar?*

R1. 6) Very little

R2. 5) Little

R3. 5) Little. *"It's easy to adapt to the device."*

R4. 4) Neither too much nor too little

R5. 6) Very little

R6. 5) Little

R7. 7) None

R8. 5) Little. *"Once it is calibrated, you get used to it very quickly."*

R9. 5) Little

R10. 6) Very little

Q4. *Regarding its usefulness, how do you consider the haptic handlebar?*

R1. 6) Useful

R2. 7) Very useful

R3. 6) Useful. *"It greatly reduces the effort that has to be made in order to move and steer the chair."*

R4. 6) Useful

R5. 7) Very useful

R6. 7) Very useful

R7. 6) Useful

R8. 7) Very useful. *"This device has really ample possibilities ."*

R9. 7) Very useful

R10. 6) Useful

Q5. *With respect to safety, how do you consider the haptic handlebar?*

R1. 6) Safe

R2. 4) Neither safe nor insecure

- R3. 6) Safe. *"The chair automatically stops if the handlebar is released, what is good. However, the system is a little slow at first, when you have to wait to hear the sound signal. What if I need to move the chair quickly to avoid an obstacle heading towards us?"*
- R4. 5) Rather safe
- R5. 6) Safe
- R6. 7) Very safe
- R7. 5) Rather safe
- R8. 6) Safe. *"I think it is well designed to avoid accidents."*
- R9. 6) Safe
- R10. 3) Rather insecure. *"Mainly during the learning period. With practice, it gets safer."*

Q6. Concerning physical and mental fatigue, how do you consider the haptic handlebar?

- R1. 6) Effortless
- R2. 5) Rather effortless
- R3. 3) Rather tiring. *"It can be rather tiring in the beginning when you are focusing on the handlebar. After getting used to it a little, it's not tiring at all."*
- R4. 4) Neither effortless nor tiring
- R5. 6) Effortless
- R6. 7) Very effortless
- R7. 6) Effortless
- R8. 6) Effortless. *"Maybe a little tiring just in the first moments. After that, it is effortless."*
- R9. 6) Effortless
- R10. 5) Rather effortless

Questions focusing on the attendant joystick:

Q1. With respect to its use, how do you consider the attendant joystick?

- R1. 4) Neither easy nor difficult
- R2. 3) Rather difficult

- R3. 3) Rather difficult. *"It is operated with only one hand, what I found more complicated and less natural than the handlebar use."*
- R4. 4) Neither easy nor difficult
- R5. 6) Easy
- R6. 5) Rather easy
- R7. 2) Difficult
- R8. 4) Neither easy nor difficult. *"The lateral movements are abrupt and it is difficult to follow a specific trajectory because of the zigzag. Only the forward movements are steady."*
- R9. 2) Difficult. *"Above all, when it is necessary to carry out little trajectory corrections."*
- R10. 3) Rather difficult

Q2. Concerning comfort, how do you consider the attendant joystick?

- R1. 3) Rather uncomfortable
- R2. 5) Rather comfortable
- R3. 2) Uncomfortable. *"It is more easy to accommodate and to steer grasping the handlebar than grasping the joystick."*
- R4. 5) Rather comfortable
- R5. 3) Rather uncomfortable. *"The hand posture is not very natural."*
- R6. 6) Comfortable
- R7. 2) Uncomfortable
- R8. 6) Comfortable. *"It is comfortable if you find the right hand posture."*
- R9. 6) Comfortable
- R10. 5) Rather comfortable

Q3. How much training do you consider is needed to use the attendant joystick?

- R1. 4) Neither too much nor too little
- R2. 3) Quite a lot
- R3. 3) Quite a lot. *"Its handling is less intuitive [than the handlebar], considering the range of maneuvers that can appear in a typical driving exercise."*

- R4. 4) Neither too much nor too little
- R5. 4) Neither too much nor too little. *"The backward driving is difficult and it requires considerable training."*
- R6. 4) Neither too much nor too little
- R7. 3) Quite a lot
- R8. 3) Quite a lot *"It requires much more training than the handlebar [in order to achieve a driving as good as that with that device]."*
- R9. 3) Quite a lot
- R10. 4) Neither too much nor too little

Q4. Regarding its usefulness, how do you consider the attendant joystick?

- R1. 5) Rather useful
- R2. 6) Useful
- R3. 5) Rather useful. *"Although in my opinion, it is more uncomfortable and unintuitive than a handlebar."*
- R4. 6) Useful
- R5. 6) Useful
- R6. 6) Useful
- R7. 3) Rather useless
- R8. 7) Very useful
- R9. 5) Rather useful
- R10. 3) Rather useless

Q5. With respect to safety, how do you consider the attendant joystick?

- R1. 5) Rather safe
- R2. 4) Neither safe nor insecure.
- R3. 3) Rather insecure
- R4. 5) Rather safe
- R5. 6) Safe
- R6. 6) Safe
- R7. 2) Insecure

R8. 4) Neither safe nor insecure. *"I think it will depend on the user's ability with one device and the other, but I think that the handlebar monitors in a better way what the attendant is doing [in order to avoid risks]. Besides, the handlebar has a softer response to certain kind of maneuvers."*

R9. 3) Rather insecure

R10. 3) Rather insecure

Q6. Concerning physical and mental fatigue, how do you consider the attendant joystick?

R1. 4) Neither effortless nor tiring

R2. 3) Rather tiring

R3. 3) Rather tiring. *"I think that driving with the joystick requires more attention and, thus, a bigger mental effort."*

R4. 5) Rather effortless

R5. 6) Effortless

R6. 5) Rather effortless

R7. 2) Tiring

R8. 5) Rather effortless. *"Effortless, although it is in a disadvantaged position compared with the handlebar, since it needs more corrections to follow a curve trajectory."*

R9. 2) Tiring

R10. 6) Effortless

Questions focusing on personal information

a) Had you used a joystick before performing the experiment (videogames, machines operating, etc.)?

R1. Yes

R2. Yes

R3. No

R4. No

R5. Yes

R6. Yes

R7. Yes

R8. Yes

R9. Yes

R10. Yes

b) *Had you used a device similar to the haptic handlebar before taking part in the experiment?*

R1. No

R2. No

R3. No

R4. No

R5. No

R6. No

R7. No

R8. No

R9. No

R10. No

c) *Are you familiar with the role of wheelchair assistant?*

R1. No

R2. No

R3. No

R4. No

R5. No

R6. No

R7. No

R8. No

R9. Yes

R10. No

d) *How old are you?*

R1. 40-45

R2. 40-45

R3. 50-55

R4. 60-65

R5. 45-50

R6. 40-45

R7. 25-30

R8. 40-45

R9. 50-55

R10. 30-35

e) *Leave, if you wish, some additional comment about your experience after having driven with both devices.*

R3. *"I think that driving with the haptic handlebar can be more advantageous for both the attendant and the person on the chair."*

R5. *"I have noted the handlebar vibration when I exert too much force in more complex maneuvers. I think that I overexert unconsciously in these cases. Sometimes, when going forward, I have observed little jerks."*

R7. *"I've found the handlebar much more intuitive than the joystick."*

R8. *"Although the joystick is also useful, the handlebar is by far a better option. It has been an interesting and fun experience!"*

Appendix B

Scientific contributions

B.1 Journals

A. Trujillo-León, W. Bachta and F. Vidal-Verdú, “Tactile Sensors Based Steering as a Substitute of the Attendant Joystick in Powered Wheelchairs,” *IEEE Transactions on Neural Systems and Rehabilitation Engineering*. (Submitted)

A. Trujillo-León and F. Vidal-Verdú, “Driving interface based on tactile sensors for electric wheelchairs or trolleys,” *Sensors*, vol. 14, no. 2, pp. 2644–2662, 2014. [Online]. Available: <http://www.mdpi.com/1424-8220/14/2/2644> (Q1)

B.2 Conferences

A. Trujillo-León, W. Bachta and F. Vidal-Verdú, “Evaluation of Tactile Sensors as an Alternative to Force Sensors in an Assistive Haptic Handlebar,” *The 13th IEEE Biomedical Circuits and Systems Conference, BioCAS2017*. Turin, Italy, October 19-21, 2017

A. Trujillo-León, W. Bachta and F. Vidal-Verdú, “Assistive haptic handlebar based on tactile sensors,” *International Workshop on Assistive and Rehabilitation Technology, IWART 2016*. University Miguel Hernández, Elche, Spain, December 14-16, 2016

A. Trujillo-León, R. Ady, F. Vidal-Verdú and W. Bachta, “A tactile handle for cane use monitoring,” *The 37th Annual International Conference of the IEEE Engineering in Medicine and Biology Society (EMBS)*. Milano, Italy, August 25-29, 2015

A. Trujillo-León, R. Ady, F. Vidal-Verdú and W. Bachta, “Tactile handle for an instrumented cane,” *The Sixth International Conference on Sensor Device Technologies and Applications*, SensorDevices 2015. Venice, Italy, August 23 - 28, 2015

A. Trujillo-León and F. Vidal-Verdú, “Self-calibration of an Attendance Device to Adapt to Different Users and Environments,” *The International Conference on Multimodal Interaction*, ICMI 2014. Boğaziçi University, Istanbul, 13-15, November, 2014

B.3 Patent

F. Vidal-Verdú, A. Trujillo-León, R. Navas-Gonzalez, J.A. Hidalgo-López, J. Castellanos-Ramos, O. Oballe-Peinado and J.A. Sánchez-Durán, “Dispositivo de conducción asistida”, wO Patent App. PCT/ES2012/000,168. [Online]. Available: <https://www.google.com/patents/WO2012172134A1>

Appendix C

Dynamic system modeling and simulations

This appendix addresses the dynamic modeling of the system and some simulations aimed to test the influence of the haptic handlebar in the general performance.

C.1 Modeling of a powered wheelchair as a differential wheeled robot

C.1.1 Powered wheelchair kinematics

A powered wheelchair may be modeled as a differential mobile robot. Although it has four wheels, the two front ones have a stabilization purpose and, therefore, they do not affect the motion [145, 146]. The parameters involved in the kinematics of this kind of nonholonomic mobile robots are shown in Figure C.1. The body of the robot rotates around a point defined as rotation center at an angular speed ω . The distance between this point and the robot's motion center (*m.c.* in Figure C.1) has been called ρ .

The linear velocity of the robot's motion center can be estimated using the angular speed as:

$$v_{mc} = \omega \cdot \rho \quad (\text{C.1})$$

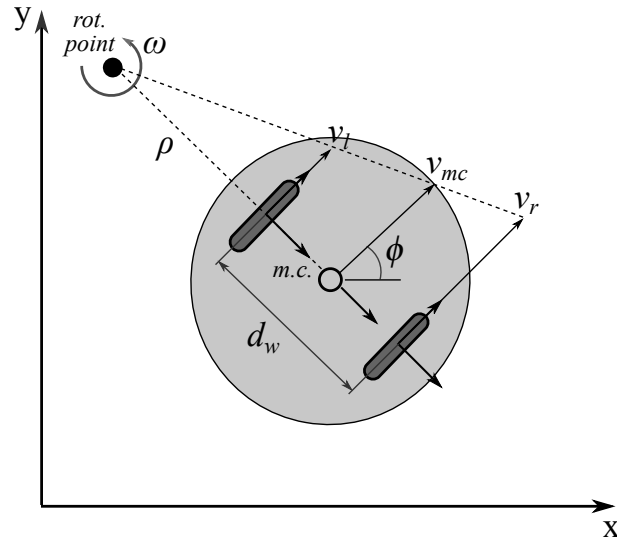


Fig. C.1 Kinematics of a differential wheeled vehicle.

Besides, the linear velocities of each wheel can be calculated as follows:

$$v_l = \omega \cdot \left(\rho - \frac{d_w}{2} \right) \quad (\text{C.2})$$

$$v_r = \omega \cdot \left(\rho + \frac{d_w}{2} \right) \quad (\text{C.3})$$

where v_l and v_r are the linear speeds of the left and right wheel, respectively, and d_w the distance between them.

From Equation C.2 and C.3, we obtain ω as:

$$\omega = \frac{v_l}{\rho - \frac{d_w}{2}} = \frac{v_r}{\rho + \frac{d_w}{2}} \quad (\text{C.4})$$

where ρ can be isolated as:

$$\rho = \frac{d_w(v_r + v_l)}{2(v_r - v_l)} \quad (\text{C.5})$$

Subtracting Equation C.3 and C.2 and using the previous form of ρ , the angular speed ω can be expressed in terms of the wheels' linear velocities:

$$\omega = \frac{v_r - v_l}{d_w} \quad (\text{C.6})$$

From Equations C.6, C.5 and C.1, the linear velocity of the PW can be calculated from the wheels' velocities and the distance between them as:

$$v_{mc} = \frac{v_r + v_l}{2} \quad (C.7)$$

In Cartesian coordinates (see Figure C.1), v_{mc} can be expressed as:

$$\begin{aligned} \dot{x} &= \frac{v_r + v_l}{2} \cos\phi \\ \dot{y} &= \frac{v_r + v_l}{2} \sin\phi \end{aligned} \quad (C.8)$$

Moreover, the linear speed of the chair wheels can be estimated using Equation C.9¹:

$$v_w = \dot{\theta} \cdot R \quad (C.9)$$

where θ is the angular position of the wheel and R its radius.

This way, the Cartesian coordinates of Equation C.8 can be rewritten as:

$$\begin{aligned} \dot{x} &= \frac{R}{2} (\dot{\theta}_r + \dot{\theta}_l) \cos\phi \\ \dot{y} &= \frac{R}{2} (\dot{\theta}_r + \dot{\theta}_l) \sin\phi \end{aligned} \quad (C.10)$$

In the same manner, ω (see Equation C.6) can be expressed as:

$$\omega = \frac{R}{d_w} (\dot{\theta}_r - \dot{\theta}_l) \quad (C.11)$$

Finally, the Jacobian matrix that links the Cartesian and joint velocities of the PW can be built with Equations C.10 and C.11:

$$\begin{bmatrix} \dot{x} \\ \dot{y} \\ \omega \end{bmatrix} = \begin{bmatrix} \frac{R}{2} \cos\phi & \frac{R}{2} \cos\phi \\ \frac{R}{2} \cos\phi & \frac{R}{2} \sin\phi \\ \frac{R}{d_w} & -\frac{R}{d_w} \end{bmatrix} \begin{bmatrix} \dot{\theta}_r \\ \dot{\theta}_l \end{bmatrix} = J_{aco}(\phi) \dot{\theta} \quad (C.12)$$

¹Provided that the following assumptions are made: there is only one point of contact between the wheels and the ground, there is no slipping and the wheels retain their shape.

C.1.2 Powered wheelchair dynamics

The dynamic model of the PW as a differential mobile robot can be calculated using the Lagrange-Euler equation, which is based on the vehicle's mechanical energy. If the PW moves on a flat surface, the potential energy can be considered zero (this assumption is made). Moreover, the kinetic energy consists of four components [147, 148]: the energy resulting from the PW's translational motion, that from its rotational motion, the energy derived from the wheels' rotational motion and that appearing when center of gravity is not on the axis of the wheels (guiding system). Regarding the last point, no exact data about the PW's center of gravity are available. It can vary slightly depending on the PW's equipped accessories, the body of the person who is seated or the angle of the seat with the ground. If the manufacturer's recommendations concerning the PW stability are followed, it should be near the guiding system so both points may be seen as coincident. This way, the fourth component of the kinetic energy can be considered negligible. The other three are shown in Equation C.13:

$$K = \frac{1}{2}M \left(\frac{R}{2}(\dot{\theta}_r + \dot{\theta}_l) \right)^2 + \frac{1}{2}J \left(\frac{R}{d_w}(\dot{\theta}_r - \dot{\theta}_l) \right)^2 + \frac{1}{2}J_w(\dot{\theta}_r^2 + \dot{\theta}_l^2) \quad (\text{C.13})$$

where M is the mass of the PW plus the person seated, J is the inertia of the PW about a vertical axis through the center of gravity (*m.c.* in Figure C.1) and J_w the inertia of each wheel around its own axis.

The dynamics of the PW is defined by Equation C.14, where the Lagrange equation (Eq. C.13) has to be solved.

$$\begin{bmatrix} \tau_r \\ \tau_l \end{bmatrix} = M_\theta \begin{bmatrix} \ddot{\theta}_r \\ \ddot{\theta}_l \end{bmatrix} = M_\theta \ddot{\theta} \quad (\text{C.14})$$

where M_θ is the equivalent inertia matrix.

Thus, by calculating the partial derivatives of Equation C.13, M_θ is:

$$M_\theta = R^2 \begin{bmatrix} \frac{M}{4} + \frac{J}{d_w^2} + \frac{J_w}{R^2} & \frac{M}{4} - \frac{J}{d_w^2} \\ \frac{M}{4} - \frac{J}{d_w^2} & \frac{M}{4} + \frac{J}{d_w^2} + \frac{J_w}{R^2} \end{bmatrix} \quad (\text{C.15})$$

The direct dynamic model provides the wheels' accelerations from their associated torques:

$$\begin{bmatrix} \ddot{\theta}_r \\ \ddot{\theta}_l \end{bmatrix} = M_\theta^{-1} \begin{bmatrix} \tau_r \\ \tau_l \end{bmatrix} = M_\theta^{-1} \tau \quad (\text{C.16})$$

As shown in Equation C.16, M_{θ}^{-1} can be obtained by calculating the inverse of the inertia matrix:

$$M_{\theta}^{-1} = \begin{bmatrix} \frac{MR^2d_w^2 + 4JR^2 + 4J_w d_w^2}{2(2J_w^2 d_w^2 + MJ_w R^2 d_w^2 + 4JJ_w R^2 + 2JMR^4)} & \frac{R^2(4J - Md_w^2)}{2(2J_w^2 d_w^2 + MJ_w R^2 d_w^2 + 4JJ_w R^2 + 2JMR^4)} \\ \frac{R^2(4J - Md_w^2)}{2(2J_w^2 d_w^2 + MJ_w R^2 d_w^2 + 4JJ_w R^2 + 2JMR^4)} & \frac{MR^2 d_w^2 + 4JR^2 + 4J_w d_w^2}{2(2J_w^2 d_w^2 + MJ_w R^2 d_w^2 + 4JJ_w R^2 + 2JMR^4)} \end{bmatrix} \quad (C.17)$$

As observed, it is necessary to know the inertia of the PW and its wheels (J and J_w) to complete the direct dynamic model. Using the model of a rectangular prism for the wheelchair, J is:

$$J = \frac{M(L^2 + W^2)}{12} \quad (C.18)$$

where L and W are the length and width of the PW.

Finally, the model of the cylinder can be used for the wheels. This way:

$$J_w = \frac{1}{2} M_w R^2 \quad (C.19)$$

where M_w is the mass of the wheel.

With these parameters, the direct dynamic model of the PW is complete.

C.2 Simulations

The kinematics and dynamics presented in the previous section are used to include the PW model in simulations. Specifically, the purpose of these simulations is to study the influence of the haptic handlebar in the whole system's performance. Therefore, three situations have been taken into account:

1. The assistant and the haptic handlebar's behaviors are not included in the simulation (only the PW model).
2. The assistant performance is included in the analysis but the haptic handlebar is not.
3. Both the assistant and the haptic handlebar' behaviors are included in the analysis.

The modeling of the human driver is a complex task that depends on many factors [149]. A quite simplified model has been used in this section, where the position feedback of the control loop is provided by the visual perception of the attendant. Thus, the error observed by

The measurements on the oscilloscope indicate that there is a delay of 16.6 ms between the input and the output of the haptic handlebar system. This time corresponds to the sampling rate of the device (60 Hz) and is imposed by the slowest element in the loop: the microcontroller PIC18F4680. This result is introduced in the simulation to model the handlebar's behavior.

Taking all the above into account, the three different scenarios described at the beginning of the section are simulated with the tool Simulink by Mathworks. Figure C.3 shows the simulation results of the path tracking (marked in dashed line). As can be observed, the main trajectory deviation is due to the PW model (1). If the driver is included, the deviation increases slightly (2). The result of addition of the haptic handlebar's behavior (3) is difficult to see, since its effect is practically nil. In the magnified area of Figure C.3, we can see that the trajectories of the second and the third scenarios are really near, almost overlapped.

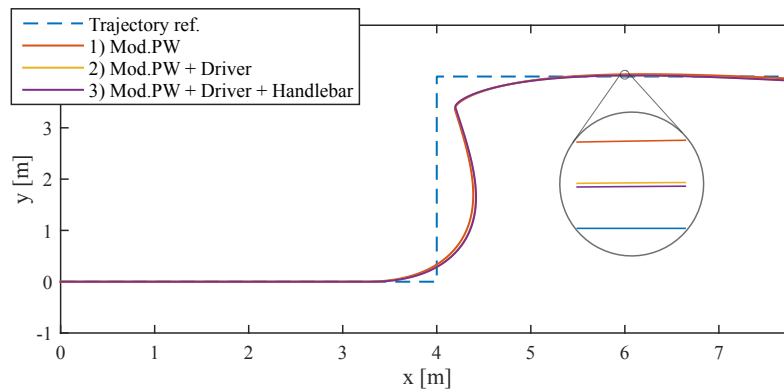


Fig. C.3 Simulation of a slalom path (dashed line) tracking considering the three following situations: 1) Only the PW model (in orange), 2) the PW and the driver model (in yellow) and 3) the PW, the driver and the haptic handlebar model (in purple).

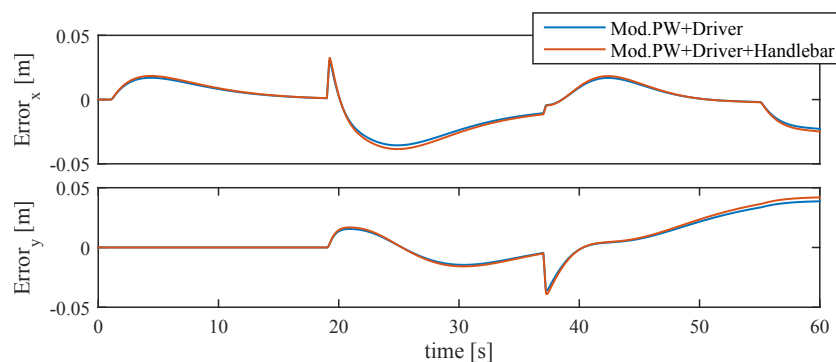


Fig. C.4 Trajectory errors when the driver model is included (in blue) and when the handlebar model is also added (in orange).

Furthermore, Figure C.4 depicts the trajectory error produced by the inclusion of the driver model and the inclusion of the driver plus the haptic handlebar model. As can be seen, errors in both situations are visually really similar. The mean error in one case and the other is $\bar{E}_{Drv_{x,y}}=(-0.0034,0.005)m$ and $\bar{E}_{Drv+HH_{x,y}}=(-0.0037,0.0054)m$. The haptic handlebar has only caused an increment of $(0.0003,0.004)m$ in the trajectory error, which is clearly negligible. This way, the simulation results show that, given the PW model, the main component of the error is produced by driver model influence and the proposed steering device hardly affects the performance of the whole system.

Appendix D

Discussion about a related proposal

The content of Chapter 2 led to the publication of the journal article in [108] (as shown in Appendix B). Authors of [151] or those of [152] cited this work in the introductory section. Furthermore, authors of [8] based their work in a quite direct way on our proposal in [108]. Although it is a preliminary study, they propose tactile sensors to estimate the user intention in a walking support robot using a bicycle-type handlebar. Due to the similarity with our work, we decided to include a discussion about what they propose, comparing it with our solution, in this appendix.

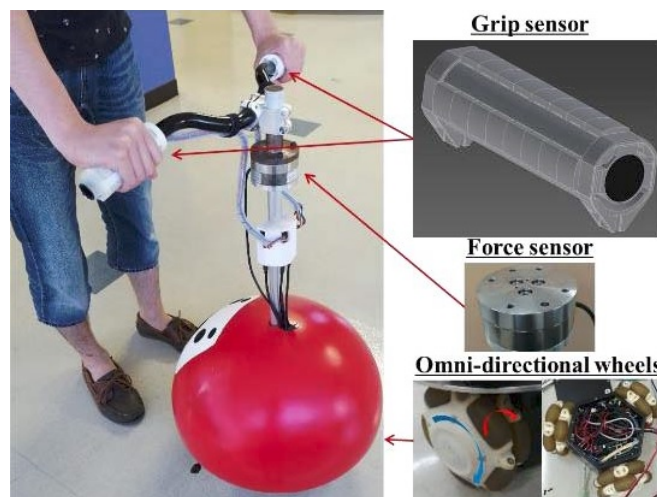


Fig. D.1 Experimental setup of the proposal in [8] (Figure extracted from the article).

The implementation of their system and the experimental setup they used is shown in Figure D.1. As with our proposal, they covered the left and right handles with FSR sensors, also from Interlink Electronics. The resulting matrices have a size of 3 rows by 8 columns. Besides, they added a force/torque sensor in the joint between the handlebar and the rest

of the structure, in the same way that it was done in the experimental setups presented in Chapter 3 of this thesis. Although the sensor model is not specified, in Figure D.1 we can see that, if it is not the same we used, it could well belong to the same family. Its purpose was also to obtain ground-truth measurements. In an experiment involving five participants they compared the signals from the tactile sensors with those extracted from the F/T sensor. The tests consisted in grasping the handlebar and turning to the right and to the left.

Their main contribution with respect to our approach in [108] lie in the way they processed the tactels information to estimate the turning intention¹. The authors use the Aggregate Output (see Section 3.1.2.2), computed for each of the handles (AO_L and AO_R)², as an estimation of the gripping force exerted with the left and right hand. Let us remember that the AO is proportional to the GF . They propose the subtraction of the previous parameters, $SUB_{AO} = AO_L - AO_R$, as a variable to control turns. The results of the experiment that they performed show a high correlation between this variable and the measurements of the F/T sensor ($r = 0.91$ for which we suppose is the best performance of the five trials).

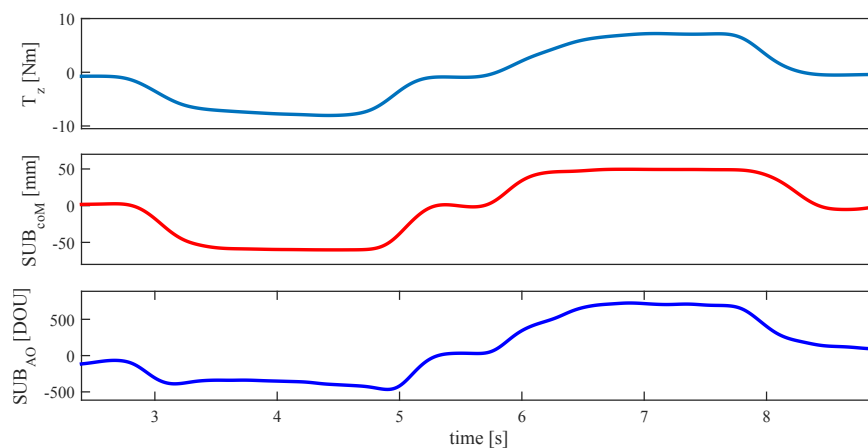


Fig. D.2 Results of the replication of the test performed in [8]: signal captured by the F/T sensor (top), parameter proposed in this thesis (center) and parameter proposed in [8] (bottom).

Since this approach is closely related to our control, we considered that it was worth to adapt it to our system and test it. The experiment was replicated using the haptic handlebar, involving also a turn to the right and another to the left. The result is shown in Figure D.2. As can be observed, both control parameters, i.e. the one proposed by the authors of [8] (graph at the bottom) and that that we use (central graph), follow closely the signal provided by the F/T sensor. The coupling is assessed with Pearson and Spearman's rank order correlation.

¹Although in the title of the work appears "user intention", that detected is only turning intention.

²In this Appendix, the nomenclature used in the paper has been changed to be in concordance with that used in this document.

For the couple formed by $\langle SUB_{AO}, T_z \rangle$, the coefficients are: $r = 0.87$ and $\rho = 0.85$. For the pair $\langle SUB_{CoM}, T_z \rangle$, they are: $r = 0.98$ and $\rho = 0.99$. Both parameters show a strong link that could be used to detect turning intentions. However, the results are better for that proposed in this thesis, SUB_{CoM} .

On the other hand, the experiment realized in [8] was quite simple and represents an ideal situation. The use of an ambulatory device such as a PW or a walking support robot involves not only turns, but also forward and backward maneuvers. There are also combinations of the latter with turns ($v \neq 0$ and $\omega \neq 0$). This scenario was reflected in experiment E1 (see Section 3.1.2), where participants followed a path of 25m that gathered an ample range of maneuvers. The data acquired in E1 could be processed to assess the degree of coupling of the parameter SUB_{AO} in a more realistic situation. This way, reminding that ten participants took part in the experiment, the correlation coefficients for $\langle SUB_{AO}, T_z \rangle$ are: $r = -0.26$ [P1], $r = -0.17$ [P2], $r = 0.26$ [P3], $r = -0.07$ [P4], $r = 0.11$ [P5], $r = -0.36$ [P6], $r = 0.27$ [P7], $r = -0.03$ [P8], $r = -0.12$ [P9] and $r = 0.12$ [P10], regarding Pearson correlation. Computing Spearman's rank order correlation, the results are: $\rho = -0.32$ [P1], $\rho = -0.17$ [P2], $\rho = 0.19$ [P3], $\rho = -0.17$ [P4], $\rho = 0.01$ [P5], $\rho = -0.33$ [P6], $\rho = 0.20$ [P7], $\rho = -0.07$ [P8], $\rho = -0.06$ [P9] and $\rho = 0.08$ [P10].

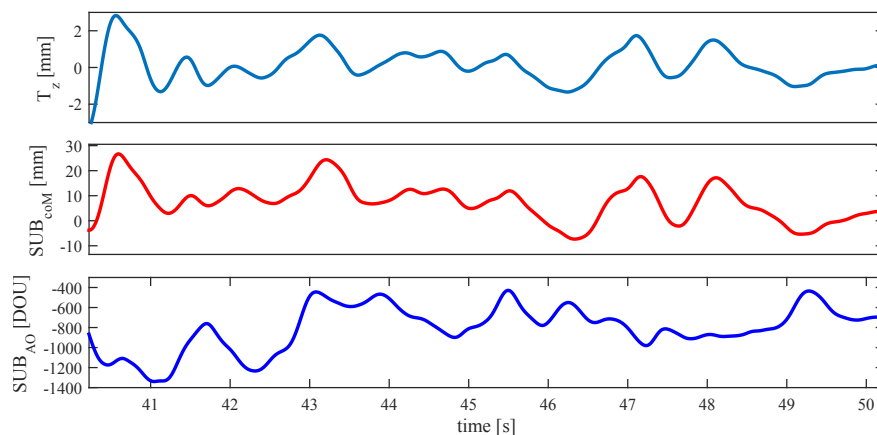


Fig. D.3 Extract from a test of E1 for an average participant: T_z (top), SUB_{CoM} (center) and SUB_{AO} (bottom).

As observed, the results are not good. Correlations are low or directly negligible. Figure D.3 illustrates an extract of a test of E1 from an average participant. As observed, whereas SUB_{CoM} (Fig. D.3 center) follows closely the variations of T_z (Fig. D.3 top), SUB_{AO} (Fig. D.3 bottom) does not change in concordance with the latter. It seems that when steering does not involve exclusively turns, SUB_{AO} is no longer a good turning intention predictor. Possibly, this parameter is also sensitive to forward and backward maneuvers, what would

make it useless as a driving control variable. Moreover, variables based on the gripping force have the drawbacks commented in previous sections and suffer from the same asymmetries as those based on the *CoM*. As said before, tactile sensors of both handles can have a slightly different response. Besides, the user could exert different gripping forces with the left and the right hand (for example, in the case of people who have suffered hand fractures in the past). This would cause that SUB_{AO} were non-zero when the user grasps the handles in rest condition. In consequence, if SUB_{AO} quantified turns, the value of the parameter in this situation should be known in order to prevent the ambulatory device from turning unintentionally. All this leads to the need of a process of stabilization of the *GF* in rest condition when the handlebar is grasped, similar to that explained in Section 3.4.1 for the *CoMs*. However, as Figure 3.46 showed, this parameter is less steady than the *CoM* and this process would take longer, so the system performance is reduced. This is another factor against the use of SUB_{AO} or a similar variable to control driving.

The discussion above and the realized test show that the proposal made by the authors of [8] seems not to be finally applicable to our system control. It seems that it would not be useful for other ambulatory devices either due to the limited range of operability.

Summary of the thesis in Spanish



UNIVERSIDAD
DE MÁLAGA

Resumen de tesis en castellano

1. Antecedentes y propuesta de la tesis

Los países desarrollados deben hacer frente al creciente envejecimiento de sus habitantes. En las próximas décadas, se estima que las pirámides de población invertirán su figura [1, 2]. En este contexto, una investigación centrada en la mejora de la calidad de vida de los mayores es más necesaria que nunca. Envejecer bien requiere salud y capacidad funcional en las actividades del día a día [3]. Las estadísticas muestran que una de cada seis personas tiene algún tipo de discapacidad en la Unión Europea. Esta cifra aumenta entre personas de la tercera edad, donde un tercio de la población mayor de 75 años cuenta con alguna discapacidad que les limita en cierta medida y más del 20% sufren limitaciones severas [4]. En Europa, el 52.9% de las personas con diversidad funcional declaran que su incapacidad les causa problemas de movilidad [5].

En este contexto, la tecnología de asistencia se ha convertido en una pieza clave en términos de mejora de calidad de vida. Este término engloba cualquier objeto, equipamiento, programa de ordenador o sistema cuyo uso aumente, mantenga o mejore las capacidades funcionales de las personas con algún tipo de discapacidad [6]. La tecnología de asistencia es especialmente útil para el colectivo de la tercera edad, ya que ayuda al desarrollo de las actividades cotidianas de forma segura, incrementando la independencia y autonomía, previniendo la comorbilidad y, por tanto, mejorando la calidad de vida y la inclusión social [7]. Cuando los usuarios pueden andar, el dispositivo de asistencia más común para el aumento de la estabilidad al caminar es el bastón. El andador es otra herramienta de asistencia para ayudar a desplazarse a personas con movilidad reducida. Sus principales características son la simplicidad, el bajo coste y el gran potencial de rehabilitación [8]. En los últimos años, la investigación ha dado lugar a varios ejemplos de estos dos comunes dispositivos de asistencia. Los autores de [9, 10, 11] trabajaron en versiones robóticas de bastones. En [12, 13, 14, 15], se presentaron andadores robóticos avanzados. Sin embargo, hay un gran número de personas cuya capacidad para andar es limitada o nula, para las cuáles este tipo de herramientas de asistencia no son suficientes. Estamos hablando de los grupos de avanzada edad, que presentan grandes ratios de deterioro físico y cognitivo. También de aquellas personas que padecen parálisis cerebral, enfermedades del sistema nervioso central, ceguera, etc.

Las sillas de ruedas son a menudo la alternativa cuando una persona tiene mermada por completo su capacidad para caminar. Aproximadamente, hay 5 millones de usuarios de sillas de ruedas en Europa [16]. Básicamente, existen dos tipos. Las sillas manuales son aquellas propulsadas por el individuo sentado en ellas a través de sus brazos. Aunque apropiadas para personas cuyas extremidades superiores no estén afectadas por ningún tipo de minusvalía, puede no ser una opción adecuada para muchos supervivientes de infartos y para personas con lesiones en la médula espinal. Tampoco son una opción apropiada para grupos de edad avanzada. En estos casos, las sillas de ruedas eléctricas son una alternativa a valorar. Su uso supone un incremento de la actividad y participación en personas de tercera edad [17]. Normalmente, son conducidas mediante un joystick ubicado en uno de los reposabrazos. Este interfaz, sin embargo, reduce el potencial de este tipo de sillas. Aproximadamente el 10% de los pacientes lo encuentran extremadamente difícil o imposible de usar en su vida cotidiana y el 40% consideran las tareas de maniobrabilidad impracticable; el 85% del personal clínico afirma haber visto pacientes que carecen de las habilidades motoras, de la fuerza y de la agudeza visual que se requiere para conducir una silla de ruedas eléctrica [18]. Los investigadores han contribuido con instrumentos destinados a ayudar con la conducción de este tipo de sillas. En [19], se propone un dispositivo de conducción para personas tetrapléjicas. El avance se controla con señales de electromiografía y los giros con el ángulo de inclinación de la cabeza del usuario. Un interfaz basado en el

movimiento corporal se presenta en [20]. Un sensor de presión colocado en el respaldo de la silla captura los cambios del centro de gravedad producidos por el movimiento del usuario y activa el movimiento de la silla en concordancia. Existen muchos más ejemplos, pues la investigación ha sido prolífica en este campo. Sin embargo, la mayor parte de ellos no llegan al usuario final por su coste de fabricación [21]. Además, hay que tener en cuenta que hay determinados pacientes que no pueden beneficiarse de este tipo de interfaces: aquellos con discapacidad severa, con problemas cognitivos como la demencia o con parálisis cerebral aguda. Los pacientes con Alzheimer o Parkinson, por ejemplo, también son excluidos. En pocas palabras, existe un grupo de personas que son usuarios potenciales de sillas de ruedas eléctricas pero que no pueden operarlas por sí mismos. En estos casos, la asistencia de otra persona es imprescindible.

Los cuidadores son personas que asisten a personas mayores o enfermas. Además de la figura profesional, a menudo es un rol llevado a cabo por familiares [22]. Las tareas de asistencia que implican el desplazamiento de personas en sillas de ruedas suelen conducir a lesiones físicas e, incluso, de carácter psicológico. Además, en gran parte de los casos son los propios cónyuges de la persona afectada, rondando una media de 70 años [23]. Teniendo en cuenta lo anterior, sería oportuno que los asistentes pudieran beneficiarse de las ventajas que las sillas de ruedas eléctricas presentan. La solución comercial más común consiste en otro joystick situado en la parte trasera de la silla y que se opera exactamente igual aquel alojado en el reposabrazos. La principal debilidad de esta propuesta es la pobre usabilidad ya descrita. Además, usados por cuidadores pueden causar oscilaciones en el movimiento al andar [24]. Algunos dispositivos orientados al asistente han sido propuestos en investigación. En [25] se propone un sistema de conducción omnidireccional para sillas de ruedas. La fuerza ejercida por el cuidador se captura mediante un sensor de fuerza colocado en el manillar. Los autores de [26] presentan una mezcla de silla de ruedas y andador basado en un control de admitancia, que podría ser útil tanto para el asistente como para la persona sentada. En [27], los autores combinan la entrada del usuario con una estimación de las perturbaciones del entorno para ofrecer un control adaptativo que permite una operabilidad mejorada. Las propuestas anteriores tienen en común el uso de un sensor de fuerza para capturar la interacción con el usuario. No son casos aislados, a menudo los dispositivos robóticos propuestos en investigación basan su interfaz en sensores de este tipo, que son precisos pero muy costosos. Esto dificulta que su llegada al mercado y su disfrute por parte de los usuarios objetivo.

En esta tesis se propone un interfaz háptico¹ para ser usado en dispositivos de asistencia para la movilidad. Como punto de partida se establecen tres objetivos:

1. Debe ser fácil de usar y no requerir mucho entrenamiento previo. Por tanto, debe ser intuitivo.
2. Debe asistir al cuidador completamente, teniendo en cuenta las maniobras típicas que se llevan a cabo durante la conducción.
3. Debe ser económico. Su coste de implementación no debe ser una barrera de cara a posibles comercializaciones.

Con lo anterior en mente, la propuesta se materializa en un **manillar táctil para sillas de ruedas eléctricas**. Un manillar es una herramienta de conducción familiar para la mayoría de las personas. Esta experiencia previa hace que su uso sea intuitivo. Está pensado para ser usado por cuidadores que deban empujar sillas de ruedas. La interacción con el usuario se lleva a cabo a través de la captura de patrones de presión por medio de sensores táctiles. Este tipo de elementos constituyen una tecnología de bajo coste. Dichos sensores están contruidos con resistencias sensibles a la fuerza (más conocidas por su nombre en inglés, *Force Sensing Resistor* o *FSR*) cuyo

¹ Término que hace referencia al sentido del tacto.

funcionamiento se basa en el principio piezorresistivo. Además posibilitan un acondicionamiento sencillo y, por tanto, también económico. También se plantea la extensión de este tipo de interfaz a otros dispositivos de asistencia. En concreto, se desarrolla un **mango táctil para un bastón instrumentado**. Este tipo de bastones equipan instrumentos de medición de forma que los distintos parámetros de su uso puedan ser capturados y usados por el personal clínico para la monitorización de terapias de rehabilitación. Se plantea el mango táctil con el fin de estudiar si las señales extraídas del sensor táctil que lo recubre se corresponden con alguno de las variables involucradas en el uso del bastón en las distintas terapias. Nuevamente, al estar basado en sensores de presión FSR, el coste de fabricación es muy bajo.

2. **Implementación del manillar háptico**

El manillar háptico se integra en el esquema de conducción como se indica en la Figura 1. La estrategia empleada ha consistido controlar el movimiento de la silla de ruedas mediante la emulación de las salidas joystick que la silla incorpora. De esta forma, la electrónica desarrollada para el manillar se conecta a la misma entrada en que el joystick va conectado en una silla de este tipo. Las flechas negras de la Figura 1 indican el flujo de funcionamiento del sistema. Cuando el usuario empuña el manillar y realiza alguna maniobra, ejerce cierto patrón de fuerza sobre los sensores táctiles que recubren el manillar. La electrónica de acondicionamiento desarrollada se encarga de leer los pertinentes mapas de presión. A través del análisis de las variaciones de presión la intención del usuario se infiere y los motores son activados generando el movimiento de la silla.

2.1. **Manillar táctil**

A diferencia de los sensores de fuerza o presión, los sensores táctiles no sólo proporcionan información acerca de la intensidad del contacto sino también acerca de la distribución de la presión en el área de los mismos. La salida de estos sensores se conoce como mapa de presiones. Otra denominación usual es la de imagen táctil, por su analogía con los sensores de imagen. Una imagen táctil está formada por la presión registrada por un grupo de elementos un determinado área, al igual que una imagen convencional se compone de una colección de registros de brillo y color asociados a un grupo de píxeles.

Un primer prototipo de manillar táctil se desarrolla usando sensores de presión FSR comerciales (FSR®402) como elementos táctiles (*tactels* o *tácteles*). Estos se organizan en forma de matriz, configuración que permite ahorrar recursos de direccionamiento. Teniendo en cuenta el tamaño de cada táctel y aquellos parámetros geométricos que optimizan la fuerza de agarre [28], se diseña un manillar con 6 x 12 elementos sensores, organizados en 6 filas y 12 columnas, con zonas activas de dimensiones de 117 x 42 mm por mango. La primera mitad de las columnas (subarray izquierdo) se destina al mango izquierdo y la segunda mitad (subarray derecho) al mango derecho. El esquemático eléctrico puede verse en la Figura 2, mientras que la implementación física en la Figura 3. Cada una de las filas de cada subarray está diseñada con una placa de circuito impreso (PCB) a la que se le han soldado los distintos sensores FSR. Estas PCB están unidas entre sí por puentes de hilo conductor y estaño.

Después de las primeras pruebas se estudia el desarrollo de un segundo prototipo. Uno de los principales motivos es la fragilidad del primer modelo. Los puentes de estaño tendían a romperse con facilidad cuando los asistentes ejercían fuerzas de agarre altas. Esto obligaba a desmontar el dispositivo y repararlo, lo que suponía una fuente de continuos retrasos.

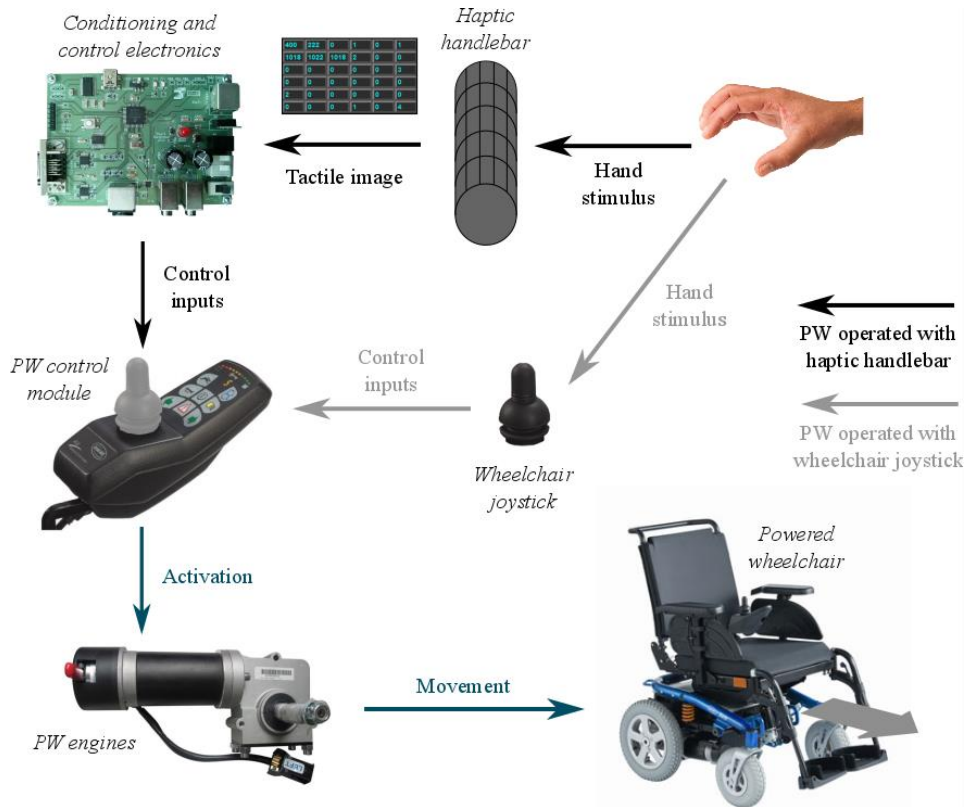


Figura 1. Esquema de funcionamiento del sistema.

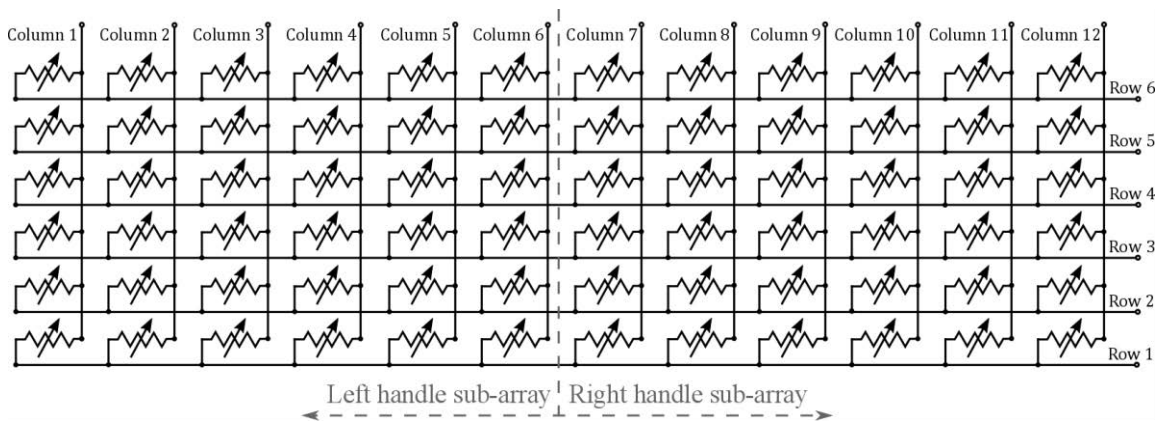


Figura 2. Esquemático del primer prototipo.

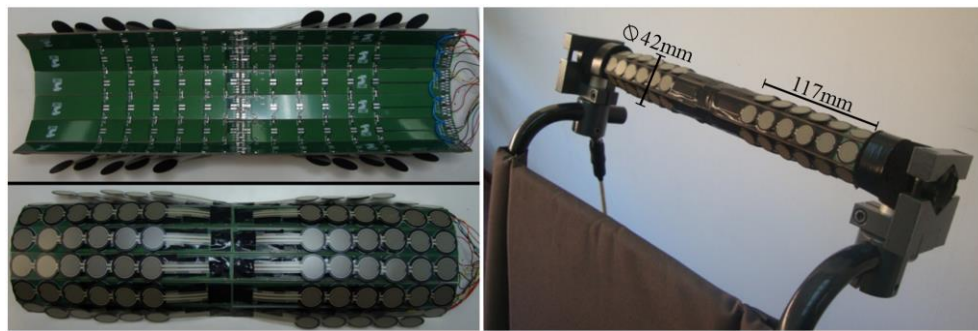


Figura 3. Matriz táctil (izquierda). Manillar táctil en silla de ruedas (derecha).

La nueva versión es más robusta. También es más económica que la primera ya que el número de tactels se reduce de 72 a 16, mediante la eliminación de los elementos del eje horizontal de la matriz (como se verá más tarde, esta medida se debe a que se observa que los patrones de presión presentan variaciones cuya relevancia reside en los desplazamientos verticales del centro de masas). La eliminación de gran parte de los elementos táctiles hace que el escaneo de la matriz también sea más rápido. Los tactels se construyen con sensores comerciales (FSR®408) adaptados a la longitud de cada uno de los mangos. Los subarrays resultantes están formados por 8 tácteles, lo que hace una matriz de 8 filas por 2 columnas. Las zonas activas son ahora de 120 x 42,5mm por mango. Tanto el esquemático del segundo prototipo como su implementación pueden verse en la Figura 4.

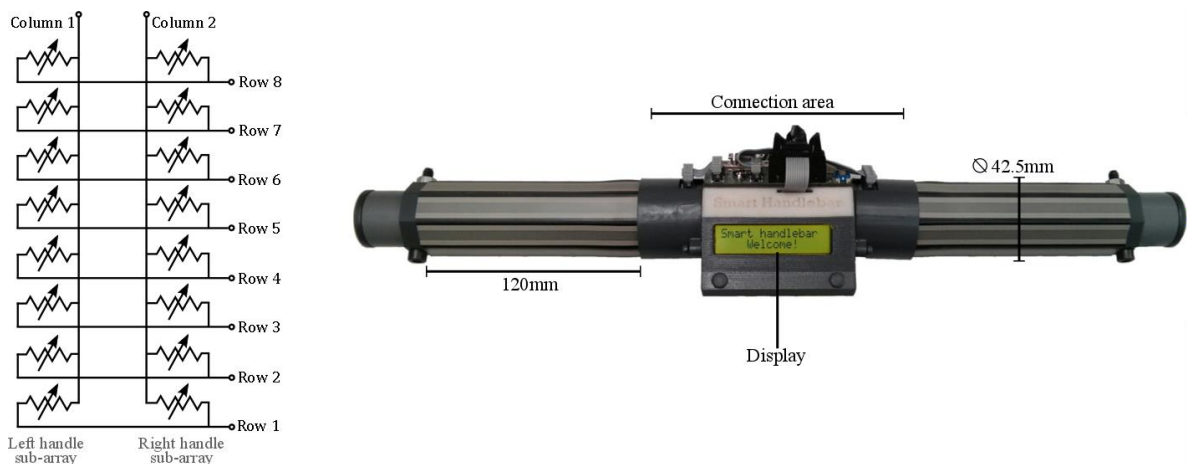


Figura 4. Esquemático de la matriz táctil del segundo prototipo (izquierda). Implementación del segundo prototipo (derecha).

2.2. Electrónica de control y acondicionamiento

La electrónica de acondicionamiento está diseñada para la adquisición de imágenes táctiles en matrices piezorresistivas. La Figura 5 ilustra el esquema de la electrónica desarrollada. Está basada en un microcontrolador PIC18F4680, que es un dispositivo versátil y de bajo coste. Las filas de la matriz están conectadas a un conjunto de llaves analógicas accionadas a través de los puertos digitales de salida del microcontrolador. Cada columna está conectada al terminal negativo de un amplificador de transimpedancia. El proceso de lectura de cada táctel es como sigue: los puertos digitales activan las llaves de forma que la fila seleccionada se pone a tierra. El resto se conecta a una tensión de referencia (V_{REF}). La entrada no inversora de los amplificadores se encuentra a esa misma tensión de referencia por lo que, debido al cortocircuito virtual, los tactels de las filas no seleccionadas tienen la misma tensión en ambos terminales. Esto cancela cualquier camino resistivo parásito que pudiera existir entre estos elementos y los de la fila de interés y, por tanto, cancela cualquier interferencia inter-táctel que pudiera darse.

Las salidas de los amplificadores están conectadas a los canales analógicos de entrada del microcontrolador para su conversión a información digital. Cuando toda la matriz táctil se ha escaneado y el mapa está digitalizado en la memoria del PIC18F4680, un algoritmo lo analiza y extrae la intención del usuario. De acuerdo con ésta, se generan las señales adecuadas para activar los motores de la silla a través de la interfaz del joystick, pasando previamente por un convertor digital a analógico. Además, la información puede enviarse vía USB a un ordenador para su

estudio posterior. La electrónica se alimenta a través de las baterías de la silla de ruedas, mediante una etapa de conversión de voltaje.

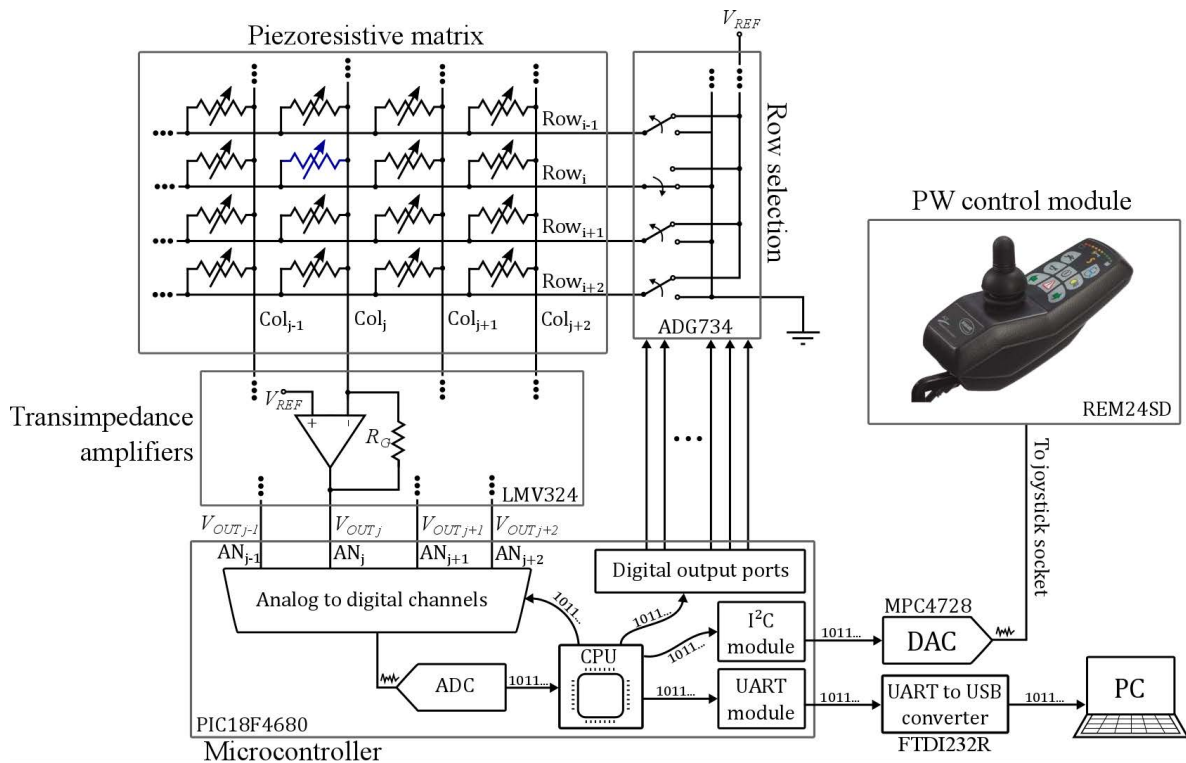


Figura 5. Esquemático de la electrónica de control y acondicionamiento.

2.3. Análisis preliminar

Los mapas de presión pueden procesarse de diversas formas. Una habitual en tareas de manipulación robótica es el cálculo del centro de masas (CoM), también conocido como centro de presión. El centro de masas concentra la lectura de todos los tactels de la matriz en una única coordenada espacial que proporciona información acerca de que cómo es la distribución de presión. De esta forma, las variaciones de presión en imágenes táctiles consecutivas pueden estudiarse a través de la evolución del centro de masas calculado para cada una de ellas. La Figura 6 muestra cuáles son los desplazamientos del centro de masas en los sensores táctiles del mango izquierdo y derecho cuando se realizaban las maniobras asociadas a la conducción de la silla de ruedas con el manillar. En la prueba mostrada se usó el primer prototipo.

Como se observa, los patrones de movimiento del centro de masas se producen en el eje vertical, característica que fue aprovechada para eliminar la resolución horizontal en el segundo prototipo, como ya se adelantó.

Un algoritmo de control de prueba se desarrolla en base a los patrones anteriores. El sentido de la variación de los centros de masas (CoMs) determina el tipo de maniobra que pretende hacer el asistente. La distancia que recorren respecto a su coordenada en *situación de reposo* se usa para estimar la intensidad de la maniobra. La situación de reposo se define como aquella en que el manillar se encuentra empuñado por el usuario, pero este no ejerce ninguna fuerza con el objetivo de conducir la silla. De esta forma, el funcionamiento es el siguiente, de acuerdo a la maniobra realizada:

- 1) Torsión a izquierda: la velocidad angular es tal que la silla produce un giro a la izquierda.
- 2) Torsión a derecha: la velocidad angular es tal que la silla produce un giro a la derecha.
- 3) Empuje hacia adelante: la velocidad lineal se incrementa.
- 4) Empuje hacia atrás: la velocidad lineal se reduce.

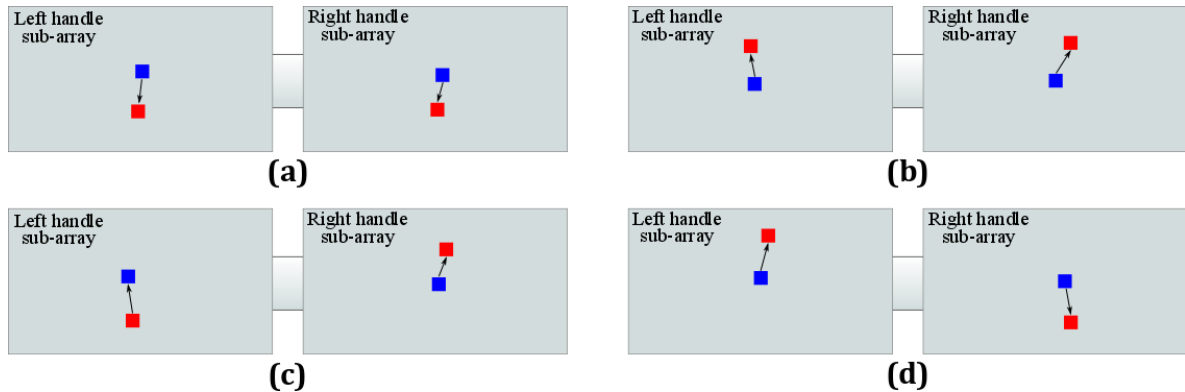


Figura 6. Desplazamiento del centro de masas desde una posición de reposo ante maniobras de: empuje hacia delante (a), empuje hacia atrás (b), giro a la derecha (c) y giro a la izquierda (d).

Como se puede observar. Empujar hacia delante o hacia detrás produce aceleraciones o deceleraciones. Por tanto, una vez alcanzada la velocidad de avance (o retroceso) que resulte adecuada para el usuario, éste no tiene que hacer más que mantener el manillar empuñado para mantenerla. Si quiere detener la silla, la empujaría hacia sí mismo haciendo que la velocidad lineal se fuera reduciendo hasta que la silla se parase. Si fuese marcha atrás, haría lo contrario. Empujaría hacia delante aumentando la velocidad lineal, que sería negativa, hasta que ésta fuera cero.

Seis voluntarios condujeron la silla usando el manillar en un circuito que incluía todas las maniobras en distinto grado. Tras la experiencia, las ideas principales extraídas son:

- Cuando se agarra el manillar se computan los CoMs de referencia, es decir, aquellos en situación de reposo. A veces el sistema no identificaba bien la intención de los usuarios, probablemente debido a un mal cómputo de estos parámetros. Esto obligaba a que tuvieran que soltar y agarrar de nuevo al manillar.
- Si el agarre era muy débil el sistema interpretaba que los mangos se habían soltado y la silla se detenía. El proceso de reiniciación de la marcha requería el nuevo cómputo de los CoMs de referencia, que tardaba varios segundos y desembocaba en una situación confusa para los usuarios.
- Si el agarre era muy fuerte, el sistema dejaba de responder adecuadamente, posiblemente debido a algún tipo de saturación.
- El hecho de que no hiciera falta mantener un empuje constante para que la silla avanzara a velocidad uniforme fue percibido como extraño y poco intuitivo, dando la sensación a veces a los usuarios de que tenían poco control sobre la conducción.

Las debilidades reportadas se usan como base para desarrollar un nuevo control del sistema. Principalmente, se requiere un estudio más profundo del **proceso de agarre** para desarrollar un método del cómputo de los centros de masa de referencia más efectivo. También se debe estudiar el efecto de la **fuerza de agarre** sobre el sistema, ya que se ha visto que cuando es excesiva limita e incluso imposibilita su uso. Además, se debe proponer otro tipo de manejo que resulte **más intuitivo**, ya que ésta era una de las principales metas definidas en esta tesis.

3. Control háptico de la conducción

Tomando como premisas las conclusiones del análisis preliminar se procede a un estudio más profundo de las características y procesos que intervienen en el uso del manillar táctil. Como resultado, se proponen unas variables de control.

3.1. Análisis del control del háptico del movimiento basado en la fuerza y el torque

Con la intención de explorar las interacciones de fuerza y torque entre el usuario y el manillar se añade un sensor de fuerza al conjunto. Se intercala entre la silla y el centro del manillar como se ve en la Figura 7. Además se usa un ordenador para capturar la información tanto de los sensores táctiles de ambos mangos como del sensor de fuerza y torque.

La interacción durante los giros se modela con el torque en el eje perpendicular a la dirección del movimiento y que pasa por el centro del manillar, T_z (ver Figura 8). Las maniobras de empuje hacia delante y hacia detrás son registradas por la fuerza en el sentido del movimiento, F_y .

En esta etapa de estudio, las señales F_y y T_z capturadas por el sensor de fuerza son usadas para la activación de los motores de la silla, que se conduce como se haría usando un manillar convencional. De esta forma, las velocidades lineal y angular serán proporcionales a una y otra señal, respectivamente. Hay que resaltar que este sensor será usado sólo para propósitos de investigación y de ninguna manera formará parte de la propuesta final, como puede esperarse de acuerdo al planteamiento inicial de esta tesis.

Se plantea el uso del manillar por parte de un grupo de voluntarios con el fin de encontrar parámetros extraídos del manillar táctil que sean equivalentes a las señales de fuerza y torque que controlan el movimiento de la silla. Después de seguir un circuito de 25m que incluía las maniobras típicas de conducción se llega a que dos variables basadas en los CoMs de cada uno de los mangos tienen gran similitud con las señales capturadas por el sensor de fuerza. Para la mayor parte de los participantes se encuentra una correlación alta o muy alta entre:

- 1) La suma de los centros de masas de los sensores táctiles de ambos mangos (SUM_{CoM}) y la señal F_y .
- 2) La resta de los centros de masas de los sensores táctiles de ambos mangos (SUB_{CoM}) y la señal T_z .

De esta forma, se proponen estos dos parámetros como variables de control para el cómputo del movimiento de la silla.



Figura 7. Montaje experimental. Se ha añadido un ordenador y un sensor de fuerza al conjunto para la extracción de datos experimentales.

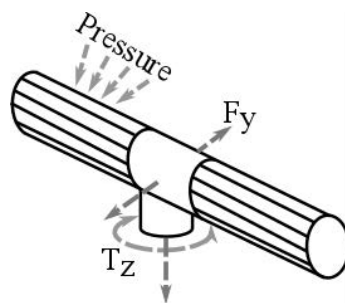


Figura 8. Fuerza y torque que intervienen durante la conducción de la silla de ruedas usando el manillar táctil.

3.2. Estudio del efecto de la fuerza de agarre

3.2.1. Efecto de la fuerza de agarre sobre el rendimiento de las variables de control propuestas

Como primera evaluación del efecto de la fuerza de agarre (GF), se comprueba cuál es la influencia que ésta ejerce sobre los parámetros de control propuestos en el punto anterior. Para

ello se estima cual es la fuerza media que ejerció durante la conducción cada uno de los voluntarios del experimento visto en el punto 3.1. La Figura 9 ilustra la relación entre este factor y las variables. Como se puede ver, conforme la fuerza de agarre aumenta la correlación calculada para cada usuario en la realización del experimento se hace menor. Es decir, conforme mayor es la fuerza de agarre peor es la correspondencia entre SUM_{CoM} y F_Y , y entre SUB_{CoM} y T_Z y, por lo tanto, peor rendimiento tienen las variables propuestas para identificar las intenciones de avance/retroceso y giro por parte del asistente. La tendencia es clara y, de hecho, la evaluación de este fenómeno mediante las correlaciones de Pearson (r) y Spearman (ρ) apunta en este sentido.

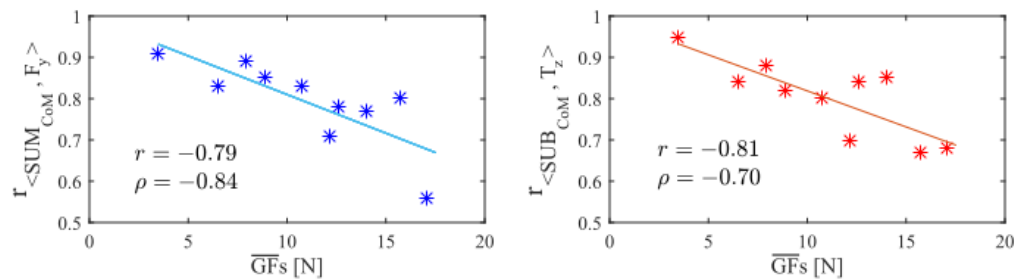


Figura 9. Efecto de la fuerza de agarre (GF) en la correlación entre las variables de control propuestas y la fuerza y torque ejercida por el usuario durante la conducción.

3.2.2. Efecto de la fuerza de agarre en la excursión de los centros de masas

Otro punto a analizar consiste en la saturación o falta de respuesta del sistema cuando se ejercen fuerzas de agarre altas, hecho que se reportó en el análisis preliminar del dispositivo. Para dicho estudio, se desmonta el manillar de la silla de ruedas y se fija a una mesa de laboratorio. Se pide a un grupo de voluntarios que empuñe el manillar y realice maniobras de empuje hacia delante y hacia detrás y giros a izquierda y derecha. Se les pide que repitan la secuencia tres veces, agarrando el manillar de forma *suave*, *normal* y *fuerte*. Analizando como varían los centros de masas conforme la fuerza de agarre aumenta se observa claramente que conforme mayor es ésta, menor es la excursión de los primeros, disminuyendo del agarre *suave* al *normal*, y del *normal* al *fuerte*. Es decir, la distancia máxima que se desplazan los centros de masas se ve afectada de forma inversamente proporcional al nivel de la fuerza de agarre de los mangos. Esto repercute en un peor rango dinámico de los parámetros de control y, por tanto, en el empeoramiento de la experiencia de conducción.

Se observa, además, que la saturación de los tácteles no es la única causa del fenómeno. Hay casos en que éste también tiene lugar sin que ningún elemento de la matriz táctil esté saturado. Se comprueba que la capacidad, a nivel anatómico, de la mano para introducir variaciones de presión disminuye conforme la fuerza de agarre aumenta.

Para compensar este efecto, se diseñan dos funciones de ganancia variable. Estas multiplican a los parámetros de control modificando su pendiente para que el sistema responda de una forma lo más uniforme posible independientemente de la fuerza con que el usuario empuñe el manillar. $\sigma_{SUM_{CoM}}$ modifica la pendiente de SUM_{CoM} y $\sigma_{SUB_{CoM}}$ la pendiente de SUB_{CoM} (ver Figura 10). Ambas funciones se diseñan teniendo en cuenta los datos experimentales que se capturaron durante la realización del experimento anterior.

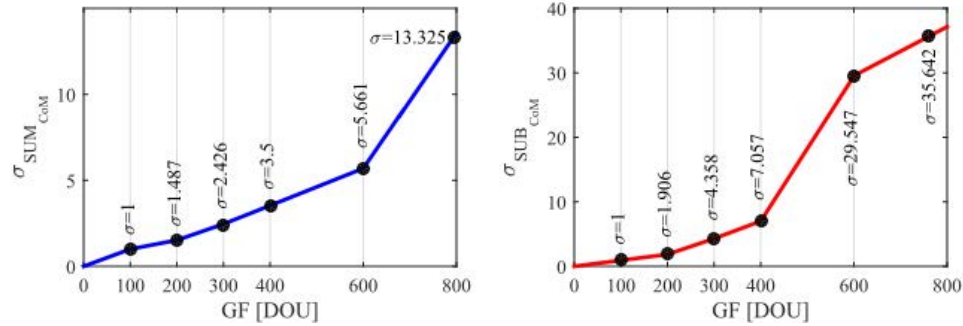


Figura 10. Funciones de ganancia variable para compensar la reducción de la excursión de los centros de masas conforme aumenta la fuerza de agarre (el eje-x muestra la fuerza de garre en unidades de salida digital de los sensores táctiles).

3.3. Estudio del efecto de la configuración de la matriz táctil

Como se dijo con anterioridad, el CoM es un parámetro que tiene forma de coordenada espacial dentro de la matriz táctil. Por tanto, su valor para un mismo mapa de presión o imagen táctil depende de que coordenada asignemos a cada tactel de dicha matriz. La Figura 11 puede ayudar a visualizar este hecho. En ella, se muestra el perfil del manillar y la posición física de cada uno los tactels, marcada desde 1st a 8th. La variable espacial 'y' asignada a cada tactel varía también, como no puede ser de otra forma, entre 1 y 8. En función de en qué tactel se comience a numerar con y=1 se dispondrá de una configuración u otra, dando lugar a 8 posibles combinaciones (A-H).

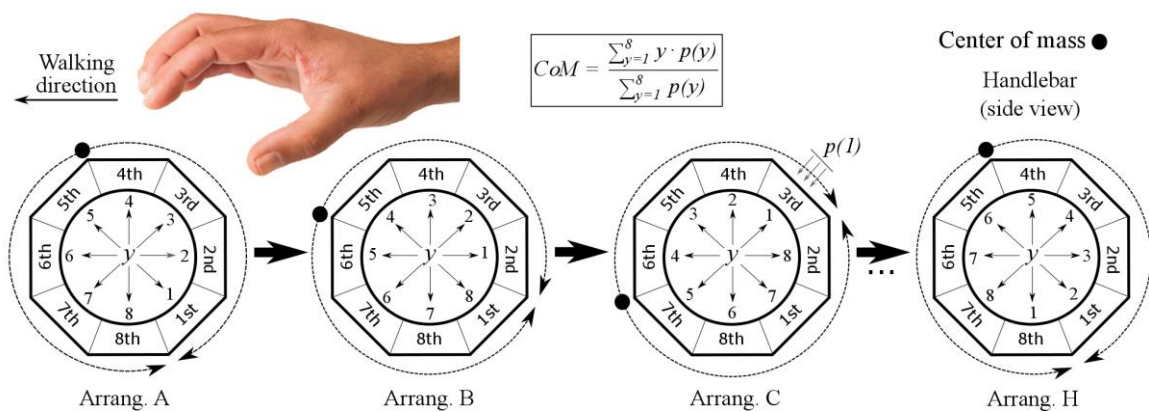


Figura 11. Distintas configuraciones de la matriz táctil, en función de la coordenada (y) asignada a cada tactel (1st-8th).

Para estudiar el efecto de la organización de los tactels dentro de la matriz, un grupo de voluntarios repite la secuencia de maniobras descrita en el experimento del punto anterior. Esta vez con el manillar fijado a la silla y con los frenos de la misma activados (las maniobras no producen movimiento). Además, las maniobras sólo se llevan a cabo una vez, con la fuerza de agarre que ellos consideran *cómoda* o *natural*. Se calcula la excursión del centro de masas durante los distintos ejercicios programados sobre el manillar y se llega a que existe una configuración de los tácteles en que la excursión del CoM es máxima para la mayoría de los usuarios. Ésta es aquella en que el tactel con coordenada y=1 es el marcado en la Figura 11 como tactel 5th. Además, se comprueba que el rendimiento de los parámetros de control, SUM_{CoM} y SUB_{CoM}, se mantiene.

La correlación entre ellos y las variables de fuerza y torque que modelan la interacción con el usuario no sólo no empeora sino que mejora en la mayor parte de los casos. No obstante, se advierte en que en algunos particulares, la correlación anterior disminuye. Como para la mayoría de usuarios existe una mejora, se selecciona esa configuración como organización de los tactels por defecto.

3.4. Estudio del proceso de agarre del manillar táctil

En este punto se procede al estudio del proceso de agarre del manillar, que cómo se observó en el análisis preliminar del apartado 2.3, resulta de especial interés para la mejora de la experiencia de conducción.

3.4.1. Estudio de la estabilización del agarre

El primer fenómeno a analizar es el de la estabilización del agarre una vez se empuña el manillar. Para ello, un grupo de voluntarios realizan un experimento consistente en agarrar el manillar y mantener esta situación durante unos segundos y soltarlo al recibir una señal. Durante el proceso no deben ejercer ninguna fuerza adicional, sólo aquella que de forma natural se imprime al tener agarrados los mangos. Una vez pasados 3 segundos, se puede considerar que el agarre se ha estabilizado. Se calcula cuál es la máxima variación del centro de masas ($\Delta_{CoM_{t>3}}$) en esa situación para cada uno de los usuarios. Tras evaluar diferentes valores, se establece el rango definido por $\overline{\Delta_{CoM_{t>3}}} + 2s_{CoM_{t>3}}$ (valor medio + 2 desviaciones típicas) como aquel rango de variación en que el centro de masas se puede considerar estabilizado. Se calcula estadísticamente que, una vez se empuña el manillar, el CoM tarda aproximadamente 0.7 segundos en estar confinado en este intervalo. De esta forma, una vez se detecta el agarre del manillar, se introduce un tiempo de espera de 0.7 segundos antes de capturar los centros de masa de referencia en situación de reposo. Recordemos que estos parámetros son necesarios para, posteriormente durante la conducción, poder computar cuánto se ha desplazado el centro de masas y poder inferir la intención del usuario.

3.4.2. Influencia de la altura en los parámetros de referencia

Con los datos extraídos durante el experimento anterior, se estudia si el valor de los parámetros de referencia está influenciado por la altura del usuario. Se llega a que existe cierta relación, aunque otros factores como el ángulo entre el antebrazo y la mano a través de la muñeca al agarrar el manillar también afectan a estos valores.

También se analiza si la fuerza de agarre está relacionada con la altura del usuario, que es un parámetro que está relacionado con el tamaño de las manos. La muestra estadística de que se dispone muestra que no existe relación entre la fuerza del agarre de los mangos y la altura de la persona.

3.4.3. Evolución del centro de masas al comienzo del agarre del manillar

En este apartado, los mismos datos son usados para analizar la evolución del centro de masas desde el preciso momento en que se detecta el contacto con el manillar y los centros de masas llegan a estabilizarse ($t < 0.7s$).

Se descubre que para la mayoría de los usuarios existe un patrón en la variación del centro de masas, que es el que se muestra en la Figura 12. El valor de este parámetro va tomando una serie de valores que están relacionados con qué parte de la mano del usuario hace contacto en cada

momento. Además, cuando se sueltan los mangos táctiles al final de la conducción, el patrón es simétrico al que se presenta en dicha figura. La identificación de este patrón puede servir para distinguir, por ejemplo, si la presión detectada en el manillar se debe al agarre del manillar para la conducción o al contacto con un objeto (o con el usuario pero sin intención de conducir, por ejemplo, apoyándose sobre el manillar para descansar).

3.5. Sistema de aviso basado en vibración

Como se ha visto en apartados anteriores, las fuerzas de agarre excesivas no son adecuadas desde el punto de vista del rendimiento del sistema. Sin embargo, tampoco lo son desde el prisma del usuario. Mantener una fuerza de agarre elevada conduce a la fatiga y el sobreesfuerzo, además de no tener sentido en un dispositivo cuya finalidad es que el asistente pueda conducir sin tener que realizar ningún esfuerzo.

Para evitar esta situación, se incorpora al manillar táctil un sistema de aviso por vibración. Cuando el cuidador aprieta los mangos por encima de un determinado umbral, el manillar comienza a vibrar para advertirle de que está ejerciendo una fuerza desaconsejablemente alta. El sistema se ha implementado con dos motores de corriente continua, uno por mango, con una pesa desbalanceada en su eje de rotación.

Finalmente, tras todo lo expuesto, se procede a la evaluación del manillar en un experimento controlado.

4. Evaluación del manillar háptico

Tomando en consideración los puntos expuestos en el apartado anterior y haciendo uso de las variables de control propuestas se procede a la evaluación del sistema. Para ello, además, se compara con el dispositivo más común para la asistencia de cuidadores que conducen sillas de ruedas eléctricas: el joystick de asistente.

Para la evaluación se realizan dos experimentos distintos:

4.1. Evaluación del rendimiento en la conducción

El primero está orientado a la obtención de datos objetivos de la conducción de la silla usando ambos dispositivos. Para ello un grupo de voluntarios conduce la misma siguiendo un circuito, primero con uno de los interfaces y luego con el otro. Dicho circuito combina maniobras suaves con giros especialmente cerrados. Además, también realizan una serie de maniobras dentro de un espacio de cerrado con obstáculos (un laboratorio de investigación).

Para el primero de los escenarios, se computa el error entre la trayectoria objetivo y aquella seguida por los usuarios. El rendimiento del manillar se muestra superior al del joystick en general para todos los voluntarios involucrados. Además, cuando realizan las maniobras en el espacio cerrado, ninguno de ellos produce colisión alguna con el entorno cuando usa el manillar mientras que el número de colisiones cuando manejan la silla con el joystick llega hasta 5 en alguno de los casos (sólo el 20% de los usuarios no produce colisiones con este dispositivo).

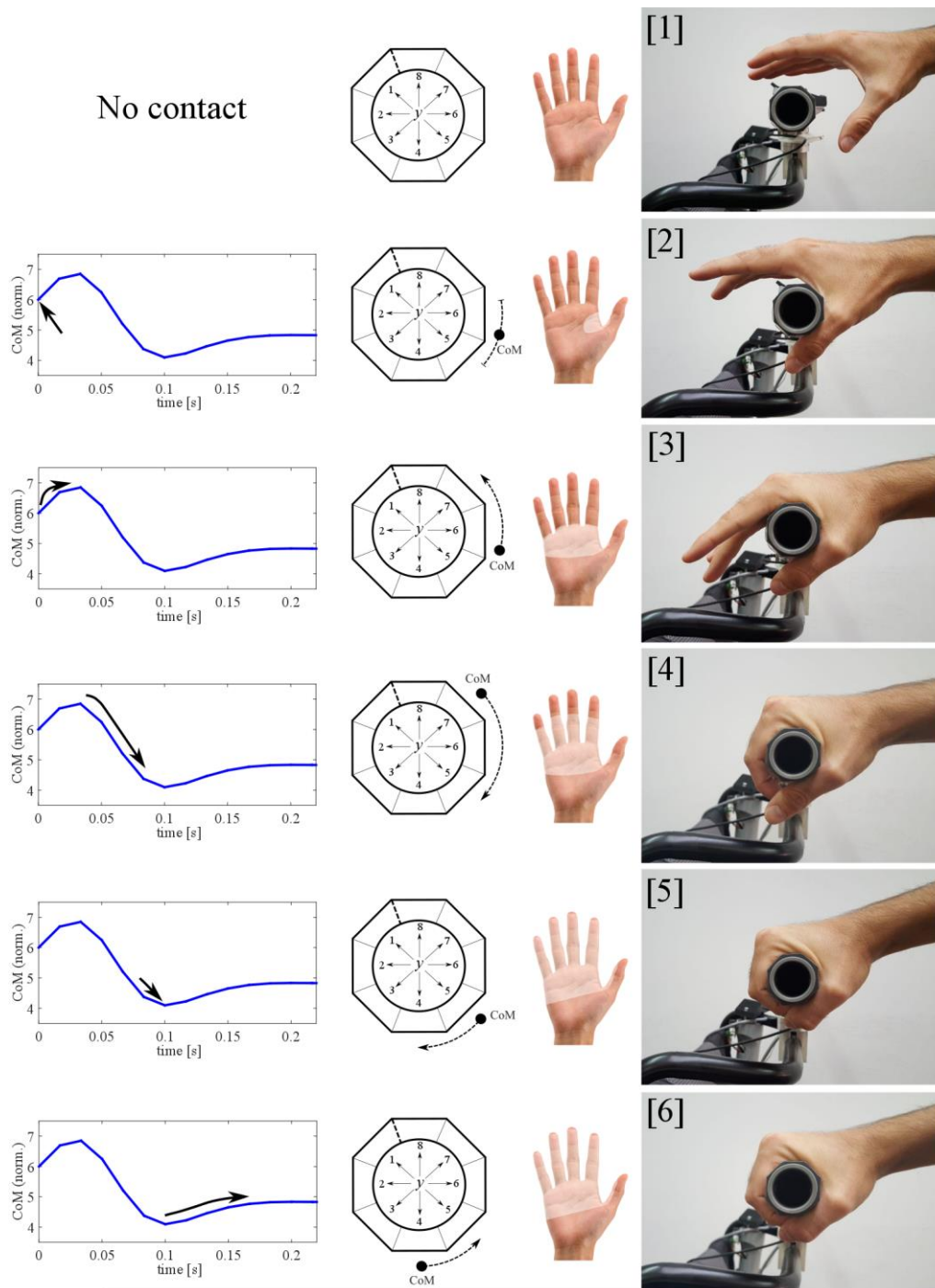


Figura 12. Evolución de los centros de masas de los sensores táctiles cuando el manillar se empuña.

4.2. Obtención de la percepción de los participantes

El segundo experimento está destinado a la valoración de la percepción subjetiva de los voluntarios durante la experiencia de conducción. También interesa conocer su opinión sobre ambos dispositivos. Para ello se les pide que rellenen un cuestionario en que se les presenta una escala de Likert donde deben escoger una de las 7 respuestas dadas a cada una de las preguntas.

Los aspectos a evaluar son: facilidad de uso, comodidad, entrenamiento previo necesario, utilidad, seguridad durante el uso y fatiga física/mental.

Las respuestas para el manillar háptico son positivas en todos los aspectos valorados, superando en cada uno de ellos al joystick de asistente. Éste tiene una imagen negativa especialmente en facilidad de uso y en entrenamiento previo necesario. Además, algunos comentarios dejados por los usuarios acerca del manillar son: "*Con un poco de práctica, es fácil controlar el movimiento*", "*Es fácil adaptarse al dispositivo*", "*Este dispositivo tiene amplias posibilidades*", etc. Sobre el joystick: "*Los movimientos laterales son abruptos y a veces se produce zigzag*", "*Requiere mucha más práctica que el manillar*", "*La postura de la mano no es muy natural*", etc.

4.3. Margen de mejora y posibles líneas de actuación

Los resultados obtenidos para el manillar son en general buenos o muy buenos. No obstante, algunos puntos a mejorar aparecieron durante el experimento:

- Para dos usuarios existía cierta asimetría en la velocidad lineal cuando empujaban hacia adelante y hacia atrás. El esfuerzo requerido para mover la silla en ambas direcciones era distinto. Además, esto no pudo corregirse cambiando la configuración de los tactels (punto 3.3). Un aumento de la resolución espacial podría dar lugar a configuraciones más precisas que permitieran un mejor ajuste de la organización de los tactels.
- Otro usuario reportó haber encontrado algo artificial el hecho de tener que esperar un poco antes de conducir mientras los CoMs de referencia se computan. Este procesamiento podría acelerarse mediante la inclusión de perfiles de usuario. Así, se podría llevar un histórico de los centros de masas en reposo para cada asistente y se podría estudiar el uso de valores por defecto para cada cuidador.
- En algunas ocasiones, aparecieron pequeños tirones durante la conducción (sobre todo al principio del ejercicio), que parecían estar modulados de cierta forma por la marcha del cuidador. Podría evaluarse la extracción de características de dicha marcha a partir de la salida de los sensores táctiles para la implementación de un método de compensación. Además, al realizar maniobras precisas en el espacio cerrado, a veces también la silla se movía de forma discontinua llevando a cabo pequeños tirones. Posiblemente, la ganancia fuera muy alta para este tipo de maniobras a baja velocidad. Por esto, se podría estudiar la incorporación de algún tipo de control adaptativo que variara la respuesta del sistema con la velocidad. Uno muy interesante es el propuesto por los autores de [29].

5. Extensión de interfaz táctil a otros dispositivos de asistencia para la movilidad

Como se adelantó en el primer apartado de este documento, la propuesta de interfaz háptico basado en sensores táctiles se extiende a un bastón instrumentado. Este tipo de bastones equipan una serie de sensores para la adquisición de datos de uso que, posteriormente, pueden ser usados por el personal clínico para mejorar terapias de rehabilitación de pacientes que han sufrido un ictus, etc.

Concretamente, se desarrolla un mango táctil para ser usado en un bastón de este tipo. La idea es estudiar qué parámetros de uso podría extraerse de los sensores del mango. El mango equipa 18 tactels formando una matriz de 4 x 5 elementos. No obstante, la cara inferior tiene solo 3 ya

que parte de ella se dedica la incrustación del mango en el bastón. En la Figura 13 puede verse la implementación del mango y su esquemático. La electrónica de acondicionamiento es muy similar a la que se diseñó para el caso del manillar táctil, con la adaptación pertinente para una matriz de diferente tamaño. Además se han incorporado bloques para la posible comunicación con placas de Arduino.

Se realiza un experimento en que un grupo de voluntarios utiliza el bastón para andar durante 5.5 metros. Llevan una suela modificada cuyo propósito es el de simular cojera, ya que los participantes no tenían problemas de movilidad. Al bastón instrumentado se le añade una unidad de medición inercial (IMU) que proporciona el **ángulo del bastón** con respecto a la vertical con el suelo. También un sensor de fuerza que captura la **fuerza** que ejerce el usuario cuando se apoya en el bastón.

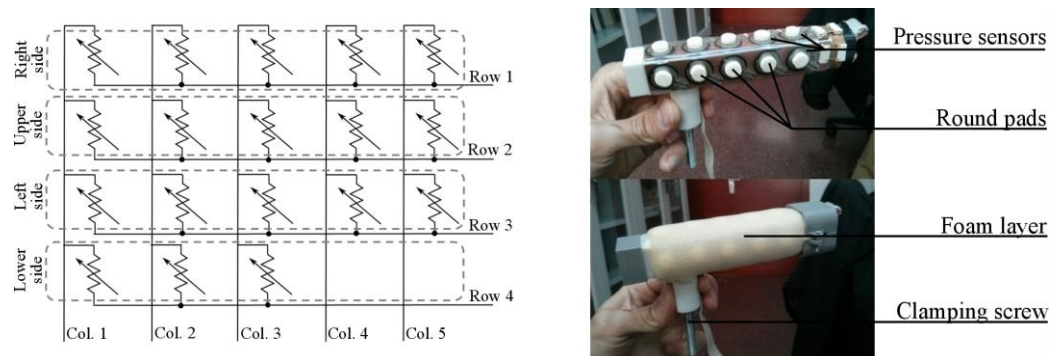


Figura 13. Esquemático (izquierda) e implementación del mango táctil para bastón (derecha).

Tras analizar los resultados, se encuentra que el **centro de masas calculado para la fila de sensores de la cara superior** del mango (CoM_U) mantiene una alta correlación con el ángulo capturado por el IMU. De la misma forma, el cómputo de la correlación entre la **suma del valor de los tactels de esta misma cara** (P_U) y la fuerza de apoyo en el bastón extraída por el sensor proporciona coeficientes cercanos a la unidad.

Lo anterior indica que estos dos parámetros pueden ser capturados en base al uso exclusivo del mango táctil, cuya implementación supone un coste muy bajo. Además se ha visto, que sólo una fila de tácteles (la superior) es necesaria para capturar este par de parámetros de uso. Esto hace que futuros prototipos puedan ser aún más baratos.

6. Conclusiones

En esta tesis se ha desarrollado un interfaz háptico basado en sensores táctiles para ser usado por cuidadores al conducir sillas de ruedas eléctricas. A pesar de los líneas de trabajo planteadas en el apartado 4.3 de este documento, la propuesta ha mostrado ser viable y cumplir con los tres objetivos de base que se plantearon: manejo sencillo, asistencia completa a la conducción y coste de implementación bajo.

Además, la tecnología se ha extendido con éxito a otros dispositivos de asistencia como son los bastones instrumentados. Se ha diseñado un mango táctil que puede proporcionar dos parámetros básicos de uso para la monitorización en terapias de rehabilitación por parte del personal sanitario.

7. **Referencias**

- [1] M. D. Wulf, "Predicted population pyramid for Western Europe in 2030," 2017, URL: <http://www.populationpyramid.net/western-europe/2030/> [accessed: February, 2017]
- [2] "World Population Prospects: The 2015 Revision," United Nations. Department of Economic and Social Affairs, Population Division, 2015, URL: https://esa.un.org/unpd/wpp/publications/files/key_findings_wpp_2015.pdf [accessed: April, 2017]
- [3] B. A. Hawkins, "Aging well: Toward a way of life for all people," Preventing Chronic Disease, vol. 2, no. 3, p. A03, July 2005.
- [4] "European Disability Strategy 2010-2020: A Renewed Commitment to a Barrier-Free Europe," COMMUNICATION FROM THE COMMISSION TO THE EUROPEAN PARLIAMENT, THE COUNCIL, THE EUROPEAN ECONOMIC AND SOCIAL COMMITTEE AND THE COMMITTEE OF THE REGIONS, 2010, URL: <http://eur-lex.europa.eu/LexUriServ/LexUriServ.do?uri=COM:2010:0636:FIN:en:PDF> [accessed: April, 2017].
- [5] Disability statistics - barriers to social integration," EUROSTAT: Statistic explained, 2015, URL: http://ec.europa.eu/eurostat/statistics-explained/index.php/Disability_statistics_-_barriers_to_social_integration [accessed: April, 2017].
- [6] "Assistive Technology Industry Association," 2017, URL: <https://www.atia.org/at-resources/what-is-at/> [accessed: March, 2017].
- [7] E. de Sousa Leite, T. P. Rodrigues, M. do Carmo Andrade Duarte de Farias, M. A. S. P. Moreira, G. K. G. D. Bittencourt, F. B. de Oliveira, C. A. Simpson, and A. O. Silva, "Influence of assistive technology for the maintenance of the functionality of elderly people: an integrative review," International Archives of Medicine, vol. 9, 2016. [Online]. Available: <http://imed.pub/ojs/index.php/iam/article/view/1501>
- [8] C. A. Cifuentes and A. Frizera, Assistive Devices for Human Mobility and Gait Rehabilitation. Cham: Springer International Publishing, 2016, pp. 1–15. [Online]. Available: http://dx.doi.org/10.1007/978-3-319-34063-0_1
- [9] R. Ady, W. Bachtta, and P. Bidaud, "Development and control of a one-wheel telescopic active cane," in 5th IEEE RAS/EMBS International Conference on Biomedical Robotics and Biomechatronics, Aug 2014, pp. 461–466.
- [10] I. Shim and J. Yoon, "A robotic cane based on interactive technology," in IECON 02 [Industrial Electronics Society, IEEE 2002 28th Annual Conference of the], vol. 3, November 2002, pp. 2249–2254 vol.3.
- [11] S. H. Pyo, M. G. Oh, and J. W. Yoon, "Development of an active haptic cane for gait rehabilitation," in 2015 IEEE International Conference on Robotics and Automation (ICRA), May 2015, pp. 4464–4469.
- [12] V. Pasqui, L. Saint-Bauzel, C. Zonga et al., "Projet MIRAS: Multimodal interactive robot for assistance in strolling," Technologies pour la sante et l'autonomie, vol. 33, no. 2, p. 165–172, April 2012.
- [13] J. Shin, D. Itten, A. Rusakov, and B. Meyer, "Smartwalker: Towards an intelligent robotic walker for the elderly," in Intelligent Environments (IE), 2015 International Conference on, July 2015, pp. 9–16.
- [14] A. Morris, R. Donamukkala, A. Kapuria, A. Steinfeld, J. T. Matthews, J. Dunbar-Jacob, and S. Thrun, "A robotic walker that provides guidance," in Robotics and Automation, 2003. Proceedings. ICRA '03. IEEE International Conference on, vol. 1, September 2003, pp. 25–30 vol.1.

- [15] K.-T. Yu, C.-P. Lam, M.-F. Chang, W.-H. Mou, S. H. Tseng, and L. C. Fu, “An interactive robotic walker for assisting elderly mobility in senior care unit,” in 2010 IEEE Workshop on Advanced Robotics and its Social Impacts, October 2010, pp. 24–29.
- [16] “Euobserver. disability in figures,” 2012, URL: <https://euobserver.com/disability/118249> [accessed: April, 2017].
- [17] A. Brandt, S. Iwarsson, and A. Stahle, “Older people’s use of powered wheelchairs for activity and participation,” *Journal of Rehabilitation Medicine*, vol. 36, no. 2, pp. 70–77, March 2004.
- [18] L. Fehr, W. Langbein, and S. Skaar, “Adequacy of power wheelchair control interfaces for persons with severe disabilities: a clinical survey,” *Journal of Rehabilitation Research and Development*, vol. 37, no. 3, pp. 353–360, May/June 2000.
- [19] G. Lee, K. Kim, and J. Kim, “Development of hands-free wheelchair device based on head movement and bio-signal for quadriplegic patients,” *International Journal of Precision Engineering and Manufacturing*, vol. 17, no. 3, pp. 363–369, 2016. [Online]. Available: <http://dx.doi.org/10.1007/s12541-016-0045-5>
- [20] S. Yokota, H. Hashimoto, D. Chugo, Y. Ohyama, J. She, and H. Kobayashi, “Supporting technology for wheelchair users,” in *Inclusive Society: Health and Wellbeing in the Community, and Care at Home: 11th International Conference on Smart Homes and Health Telematics, ICOST 2013, Singapore, June 19-21, 2013, Proceedings*, vol. 7910. Springer, 2013, p. 118.
- [21] J. C. Garcia, M. Marron, J. Urena, and D. Gualda, “Intelligent wheelchairs: Filling the gap between labs and people,” *ASSISTIVE TECHNOLOGY RESEARCH SERIES*, no. 33, pp. 202–209, September 2013.
- [22] F. G. Wood, “The meaning of caregiving,” *Rehabilitation Nursing*, vol. 16, no. 4, pp. 195–198, July-August 1991.
- [23] A. R. BROWN and G. P. MULLEY, “Injuries sustained by caregivers of disabled elderly people,” *Age and Ageing*, vol. 26, no. 1, p. 21, 1997. [Online]. Available: [+http://dx.doi.org/10.1093/ageing/26.1.21](http://dx.doi.org/10.1093/ageing/26.1.21)
- [24] G. Lacey and S. MacNamara, “User involvement in the design and evaluation of a smart mobility aid,” *Journal of rehabilitation research and development*, vol. 37, no. 6, p. 709, 2000.
- [25] H. Kitagawa, K. Terashima, T. Miyoshi, J. Urbano, and S. Nishisaka, “Power assist system for omnidirectional transport wheelchair using fuzzy reasoning,” in *Proceedings of the 2004 IEEE International Conference on Control Applications, 2004.*, vol. 1, Sept 2004, pp. 123–130 Vol.1.
- [26] C. Zhu, M. Oda, M. Yoshioka, T. Nishikawa, S. Shimazu, and X. Luo, “Admittance control based walking support and power assistance of an omnidirectional wheelchair typed robot,” in 2010 IEEE International Conference on Robotics and Biomimetics, Dec 2010, pp. 381–386.
- [27] S. Katsura and K. Ohnishi, “A wheelchair type mobile robot taking environmental disturbance into account,” in 7th International Workshop on Advanced Motion Control. Proceedings (Cat. No.02TH8623), 2002, pp. 500–505.
- [28] C. S. Edgren, R. G. Radwin, and C. B. Irwin, “Grip force vectors for varying handle diameters and hand sizes,” *Human Factors*, vol. 46, no. 2, pp. 244–251, 2004, PMID: 15359674. [Online]. Available: <http://dx.doi.org/10.1518/hfes.46.2.244.37337>
- [29] M. Spenko, H. Yu, and S. Dubowsky, “Robotic personal aids for mobility and monitoring for the elderly,” *IEEE Transactions on Neural Systems and Rehabilitation Engineering*, vol. 14, no. 3, pp. 344–351, Sept 2006.



UNIVERSIDAD
DE MÁLAGA